LIVE LOAD TESTING OF APPALACHIA, VA CONCRETE ARCH BRIDGES FOR LOAD RATING RECOMMENDATION

Nathan Paul Thornton

Thesis submitted to the faculty of the

Virginia Polytechnic Institute and State University

in partial fulfillment of the requirements for the degree of

Master of Science

In

Civil Engineering

Thomas E. Cousins, Chair

Carin L. Roberts-Wollmann

Roberto T. Leon

September 13, 2012

Blacksburg, Virginia

Keywords: open-spandrel concrete arch bridge, live load test, Virginia Department of Transportation (VDOT), finite element modeling

LIVE LOAD TESTING OF APPALACHIA, VA CONCRETE ARCH BRIDGES FOR LOAD RATING RECOMMENDATION

Nathan Paul Thornton

(ABSTRACT)

As America's infrastructure ages, many of the nation's bridges approach the end of their service life. In order to develop a method for handling the rising number of deficient and functionally obsolete bridges, nondestructive tests and evaluations must be undertaken. Valuable information from these tests regarding the strength and condition of bridges will help in making decisions about their rehabilitation and replacement.

Two adjoining open spandrel reinforced concrete arch bridges in downtown Appalachia, Virginia were selected for live load testing by Virginia Department of Transportation (VDOT). Both bridges have supported an increasing amount of extreme coal truck traffic throughout their service life and are essential to the efficient transport of coal in the region. Because of their age, having been built in 1929, and the amount of visible damage and repairs, VDOT was concerned about their remaining capacity and safe operation.

The live load tests focused on global behavior characteristics such as service strain and deflection as well as local behavior of the arches surrounding significant repairs. It was found that the strain and deflection data collected during load testing displayed linear elastic behavior, indicating excess capacity beyond the test loads. Also, given the loading applied, the measured strains and deflections were small in magnitude, showing that the bridges are still acting as stiff structures and are in good condition.

Data collected during these tests was compared to results from a finite element model of the bridges to determine the coal truck size which is represented by the live load test loading configurations. The model comparisons determined the test loads produced comparable deflections to those produced by the target coal truck load. Through this approach, a recommendation was given to VDOT regarding the satisfactory condition of the aging bridges to aid in the process of load rating and maintenance scheduling for the two bridges.

Acknowledgements

I would like to express my thanks to everyone that helped me with this research. To my committee members, Dr. Tommy Cousins, Dr. Carin Roberts-Wollmann, and Dr. Roberto Leon, thank you for your guidance and patience during this process. Your experience and instruction during this project has provided me with many lessons to learn from. I would like to thank those from the research lab who helped with the live load tests including Brett Farmer, David Mokarem, Marc Maguire, and Drew Woerheide. Without your hard work on those trips, the test would never have happened. Thank you to those from VCTIR including Mike Brown and Bernie Kassner for your help during the testing and report writing process. Further, I would like to thank the VDOT Bristol District engineers, Jason Kelly and Gary Lester, for their help and supervision during the live load tests. Last but not least, I would like to thank my wife, Lindsey, for her love and support through these last couple years. All photos by author, 2011-2012.

TABLE OF CONTENTS

LIST OF FIGURES

LIST OF TABLES

Chapter 1 – Introduction

As the population continues to increase in America, the demand on the nation's infrastructure is reaching a critical juncture. According to the U.S. Department of Transportation in 2008 there are a total of 600,905 bridges across the country. Of these bridges, 72,868 (12.1%) were found to be structurally deficient and 89,024 (14.2%) were considered functionally obsolete (AASHTO 2008). This equates to one out of every four bridges in the nation having limited structural capacity or failing to accommodate the increasing traffic demand. With the typical bridge built to last 50 years in our country, the average bridge is now 43 years old. To compound the problem, heavy truck traffic continues to increase both in volume and weight, having doubled over the last 20 years. Of the 3 trillion total vehicle miles traveled over bridges per year, 223 billion miles come from heavy trucks (AASHTO 2009). The increase in truck traffic is a significant factor in the deterioration of bridges and is projected to increase at a more rapid rate in the future.

With prices for construction and materials continuing to rise, the amount of money needed to address the aging bridge population far outweighs the funds available at local, state, and national levels. In 2008, the American Association of State Highway and Transportation Officials (AASHTO) estimated it would cost $140 billion dollars to properly repair and improve every structurally deficient and functionally obsolete bridge in the country (AASHTO 2008). Because of these rising expenses, cost-effective strategies for repairing and rehabilitating bridges are essential to extending the lifespan of bridges without necessitating the need for total replacement. The first step in determining the condition of a bridge is through load testing or other non-destructive evaluation techniques. These tests provide information about the bridge's

global behavior, remaining strength capacity, and other important characteristics. Testing is crucial in relating the performance, deterioration, and resiliency of bridges to help in deciding what further steps must be taking in the rehabilitation process.

1.1 Appalachia, Virginia Bridges

Appalachia, Virginia is a small town located in the southwest corner of Virginia along the Kentucky border as seen in Figure 1-1. The town is an important part of the coal industry in the region, being south of several coal mines and handling large amounts of coal truck traffic daily.

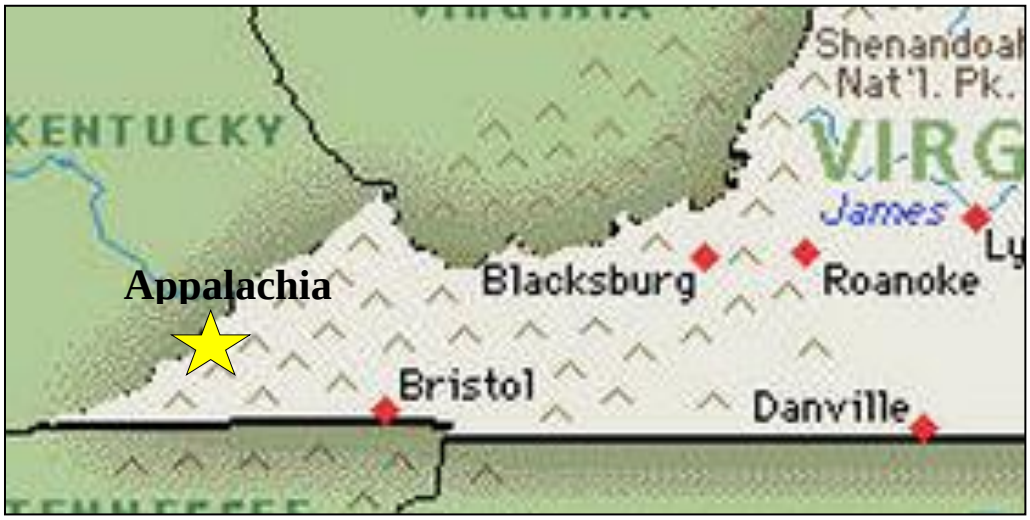

Figure 1-1. Appalachia, Virginia

(Courtesy: www.wwp.greenwichmeantime.com)

Two adjoining concrete arch bridges in downtown Appalachia are crucial to the efficient transit of coal traffic to and from the mines. They are located along Main Street and Depot Street and span Callahan Creek which flows southeast through town. In Figure 1-2, the Main Street Bridge is represented by the red dashed line while the Depot Street Bridge is shown as the

yellow dashed line and the routes to and from the mines are shown in light blue and dark blue, respectively.

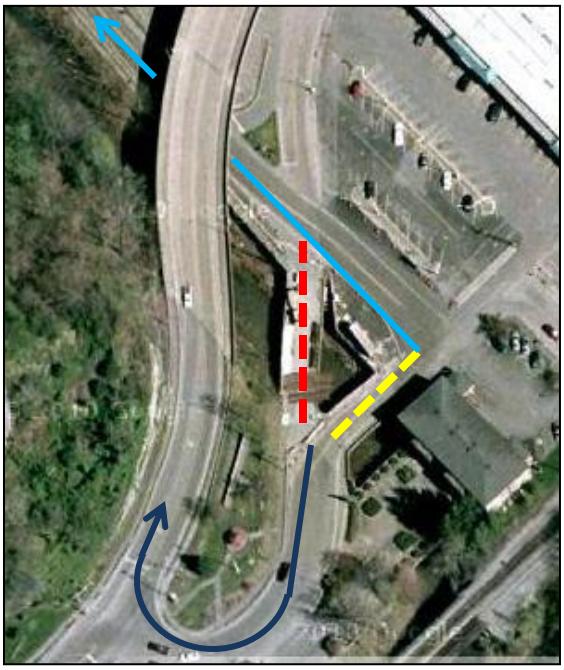

Figure 1-2. Bridge Orientation

(Courtesy: Google Maps ©2012)

Both bridges were built as open spandrel reinforced concrete arch bridges in 1929, making them 83 years old. They each consist of a reinforced concrete deck supported by beams, columns, and three reinforced concrete arch ribs. The arch ribs are nonprismatic over their length, being most slender at the top and increasing in depth as they approach each end. At the south end, the two bridges are joined by several beams connecting their superstructures directly underneath their decks. This connection can be seen in Figure 1-3 with the Main Street Bridge on the right and the Depot Street Bridge to the left.

Figure 1-3. Adjoining Bridge Framework

To simplify lane references for both bridges, each bridge will consist of an upstream and downstream lane.

1.1.1 Main Street Bridge

The Main Street Bridge has a total span length between abutments of 120 ft. Due to the bridge's unsymmetrical arch plan, the downstream and center arches span approximately 102 ft. while the upstream arch spans 95 ft. The arch ribs are skewed at an angle of 33°. A profile view of the bridge as seen from upstream is shown in Figure 1-4.

Figure 1-4. Main Street Bridge from Upstream

As stated previously, the superstructure of the bridge consists of three arches with several columns and web walls supporting the bridge beams located underneath the deck. The arches are spaced at 11 ft on center with a 5 ft-3 in. clear distance between the center of the outer arches and the edge of the deck. Further, the Main Street Bridge has a 32 ft-6 in. wide continuous reinforced concrete deck with a depth of 16 in. that is supported by the superstructure. A closer look at the superstructure is shown in Figure 1-5.

Figure 1-5. Bridge Superstructure

As seen in Figure 1-2, the Main Street Bridge is oriented such that traffic flows both north and south. The Main Street Bridge handles the majority of the coal truck traffic as the primary route to the mines, with two lanes of traffic and a sidewalk on the upstream side of the bridge. A precast concrete and aluminum guardrail system runs along the exterior on each side. The deck and guardrails have been improved and replaced since the original construction of the bridge. A view of the bridge lanes as viewed from the south is shown in Figure 1-6.

Figure 1-6. Traffic Lanes of Main Street Bridge

1.1.2 Depot Street Bridge

The Depot Street Bridge has a total span between abutments of 77 ft. As opposed to the Main Street Bridge, the Depot Street Bridge has a symmetrical arch plan with each arch spanning the entire 77 ft between abutments. There is also no arch skew in the Depot Street Bridge. A profile view of the bridge as seen from upstream is shown in Figure 1-7.

Figure 1-7. Depot Street Bridge from Upstream

The superstructure of the Depot Street Bridge is similar to that of the Main Street Bridge. The arches are spaced at 12 ft-4 in. on center with a 5 ft-6 in. clear distance between the center of the outer arches and the edge of the deck. The continuous deck has a width of 35 ft-8 in. and a depth of 16 in.

The Depot Street Bridge is oriented such that traffic flows to the northeast and southeast. This bridge is primarily used for local traffic and provides a secondary route for coal truck traffic in the event of detour. The bridge supports two lanes of traffic with a sidewalk on each side. The upstream side contains a newer precast concrete and aluminum guardrail while the downstream contains the original guardrail which has fallen into disrepair. The traffic lanes can be seen in Figure 1-8.

Figure 1-8. Traffic Lanes of Depot Street Bridge

1.2 Need for Evaluation

Over their long service lives the bridges have experienced extreme coal truck loadings and environmental exposure, contributing significantly to their deterioration. The visible deterioration, including concrete spalling and cracking as well as steel reinforcement corrosion can be seen in Figure 1-9 and Figure 1-10. Significant patching of the arch ribs and retrofit columns have been added over the years to mitigate the significant damage to the bridges.

Figure 1-9. Patched Concrete Arch Cracks

Figure 1-10. Steel Reinforcement Corrosion

Because of the damage, VDOT became concerned with the bridges' remaining strength. Combining the economic and political importance of the coal industry in the region with the vital location of these bridges, VDOT needed an evaluation of the bridges to decide if they were safe enough to support the continuous heavy loading.

1.2.1 Coal Truck Weight Limits

Another cause for concern is the inspection method that is used to evaluate coal truck weights. Due to the significant contribution of the coal industry to the region's economic vitality, political legislation aids in allowing large truck loads coming to and from the coal mines. Because of the inaccurate weight inspection methods used to limit the truck weights, it is difficult to determine with certainty the loads being carried by coal trucks. A typical six-axle coal truck is shown in Figure 1-11.

Figure 1-11. Typical Coal Truck

The typical coal truck has six axles with a tri-axle configuration in the rear of the trailer. The rear axles, carrying more load than the other truck axles, are the most critical loading component when examining coal truck loads on bridges. This setup with approximate dimensions given is shown in Figure 1-12.

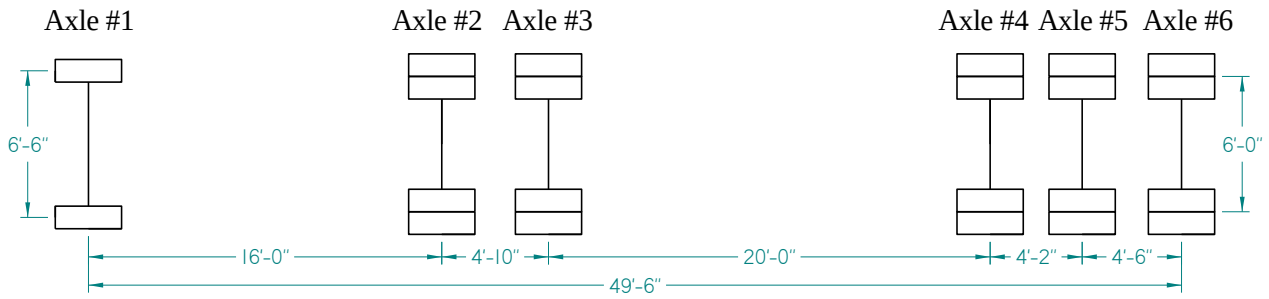

Figure 1-12. Typical Coal Truck Dimensions

The calibration of legal coal truck weight limits is based on the payload weight of the truck and the standard unit weight of coal. The payload weight is found by subtracting the empty truck weight from the total gross weight allowed and the assumed unit weight of coal used in the calculations is 52 pounds per cubic foot. By dividing the payload weight by the unit coal weight, an allowable payload volume is found. This volume is then divided by the inside area of the truck bed to determine the maximum payload height. At this height, a 2 in. wide by 6 in. long opening, as shown in Figure 1-13, is cut into the side of the truck bed to expose the interior material being hauled. If coal cannot be seen through this hole, the truck is judged to be carrying a legal amount of material.

Figure 1-13. Slot Determining Legal Coal Truck Weights

Although this provides for a simple method for determining legal permit loads for coal trucks, there are inaccuracies in the method which can result in larger loads. First, the assumed unit weight of coal at 52 pounds per cubic foot is a rough estimate that can be a severe underestimation depending on the material mixture being hauled with coal. Also, the material can be loaded in such a way that it is not seen through the permitted slot and exceeds the allowable payload volume determined in the calibration method.

Because of these discrepancies in the calibration process, coal truck loads vary greatly and can easily exceed the allowable loads designated by VDOT. A comparison of the allowed loads and common truck loads is shown in Table 1-1. The legal limit weights in the table represent the maximum allowed for coal haulers from the Code of Virginia, Chapter 10, Title

46.2-1143.B. The actual coal truck weights represent field measured loads as reported by the Virginia Department of Transportation.

Table 1-1. Legal and Actual Coal Truck Weights (in kips)

Load	Gross Weight	Single Axle	Tandem Axle	Tri-Axle
Legal Limit	110	24	44	54.5
Actual	160	20	68	72

The live load tests performed in this study attempt to simulate the loads seen by the trucks that exceed the legal weight limits as determined using the calibration method.

1.3 Scope and Objectives of Study

For this study, live load tests were performed on each of the bridges. The goals for these tests were to investigate the global behavior of the bridges, their remaining strength capacity, and the effect of bridge deterioration on their overall safety. The main characteristics being observed were service strains and service deflections. The deflections provide knowledge of how the bridge distributes loads throughout its components. However, the strains reveal whether the arches are acting in the elastic or inelastic range. By analyzing the results, decisions can be made about the condition of the bridges.

After using the tests to determine behavior, finite element models of the bridges were developed to analyze and compare the results. Because live load tests have constraints related to loading and time, analytical models allow a more thorough examination of the bridge. The main purpose for the models is to determine the coal truck loading which is equivalent to the test truck loadings. Also, the model can be refined for later use if the bridges need to be analyzed further.

1.4 Thesis Organization

This thesis is divided into six chapters. Chapter 2 contains a literature review of concrete arch bridges, live load testing, and bridge load rating. The experimental testing procedure used for the live load tests is covered in Chapter 3. The techniques and assumptions used in developing the SAP2000 finite element model of the bridges are found in Chapter 4. The results and analysis from the live load tests and finite element model are presented in Chapter 5. Finally, Chapter 6 summarizes the conclusions of the study and provides recommendations for the load rating of the bridges.

Chapter 2 - Literature Review

The following chapter reviews literature that is useful in accomplishing the objectives of this study. First, the arch bridge design and its unique behavior are examined. Next, finite element modeling of arches is discussed briefly followed by live load testing as an accurate method for obtaining bridge characteristics. Load rating procedures and how they can be applied to arch bridges using AASHTO LRFD load rating equations are discussed last.

2.1 Reinforced Concrete Arch Bridges

The arch is a fundamental structural shape that has been used and improved by engineers over the past 2500 years. Civil engineering advancements are based on tangible results rather than abstract ideas and would not be possible without past engineers pushing the envelope (Radic, et al 2006). One such engineer, when discussing the progression of arch bridges, was Robert Maillart, who built exquisite arch bridges in Switzerland. Through his designs, Maillart not only showed how the arch is a simple, functional structural shape but also how it results in a bridge which is an aesthetically-pleasing work of art (Laffranchi and Marti 1997).

There are several types of arch bridges used in construction today, using both steel and concrete materials. The through arch bridge contains a steel arch/truss structure above the deck such that the traffic travels underneath the arch. Through arch bridges are not in the scope of this study. Deck arch bridges are designed with the deck located above the arch and other supporting structural components. Within deck arch bridges there are open-spandrel and closed-spandrel designs. The closed-spandrel arch bridges, also known as filled or buried arch bridges consist of at least one arch that supports a deck above with earth or material filling the spandrel area (Weidner, et al 2009). The focus of this study is on open-spandrel arch bridges where the deck is

supported by arch ribs and the spandrel area containing columns and beams. Due to the many components working together to distribute the loads experienced on open-spandrel arch bridges, it is difficult to determine their true behavior. At times they can behave more like multilayer continuous structures with high structural redundancy rather than true arches. The typical load path of an open-spandrel arch bridge follows the superstructure and arch ribs to the end supports. The distribution of the loads is dependent on the ratio of flexural stiffness between the structural components (Baxter and Balan 2008). Due to their complexity, when analyzing damaged bridges of this type it is important to note that failure mechanisms will not always develop as a result of cracking because the structure will redistribute the load path (Marefat, et al 2004).

2.1.1 Arch Behavior

When analyzing a continuous arch, it can be considered as a unique type of curvilinear beam built in from the end supports. Due to this, arches are statically indeterminate meaning statics equations alone cannot determine stresses and reactions within the structure (Viola, et al 2007). Because of its indeterminacy and the myriad geometric variations possible, arch behavior can be complex to explain. However, when simplifying these parameters, the general behavior of arches in terms of compression and thrust is quite simple.

In an arch bridge the ribs act as the main load-resisting members, determining how the bridge performs (Zhang, et al 2007). It is important to point out the main external characteristics that classify the structural shape as an arch. Every arch is supported at either end by abutments with the clear span defined as the distance between the centerlines of each support. Arches reach a maximum height at the crown, following a certain geometric profile throughout the span. The geometric profile of an arch can be determined by a constant circular radius, parabolic, or

elliptical equation (Viola, et al 2007). The maximum height at the crown is called the rise and has a large effect on the arch response that will be discussed later in this section.

The amount of arch and beam action experienced within the arch rib is determined by the arch profile, fixity of the supports, and construction procedure (Baxter and Balan 2008). The imaginary plane that marks the end of the arch and beginning of the end support is called the arch skewback. For a structure to be classified as an arch both end supports must have horizontal reactions to resist the outward thrust transmitted through arch (compressive) action. If the supports have horizontal flexibility due to settlement or material properties, arch action will decrease as beam action and tensile stresses increase. Although outside the scope of this study, it is important to recognize that elastic rib shortening, concrete creep, and shrinkage will produce moments within the arch rib regardless of its shape (Baxter and Balan 2008).

Each arch has a thickness that can be constant or vary along its length. The inner edge of the thickness is defined as the intrados and the outer edge is known as the extrados. Within each arch cross-section is the core of the section, defined by an upper curve and lower curve. For rectangular sections the upper curve is located at a distance of one-third the arch thickness from the extrados and likewise for the lower curve from the intrados (Viola, et al 2007). This section core is significant when discussing the thrust line of the arch. The thrust line is the line containing all the stress resultants acting at each section along the span of the arch. Since the thrust line summarizes the arch response in a comprehensive manner, it is very important to understand how it behaves under various geometric and loading scenarios (Viola, et al 2007). For an arch to satisfy the assumption that it is in pure compression at every section along its span, the geometric profile of the arch must follow the thrust line, balancing the compressive loads at every spandrel joint (Baxter and Balan 2008). When this occurs, the thrust line will fall within

the core of every section along the arch (Viola, et al 2007). However, if the geometry of an arch differs from the line of thrust, beam action and tensile stresses will increase while arch action and compressive stresses decrease in the arch rib. For an arch similar to those in the study with spandrel columns, the thrust line forms a polygon with vertices where the arch and columns intersect (Baxter and Balan 2008).

Because the thrust line determines the amount of arch action and beam action experienced within the arch rib, its location is vital when assessing the safety of an arch. The eccentricity between the location of the thrust line and the geometrical axis of the arch is dependent on the ratio of the moment and axial force within an arch section (Viola, et al 2007). As the eccentricity becomes large enough for the thrust line to pass outside the core of any section along the arch, hinges could form within the structure. When a certain number of hinges is reached, a collapse mechanism is formed and the failure of the arch occurs. Arches have shown to fail in a manner that occurs when it breaks apart in four pieces. However, the location of the four fractures at the arch intrados is still complex. Parameters such as arch rise and support settlement have been analyzed to determine their effect on the location of the thrust line (Viola, et al 2007). It was shown that as the rise increases, the moments and shear increase as the arch shows more beam action. This causes the thrust line to move further from the geometrical arch axis and eventually cause cracking of the arch and redistribution of stresses within the arch. Further, it was shown that settlement of supports is also an important factor in the failure of arches. As settlement increases at a support, moments increase at the opposite end of the arch, causing the thrust line to shift outside the section core. Because of these findings, it is important to know the behavior of the thrust line as it relates to arch geometry, loading scenarios, and material properties (Viola, et al 2007).

2.2 Finite Element Modeling of Arches

Finite element models provide useful information when investigating the behavior of a structure, especially when studying unique structures like arches where behavior is complex. The models can be as refined as the study requires, ranging from general representations of a structure to extremely detailed replicas. Because modeling allows economic and efficient analysis of a structure with a wide range of variables, it has proven to be an important tool for research studies as well as design work (McGrath and Mastroianni 2002).

2.2.1 Element Formulation

Finite element modeling makes understanding the behavior of complex structures much easier through the use of computational power. However, due to assumptions made within structural analysis programs, it is important to understand the theory behind the formulation of the finite elements being used.

Development of arch theory including shear deformations follows that of a Timoshenko straight beam except a curvilinear coordinate system is used and there is a coupling of the axial and transverse directions (Viola, et al 2007). Several assumptions such as a global coordinate system, boundary conditions and a plane, prismatic isotropic arch are made before deriving the differential equations used in the element formulation. The strain-displacement relationships are then defined for an arch, including normal and shear strain as well as curvature. The equilibrium equations for an infinitesimal arch are represented by a system of three coupled differential equations. By combining these equilibrium equations with the constitutive relations for the internal forces of shear, axial, and moment and the strain-displacement equations, all aspects of the problem are included in the three coupled differential equilibrium equations (Viola, et al

2007). A third order differential equation in terms of curvature is obtained and used to determine a solution for the coupled system of equations, also in terms of curvature. By de-coupling the equilibrium equations, the exact solution is expressed in terms of six constants, three for each node of the finite element. The six constants must be found by satisfying the geometric and natural boundary conditions of each beam end. After solving the problem for the coupled displacement equations, the element stiffness matrix is found based on shape functions. The stiffness matrix is made up the stiffness matrices for the axial, shear, and bending moment forces (Viola, et al 2007).

2.2.2 Arch Modeling Procedure

By knowing structural parameters such as material properties, dimensions, end connection details, the type of analysis being conducted, and desired results, the modeling process will be more efficient, eliminating steps that could be unnecessary. When preparing to model a complex structure using a structural analysis software package, it is important to be familiar with the program's operation and terminology. Also, it is vital to study the modeling methods used in past studies of similar structures and determine which parameters will be included in the model.

The structural analysis program, SAP, uses finite element analysis and was created at the University of California, Berkley in the early 1980s. Its latest release, SAP2000, is popular among structural engineers for analysis and design purposes (Lok and Lamanna 2006). In past studies, open-spandrel arch bridges were modeled as planar frames, using a series of frame elements for the arches, beams, and columns. In a study by Garrett, it was found that this simplified approach produced accurate results when compared to a complex three-dimensional

model with many more degrees of freedom (Garrett 2007). Frame elements are used in SAP2000 because displacements, reactions, and internal forces can be found from live loads acting on the structure (Lok and Lamanna 2006). To account for arches and other structural components with varying thickness along their length, several frame elements with different geometric traits can be joined to create a continuous structural element (Zanardo, et al 2004). The number of frame elements used in the entire model is subject to the convergence check performed after the analysis. This is done to optimize the model by finding the minimum number of elements needed to produce satisfactorily accurate results. Other details from past studies include modeling the arch boundary conditions as fixed and the vehicle tire loads as point loads along the deck (Lok and Lamanna 2006).

Because some structural behavior can only be determined by field testing, it is important to only include parameters that are known. This is especially true with damaged structures when trying to model cracking and corrosion of concrete or steel. However, past studies provide insight on how to account for these intricate behaviors. To account for corrosion in the reinforcement steel, the effective area of steel can be reduced to simulate a decrease in capacity (Zhang, et al 2007). Further, cracking has been represented by a reduction in the tensile strength of the concrete. The tensile strength is reduced from the typical $7.5\sqrt{f'_c}$ because it is assumed that the crack will be closed under compression (McGrath and Mastroianni 2002). Another method for modeling damaged concrete structures is to reduce the moment of inertia of the damaged element, decreasing the element's stiffness (Garrett 2007). These modeling assumptions have been verified in past studies but it is still important to note that each structure behaves uniquely.

2.3 Live Load Testing

As the condition of our nation's bridges continues to worsen, it has become more important than ever to correctly assess the condition of these structures (Chajes, et al 2000). By accurately determining the load-carrying capacity of existing bridges, informed decisions can be made regarding limited funds and resources available for projects (Chajes and Shenton 2005). When engineers design bridges they must rely on AASHTO LRFD Bridge Design Specifications that are developed using simplifying assumptions which allow them to design structures safely without increasing burdensome calculations. Because these codes are used to predict global performance they tend to be overly conservative and do not take into account the multitude of variables that are present in a structure (Sartor, et al 1999). Due to their idealized nature, design codes may not represent actual conditions and are sometimes poor predictors of load carrying capacity for existing bridges (Cai, et al 1999). Analytical tools such as finite element models are also used to determine bridge behavior such as stresses and displacements under certain loading scenarios. However, these models do not always provide the best results because it is difficult to accurately portray certain structural unknowns such as complex interaction between components in a structure. Live load field testing is one way to ensure precise results that account for the actual conditions of the bridge (Sartor, et al 1999). Only by investigating the bridge's behavior through live load testing can engineers understand the inadequacies of theoretical evaluation methods (Bakht and Jaeger 1990). Live load testing presents the best solution to determining a bridge's remaining capacity and advancements have made efficient testing much more feasible (Chajes, et al 2000). With each bridge presenting unique challenges, live load tests always manage to surprise, leaving valuable lessons for engineers to learn from (Bakht and Jaeger 1990).

Live load tests provide numerous benefits when investigating the behavior of an existing bridge such as evaluation of the load distribution between members, measurement of stresses at connections, and most importantly the effective capacity of the bridge (Sartor, et al 1999). As a result of the test, decisions can be made regarding the need for bridge repairs and proper load ratings can be established (Cai, et al 1999). As stated earlier, theoretical capacity calculations tend to be overly conservative because of the assumptions made. Field tests reveal that actual capacities often exceed the calculated capacity, with the bridge having the ability to carry much greater loads than previously thought (Bakht and Jaeger 1990). The higher actual capacity represents an increase in stiffness and can be due to several differences between actual and assumed structural properties. These could include differences in material properties, support rigidity, load distribution, or unexpected composite action with the deck. The larger capacity will result in higher load ratings which could eliminate unnecessary repairs and prevent bridges from being posted for loads (Saraf, et al 1996). Deteriorating bridges, appearing in desperate need of repair, have been found through testing to possess normal capacities, showing that damage can be misleading at times (Bakht and Jaeger 1990). Bridge capacities exceed that of the test load when the data collected displays elastic behavior through linear relationships (Saraf, et al 1996). This concept is illustrated with a typical load-deformation curve in Figure 2-1.

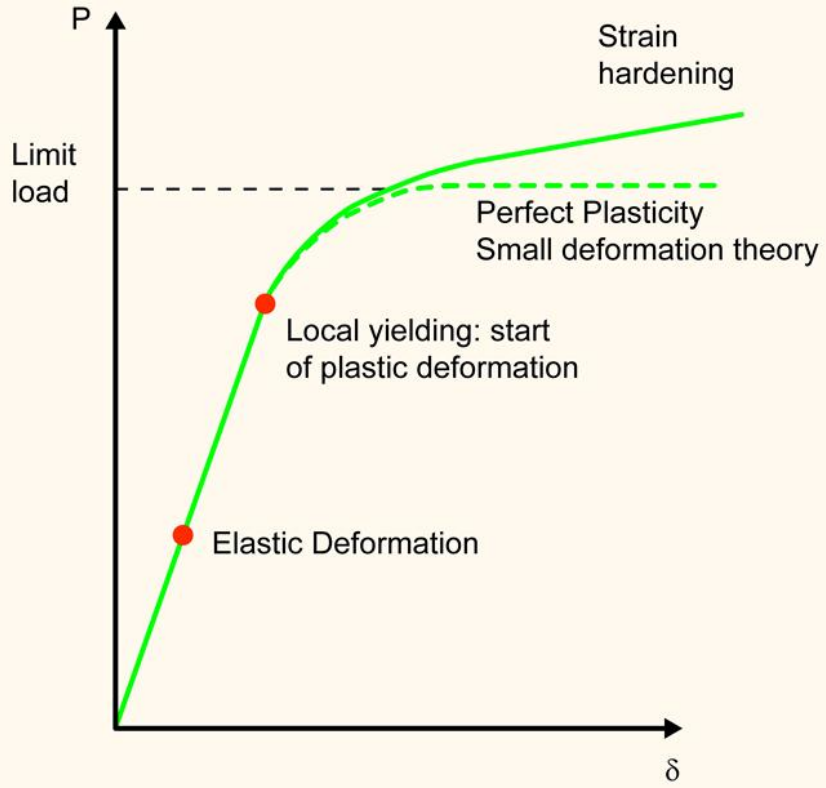

Figure 2-1. Load-Deformation Curve

(Courtesy: http://www.strath.ac.uk)

From the linear portion of the curve, deflections increase at a rate proportional to the load increase. As the specimen yields and approaches ultimate capacity it begins to experience nonlinear behavior where the increases in deflection are much greater for small increases in load. Therefore, if a bridge is tested with a certain load level and displays elastic behavior through linear relationships, it can be concluded that the ultimate capacity of the bridge is greater than the test load.

2.3.1 Types of Live Load Testing

Several nondestructive field testing methods exist to provide results for varying objectives. The most common among these are diagnostic tests, proof tests, and in-service monitoring. The testing employed for this study used both diagnostic and proof load testing with different truck load combinations.

Diagnostic testing uses predetermined loads to quantify the bridge response accurately (Chajes, et al 2000). It provides a better understanding of bridge behavior and unknown characteristics such as damage level, material properties, and load distribution. Diagnostic testing is used when the condition of the bridge is in question and the bridge loading patterns are known, providing feedback that can help with repair decisions (Cai, et al 1999). Some drawbacks to this type of test include the need for traffic control, setup time, and the brief period of test time represented in the data (Chajes, et al 2000).

Proof load testing is performed to determine the ultimate live load capacity of a bridge (Saraf, et al 1996). Loading is done incrementally, checking bridge behavior for nonlinearity at each loading step, until the target load is reached. Proof tests require much larger loads than diagnostic tests and must be carefully monitored to prevent damage to the bridge (Cai, et al 1999).

In-service bridge monitoring is another type of bridge evaluation, being used to capture bridge behavior over longer durations of time. This method provides statistical feedback for response to normal daily traffic, requires little setup, and can be overseen from a remote location. However, this type of test makes it difficult to quantify bridge response as the weights of the truck loadings are not known (Chajes, et al 2000).

2.3.2 Loading Application

During live load testing, vehicular loads are applied to the bridge with the response being captured by instrumentation attached to bridge components at specific locations. Diagnostic tests are usually performed with dump trucks filled to a specific weight while proof tests use extreme loadings to obtain their target load (Saraf, et al 1996). The diagnostic test trucks are often filled to weights in the range of the 72 kip AASHTO HL-93 design truck to compare actual behavior to calculated responses (Sartor, et al 1999).

For the test, vehicles make passes in each direction along predetermined paths marked along the bridge (Neely, et al 2004). The test plan can include passes with single trucks, side-by-side trucks, or multiple trucks in a train (Chajes and Shenton 2005). The loading levels and positions are determined to produce the maximum response at critical locations along the bridge. Depending on the testing plan, trucks make multiple passes at varying speeds ranging from a crawl to highway speed to capture impact of dynamic effects on response. As in this study, static testing can be deemed the appropriate method, where trucks are stopped at critical locations along the bridge to capture a steady response over several seconds (Cai, et al 1999). It is important to assess the impact on daily traffic volume on the bridge if considering closing lanes for the loading procedure. If possible it is best to avoid multiple lane closures to limit the delay to the traveling public (Sartor, et al 1999).

2.3.3 Data Collection

During live load tests, bridge behavior is measured by instrumentation planned to capture specific characteristics of the response. The most common elements of behavior that are recorded are girder and deck strains, girder deflections, thermal effects, and bearing rotation. The

instruments are located at critical positions along the bridge as determined by theoretical calculations, analytical models, or engineering judgement (Saraf, et al 1996). Other factors that are considered when planning the instrumentation setup include locations of maximum stress, bending moment, or deflection, as well as traffic control, and attachment feasibility (Nowak, et al 2000).

Strains are generally recorded through the use of vibrating wire gages, foil strain gages, or strain transducers. The type of instrument used depends on the material of the structure being tested, as well as the location on the structure (Cai, et al 1999). All gages can be attached to the face of girders or decks with epoxy or C-clamps to measure surface strains and vibrating wire gages can be embedded or post-installed in concrete to measure internal strains. Full bridge strain transducers, such as in the BDI instruments used in this test, are recommended because they produce higher output, decreasing the chance of noise affecting the data collected (Chajes and Shenton 2005). Depending on the type of test, it is important to make sure the portable strain monitoring system can collect reliable data in various testing environments (Sartor, et al 1999).

Deflection measurements have been recorded in many different ways in past studies. The most reliable methods include using linear variable displacement transducers (LVDTs) (Cai, et al 1999) or homemade instruments known as deflectometers or twangers (Neely, et al 2004). LVDTs can measure vertical deflection but are best suited for measuring horizontal displacements such as those over expansion joints in bridge decks (Cai, et al 1999). Deflectometers measure deflection through the use of a cantilever arm attached to a fixed ground wire. These instruments were used in this study and are described in Chapter 3.

Each instrument is connected to a data acquisition system which runs the test program and saves the recorded data throughout the test (Cai, et al 1999). These systems range from cumbersome wired units which require hundreds of feet of cable to newer wireless systems with less harrowing setups (Chajes and Shenton 2005). Depending on the speed of the test, the sampling rate can be increased in the test program to meet the data requirements. Static and crawling tests require much lower rates than high-speed tests. This study used a rate of 4 Hz due to its static nature while high-speed tests require rates close to 200 Hz to measure dynamic effects. When analyzing the results following the test, data filtering can be performed to remove unnecessary data (Nowak, et al 2000).

2.3.4 Bridge Structural Identification

By revealing how certain stiffness parameters affect a bridge's performance, live load testing plays an important role in structural identification. Structural identification is a process that quantifies characteristics of a structure by correlating simulated responses from analytical models and measured responses from field testing (Weidner, et al 2009). The structural identification process is driven by a specific objective, usually formulated by the owner, and the testing methods and modeling options are determined by the structure type.

Since finite element modeling acts as a guideline for a structure's idealized behavior (Cai, et al 1999), live load testing can reveal differences between the idealized and actual structure. By comparing test results from the actual bridge to data from an idealized model, damage and deterioration can be identified. The goal of structural identification is to use these data comparisons to develop field calibrated models that quantify how stiffness parameters have changed over time (Weidner, et al 2009). With this knowledge, owners can make informed

decisions with respect to their original objective. These decisions can range from avoiding unfavorable postings to discovering a bridge is in need of immediate repair. Regardless of the objective, structural identification provides an accurate method that allows owners and engineers to make responsible decisions regarding deteriorating structures (Weidner, et al 2009).

2.4 Bridge Load Ratings

As bridges deteriorate because of aging, harsh environments, and extreme loadings (Cai and Shahawy 2003), it becomes more important to use the results of load tests to calculate accurate load ratings (Ranasinghe and Gottshall 2002). Load ratings are simplified expressions of a bridge's live load capacity. They are calculated by first subtracting the stress caused by dead loads and other factors from the total capacity of a member, with the remaining stress representing the live load capacity of the member. This live load capacity is compared to the stress caused by a standard design load, such as an HL-93 truck, providing a ratio that signifies the member load rating. Because several members comprise a structure, the lowest rated member controls the load rating of the structure (Carrato, et al 2000). With the *Manual for Condition Evaluation of Bridges (*MCE) giving little direction for reinforced concrete arches (Garrett 2007), there is relatively no standardized methods for load rating these types of structures (Ranasinghe and Gottshall 2002).

As stated earlier, live load tests reveal that theoretical capacities are often underestimations of the actual bridge capacity. Similarly, theoretical load ratings based on original designs underestimate the true bridge rating (Chajes, et al 2000), tending to be very conservative (Chajes and Shenton 2005). The more accurate ratings are based on test results that reveal much lower measured live load stresses and distribution factors than calculated values

from analytical models (Cai and Shahawy 2003). Accurate load ratings are important because ratings are used to prioritize repairs, place postings on bridges that have insufficient capacities, and determine safe routes for heavy permit loads. Inaccurate ratings can be dangerous for the public's safety, lead to inefficient fund allocation, and traffic problems for heavy truck loads (Chajes, et al 2000).

Bridges are rated at two different load levels known as the inventory and operating rating levels (Carrato, et al 2000). The inventory rating is based on a normal traffic load which the bridge can support for an indefinite amount of time. The operating rating level is based on a maximum live load which the bridge can support in sporadic intervals. This maximum live load would cause damage to the bridge if it occurred more frequently on the bridge (Garrett 2007).

Rating a bridge requires engineering judgment to interpret the many factors that affect bridge behavior. Factors that affect ratings include redundancy, load distribution, support fixity, composite action, and effect of secondary members (Carrato, et al 2000). Redundancy is defined as the presence of several load-carrying mechanisms within a structure. If one of these fails, there are multiple ways to carry the load to prevent failure of the structure. There are three types including load path, structural, and internal redundancy. Recognizing any type of redundancy in a bridge is vital to allowing heavy loads because the capacity is higher than calculations show. Live load distribution is simplified in the AASHTO design codes so if the analytical load rating is unfavorable it is important to establish more accurate load distribution behavior from field testing or advanced finite element models (Carrato, et al 2000). Support fixity and composite action always vary from the idealized structure used in theoretical ratings, making it important to quantify the actual behavior from field testing. This is also the case with secondary members as they contribute to the structural stiffness, boosting the capacity and rating of the bridge. Since the

rating process is a force based approach, it is more important to record strains than deflections when using field testing to improve the load rating (Chajes and Shenton 2005).

2.4.1 AASHTO Load Ratings

Analytical load ratings in the AASHTO Bridge Design Specification are determined by two basic equations. The equation used to determine the rating factor of a member is given by:

$$RF = \frac{C - A_1 D}{A_2 L_{rat}(1 + I)}$$

where RF = rating factor for live-load capacity; C = capacity of the member; D = dead load effect on the member; L_{rat} = live load effect on the member; I = impact factor; A_1 = dead load factor; and A_2 = live load factor (Garrett 2007). The capacity (C), dead load effect (D), and live load effect (L_{rat}) can be represented by a stress or moment capacity, depending on the desired units. The live load effect (L_{rat}) is the stress or moment caused by a standard rating vehicle, such as the HL-93 loading (Cai and Shahawy 2003).The dead load and live load factors (A_1, A_2) depend on the method used, being allowable stress design (ASD), load factor design (LFD), or load and resistance factor design (LRFD). For ASD, $A_1 = A_2 = 1.0$ and for LFD, $A_1 = 1.3$ and $A_2 = 1.3$ for operating rating level or 2.17 for inventory rating level (Carrato, et al 2000). To determine the bridge member rating in tons (RT), the rating factor (RF) is multiplied by the weight (W) of the design load used for calculating the live load effect (L) in the Equation 2-1 (Garrett 2007). This is presented below:

$$RT = \text{RF(W)}$$

First order elastic ratings are most common when calculating load ratings. However, if a more detailed rating is needed second order ratings can be performed. Several methods are

available to perform this analysis while incremental methods and moment magnification are the simplest. Geometric and material nonlinearity is accounted for and the tangent stiffness matrix updated at each increment. At the end of the process, new loads are calculated which are applied to the structure, producing different capacities and load effects to be used in the rating factor equation (Garrett 2007).

2.4.2 Experimental Calculation of Load Ratings

The nature of the design codes causes analytical load ratings to be conservative, producing unfavorable results at times when they could be avoided. In many instances, field tests reveal that the calculated stresses are much higher than the measured values (Cai and Shahawy 2003). Because of this, it is important to consider using field tests when load rating structures, especially when the analytical rating may cause unnecessary postings or repairs. Due to the different load levels, proof testing and diagnostic testing produce different load rating values.

Proof testing loads a bridge up to a heavy target load until nonlinear behavior is observed. This final test load is used to rate the bridge in the equation given by:

$$RF = \frac{M_{test}}{A_2 M_{rat}(1 + I)}$$

where M_{test} = measured moment from load test due to final target load used; M_{rat} = calculated moment due to standard rating vehicle load (Cai and Shahawy 2003). Proof load tests are used mainly for operating ratings and need to be reduced by a factor of 1.67 to reach the corresponding inventory level. The ratings from proof load tests establish a lower bound capacity because they are based on a target load that is assumed as the ultimate load. Since the bridge can

support more load, the minimum capacity reflected in the rating produces the lower bound (Cai and Shahawy 2003).

Diagnostic testing uses lower loads than proof load testing. Because of this, the rating obtained from this test is actually a linear extrapolation of the measured test performance to the ultimate capacity. This is represented, in terms of stress, given by:

$$RF = \frac{\sigma_{test}}{\sigma_{test}^{m}} RF_a$$

where RF_a = AASHTO analytical load rating factor; σ_{test} = predicted analytical stress caused by the test vehicle; σ_{test}^{m}= measured live load stress caused by test vehicle (Cai and Shahawy 2003). The analytical rating factor (RFa) and stress (σ_{test}) can be determined with a simplified or complex analytical model. It is recommended that the test vehicle be similar to the service load level to ensure the rating results are reliable. The linear extrapolation in the diagnostic rating is not conservative because it assumes linear bridge behavior from the test load up to the ultimate limit state. Because of this, diagnostic ratings are considered as an upper bound capacity. The actual rating of the bridge lies between the lower bound proof load rating and the upper bound diagnostic load rating (Cai and Shahawy 2003).

2.5 Literature Review Summary

This literature review was focused on examining arch bridges, live load testing, and load rating procedures. The behavior of arch bridges is complex and difficult to analyze. It was determined that the location of the thrust line in proximity to the arch's geometric profile plays a significant role in the amount of arch and beam action within the arch. It was also found that the typical failure mode of an arch is to rupture at the intrados of the arch and break apart in four

segments. The method of structural identification was discussed where load tests are used to create accurate models of the bridge for determining the bridge's condition. Finite element models provide a baseline for structural behavior to be used as a guideline during load testing. Live load testing was shown to predict larger bridge capacities than the conservative guidelines provided in design codes. Structures displaying linear elastic behavior from test loads have excess capacity beyond these loads. The study consisted of diagnostic load testing used to determine the general behavior of the bridge and proof load testing used to find the ultimate live load capacity. Due to the nature of arch bridges, there are not any simplified methods for load rating these structures. Load rating is controlled by the lowest rated member within the structure. There are two types of load ratings, inventory and operating. The inventory rating level is calculated based on normal traffic loads over and indefinite time period while the operating level is based on large loads that the bridge can support sporadically. Similar to predictions for capacity, theoretical calculations of load ratings are often conservative. The use of live load tests in determining load ratings was examined and compared to current analytical AASHTO rating approaches. It was found that proof load tests provide a lower bound load rating and diagnostic tests provide an upper bound rating. The actual load rating of the bridge is between these two ratings. The different elements of the literature review combine to present a clear picture of how a bridge is behaving in its current state.

Chapter 3 - Testing Procedure

The Appalachia concrete arch bridges were tested on separate occasions. Due to its significance as the primary route for coal truck traffic, the Main Street Bridge was tested first on August 18, 2011. The live load test for the Depot Street Bridge was performed on September 29, 2011. The bridge instrumentation, testing, and teardown were completed within the same day for each test.

3.1 Data Collected

Live load tests were performed to understand the global and local behavior of the concrete arch bridges. To provide a load rating recommendation for the bridges, knowledge of their remaining strength capacity was needed. Bridge performance characteristics such as the strength capacity are dependent on certain structural stiffness parameters. Specific data was captured during the testing to understand how these parameters were affecting bridge performance under simulated coal truck loading. The data collected during the tests includes the surface strains and global deflections at different locations along the concrete arch ribs. Also, local behavior around damaged and repaired portions of the bridge was investigated to further understand the effects of long term deterioration.

3.2 Bridge Instrumentation

Instrumentation for the tests was chosen based on the data being collected. Strain transducers and deflectometers were attached at nine locations along the concrete arches of each bridge. These locations were determined using engineering judgment to be the critical locations along the bridge. Finite element modeling was not done prior to testing due to time constraints

surrounding the study. Testing the condition of the bridges was paramount to determining their safety and was required before modeling could be undertaken.

3.2.1 Deflectometers

The deflections at nine locations on each bridge were measured by deflectometers or "twangers". These instruments were made in the research laboratory and have been used as an accurate method for measuring deflections during live load testing for many years. They were shown in calibration to be accurate to 0.001 in. A picture of a deflectometer, as seen from directly below, is shown in Figure 3-1.

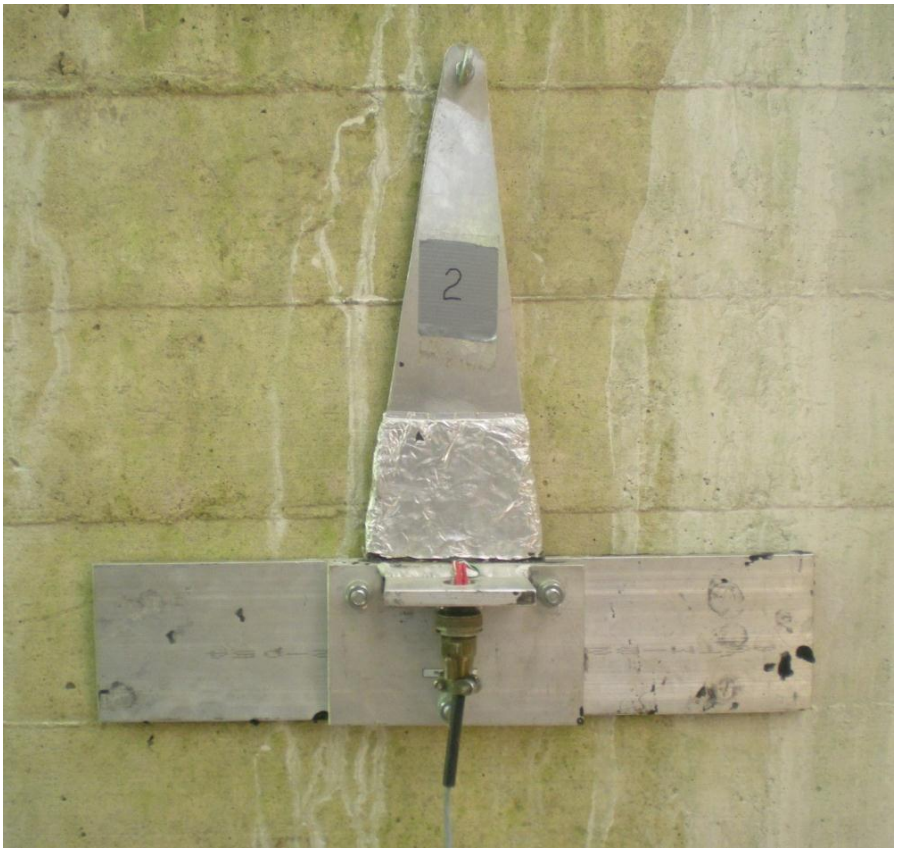

Figure 3-1. Deflectometer

Deflectometers are made using three aluminum plates. Two rectangular plates fixed on either side of a third, triangular plate act together to create a cantilever structure. The bottom plate is used to attach the deflectometer to the bridge using epoxy glue and accelerant combination or C-clamps depending on the structure. Due to the roughness of the concrete arches, a grinder was used to provide a smooth surface for the instruments. This process can be seen in Figure 3-2. The smaller rectangular plate contains a connection for wiring to the data acquisition system. Finally, the triangular plate contains a full bridge strain gage protected by aluminum foil as shown previously in Figure 3-1.

Figure 3-2. Smoothing Concrete Arch Surface with Grinder

The cantilever end of the deflectometer contains an eye-hole screw that allows for picture wire to be attached. The picture wire is then stretched taut to the ground and connected to a 6 in. by 12 in. concrete cylinder weight. This provides an initial downward deflection to the tip of the

deflectometer which changes during the load test. This is shown in Figure 3-3. As the bridge is loaded during testing, the arch and the attached deflectometer base deflect simultaneously. The change in strain between the loaded and unloaded conditions, as measured by the strain gage within the deflectometer, provides the deflection value for the girder.

Figure 3-3. Deflectometer Attached to Weight

Nine critical locations for the placement of the deflectometers were determined for the tests, with three along each arch. These were located at the approximate quarter points and at midspan on each of the three arches.

3.2.2 Strain Transducers

During the live load tests, surface strains of the arch rib were measured by strain transducers. The ST350 strain transducer model from Bridge Diagnostics, Inc. (BDI) was chosen as the most accurate and efficient instrument for the tests. A picture of the ST350 fixed to the concrete arch is shown in Figure 3-4.

Figure 3-4. BDI ST350 Strain Transducer

The BDI strain transducers contain a full Wheatstone bridge with four active 350 watt foil gages inside of a waterproof and weather-resistant aluminum exterior. When measuring strain, strain gages produce a linear change in electrical resistance which is transmitted to the data acquisition system. The resistance of each foil gage within the bridge can be measured with an ohmmeter. With strain gages, the level of resistance is directly related to the sensitivity of the instrument, giving gages with higher resistance a higher sensitivity. Because measured strains are usually very small, often being measured in microstrain, it is important to have strain gages with

higher resistance and subsequently sensitivity. Also, the BDI transducer contains a completed circuit with the four gages, meaning its output is three times higher than a single quarter-arm foil gage setup, allowing for an enhanced signal-to-noise ratio. This provides higher-resolution strain readings and eliminates the possibility of interference that can occur with long cables required to span the distance between the instrument and the data acquisition system. Overall, the strain transducer has a three inch gage length and is calibrated by BDI to accuracy within two percent of the measured strain value.

Strain transducers can be attached to both steel and concrete structures, using an epoxy glue and accelerant combination. The combination used during these tests was Loctite 410 glue and Loctite 7452 accelerant. Similar to the deflectometer installation, smoothing of the rough concrete prior to placing the transducers provided a more suitable bonding surface on the arch. After applying glue and accelerant to each of the transducers tabs, the ST350 strain transducers were fixed to their proper location on the bridge and bonded within a few seconds. Each strain transducer attached to the bottom face of the arch was placed approximately one inch behind the deflectometer. This setup is shown in Figure 3-5.

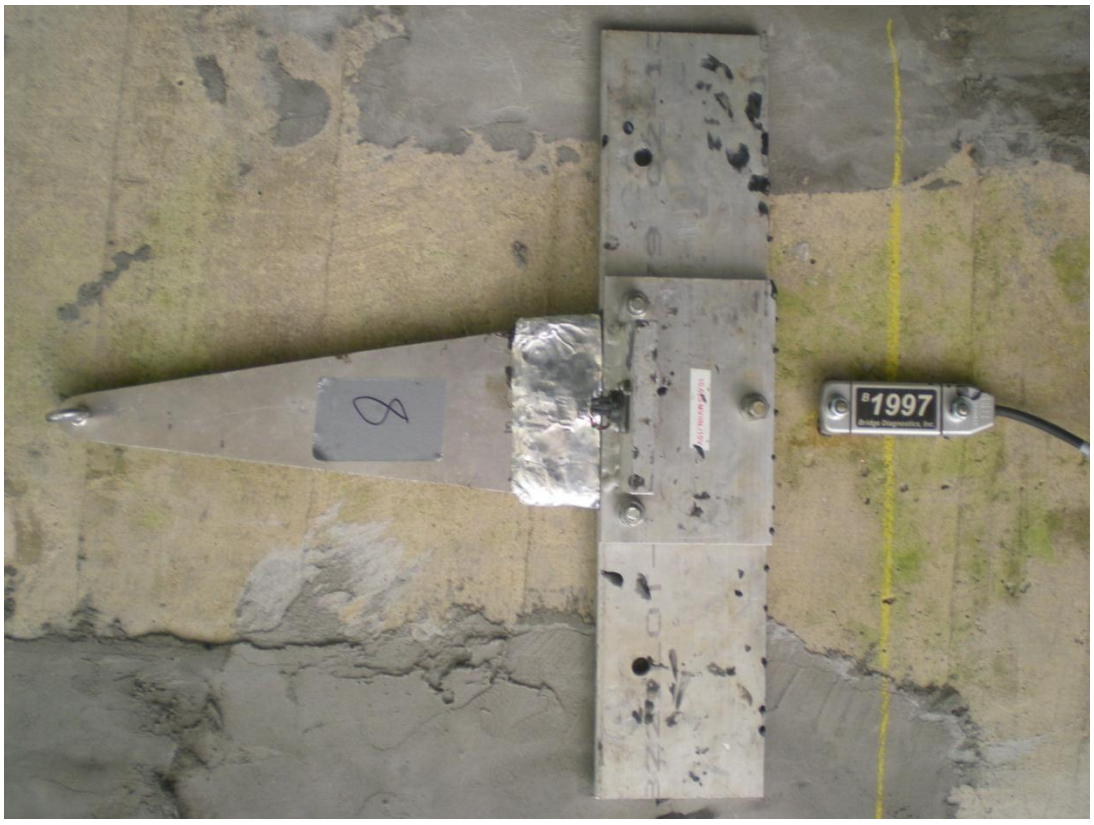

Figure 3-5. Deflectometer and Strain Transducer Test Setup

A total of thirteen strain transducers were placed on each bridge during the tests. They were placed at the midspan and both quarter points of each arch. At seven of these positions a single transducer was attached as shown in the setup in Figure 3-5. However, in two locations, three strain transducers were placed such that one strain transducer was fixed to the top, bottom, and side of the arch. These selected locations were at the north quarter point on the center and downstream arches on both bridges. Measuring the strain at different depths in the arch was crucial in developing strain distribution plots which help in determining if the arch is exhibiting linear-elastic behavior. This triple configuration can be seen in Figure 3-6.

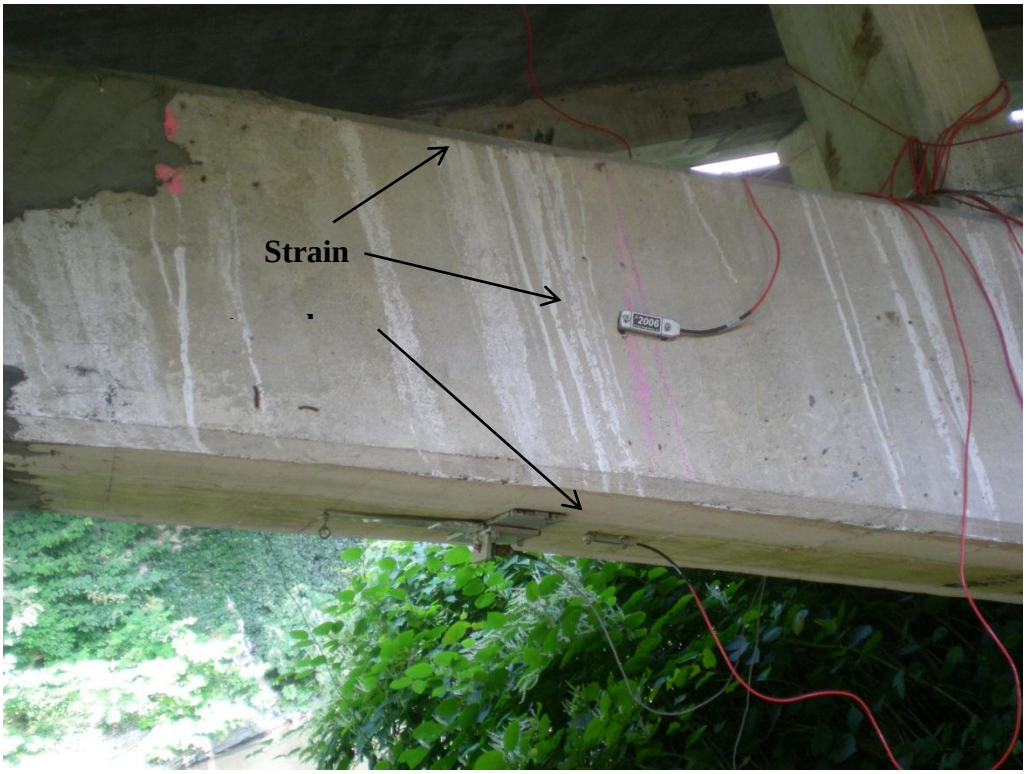

Figure 3-6. Strain Transducers through Arch Depth

3.2.3 Instrument Layout

The instrument layout for the live load tests was developed to capture critical bridge behavior at certain locations along the arch span. These locations, at the midspan and quarter points of each arch, were determined to be where maximum strain and deflection would occur during loading. The layout was similar for the Main Street and Depot Street bridges.

When developing the instrument plan for the Main Street Bridge, arch skew was taken into account. The midspans of each outside arch were found using a plumb-bob and then a string was stretched taut to mark the midspan across all three arches. When determining the quarter point location of the arches, it was determined that the best place for the instruments was halfway between the web wall and the first column. This was chosen as the suitable location

because it was as close to the critical location at the quarter point as possible without being directly under a column or web wall. The instrument layout for the Main Street Bridge is not symmetric due to the arch skew as well as the shorter upstream arch. The plan is shown in Figure 3-7. Each location is marked with a number and designation indicating the instruments there. Locations 1 and 2 contained three strain transducers to measure the strain through the arch depth while most other places contained only one strain transducer. The only exception is locations 3 and 9, where only deflectometers were used. At location 2, additional strain transducers were placed on the bottom of bridge beam and on the bottom of the arch beneath the center supporting column. There was also a strain transducer attached to the bridge beam at location 1. These additional instruments are not represented in Figure 3-7. A total of 23 instruments were used on the Main Street Bridge, including fourteen strain transducers and nine deflectometers.

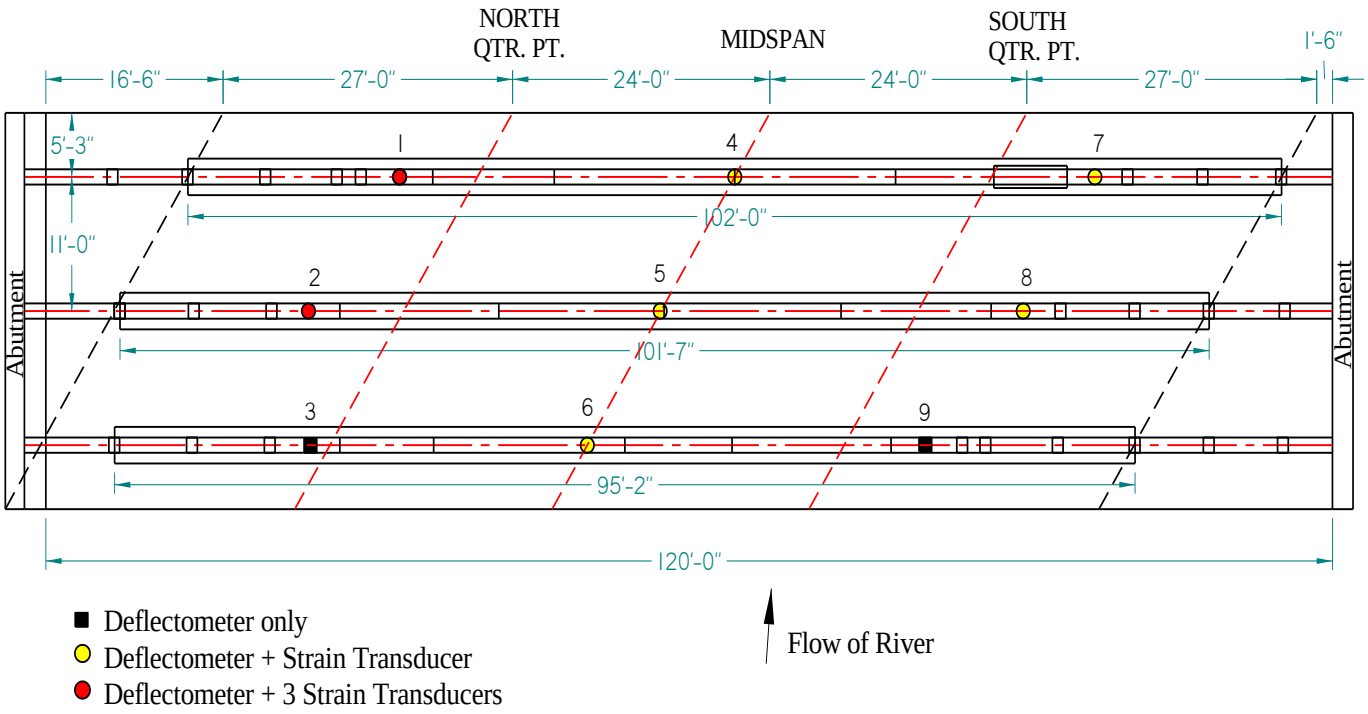

Figure 3-7. Main Street Bridge Instrumentation

Due to the successful instrument plan used on the Main Street Bridge, the instrumentation of the Depot Street Bridge was done in the same manner. However, since this bridge has a symmetrical plan the setup was simpler in terms of geometry. The instrument setup is seen in Figure 3-8. Locations 3 and 6 were chosen for measuring the strain through the arch depth using three transducers. Further, a deflectometer could not be attached at location 1 due to the roughness of the concrete. This was not a concern because this location was not considered to provide relevant information due to the connection between bridges at this end. Although strain transducers were attached to the bottom of the bridge beam in the Main Street Bridge setup, they were deemed unnecessary for the Depot Street Bridge. Therefore, a total of 21 instruments were attached to the bridge, with thirteen strain transducers and eight deflectometers.

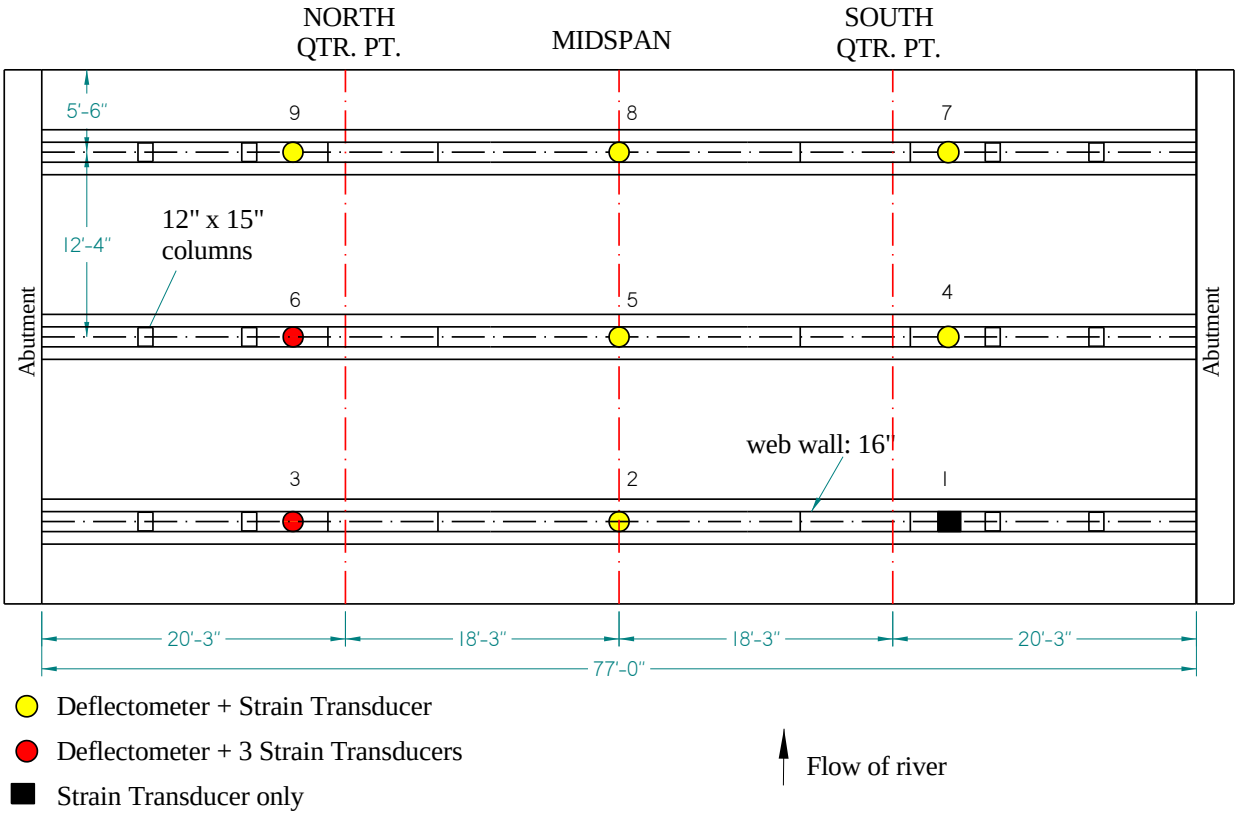

Figure 3-8. Depot Street Bridge Instrumentation

3.3 Data Acquisition

Different data acquisition systems were used for each live load test. A wired system was used on the Main Street Bridge while a wireless system was used on the Depot Street Bridge.

3.3.1 CR9000X

For the Main Street Bridge, the CR9000X Datalogger from Campbell Scientific, Inc. was chosen for its reliability and proven record in many past tests. The program CR Basic Editor and RTDAQ software were used to run the test. A picture of the CR9000X is shown in Figure 3-9.

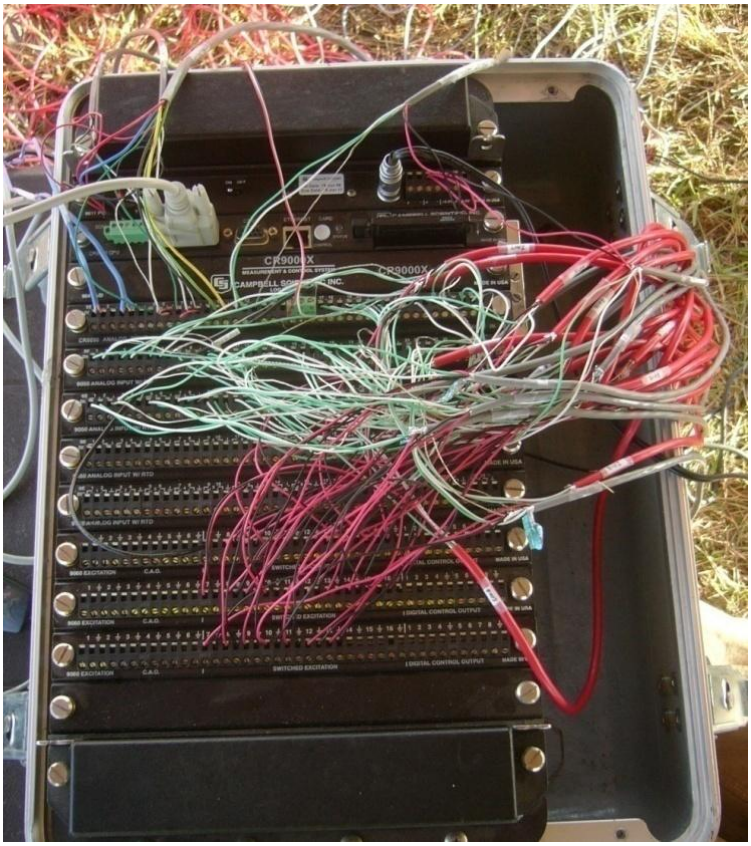

Figure 3-9. CR9000X Datalogger

Each instrument was connected to the CR9000X from its position on the bridge, requiring hundreds of feet of wiring. The planning and setup for this system involves calculations for

instrument wire lengths and a tedious process of wiring the CR9000X. It also takes longer to setup instruments prior to starting the live load test. For the Main Street Bridge data was recorded at 4 Hz for each instrument, allowing for a manageable amount of data. A picture of the wires connected to the bridge is shown in Figure 3-10.

Figure 3-10. Bridge Instrument Wiring

3.3.2 STS Wireless System

A new wireless data acquisition system was used for the Depot Street Bridge test. This was the first time the system had been used by Virginia Tech in any field testing. The STS-WiFi Structural Testing System is manufactured by Bridge Diagnostics, Inc. and operates on 802.11g broadband. The system relays signals wirelessly from several nodes to a hotspot and then to a

laptop where the data is recorded in the STS software. Each node can operate up to four different instruments during the same test and requires a specific Intelliducer connection for each deflectometer and strain transducer. The initial setup requires careful planning because each node must be placed in a direct line of sight to the hotspot. The wireless signals cannot travel through solid objects such as concrete and steel. A total of six nodes were required for the 21 instruments on the Depot Street Bridge. A picture of a single node on the bridge is shown in Figure 3-11.

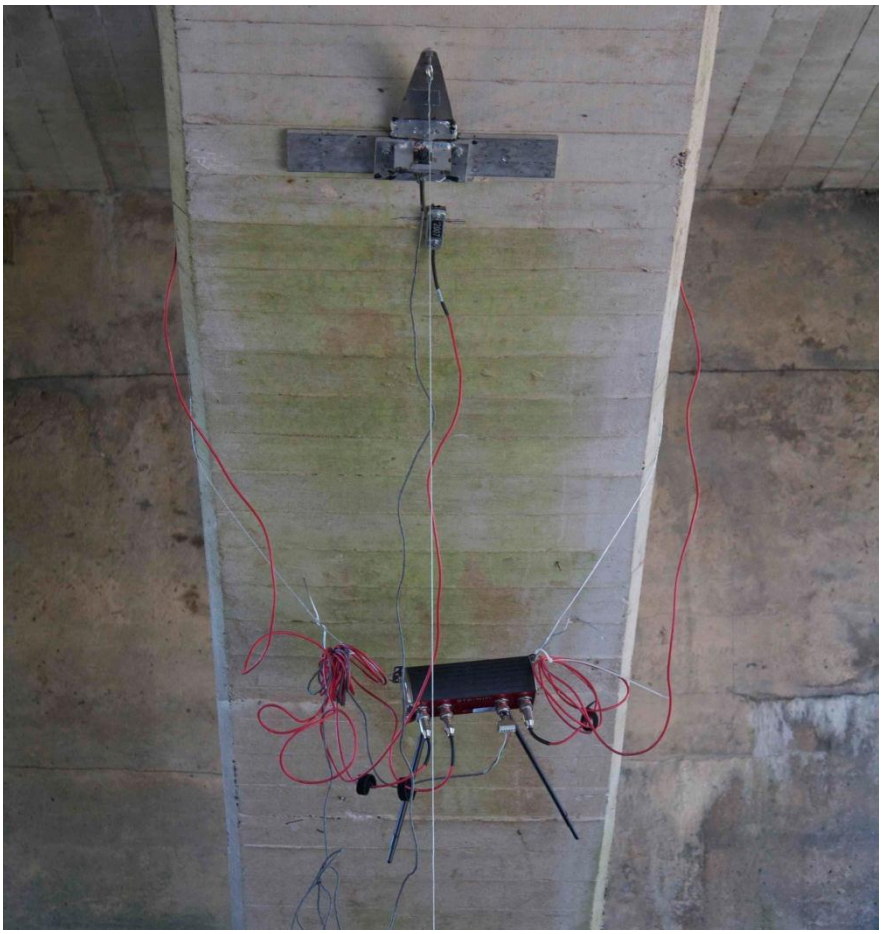

Figure 3-11. STS Wireless Node

The STS software, WinSTS, provides a simple user-friendly interface which shows real time results during the test. Unlike the CR9000X it does not require meticulously written programming for each live load test. Also this system provides a much quicker setup and teardown time during the live load test. A picture of the STS hotspot is shown in Figure 3-12.

Figure 3-12. STS Wireless Hotspot

3.3.3 Instrument Calibration

Prior to each test, instruments were calibrated, and their calibration values input into the appropriate software program. The ST-350 strain transducers were calibrated by the manufacturer, BDI, and the deflectometers required manual calibration in the research laboratory. The deflectometers were fixed to a table with C-clamps and deflected approximately one inch using a wire connected to a caliper. The recorded values were then input into Microsoft Excel and a two point calibration was performed. Due to the angle of the arch, several of the deflectometers were calibrated on a slope to provide accurate calibration values.

3.4 Test Loading Procedure

The same live load testing procedure was used on the Main Street and Depot Street bridges. Due to the nature of the loading procedure and the bridge approaches, the tests resembled quasi-static load tests more than true live load tests. For loading, three dump trucks were arranged in different orientations with the objective of mimicking the loading of a six-axle coal hauling truck.

3.4.1 Truck Description

The Virginia Department of Transportation (VDOT) provided three dump trucks to use during testing. The three-axle dump trucks, as seen in Figure 3-13, were filled to varying weights with aggregate, with each test having varying combinations of these trucks. The truck weights used on the Main Street Bridge were 28.5, 53.8, and 59.1 kips while those used on the Depot Street Bridge were 32.1, 52.8, and 54.5 kips.

Figure 3-13. Three-Axle Dump Truck

The measured axle dimensions, as shown in Figure 3-14, were identical for each truck. Prior to arriving at the test site, the trucks were weighed by VDOT and the tire load distribution recorded. A typical dump truck with axle designations is shown in Figure 3-15 with the axle load distributions for each test reported in Table 3-1 and Table 3-2.

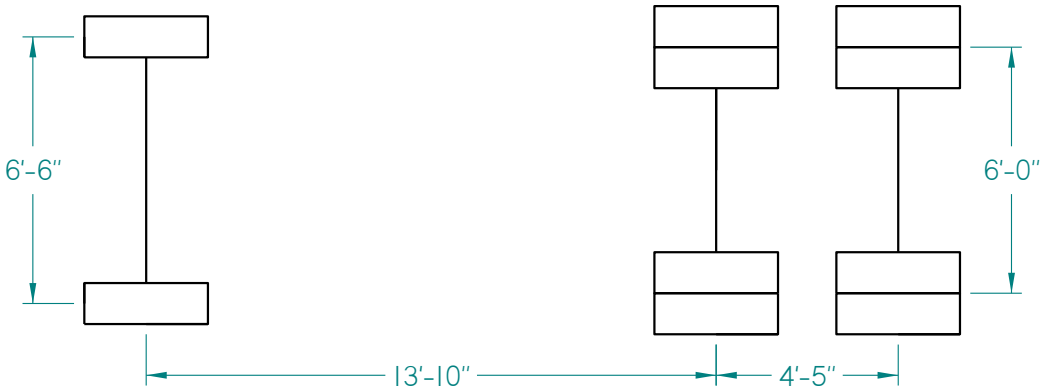

Figure 3-14. Dump Truck Axle Dimensions

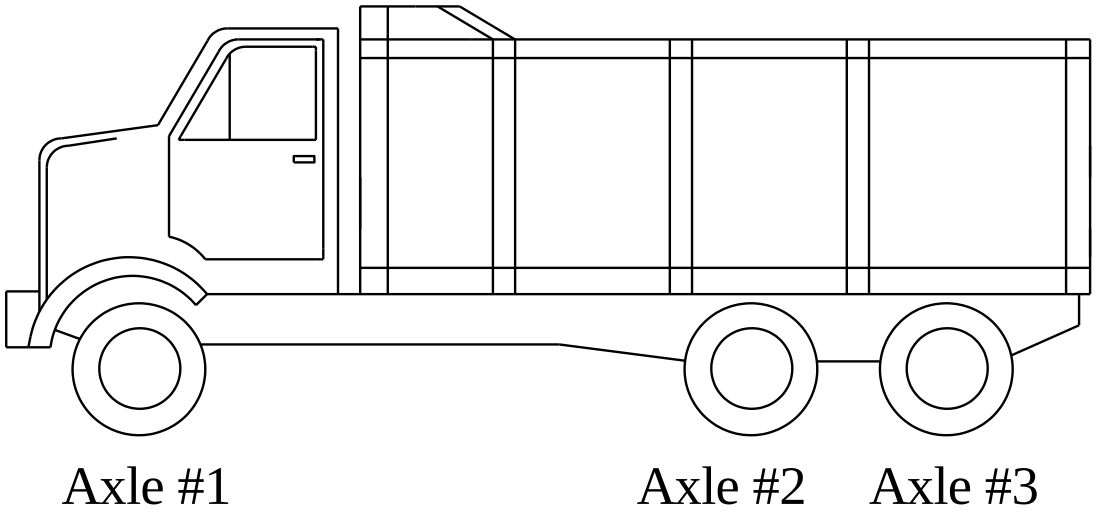

Figure 3-15. Dump Truck Axle Designations

Table 3-1. Main Street Truck Axle Load Distributions

Truck	Axle #1 (kips)	Axle #2 (kips)	Axle #3 (kips)	Total (kips)
1	12.1	8.4	8	28.5
2	12.5	20.3	21	53.8
3	18	20.5	20.6	59.1

Table 3-2. Depot Street Truck Axle Load Distributions

Truck	Axle #1 (kips)	Axle #2 (kips)	Axle #3 (kips)	Total (kips)
1	12.3	9.9	9.9	32.1
2	15.7	18.6	18.5	52.8
3	15.8	19.5	19.2	54.5

3.4.2 Truck Combinations and Orientations

Each bridge was loaded using five different truck combinations in each traffic lane, creating ten separate loading scenarios for each live load test. During each pass, the truck(s) were stopped at both quarter points and the midspan of the bridge for approximately five to ten seconds. This length of time allowed the instruments to capture a steady response from the bridge at each location, eliminating the dynamic effects of moving trucks.

Due to the restrictions of using dump trucks, it was difficult to simulate the loading caused by coal trucks. However, all three trucks were placed on the bridge in a way that maximized the amount of load over the points of interest as shown in Figure 3-16. By using this approach, the bridge's effective strength capacity was evaluated using loads comparable to that seen in daily coal traffic.

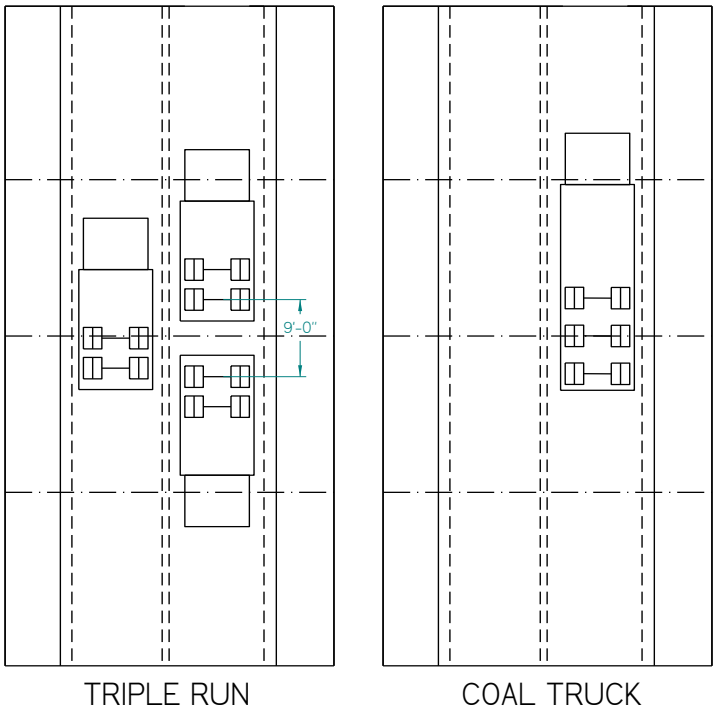

Figure 3-16. Coal Truck Comparison to Test Configuration

Two separate runs with single trucks were done on each lane using the lighter truck and a heavier truck in each test. Next, two separate runs were performed on each lane using two trucks back-to-back. The combinations for both tests included the light truck with a heavier truck and then the use of both heavy trucks. Finally, a combination of all three dump trucks was used with the objective of simulating the loading of the three rear axles of a 150 kip coal truck. The rear triple axle was chosen as the basis for testing because it is the largest concentrated force the bridge will experience. The majority of the load in coal trucks is carried by the rear axles and represents the most extreme loading could cause damage to the bridge. The truck configurations for the Main Street Bridge test are shown in Figure 3-17 with Table 3-3 and providing truck combination and total weight information for each scenario. In Table 3-3 total test weight represents the weight of all truck axles on the bridge during each load case while the

concentrated weight represents only the axles that are located directly over the instrument location. The ratio of the concentrated axles to the triple rear axle of actual coal trucks is given to show how accurately the test load combinations simulated the triple rear axle.

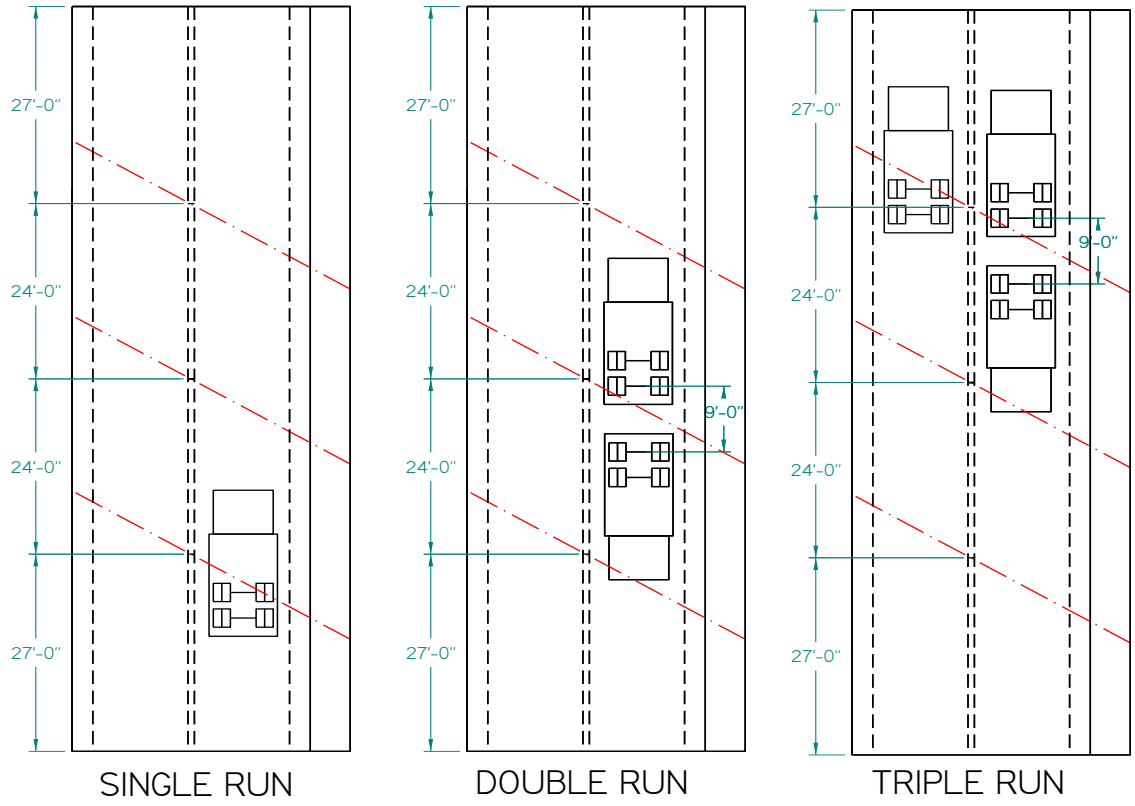

Figure 3-17. Main Street Truck Loading Configurations

Table 3-3. Main Street Truck Load Cases (in kips)

Case	Truck Combination	Total Test Weight	Concentrated Axle Weight	Actual Coal Triple Axle	Ratio of Test to Actual
1	#1	28.5	16.4	72	0.23
2	#2	53.8	41.3	72	0.57
3	#1 (front), #2 (back)	82.3	57.7	72	0.80
4	#2 (front), #3 (back)	112.9	82.4	72	1.14
5	#2 (front), #3 (back), #1 (beside in other lane)	141.4	98.8	72	1.37

Each load case shown in Table 3-3 was performed on the upstream and downstream lanes. As seen in Figure 3-17, the skew of the bridge was taken into account when marking the quarter points and midspan. Similar information for the Depot Street Bridge test is shown in Figure 3-18 and Table 3-4.

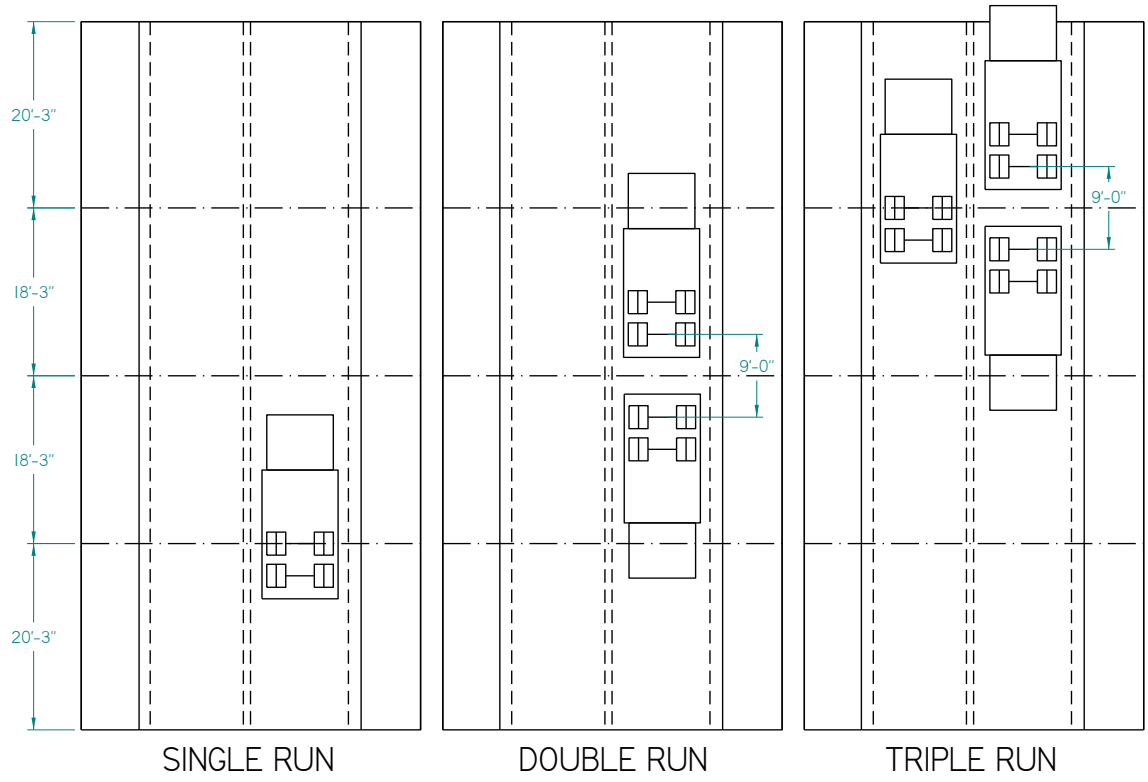

Figure 3-18. Depot Street Truck Loading Configurations

Table 3-4. Depot Street Truck Load Cases (in kips)

Case	Truck Combination	Total Test Weight	Concentrated Axle Weight	Actual Coal Triple Axle	Ratio of Test to Actual
1	#1	32.1	19.8	72	0.28
2	#3	54.5	38.7	72	0.54
3	#1 (front), #3 (back)	86.6	58.5	72	0.81
4	#3 (front), #2 (back)	107.3	75.8	72	1.05
5	#3 (front), #2 (back), #1 (beside in other lane)	139.4	95.6	72	1.33

Lines marking the quarter points, midspan and exact stopping points for truck tires were painted on the bridge deck as shown in Figure 3-19. During the test, the trucks were moved into position using these lines as guidance. As shown in the above figures, Axle #2 was positioned over the point of interest when a single truck was on the bridge. When the double truck configuration was used, the rear axles were positioned nine feet apart, straddling the quarter point or midspan. In the triple truck configuration, the third truck was placed alongside the back-to-back scenario with Axle #2 over the marked position.

Figure 3-19. Truck Reference Lines on Bridge Deck

In each loading scenario, the trucks were positioned centrally in each lane. Due to the variations in lane width for each bridge, diagrams in Figure 3-20 and Figure 3-21 show the spacing of trucks within each lane. Due to the different layouts of the sidewalks and lanes, each bridge distributed the loading differently between the arches. As can be seen in Figure 3-20, the positioning of the trucks on the Depot Street Bridge is symmetric in relation to the arches because of sidewalks on both sides of the bridge. However, in Figure 3-21, without the sidewalk

on the downstream side of the bridge, the Main Street Bridge lanes are not symmetrically located about the bridge center line. Because of this, the downstream lane is located directly over the downstream arch and the upstream lane is shifted closer to the center arch. This is taken into account when looking at the measurements recorded during the tests.

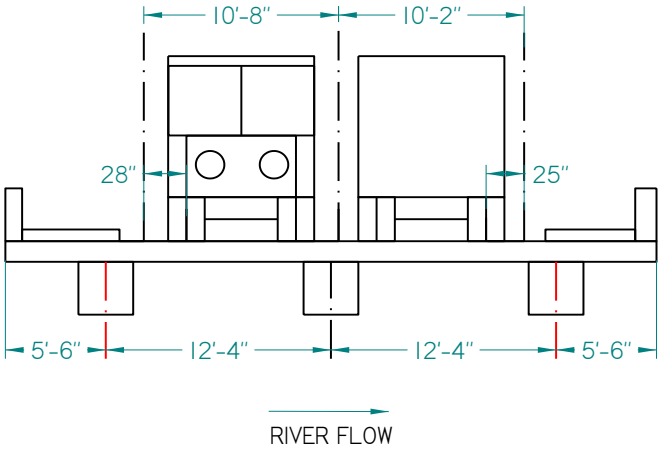

Figure 3-20. Depot Street Bridge Truck Positioning

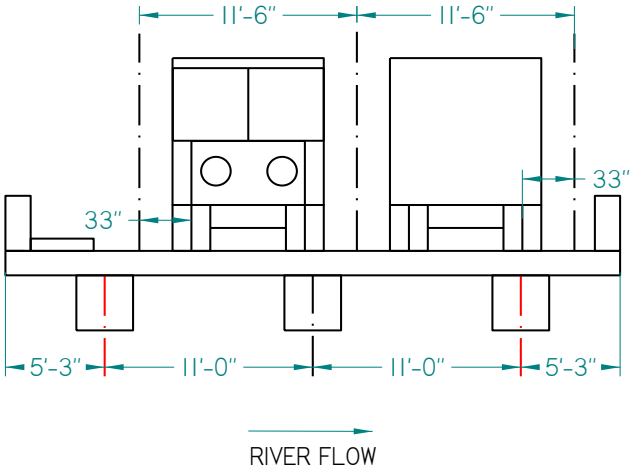

Figure 3-21. Main Street Bridge Truck Positioning

Each scenario was tested in one lane of the bridge and then turned around to record data in the opposite lane of the same bridge. For each crossing, the truck(s) began at one end of the bridge and stopped at each quarter point along the span to obtain static loading measurements. This allowed for efficiency in the test and organization in the data collection. Due to restrictions with traffic control and proximity to intersections, dynamic tests with trucks travelling at speed were not possible. The back-to-back truck configuration is shown in Figure 3-22.

Figure 3-22. Trucks during Live Load Test

3.5 Data Organization and Reporting

The live load tests were done using different data acquisition systems. Because of this the data was collected in different software programs, RTDAQ for the CR9000X and WinSTS for the STS-WiFi system. For the Main Street Bridge test, the data was downloaded after each test as a text data file and saved on a laptop. The Depot Street Bridge also recorded in the text data file format but provided a more user-friendly interface within the WinSTS software. Since both tests recorded all instruments at a sampling rate of 4 Hz, the text data files were small enough to be

managed in Microsoft Excel. The text data file was imported into Excel and manipulated for easier analysis of the results. First, the recorded time taken during the test was reset from zero and data points incremented at every quarter-second. Following this, the recorded data was zeroed. To achieve this, the initial recorded value on each instrument was subtracted from every subsequent reading, providing a difference representative of the recorded value during the test. Plots were developed, as shown in Figure 3-23, using the data for the strain transducers and deflectometers to show the response of the instruments for each loading scenario.

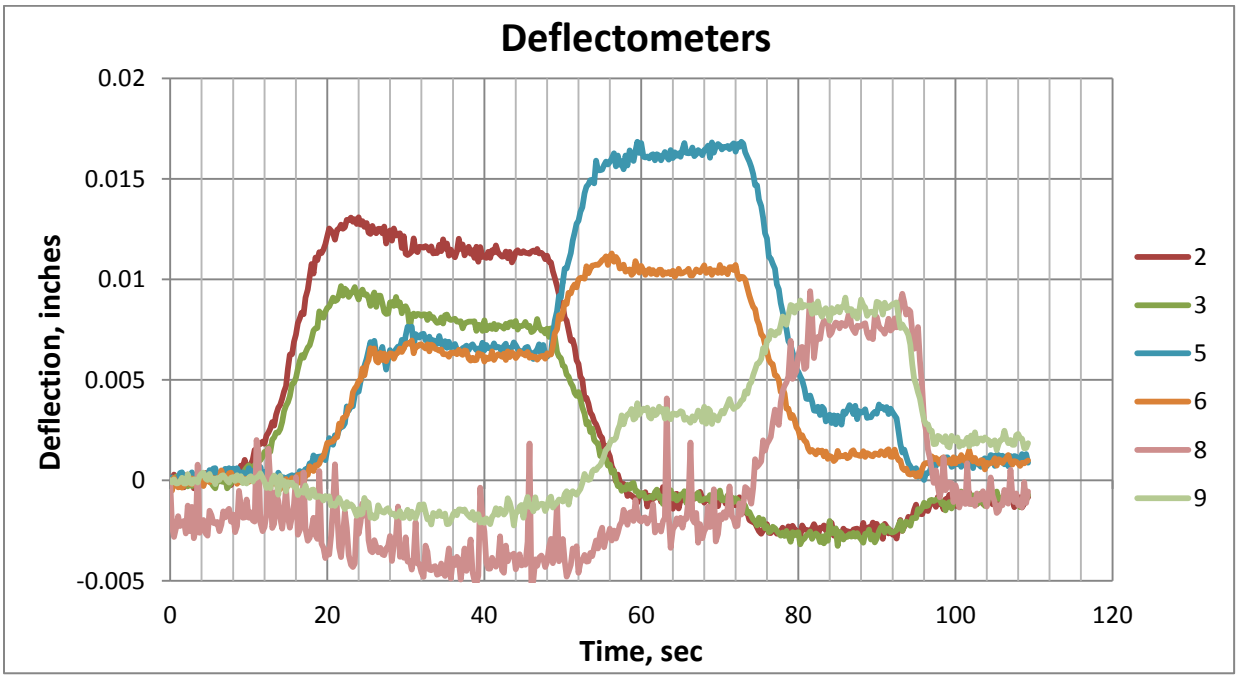

Figure 3-23. Example of Data Organization

The data is presented in subsequent chapters based on the accuracy of the instruments and the resolution of their measurements. Strains from the BDI instruments are reported to the nearest tenth of a microstrain. Deflections are reported throughout to the nearest thousandth of an inch.

Chapter 4 - Finite Element Modeling

In addition to performing live load tests, finite element models were developed of both the Main Street and Depot Street bridges. These models were used to analyze the structures with various truck loads used in the live load test and seen in daily traffic.

4.1 Modeling Objectives

The main objective of the finite element models in this study was to see how the actual live load test responses would compare to the predicted responses from the model analyzed with test loads and a coal truck rear tri-axle load. With the dump trucks available during the live load tests, certain loads were not able to be simulated. Since the bridges see large amounts of coal truck traffic it was important to see the bridge responses under this loading. To simulate this in the live load tests, a triple truck configuration was used with two trucks back-to-back in one lane and another beside in the other lane. Even though this combination approached the total weights of coal trucks their positioning did not exactly replicate the axles of the coal trucks. To do this, six, 12 kip tire point loads representing the legal 72 kip rear tri-axle of the coal truck were placed at each quarter point in both lanes in the exact way of the live load test runs. After applying the loads, peak strains and deflections were recorded at the same locations as in the live load tests.

The models were also used to investigate the interaction between different structural components in the bridge. Each bridge consisted of three arches with columns along their span connecting to bridge beams which supported the deck. Each arch had fixed end supports that looked to be in good condition with no cracking or visible deterioration. Because of this, the end supports were only modeled as fixed with no settlement taken into account. Since only nine locations were instrumented during the tests the amount of information regarding the bridge's

behavior was limited. The objective was to study the interaction between these components, gaining a better understanding of the load path and distribution within the structure.

4.2 Modeling Assumptions

The bridges were modeled in SAP2000 v14, a structural analysis program developed by Computer and Structures, Inc. The complexity and uncertainty involved with the bridges presented many challenges when approaching the modeling process. Because of these uncertainties, several assumptions were made while modeling. In each bridge, all three arches were modeled along with the spandrel columns, beams, and deck.

The locations of end connections for each bridge varied for the arches and bridge beams. The arches and beams in the Depot Street Bridge spanned to the concrete wall abutment, creating a symmetric profile. However, due to the skew of the Main Street Bridge the arches end in the bank of the creek while the beams meet the concrete wall abutment. The end connections were assumed to be fixed, preventing rotation and translation at the end of the arches and bridge beams.

When gathering material properties during the Main Street Bridge test, only two sample cores were allowed to be removed from the bridge at the south side of the downstream and center arches. The strengths of these samples were determined to be 6.09 ksi for the downstream arch and 7.03 ksi for the center arch. However, this does provide at best an approximate representation of the material properties throughout the Main Street Bridge and does not provide any direct information for the Depot Street Bridge. To accommodate this in the model a moderate compressive strength of 4 ksi and modulus of elasticity of 4000 ksi were assumed for all concrete in both bridges. This assumption for the compressive strength in the models was

considerably less than the actual compressive strengths measured from the sample cores. This was done intentionally in an attempt to simulate the compressive strength lost due to damage and deterioration. Reducing the strength was an effective method used for achieving softening behavior within the models.

Both bridges have significant cracking and patching along the arches and bridge beams. Due to the large variance and random nature of the cracks and patches they were not modeled discretely in the bridges. To account for the damage to the concrete arches and beams, the gross moment of inertia for each component was reduced as per ACI 318-08 Section 10.10.4.1. The compression members including only columns were reduced to $0.7I_g$. The entire deck was reduced to $0.25I_g$ due to its classification as a flat slab and the flexural beams and web walls were reduced to $0.35I_g$. When considering the arch stiffness reduction, it was determined that it should also be reduced to $0.35I_g$ even though it acts in compression. This was chosen due to the extensive damage seen in the arches and the need to calibrate the models to the test results. This reduction in stiffness allowed the model to deflect and behave as if it had been softened by the damage seen in the real bridges.

4.3 Modeling Procedure

Prior to modeling the bridges detailed measurements of the dimensions and geometry of each bridge were taken. These measurements were then used to develop the most accurate models possible. Due to varying measurements in some instances, assumptions had to be made to construct consistent, functioning models. Each model consisted of various frame and shell elements. The arches, columns, and bridge beams were modeled using frame elements while the

web walls and deck were modeled with shell elements. The bridge superstructure was modeled first followed by the addition of the deck.

The nonprismatic concrete arches were the first component modeled in the process. Due to the absence of detailed as-built drawings of the bridges, an exact formulation of the arch shape was not possible. To simplify the arch shape, arch depths were measured at nine locations along the span including each column location as well as the beginning and end of the web walls and again at the crown. With these measurements, the parabolic arch was developed consisting of ten individual beam elements with varying arch depths. Each nonprismatic beam element was connected to the adjacent elements by the common joints, allowing the entire arch to act was one frame element. The arches had a constant 3 ft width with the arch being deeper at the supports and shallower at the crown. The columns were added to the arches at the appropriate locations with each being 12 in. by 15 in. The columns were subdivided into two elements to refine the model.

The web wall was then modeled using the generally recommended thin shell element with a thickness of 16 in. The thin shell element was used because the thickness and depth of the web walls were such that shear deformations were not of concern and could be neglected. Several different web wall variations were modeled to try and calibrate the model to act more closely to the actual bridges. These variations included eliminating the web wall which created unsatisfactorily large deflections at midspan. Other attempts ranged from using a couple of columns to as many as twenty slender columns over the length of the wall. These variations proved not to be as realistic as the thin shell element which provided more accurate results. The web walls were divided into a mesh that provided elements with satisfactory aspect ratios. Following this, the bridge beam was added above the columns and web wall and divided into

smaller elements along its length. The superstructures of the Depot Street Bridge can be seen in Figures 4-1 and 4-2.

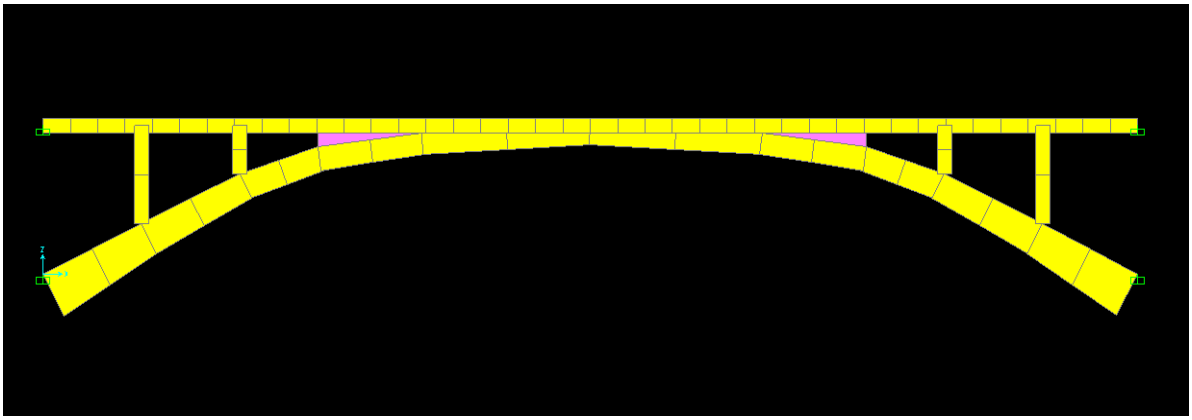

Figure 4-1. Two-Dimensional View of Typical Depot Street Arch

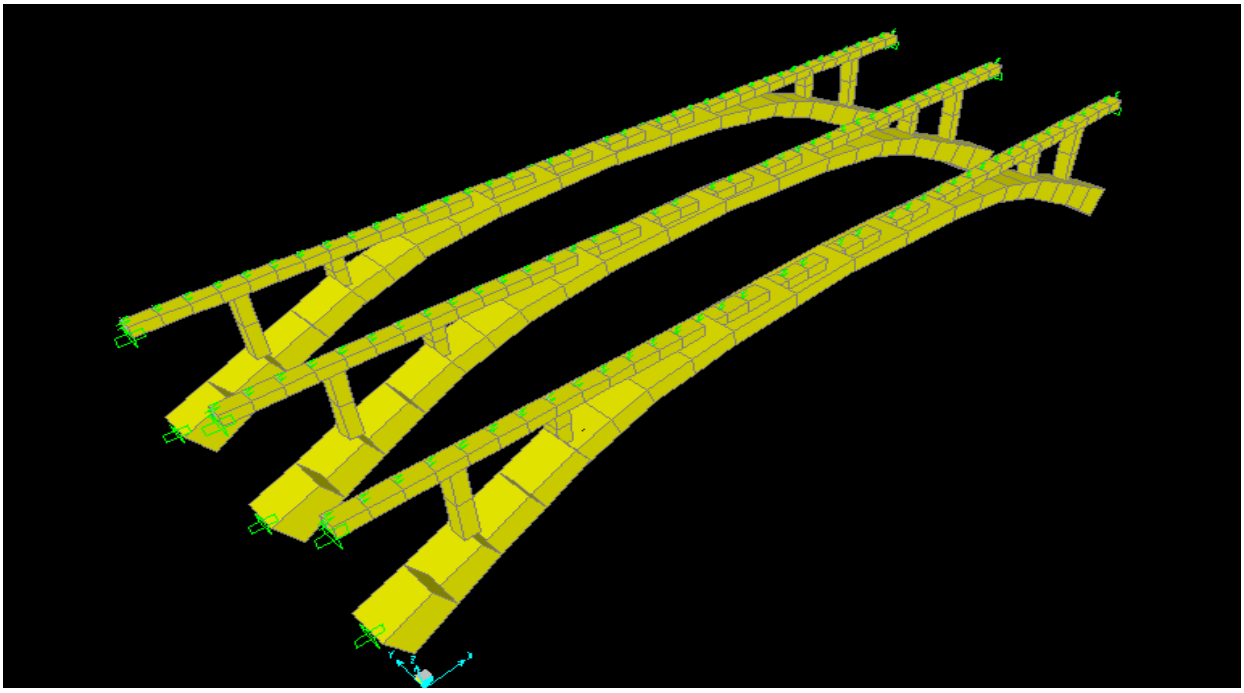

Figure 4-2. Three-Dimensional View of Depot Street Bridge Superstructure

Following the superstructure, the deck was modeled using thin shell elements and was divided into elements with near equal aspect ratios. When subdividing the deck it was important

to develop a mesh where element edges were located along the lane and truck axle widths. This was necessary so that the tire point loads could be applied to the nodes at these joints. The biggest challenge when modeling was trying to get the deck and superstructure to act as a single structure. To create this composite action the deck needed to be meshed or attached to the three bridge beams. This was achieved through the use of rigid link elements which act as springs that have an infinite stiffness. The joints of the bridge beam were connected with these rigid links to the deck joints located directly above providing joint connectivity. When loads were applied to the deck, the deflections experienced at the deck joints connected to rigid links were also experienced at its connected joint along the bridge beam. The skew in the Main Street Bridge arches as viewed from the upstream side can be seen in Figures 4-3, 4-4, 4-5, and 4-6.

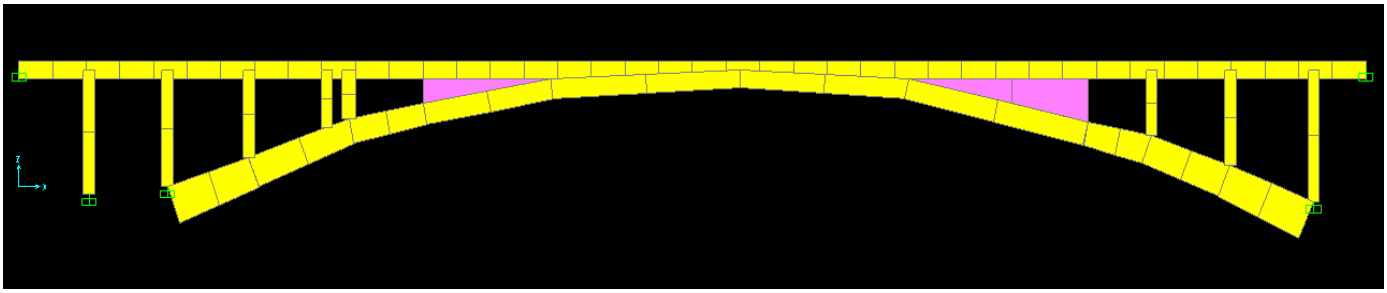

Figure 4-3. Two-Dimensional View of Main Street Bridge Downstream Arch

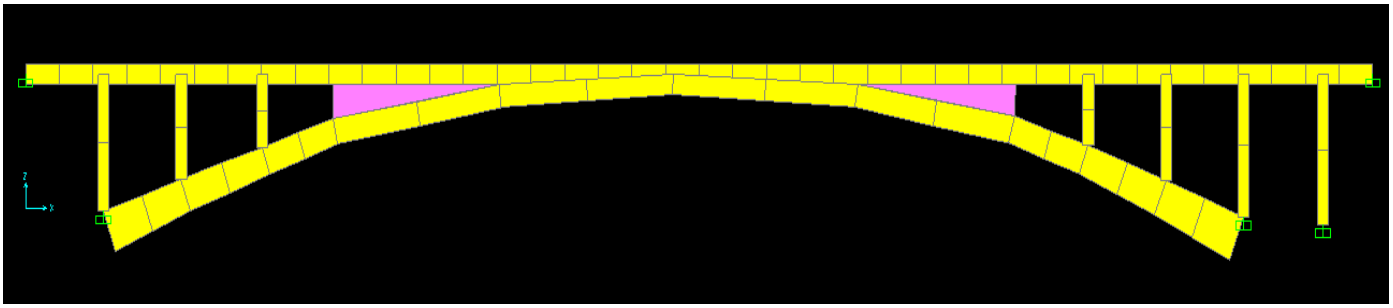

Figure 4-4. Two-Dimensional View of Main Street Bridge Center Arch

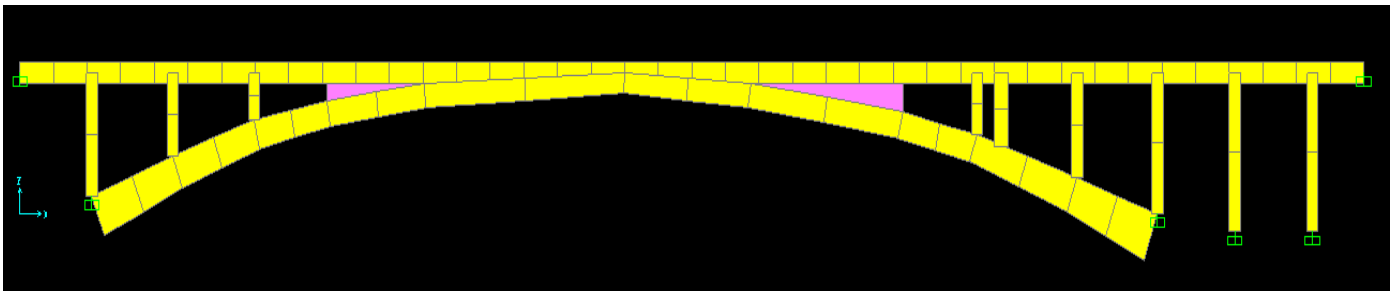

Figure 4-5. Two-Dimensional View of Main Street Bridge Upstream Arch

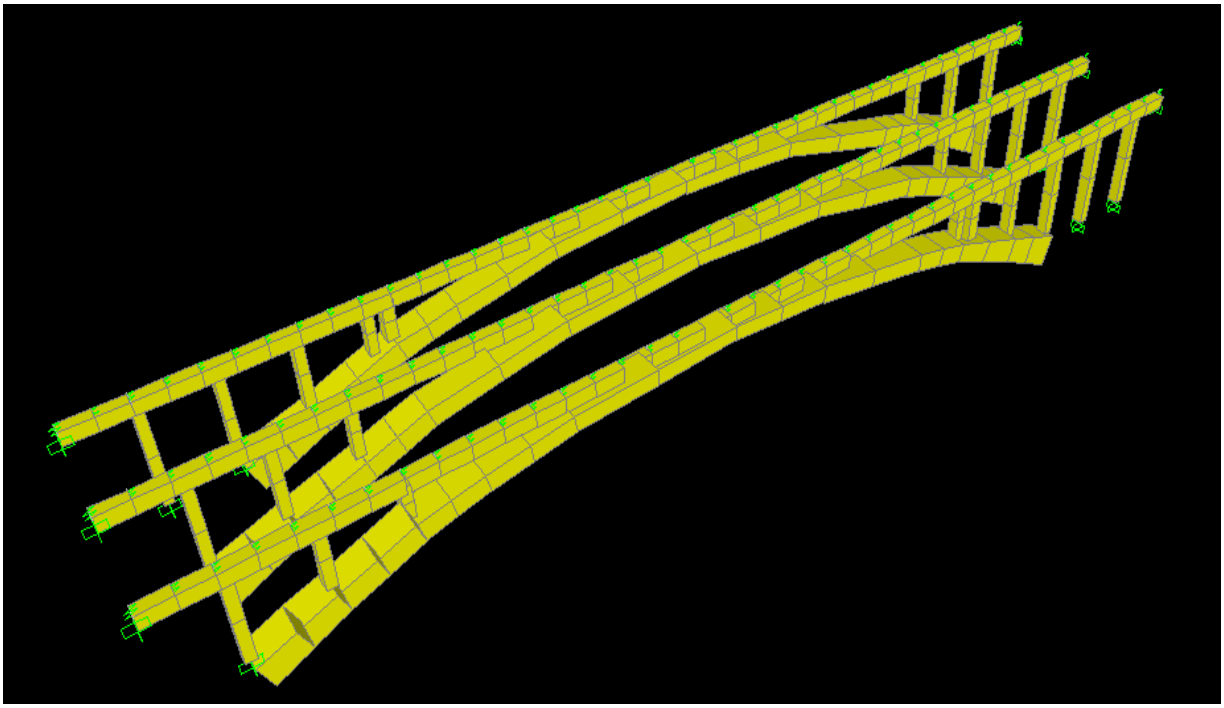

Figure 4-6. Three-Dimensional View of Main Street Bridge Superstructure

When analyzing the bridge, tire point loads were placed at the exact locations as during the live load testing in the field. It was determined that testing all the truck configurations used during testing would provide a large amount of inconsequential data. Instead, the most critical load case using all three dump trucks was chosen to be analyzed in the models. These tire point loads were placed at the north and south quarter points and midspan in both lanes and the

deflections and strains were recorded. The stresses at each location were determined for the top and bottom of the arch using the equation that combined axial and bending stresses, given by:

$$\sigma = P/A \pm M/Z$$

where P = member axial force; A = member cross-sectional area; M = moment about the local 3-axis; and Z = member section modulus. The sign convention used in SAP2000 for element local axes and internal forces is shown in Figure 4-7.

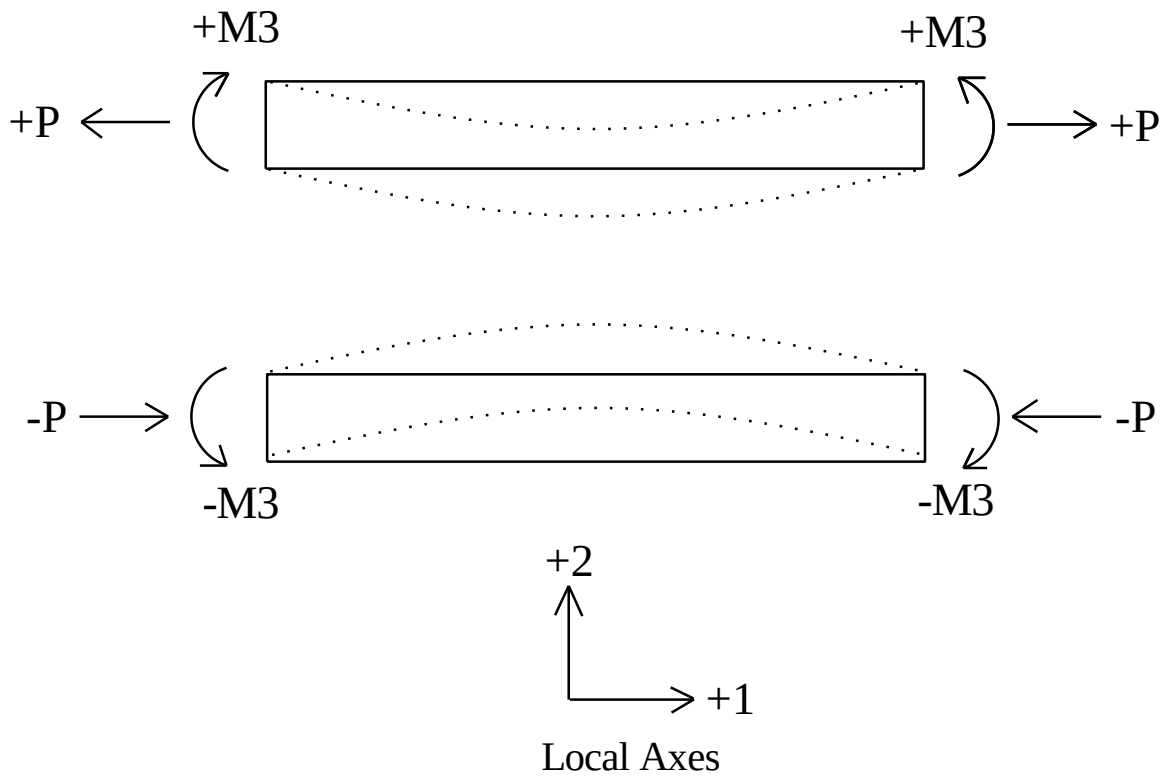

Figure 4-7. SAP2000 Element Sign Convention

This sign convention was used to establish which sign to use for the bending stress when calculating top and bottom stresses at each location. It was determined that the arch bottom

stresses were found by adding the bending stresses and the arch top stresses by subtracting the bending stresses. The strains were then calculated by Hooke's Law, shown by:

$$\varepsilon = \sigma / E$$

where E = modulus of elasticity; and σ = total stress. The results of the analysis are summarized in Section 5.3. The cross-section of the completed Depot Street Bridge can be seen in Figure 4-7.

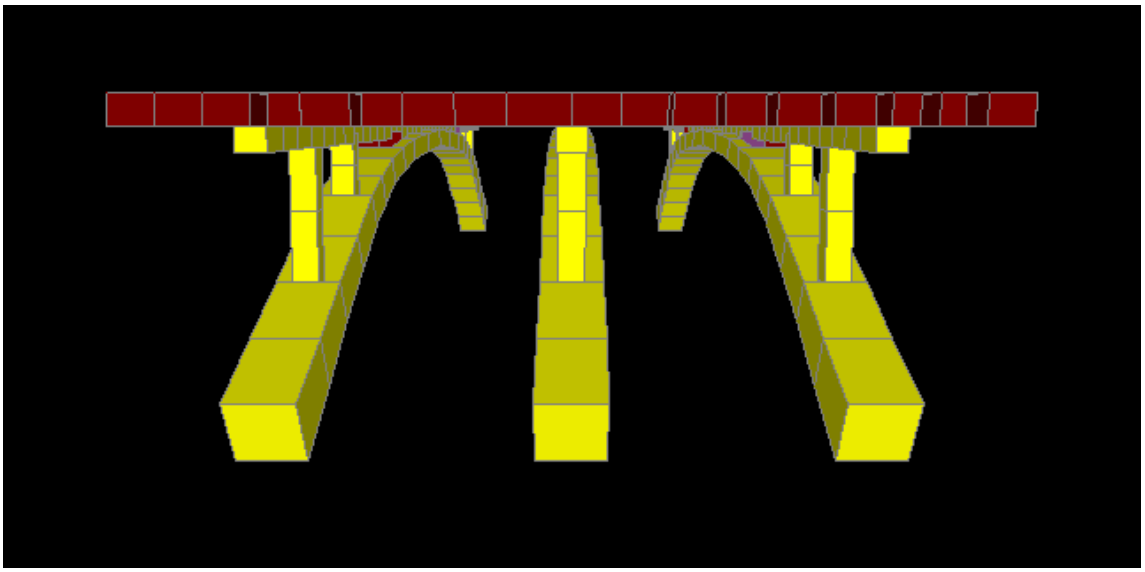

Figure 4-8. Depot Street Bridge Viewed from North

Chapter 5 - Test Results

The majority of this chapter summarizes the results from the live load tests. In section 5.3, results from the finite element modeling are discussed and compared to the test results. To provide clarity throughout, the results are separated according to the Main Street and Depot Street bridge tests.

Data values were recorded from the time the trucks entered the bridge until the time they exited. Only the data recorded while the trucks were stopped at the quarter points and midspan are relevant to the study. The three times when the trucks were stationary during each run were found by analyzing the graphs of each run and finding where the resulting data plateaus. One such graph is shown in Figure 5-1. Unless otherwise stated, the values presented in this chapter are averages of the data in the time ranges when the trucks were stopped.

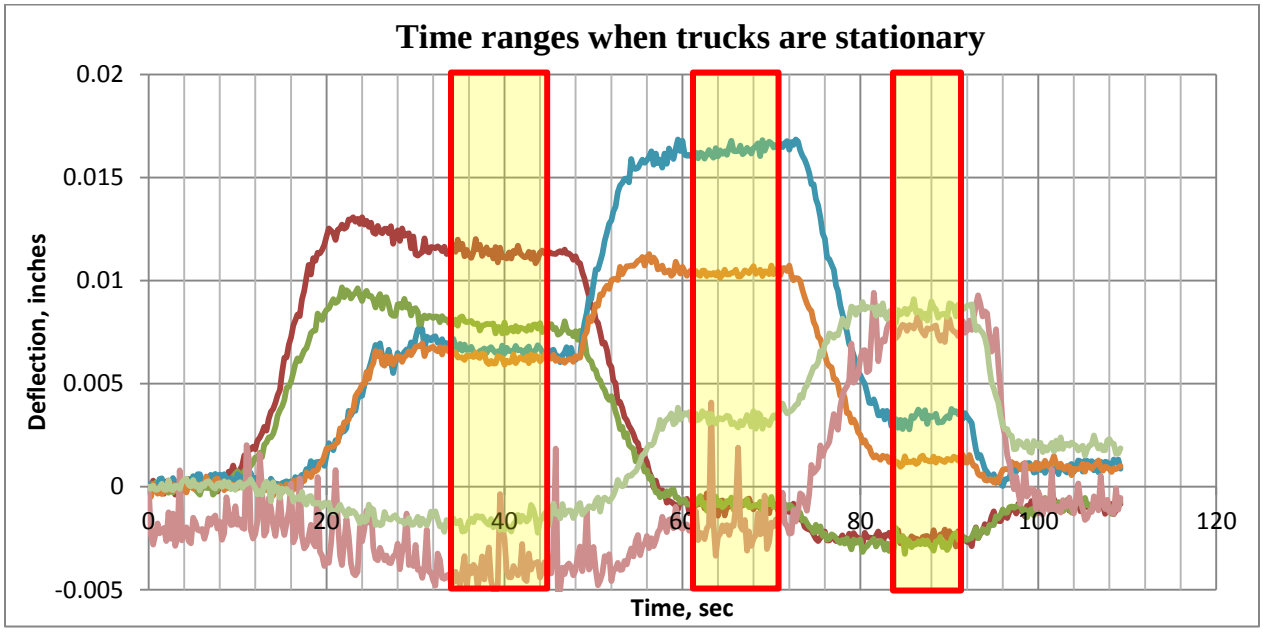

Figure 5-1. Example of Finding Relevant Data

Within each test, the recorded deflections are presented in units of inches to the nearest thousandth of an inch. Positive values represent downward displacement and negative values signify uplift of the arch. The strains are reported in units of microstrain to the nearest tenth of a microstrain. The compressive strains are reported as negative values while the tensile strains are positive. Strains reported throughout the thesis are based solely on applied live loads. Therefore the strains in this study are relative to the dead load stresses already present in the arch. Because of this, a tensile strain reported in this study does not necessarily represent an overall tension state in the arch at that location.

5.1 Material Properties

With the bridges being 83 years old, the condition of the concrete and reinforcing steel needed to be determined. During testing, sample cores, as shown in Figure 5-2, were taken out of the center and downstream arches of the Main Street Bridge. The sampling was performed by Mike Brown, associate director of The Virginia Center for Transportation Innovation and Research (VCTIR). Due to the destructive nature of removing concrete core samples, only two cores were tested. The results are an estimation of, not a comprehensive representation of, the material properties throughout the bridge.

Figure 5-2. Extracted Concrete Sample Cores

Compressive tests were performed on each cylinder according to ASTM C469 guidelines to determine their compressive strength and modulus of elasticity. These tests were performed by Virginia Tech research associate David Mokarem. The concrete compressive strengths were found to be 7.03 ksi for the center arch and 6.09 ksi for the downstream arch. The moduli of elasticity found for the samples are 6.88×10^6 psi for the center arch and 4×10^6 psi for the downstream arch. Further, the moduli of rupture for each core were calculated using the ACI equation, $f_r = 7.5\sqrt{f_c'}$, with the center arch being 629 psi and the downstream arch 585 psi.

A tensile coupon test was performed on the extracted rebar by doctoral student Will Collins and the results can be seen in the stress-strain relationship shown in Figure 5-3. The yield strength for the rebar was found to be 59.7 ksi.

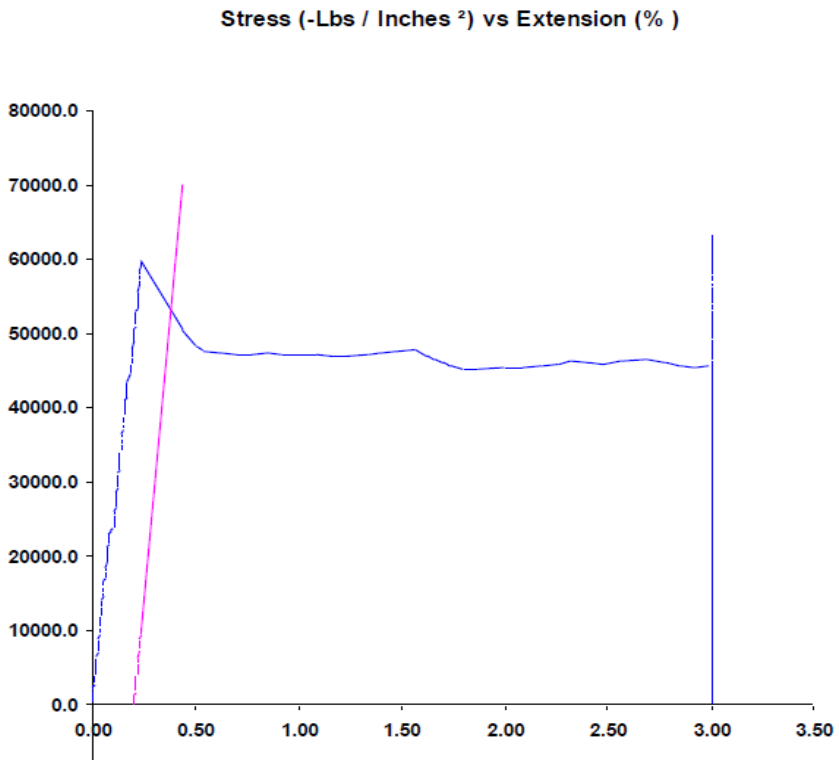

Figure 5-3. Stress-Strain Curve for Extracted Rebar

5.2 Main Street Bridge Results

The Main Street Bridge test was conducted using the five truck load cases discussed in Section 3.4.2. During the test, the upstream lane was loaded first, followed by the downstream lane. The following is a summary of strains and deflections experienced by the three reinforced concrete arches of the bridge. To ensure clarity when presenting the results, the locations are shown in Figure 5-4.

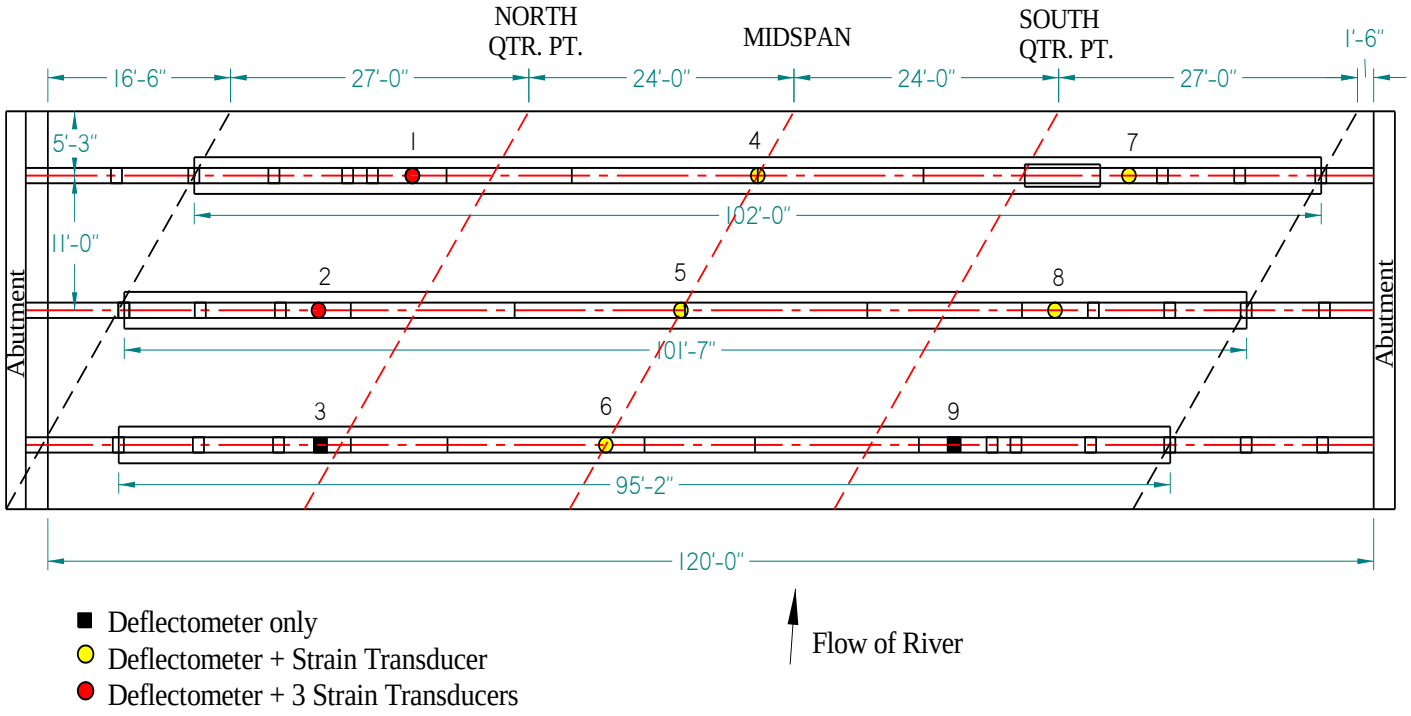

Figure 5-4. Main Street Bridge Instrument Locations

5.2.1 Service Strains

As the bridge was loaded, peak strains at all locations were of concern as well as how the strain was distributed through the arch depth. The peak strains for each instrument occurred when the trucks were located directly above that instrument. As expected for an arch, the majority of the strains recorded were compressive strains. The peak strains at location 1 were plotted to check for linear distribution of strain through the arch depth. Distributions were plotted when the load was placed at every quarter point along the bridge to determine if the arch would behave as expected. The plot shown in Figure 5-5 and the values in Table 5-1 give the peak strains recorded when the trucks were directly over the north quarter point (location 1).

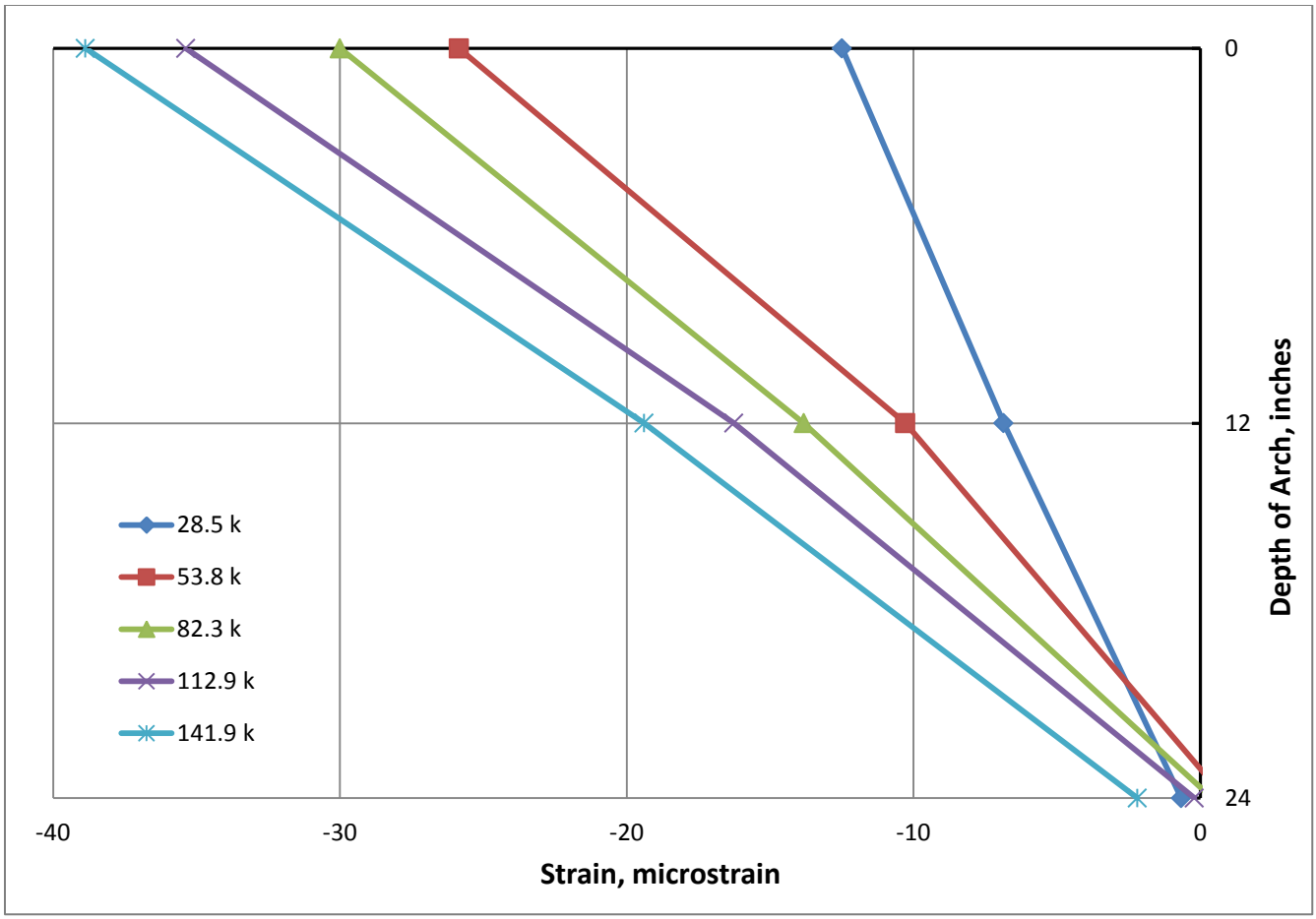

Figure 5-5. Main St. Bridge Location 1 Strain Distribution (Load at Location 1)

Table 5-1. Main St. Bridge Location 1 Strains (Load at Location 1)

Load (kips)	Arch Depth Location		
	Bottom	Middle	Top
28.5	-0.7	-6.9	-12.5
53.8	0.9	-10.3	-25.8
82.3	0.4	-13.8	-30.0
112.9	-0.2	-16.3	-35.4
141.4	-2.2	-19.4	-38.9

As shown in the plot and table, the strain distribution in Figure 5-5 is linear for each load increment. Also, the maximum strain (and therefore stress) seen in the arch at location 1 is about

40 microstrain of compression at the top. This is not a significant amount of strain given the amount of load being applied totals 141.9 kips. The corresponding stress can be calculated using the modulus of elasticity for the downstream arch given earlier and is 160 psi. This is well below the compressive strength of the concrete of 6090 psi. A similar strain distribution is plotted for location 1, in Figure 5-6, when the load is over the opposite end of the bridge at the south quarter point (location 7). Table 5-2 shows the values plotted in Figure 5-6.

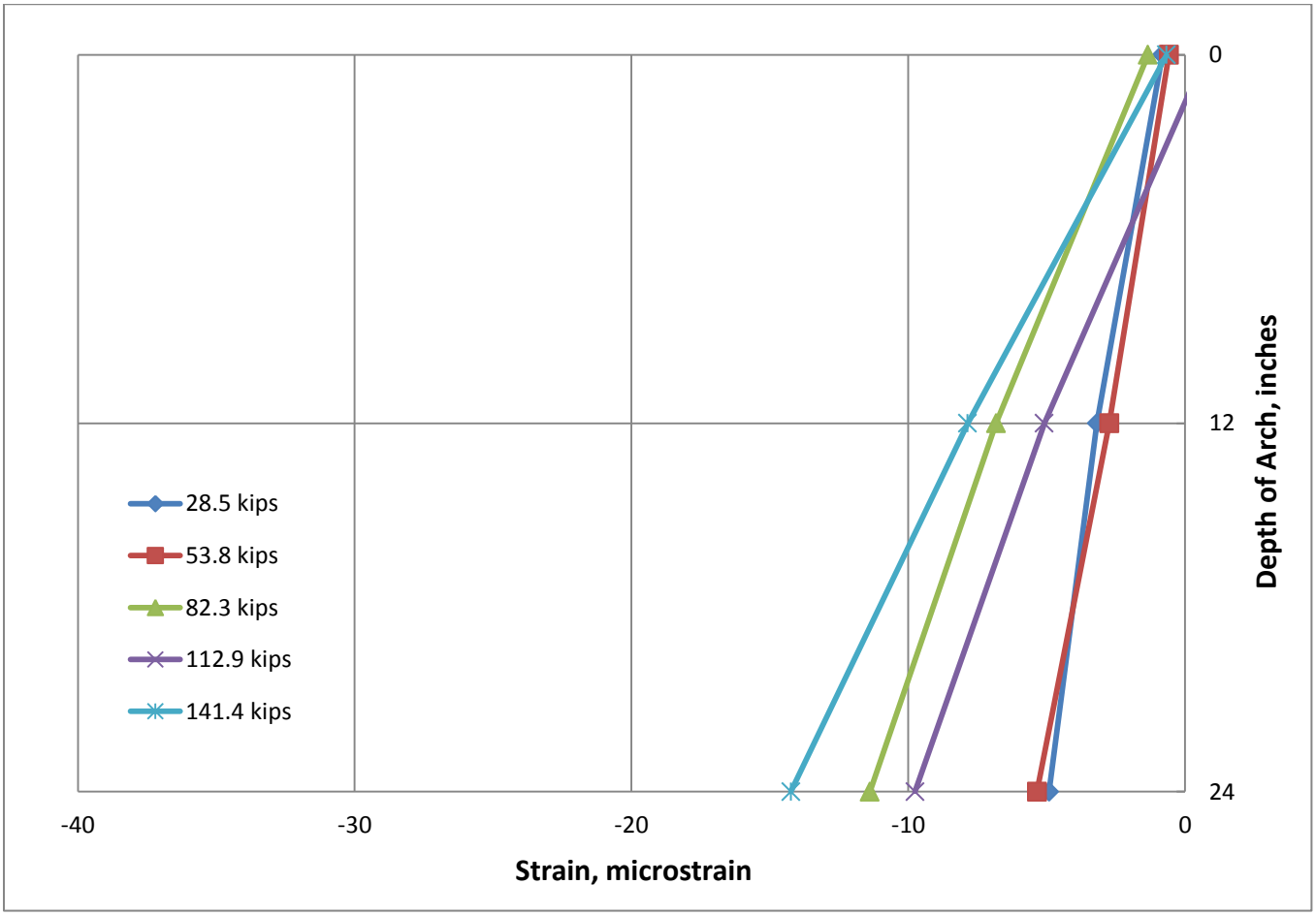

Figure 5-6. Main St. Bridge Location 1 Strain Distribution (Load at Location 7)

Table 5-2. Main St. Bridge Location 1 Strains (Load at Location 7)

Load (kips)	Arch Depth Location		
	Bottom	Middle	Top
28.5	-4.9	-3.2	-0.8
53.8	-5.3	-2.7	-0.6
82.3	-11.4	-6.8	-1.3
112.9	-9.7	-5.1	0.8
141.4	-14.2	-7.8	-0.7

It is apparent that linear strain behavior is displayed when the load is on the other end of the bridge. However, the compressive stress is now located on the bottom of the arch rather than the top. Also, the small strains shown at the top are assumed to be negligible. From Figure 5-6 the maximum compressive stress is around 15 microstrain with corresponding stress of 60 psi at the bottom of the arch. This is still a very small amount of stress for the loads applied.

Another interesting observation can be made by comparing Figures 5-5 and 5-6. When the test trucks are directly over location 1 (Figure 5-5), there is a large amount of compression in the top of the arch and only a small amount of compression or tension in the bottom. When the test trucks are on the other end of the bridge at location 7 the strain distribution at location 1 is reversed with smaller compressive strain in the bottom due to the proximity of the load. This is expected because downward deflection occurs directly under the load while uplift occurs on the opposite end of the arch. With downward deflection the arch will experience compression at the top and tension at the bottom and vice versa where uplift occurs on the end opposite the load.

Looking at the strain distribution when the load is over midspan (location 4) provides insight into how the arch is behaving with the different loading scenarios. The strain distribution,

in Figure 5-7, shows that the entire arch cross-section is in compression. Although the strain distributions in Figures 5-5 and 5-6 showed the distributions vary with compression in either the top or bottom, the strain in this instance is more consistent, varying less through the arch depth. Again, Table 5-3 summarizes the strain values at location 1 when the load is at midspan.

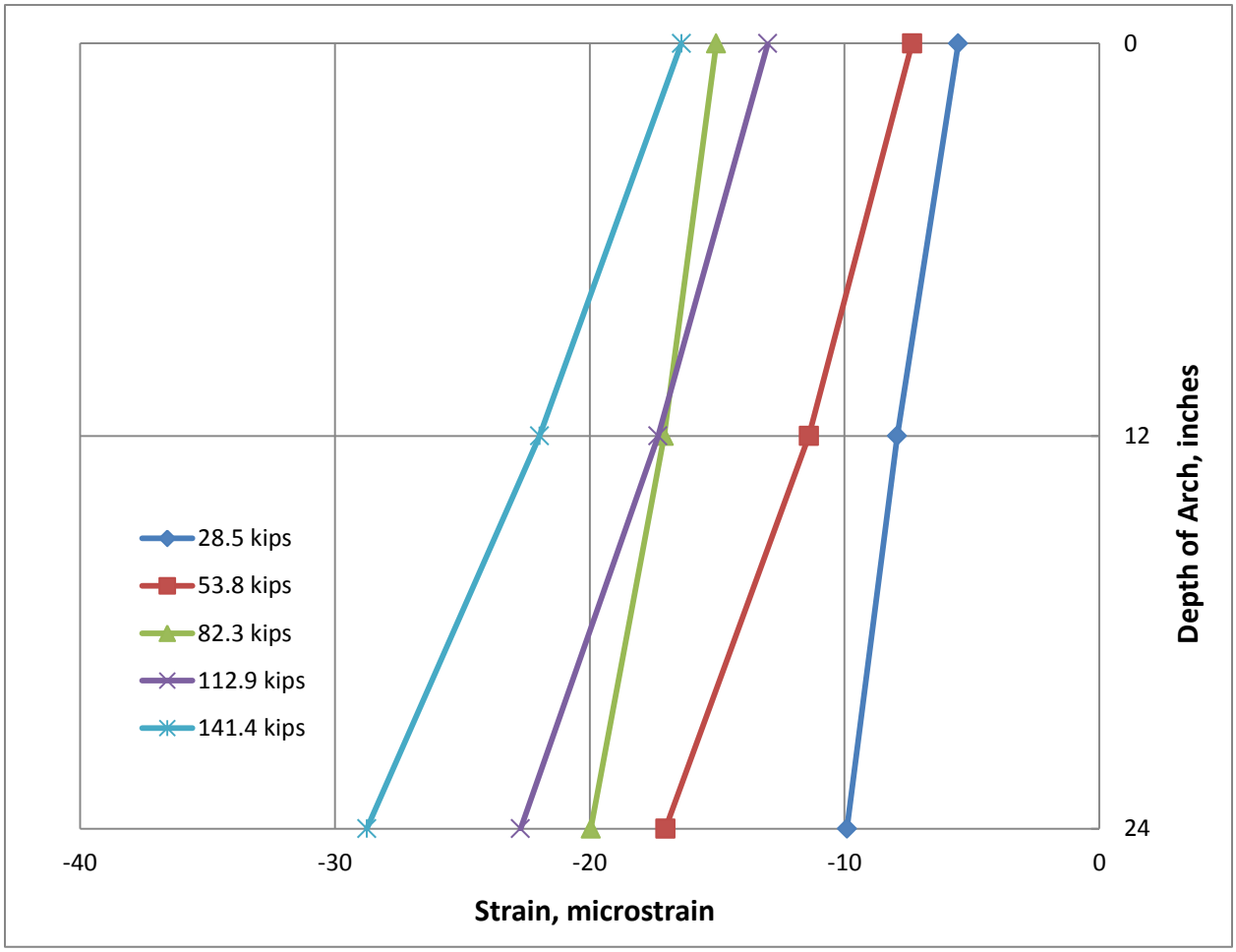

Figure 5-7. Main St. Bridge Location 1 Strain Distribution (Load at Location 4)

Table 5-3. Main St. Bridge Location 1 Strains (Load at Location 4)

Load (kips)	Arch Depth Location		
	Bottom	**Middle**	**Top**
28.5	-9.9	-7.9	-5.5
53.8	-17.0	-11.4	-7.3
82.3	-20.0	-17.1	-15.0
112.9	-22.7	-17.3	-13.0
141.4	-28.7	-22.0	-16.4

Examining these results shows that the strains seen at location 1 are behaving as expected. When the load is directly over that location, downward deflection will occur, resulting in tension in the bottom and compression in the top. When the load is at the other end of the bridge, uplift will occur, creating tension in the top and compression in the bottom. When the load is at midspan, downward deflection will occur under the load with slight uplift on either end. These deflection shapes can be seen in Figure 5-8. The maximum compressive strains at location 1 were -14.2, -28.7, and -38.9 με with the load at the south quarter point, midspan, and north quarter point respectively. The decreasing strains experienced at this arch location as the load moves further away show appropriate behavior.

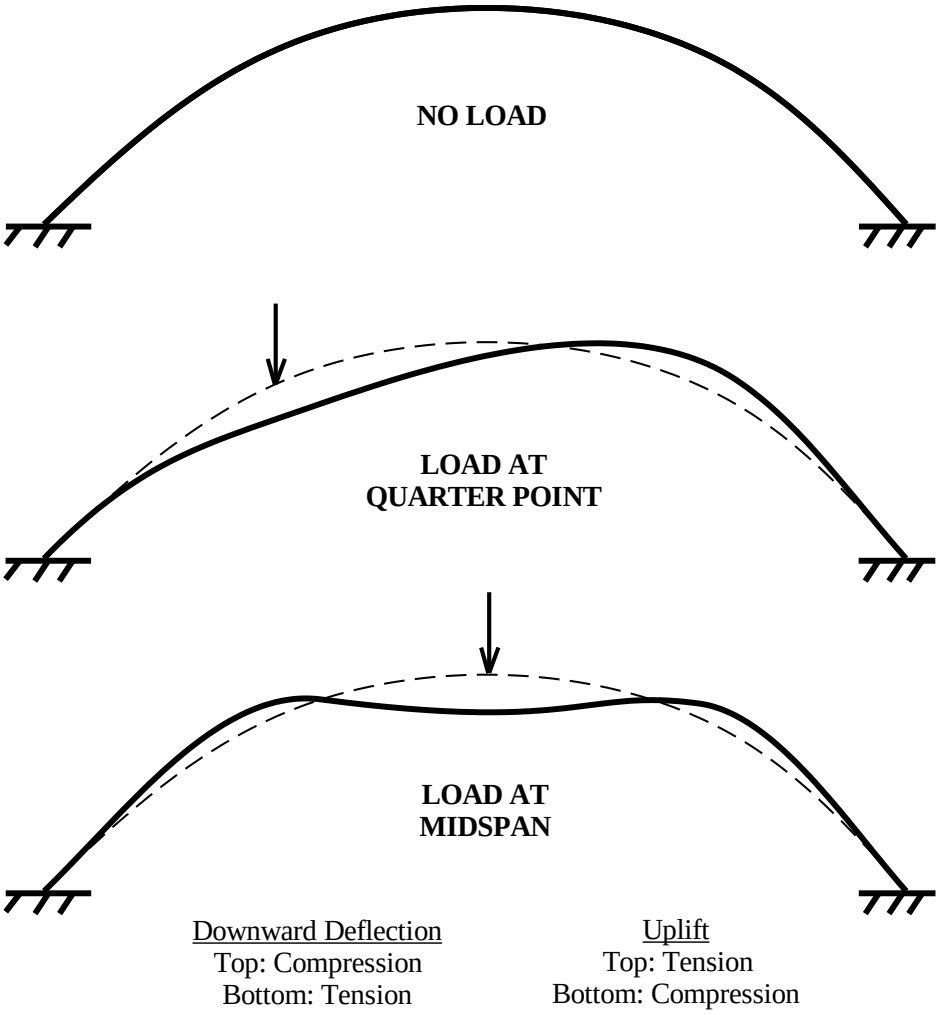

Figure 5-8. Typical Arch Deflection Shapes

5.2.2 Service Deflections

To examine the global behavior of the bridge, arch deflections from the test were analyzed. A plot of load versus deflection was created for each deflectometer with the five truck orientations located over the deflectometer in question. This plot and a table of the maximum deflections can be seen in Figure 5-9 and Table 5-4, respectively.

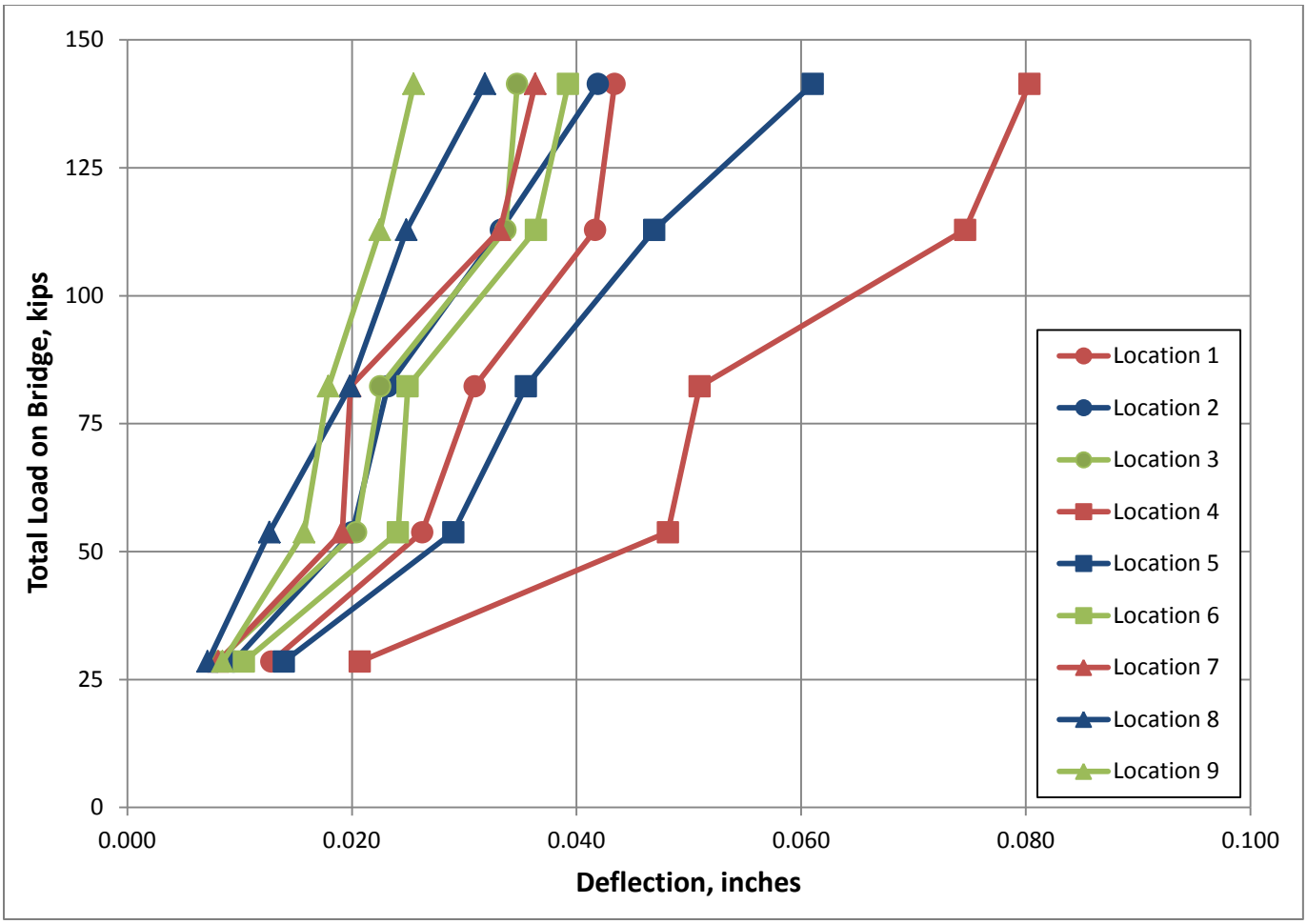

Figure 5-9. Maximum Arch Deflections for Main St. Bridge

Table 5-4. Maximum Arch Deflections for Main Street Bridge (in.)

Loads (kips)	Location 1	Location 2	Location 3	Location 4	Location 5	Location 6	Location 7	Location 8	Location 9
28.5	0.013	0.009	0.008	0.021	0.014	0.010	0.008	0.007	0.009
53.8	0.026	0.020	0.020	0.048	0.029	0.024	0.019	0.013	0.016
82.3	0.031	0.023	0.023	0.051	0.035	0.025	0.020	0.020	0.018
112.9	0.042	0.033	0.034	0.075	0.047	0.036	0.033	0.025	0.022
141.4	0.043	0.042	0.035	0.080	0.061	0.039	0.036	0.032	0.026

In Figure 5-9 the data sets are color coded and shape oriented to distinguish between arches and quarter point locations. The red lines represent the deflectometers along the downstream arch, the blue for the center arch, and the green represent the upstream arch. The triangle markers show the south quarter point of the bridge, the circles represent the north quarter point, and squares stand for the mid-span deflectometers. Following this system, it can be seen that the north span deflectometers and the downstream arch showed greater deflections. This was expected for the downstream arch since it takes a more direct load due to the absence of a sidewalk as seen in Figure 3-21. The greater deflections experienced by the north end of the span can be explained by the presence of connecting beams between bridges on the south span. Because of this detail the load is transferred between the connected structures resulting in the south end of the span being stiffer than the north. Also, the deflections are very small, generally linear with respect to increasing load (the slight nonlinearity shown is attributable to load location rather than magnitude), and show that the arch bridge is a stiff, linear elastic structural system.

5.2.3 Arch Load Distribution

To determine how the bridge distributes load between arches, deflections at each quarter point were compared. From the data, six transverse load distribution plots were developed for when the load was stopped at each quarter point in both lanes. The load distribution between the three arches for when the load is in the downstream lane is shown in Figures 5-10, 5-11, and 5-12 for the north quarter point, midspan, and south quarter point, respectively. Tables 5-5, 5-6, and 5-7 show the distribution percentages of the total deflection at that quarter point.

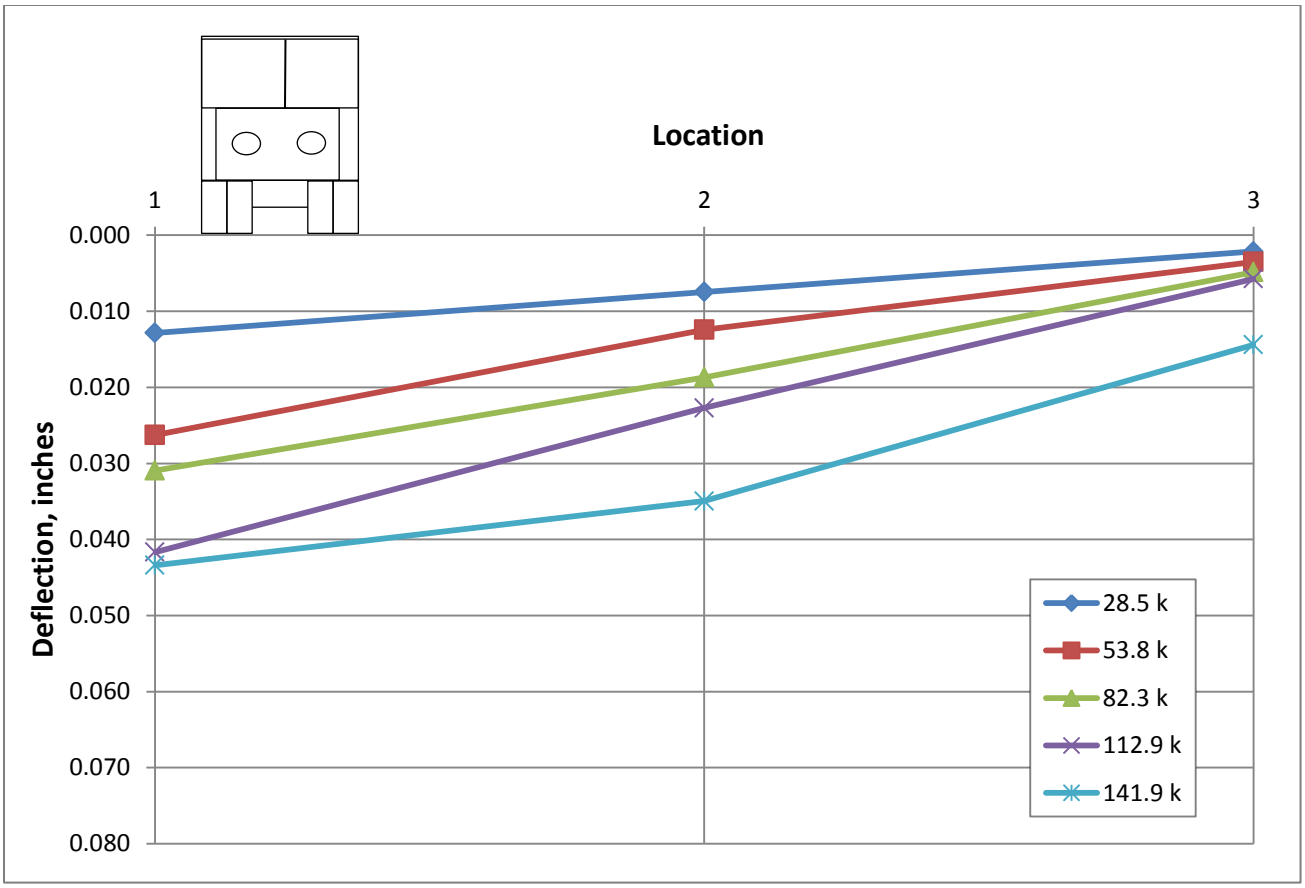

Figure 5-10. Main St. Bridge North Quarter Point Load Distribution (Load in D-S Lane)

Table 5-5. Main St. North Quarter Point Load Distribution (Load in D-S Lane)

Run	Load	1	2	3
2	**28.5**	57.2%	33.3%	9.5%
4	**53.8**	62.3%	29.4%	8.3%
6	**82.3**	56.8%	34.3%	8.9%
8	**112.9**	59.4%	32.4%	8.2%
10	**141.9**	46.8%	37.7%	15.5%

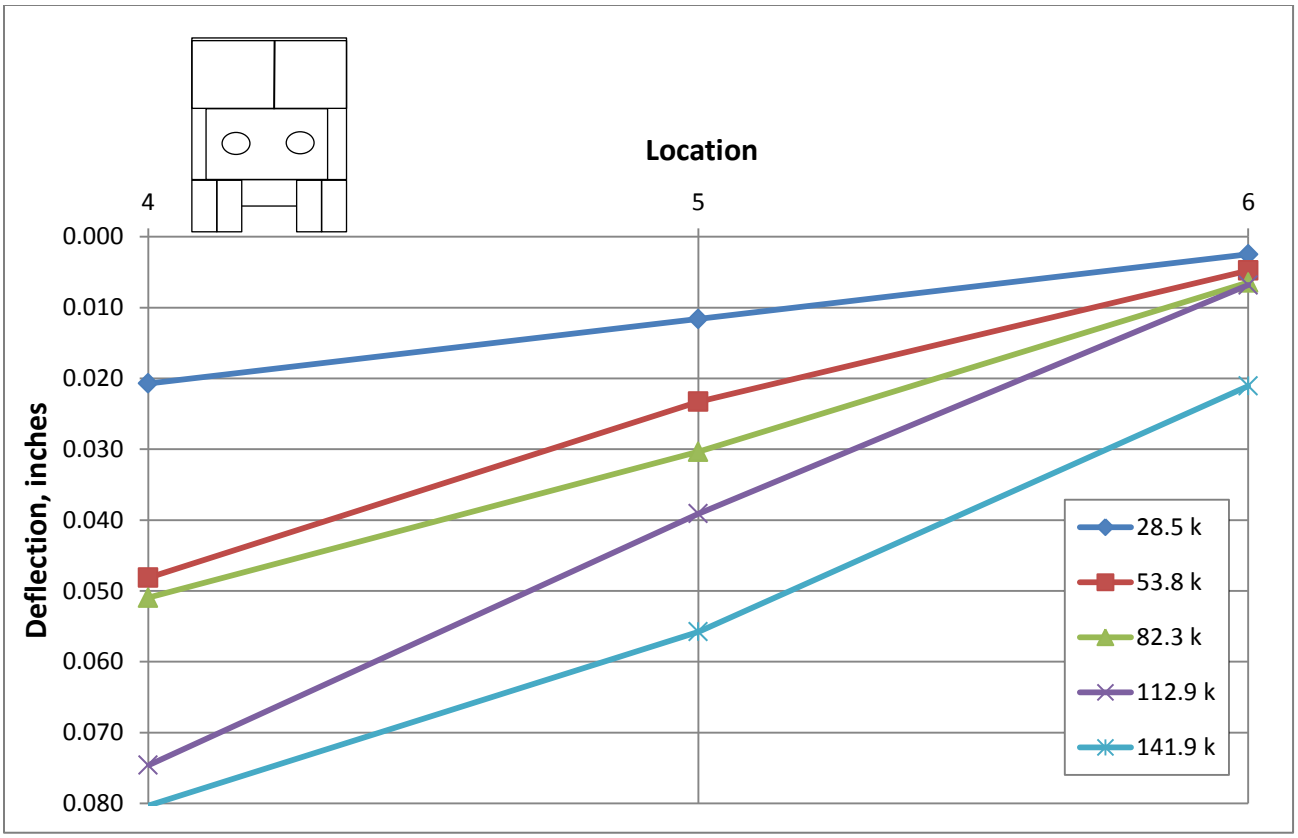

Figure 5-11. Main St. Bridge Midspan Load Distribution (Load in D-S Lane)

Table 5-6. Main St. Midspan Load Distribution (Load in D-S Lane)

Run	Load	4	5	6
2	**28.5**	59.5%	33.3%	7.1%
4	**53.8**	63.2%	30.6%	6.2%
6	**82.3**	58.1%	34.6%	7.3%
8	**112.9**	61.9%	32.4%	5.7%
10	**141.9**	51.1%	35.5%	13.4%

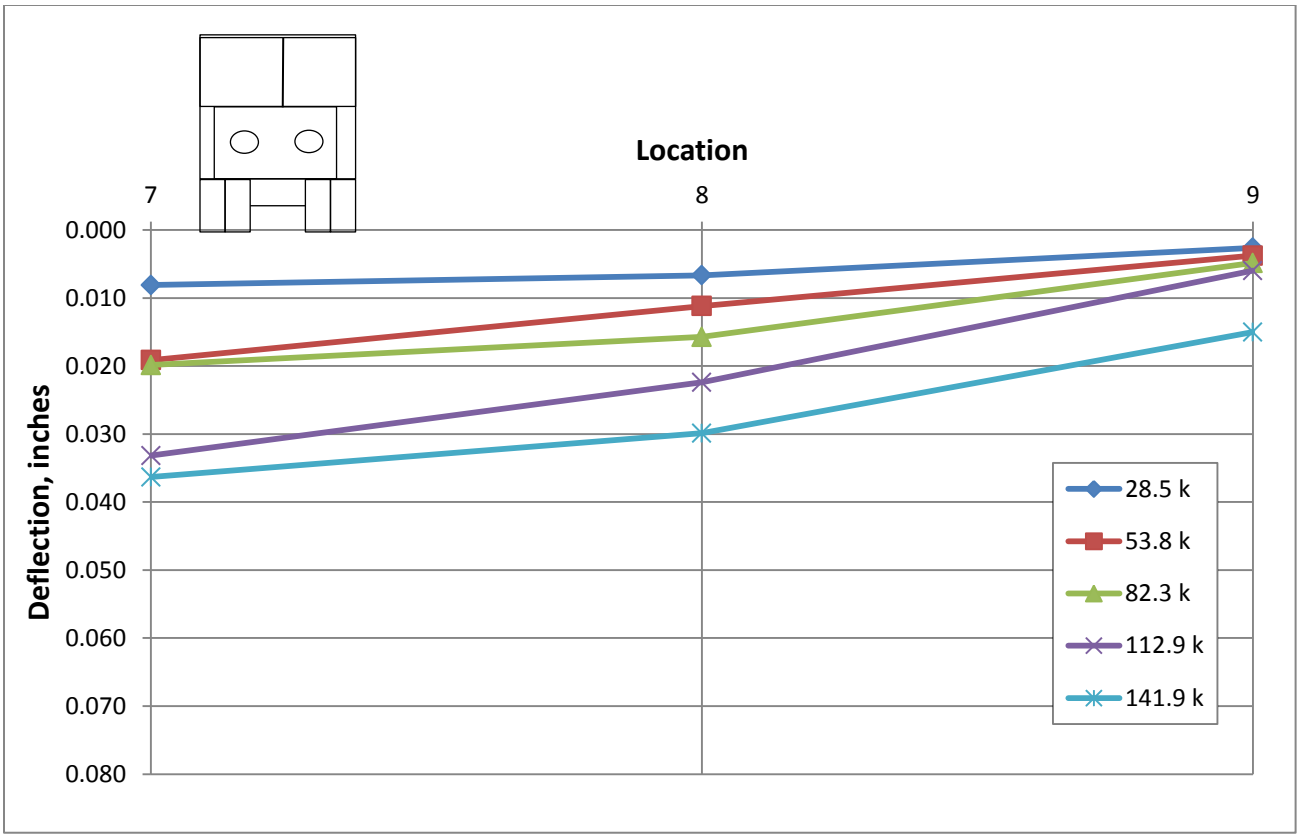

Figure 5-12. Main St. Bridge South Quarter Point Load Distribution (Load in D-S Lane)

Table 5-7. Main St. South Quarter Point Load Distribution (Load in D-S Lane)

Run	Load	7	8	9
2	**28.5**	46.6%	38.3%	15.1%
4	**53.8**	56.1%	32.8%	11.1%
6	**82.3**	49.1%	38.9%	12.0%
8	**112.9**	53.9%	36.4%	9.7%
10	**141.9**	44.7%	36.8%	18.5%

From the plots, the transverse load distribution shows linear increases in deflection across the three arches with proximity to loading. The deflections also increase with respect to the magnitude each subsequent load case. With the load in the downstream lane, the downstream arch is getting the load directly and it is shared less with the other arches as shown in each plot.

The maximum downward deflections for each quarter point are 0.043 in. for the north, 0.080 in. for midspan, and 0.036 for the south. These maximum deflections were all recorded on the downstream arch under the 141.9 kip loading. As seen in Table 5-4 for the 141.9 kip load, the north end had deflections of 0.043, 0.042, and 0.035 in. for the downstream, center, and upstream arches, respectively. The corresponding deflections on the south end for the same load were 0.036, 0.032, and 0.026 in. From these values, evidence shows that the north end of the span is more flexible than the south end with deflections ranging between approximately twenty and thirty percent greater on the north end than the south. This is shown in Table 5-8.

Table 5-8. Comparison of Max. Deflections between Main St. Span Ends

Span	Location	Deflection	Span	Location	Deflection	Percent Difference
North End	**1**	0.043	**South End**	**7**	0.036	19
	2	0.042		**8**	0.032	31
	3	0.035		**9**	0.026	35

In the load distribution tables, the percentages represented the deflection of that arch compared to the total deflection of the three arches at that quarter point. The arches displayed consistent behavior throughout the span of the bridge. Generally, the downstream arch had between fifty and sixty percent of the total deflection, the center arch between thirty and forty percent, and the upstream arch between five and fifteen percent.

In Figures 5-13, 5-14, and 5-15 and Tables 5-9, 5-10, and 5-11 the load distributions are plotted and reported as the load is in the upstream lane. Due to the sidewalk on this side of the bridge, the load is located between the center and upstream arches with the load being shared between the two as shown in Figure 3-20.

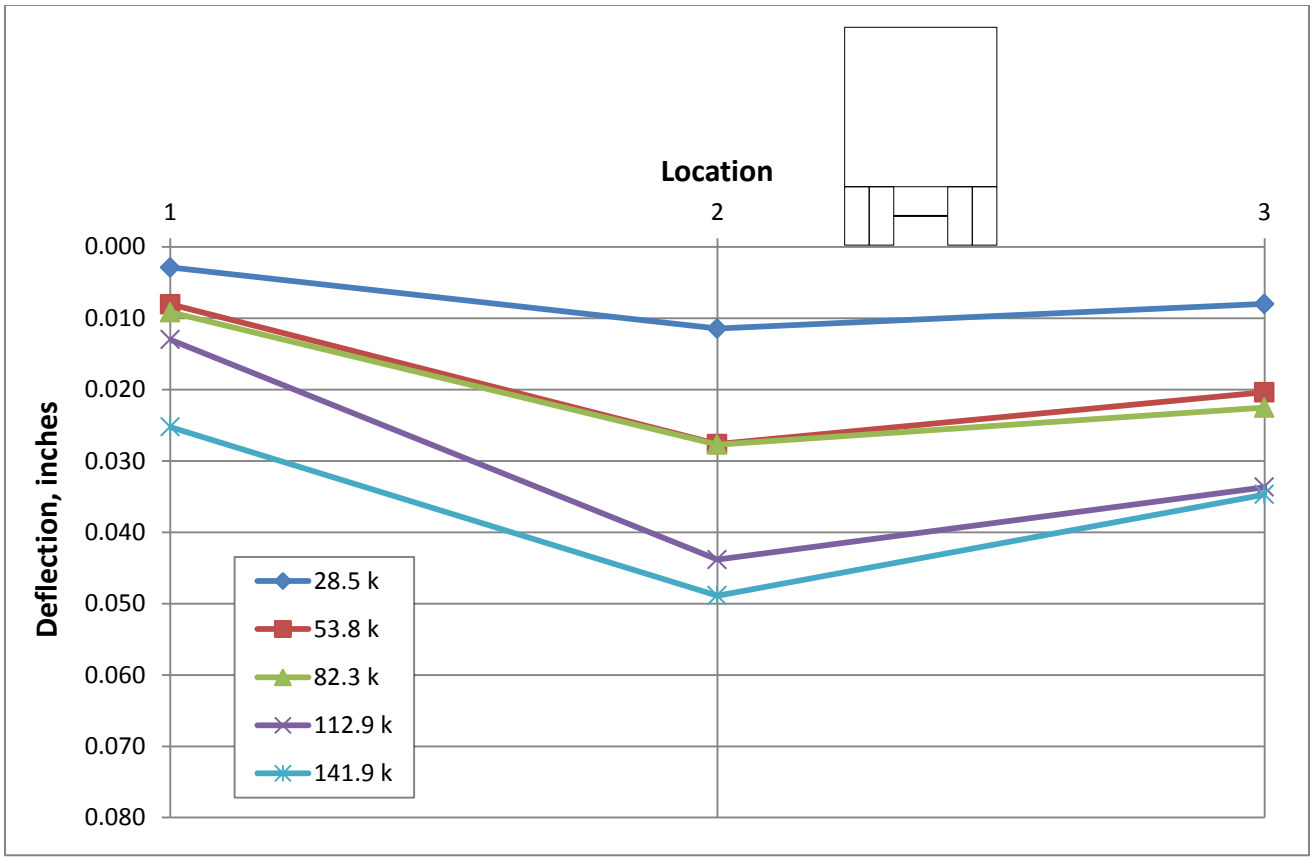

Figure 5-13. Main St. Bridge North Quarter Point Load Distribution (Load in U-S Lane)

Table 5-9. Main St. North Quarter Point Load Distribution (Load in U-S Lane)

Run	Load	1	2	3
1	**28.5**	12.9%	51.3%	35.8%
3	**53.8**	14.3%	49.3%	36.3%
5	**82.3**	15.4%	46.6%	37.9%
7	**112.9**	14.4%	48.4%	37.2%
9	**141.4**	23.2%	44.9%	31.9%

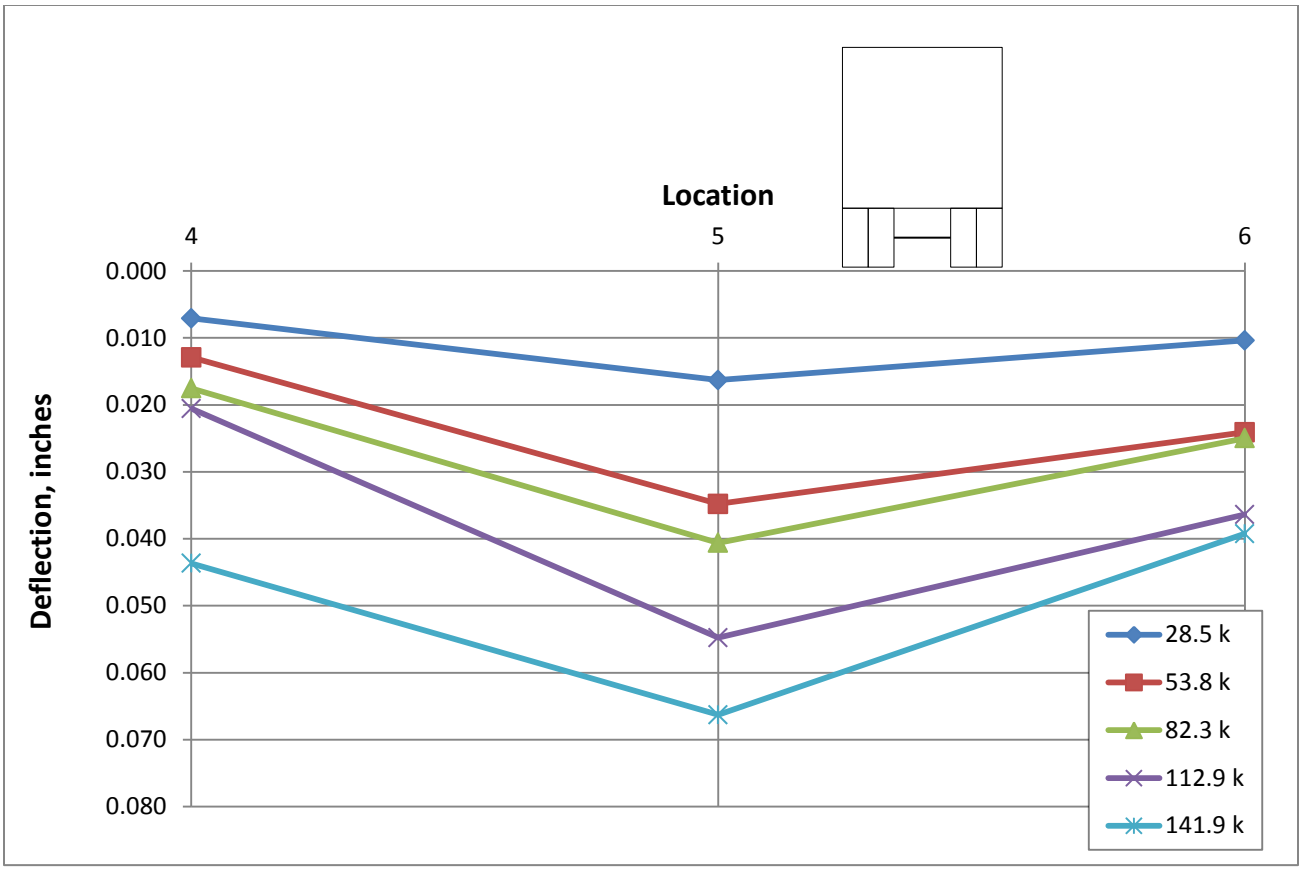

Figure 5-14. Main St. Bridge Midspan Load Distribution (Load in U-S Lane)

Table 5-10. Main St. Midspan Load Distribution (Load in U-S Lane)

Run	Loads	4	5	6
1	**28.5**	21.0%	48.3%	30.8%
3	**53.8**	18.0%	48.5%	33.6%
5	**82.3**	21.1%	48.9%	30.0%
7	**112.9**	18.4%	49.0%	32.6%
9	**141.4**	29.3%	44.4%	26.3%

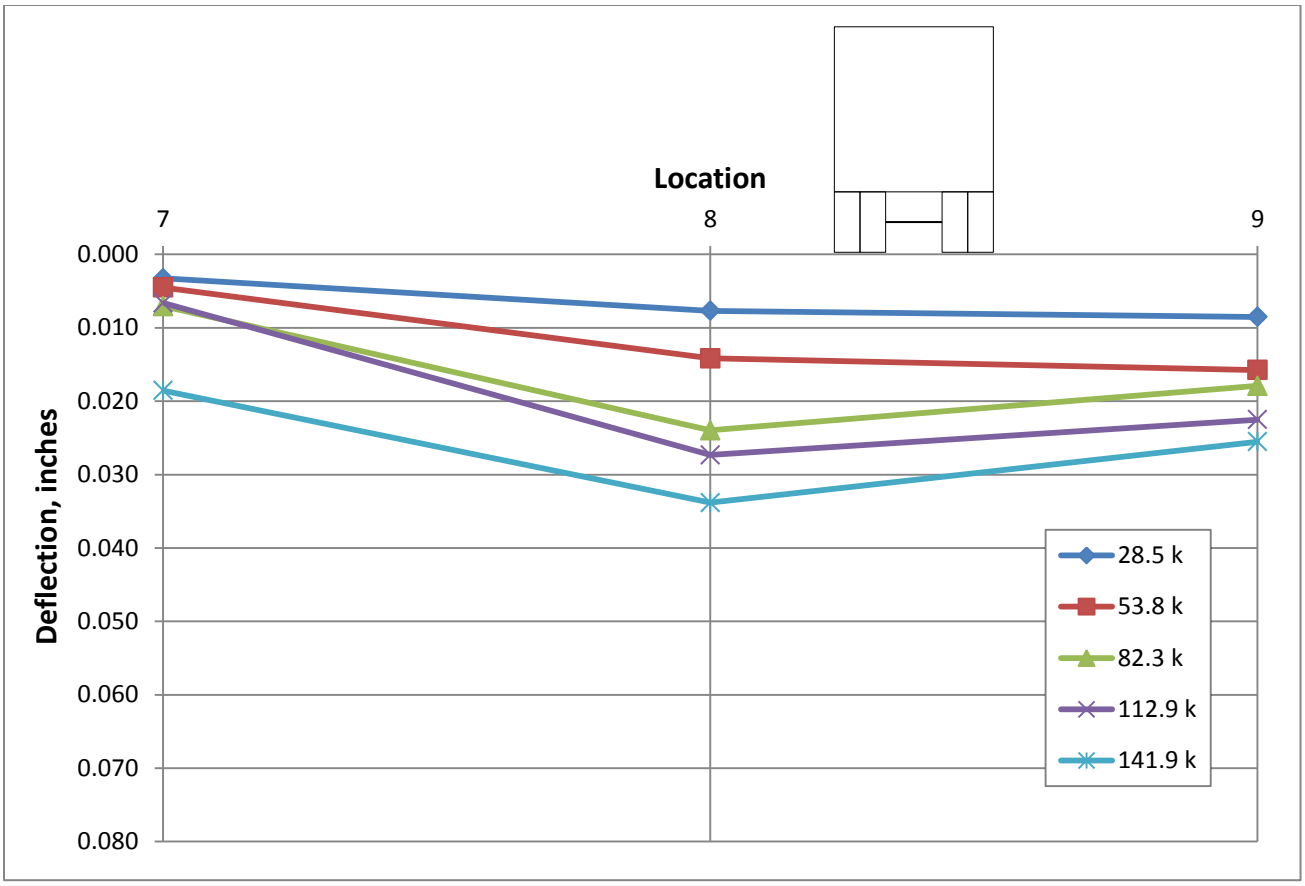

Figure 5-15. Main St. Bridge South Quarter Point Load Distribution (Load in U-S Lane)

Table 5-11. Main St. South Quarter Point Load Distribution (Load in U-S Lane)

Run	Load	7	8	9
1	**28.5**	16.8%	39.5%	43.7%
3	**53.8**	13.1%	41.1%	45.8%
5	**82.3**	14.4%	49.0%	36.6%
7	**112.9**	11.7%	48.4%	39.9%
9	**141.4**	23.8%	43.4%	32.8%

From the plots, the transverse load distribution shows linear increases in deflection across the three arches with proximity to loading. The deflections also increase with respect to the magnitude each subsequent load case. These plots show that the load is distributed more to the

center arch due to the truck's closer proximity to the center of the bridge. The maximum deflections seen with this load case are 0.049 in. for the north, 0.066 in. for midspan, and 0.034 in. for the south. These maximum deflections were all recorded on the center arch under the 141.9 kip loading. This follows the trend of small deflections in this bridge as well as the stiffer south span as the north span deflections are thirty percent larger.

From the tables, the percentages represented the deflection of that arch compared to the total deflection of the three arches at that quarter point. The arches displayed consistent behavior throughout the span of the bridge. Generally, the downstream arch had between fifteen and thirty percent of the total deflection, the center arch contained between forty and fifty percent, while the upstream arch held between thirty and forty percent.

5.3 Depot Street Bridge Results

The Depot Street Bridge test was conducted using the same five truck load combinations as the Main Street Bridge. The data analysis performed on the Main Street Bridge was replicated for the Depot Street Bridge. During the test, the downstream lane was loaded first, followed by the upstream lane. The following is a summary of strains and deflections experienced by the three reinforced concrete arches of the bridge. To ensure clarity when presenting the results, the locations are shown in Figure 5-16.

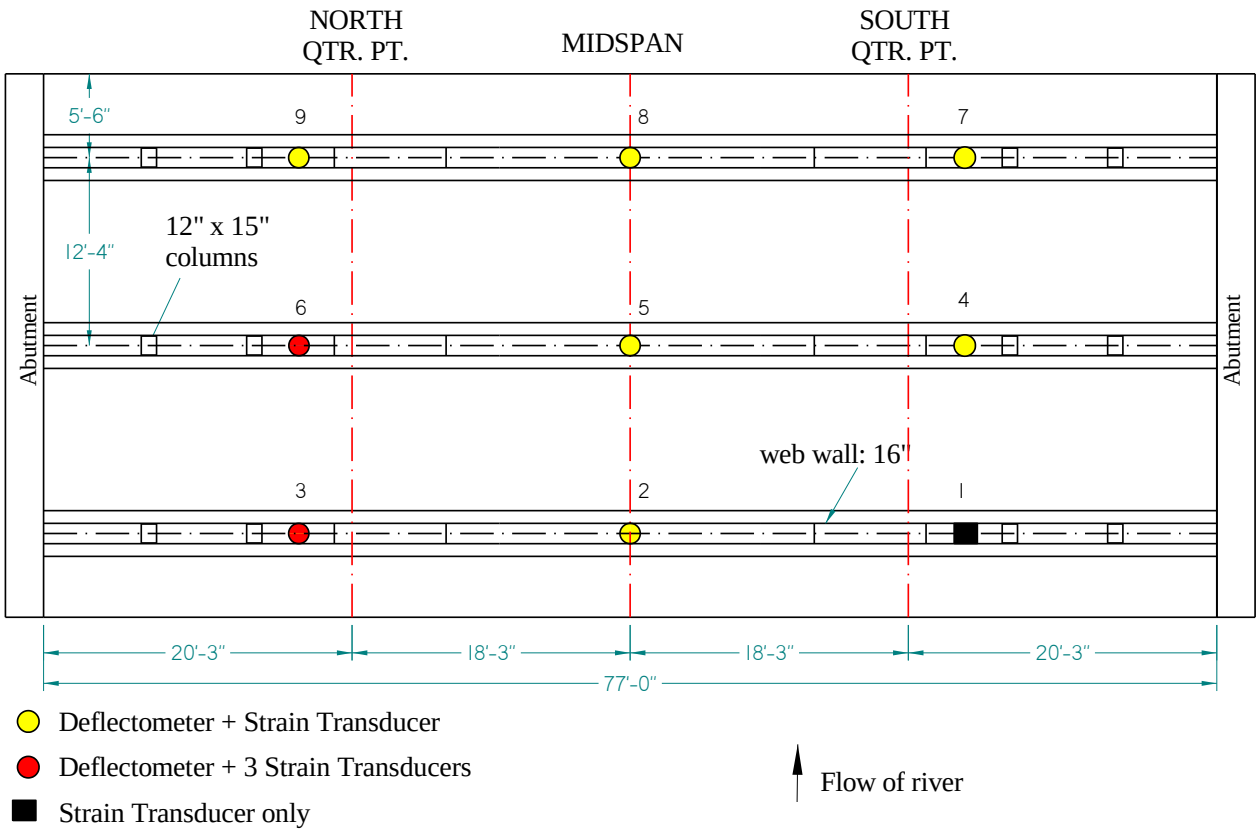

Figure 5-16. Depot Street Bridge Instrument Locations

5.3.1 Service Strains

The strains were recorded in the same manner as the Main Street Bridge and the peak sgtrains were plotted to check the arch behavior. The peak strains for each instrument occurred when the trucks were located directly above that instrument. The results at location 3 were then plotted to check for linear distribution of strain through the arch depth. The plot shown in Figure 5-17 and the values in Table 5-12 demonstrate the peak strains recorded when the trucks were directly over the north quarter point (location 3).

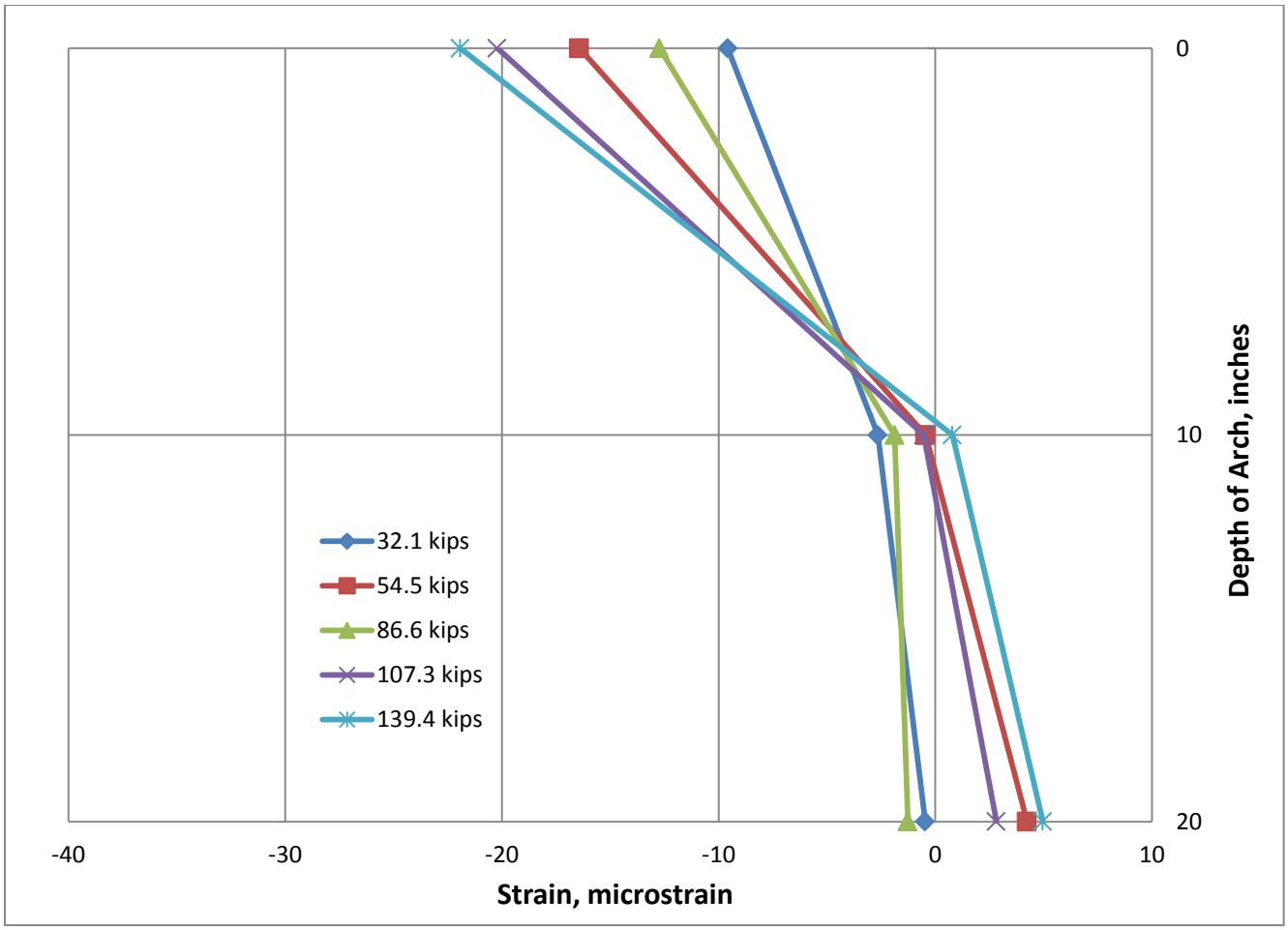

Figure 5-17. Depot St. Bridge Location 3 Strain Distribution (Load at Location 3)

Table 5-12. Depot St. Bridge Location 3 Strains (Load at Location 3)

Load (kips)	Arch Depth Location		
	Top	Middle	Bottom
32.1	-9.6	-2.7	-0.5
54.5	-16.4	-0.5	4.2
86.6	-12.7	-1.9	-1.3
107.3	-20.2	-0.5	2.8
139.4	-21.9	0.8	5.0

From Figure 5-16, it is shown that the maximum strain observed in the arch at location 3 is approximately 20 microstrain of compression at the top. This is not a significant amount of strain given the magnitude of load being applied. The corresponding stress can be calculated using the modulus of elasticity reported earlier for the companion structure and is 80 psi. When the load is applied on the other quarter point at location 1, location 3 still has a linear strain distribution as seen in Figure 5-17 and Table 5-13.

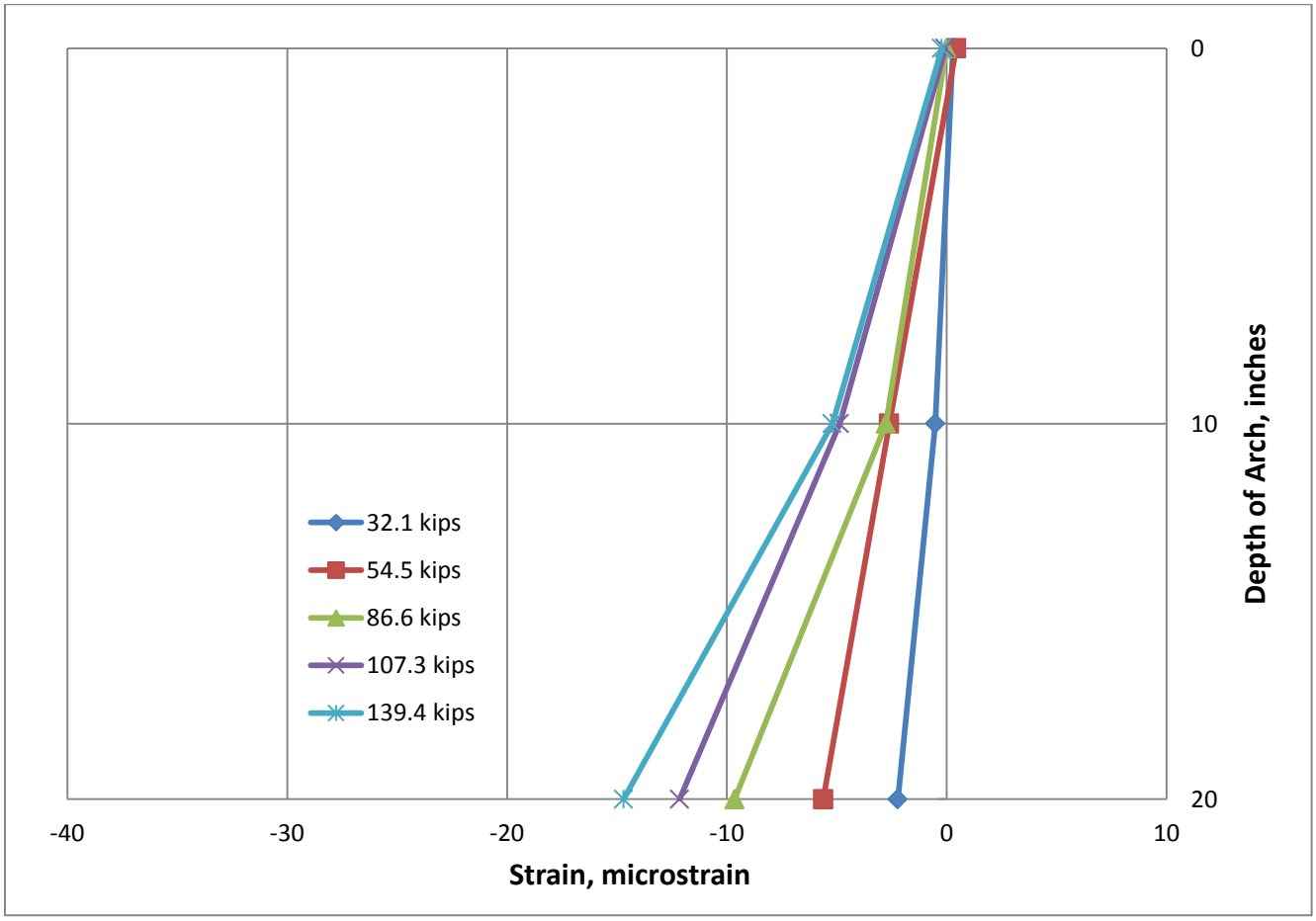

Figure 5-18. Depot St. Bridge Location 3 Strain Distribution (Load at Location 1)

Table 5-13. Depot St. Bridge Location 3 Strains (Load at Location 1)

Load (kips)	Arch Depth Location		
	Top	**Middle**	**Bottom**
32.1	0.3	-0.5	-2.2
54.5	0.4	-2.6	-5.6
86.6	0.0	-2.8	-9.6
107.3	-0.1	-4.9	-12.1
139.4	-0.2	-5.2	-14.7

From Figure 5-18 the maximum compressive stress is approximately 14.7 microstrain. This is still a small strain for the loads applied. The corresponding maximum compressive stress was calculated to be 60 psi.

Another interesting observation can be made by comparing Figures 5-17 and 5-18. When the test trucks are directly over location 3 (Figure 5-17) there is a large amount of compression in the top and small compression or tension in the bottom of the arch. When the test trucks are on the other end of the bridge the strain distribution at location 3 is reversed. This is expected and is typical of concrete arch behavior.

Looking at the strain distribution when the load is over midspan (location 2) provides a picture of how the strain distribution changes when the load is moving away from the strain transducer. The strain distribution, in Figure 5-19, shows that the entire arch cross-section is in compression. The compressive strains in the arch are very small in magnitude and nearly constant throughout the depth.

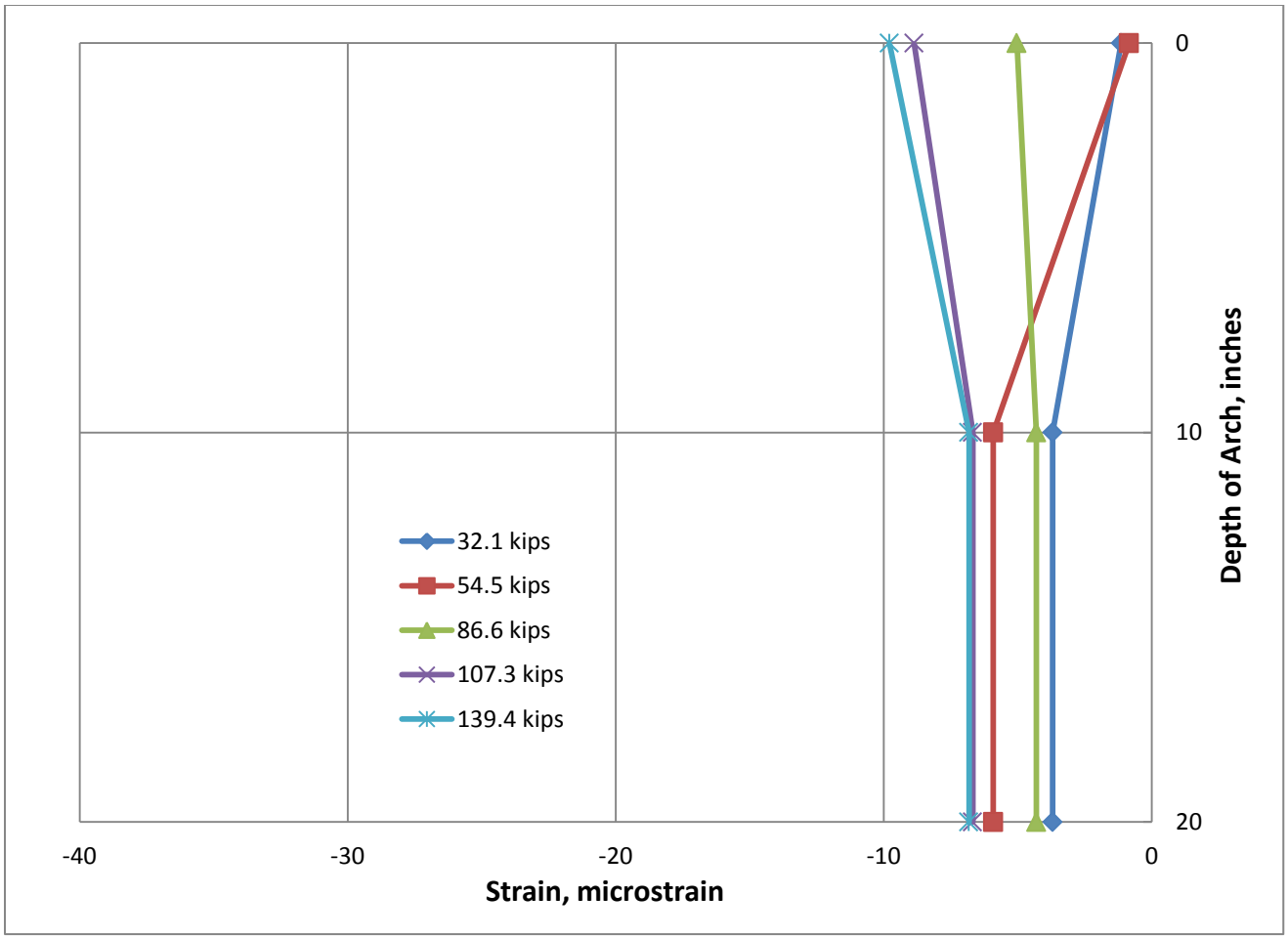

Figure 5-19. Depot St. Bridge Location 3 Strain Distribution (Load at Location 2)

Table 5-14. Depot St. Bridge Location 3 Strains (Load at Location 2)

Load (kips)	Arch Depth Location		
	Top	Middle	Bottom
32.1	-1.1	-3.7	-3.7
54.5	-0.8	-5.9	-5.9
86.6	-5.0	-4.3	-4.3
107.3	-8.9	-6.7	-6.7
139.4	-9.8	-6.8	-6.8

Examining these results shows that the strains seen at location 3 are behaving in a linear fashion. When the load is directly over that location, downward deflection will occur, resulting in tension in the bottom and compression in the top. When the load is at the other end of the bridge, uplift will occur, creating tension in the top and compression in the bottom. When the load is at midspan the deflection will be more neutral with the thrust acting through the arch. The maximum compressive strains at location 1 were -21.9, -9.8, and -14.7 με with the load at the north quarter point, midspan, and south quarter point respectively. Although the strains do not follow an exact linear decline as the load moves away from location 3, the behavior is similar to that seen from the Main Street Bridge.

5.3.2 Service Deflections

To examine the global behavior of the bridge, arch deflections from the test were analyzed. A plot of load versus deflection was created for each deflectometer with the five truck orientations located over the deflectometer in question. This plot and a table of the maximum deflections can be seen in Table 5-15 and Figure 5-20, respectively.

Table 5-15. Maximum Arch Deflections for Depot Street Bridge (in.)

Loads (kips)	Location 2	Location 3	Location 4	Location 5	Location 6	Location 7	Location 8	Location 9
32.1	0.012	0.009	0.011	0.018	0.015	0.008	0.012	0.012
54.5	0.022	0.018	0.020	0.034	0.026	0.017	0.022	0.024
86.6	0.025	0.018	0.021	0.035	0.027	0.015	0.022	0.025
107.3	0.032	0.026	0.026	0.045	0.035	0.021	0.030	0.031
139.4	0.034	0.027	0.038	0.063	0.041	0.025	0.034	0.036

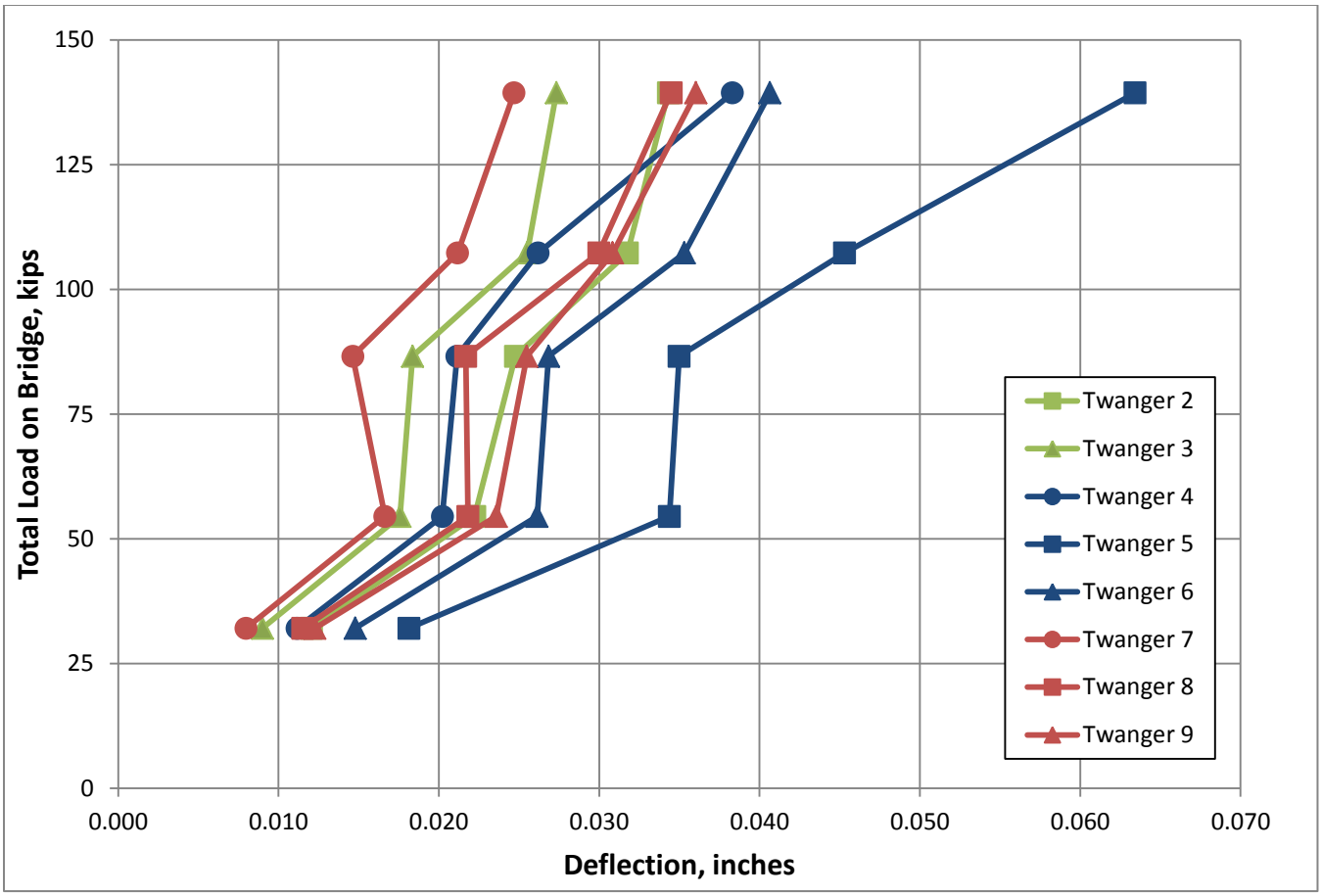

Figure 5-20. Maximum Deflections for Depot St. Bridge

In Figure 5-20, the red lines represent the deflectometers along the downstream arch, the blue represent the center arch, and the green represent the upstream arch. The triangle markers show the deflectometer values from the south quarter point of the span, the circles represent the north quarter point, and squares indicate the mid-span. Following this system, it can be seen that the midspan and the center arch showed greater deflections. This was expected for the center arch since the truck loads are located closer to the center arch than the outside arches of each lane (see Figure 3-20). Also, the deflections are very small, generally linear with respect to increasing load (the slight nonlinearity shown is attributable to load location rather than magnitude), and show that the arch bridge is a stiff, linear-elastic structural system.

5.3.3 Arch Load Distribution

From the data, the transverse load distribution amongst the arches was considered. In Figures 5-21, 5-22, and 5-23 and Tables 5-16, 5-17, and 5-18 the load distribution of the three arches is shown by plots of the arch deflections and percentages. The figures represent the deflections of the arches when the load is over each quarter point while in the downstream lane.

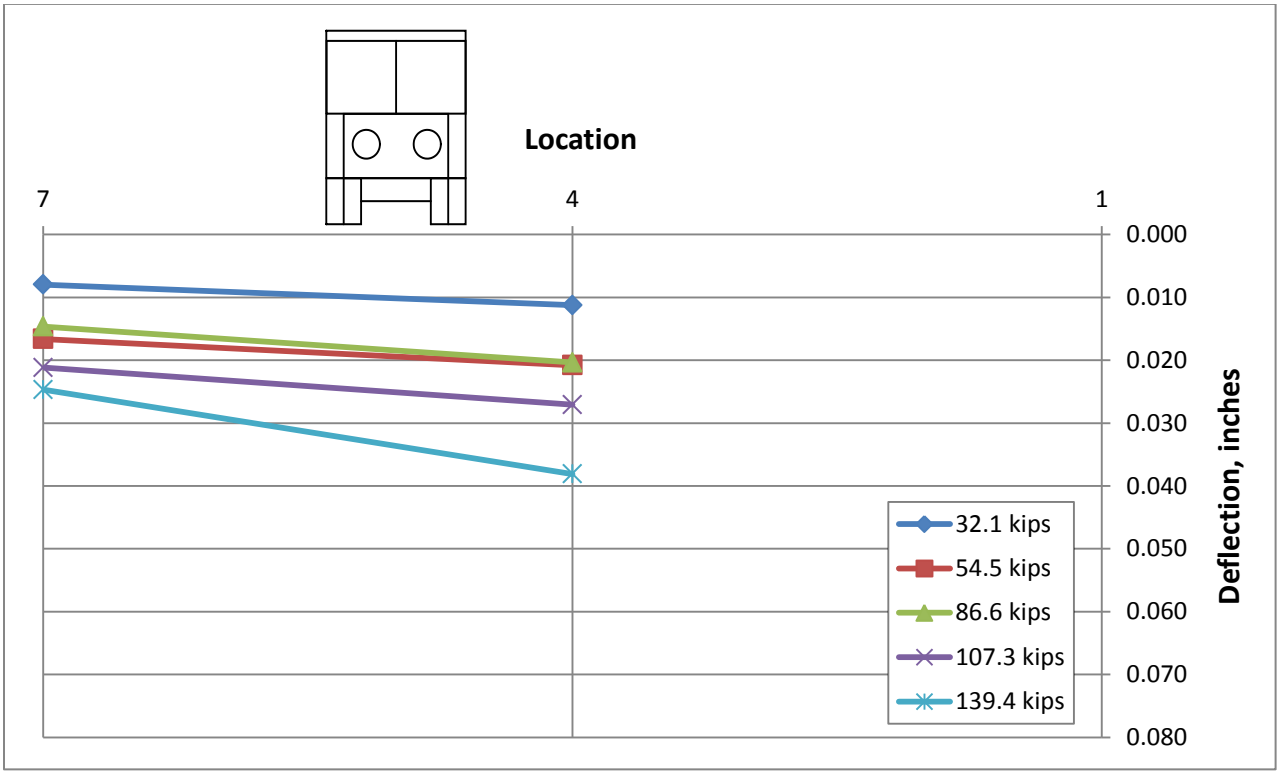

Figure 5-21. Depot St. Bridge South Quarter Point Load Distribution (Load in D-S Lane)

Table 5-16. Depot St. South Quarter Point Load Distribution (Load in D-S Lane)

Run	Load	4	7
1	**32.1**	58.5%	41.5%
3	**54.5**	55.6%	44.4%
5	**86.6**	58.2%	41.8%
7	**107.3**	56.1%	43.9%
9	**139.4**	60.7%	39.3%

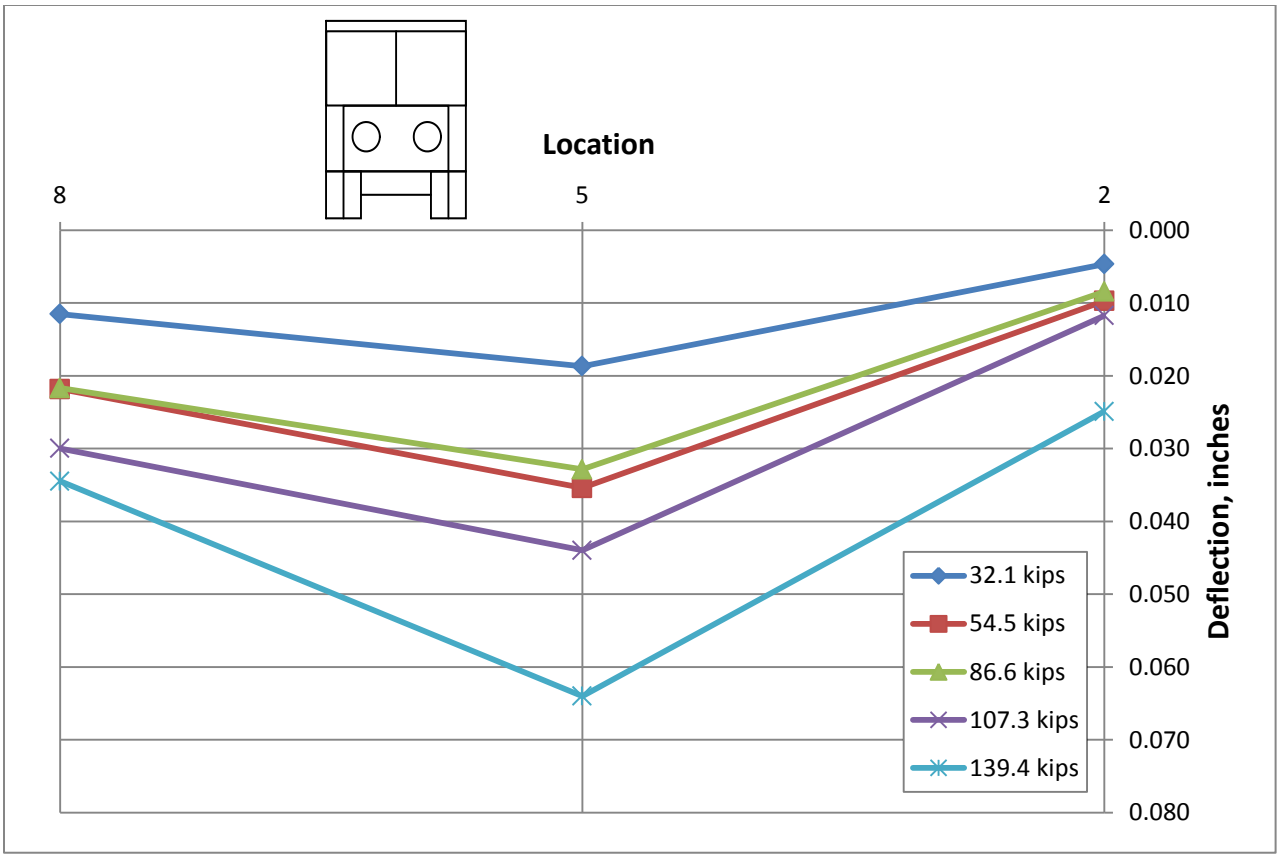

Figure 5-22. Depot St. Bridge Midspan Load Distribution (Load in D-S Lane)

Table 5-17. Depot St. Midspan Load Distribution (Load in D-S Lane)

Run	Load	2	5	8
1	**32.1**	13.4%	53.6%	33.0%
3	**54.5**	14.5%	52.9%	32.6%
5	**86.6**	13.4%	52.2%	34.4%
7	**107.3**	13.7%	51.3%	35.0%
9	**139.4**	20.2%	51.9%	27.9%

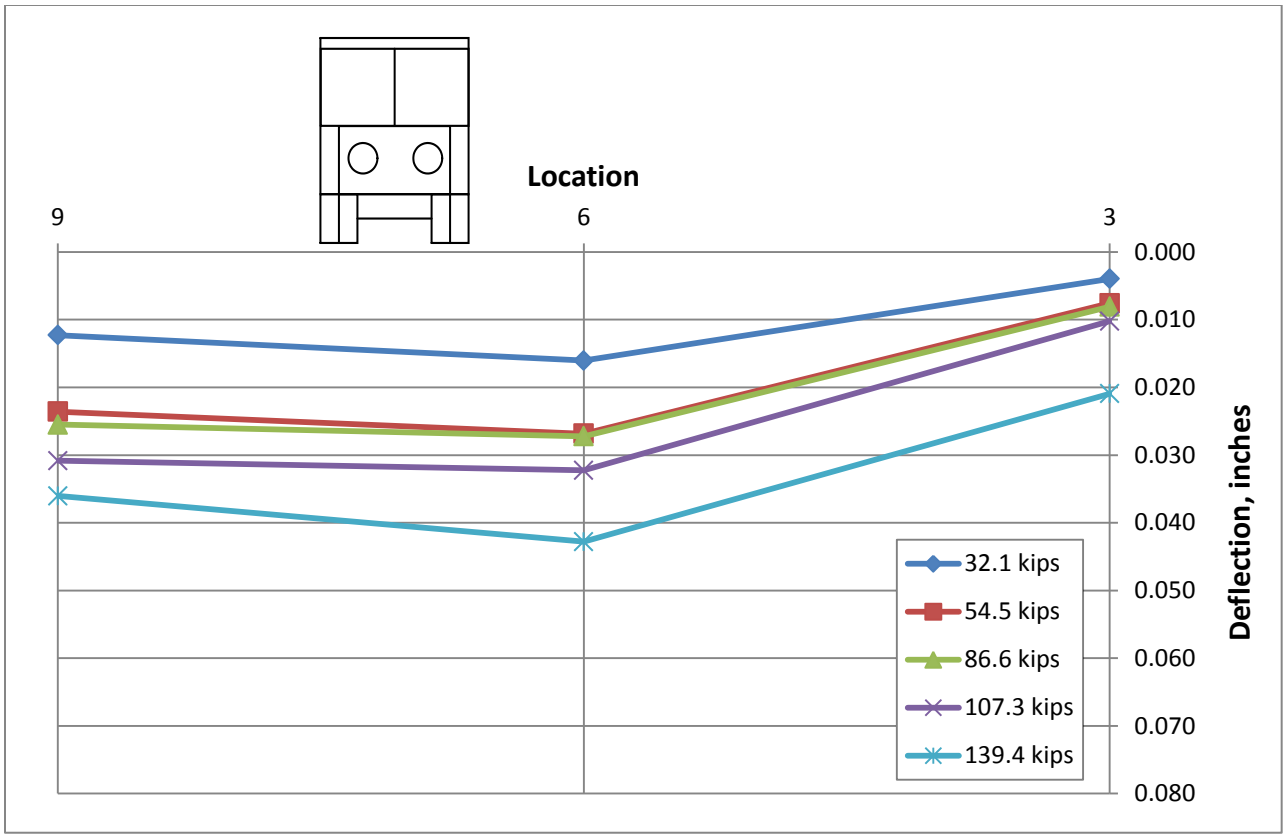

Figure 5-23. Depot St. Bridge North Quarter Point Load Distribution (Load in D-S Lane)

Table 5-18. Depot St. North Quarter Point Load Distribution (Load in D-S Lane)

Run	Load	3	6	9
1	**32.1**	12.3%	49.7%	38.0%
3	**54.5**	13.1%	46.3%	40.7%
5	**86.6**	13.3%	44.8%	41.9%
7	**107.3**	13.9%	44.0%	42.1%
9	**139.4**	21.0%	42.9%	36.1%

From the plots, the transverse load distribution shows linear increases in deflection across the three arches with proximity to loading. The deflections also increase with respect to the magnitude each subsequent load case. Due to the absence of a deflectometer at location 1, the plot for the north quarter point displays the deflections for the center and downstream arches

only. The maximum downward deflections for each quarter point are 0.043 in. for the north, 0.080 in. for midspan, and 0.036 for the south. The north deflections are slightly larger than the south and the deflections are very similar to those from the Main Street Bridge with similar loading. This leads to the conclusion that the bridges have stiffnesses that closely match each other.

From the tables, the percentages represented the deflection of that arch compared to the total deflection of the three arches at that quarter point. The arches displayed consistent behavior throughout the span of the bridge. Generally, the downstream arch had between ten and twenty percent of the total deflection, the center arch contained between forty and fifty percent, while the upstream arch held between thirty and forty percent. For the deflections at the south quarter point, the percentages do not show a representation of the three arches and are therefore not accurate. However, it does show that the center arch had more deflection than the downstream arch at all loading increments.

In Figures 5-24, 5-25, and 5-26 the load distributions are plotted as the load is in the upstream lane. Tables 5-19, 5-20, and 5-21 show the percentages of each arch's deflection in comparison to the total of the three arches at that quarter point. Since sidewalks are located on each side of the bridge, the load is located symmetrically in each lane between the center and outside arches.

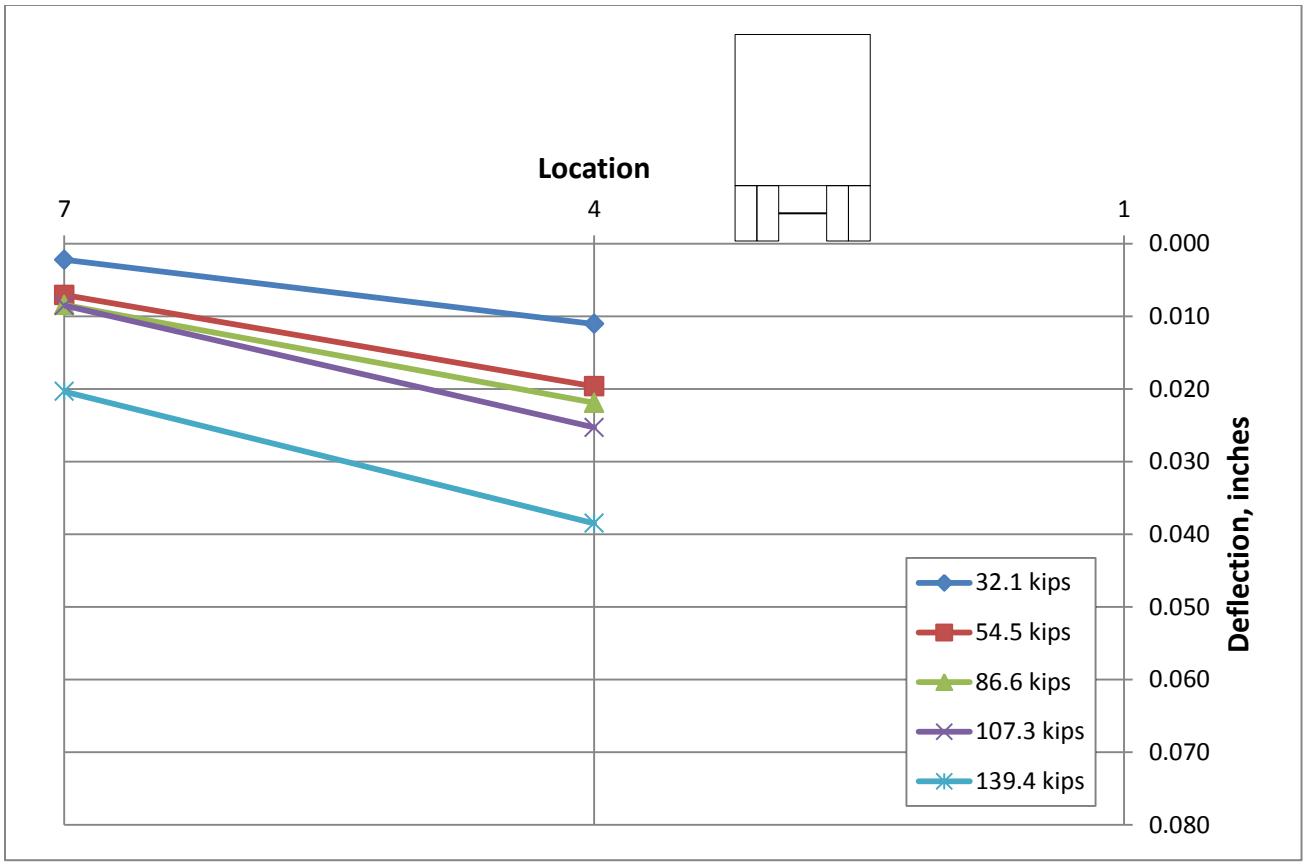

Figure 5-24. Depot St. Bridge South Quarter Point Load Distribution (Load in U-S Lane)

Table 5-19. Depot St. South Quarter Point Load Distribution (Load in U-S Lane)

Run	Load	4	7
2	**32.1**	83.3%	16.7%
4	**54.5**	73.6%	26.4%
6	**86.6**	72.2%	27.8%
8	**107.3**	74.8%	25.2%
10	**139.4**	65.4%	34.6%

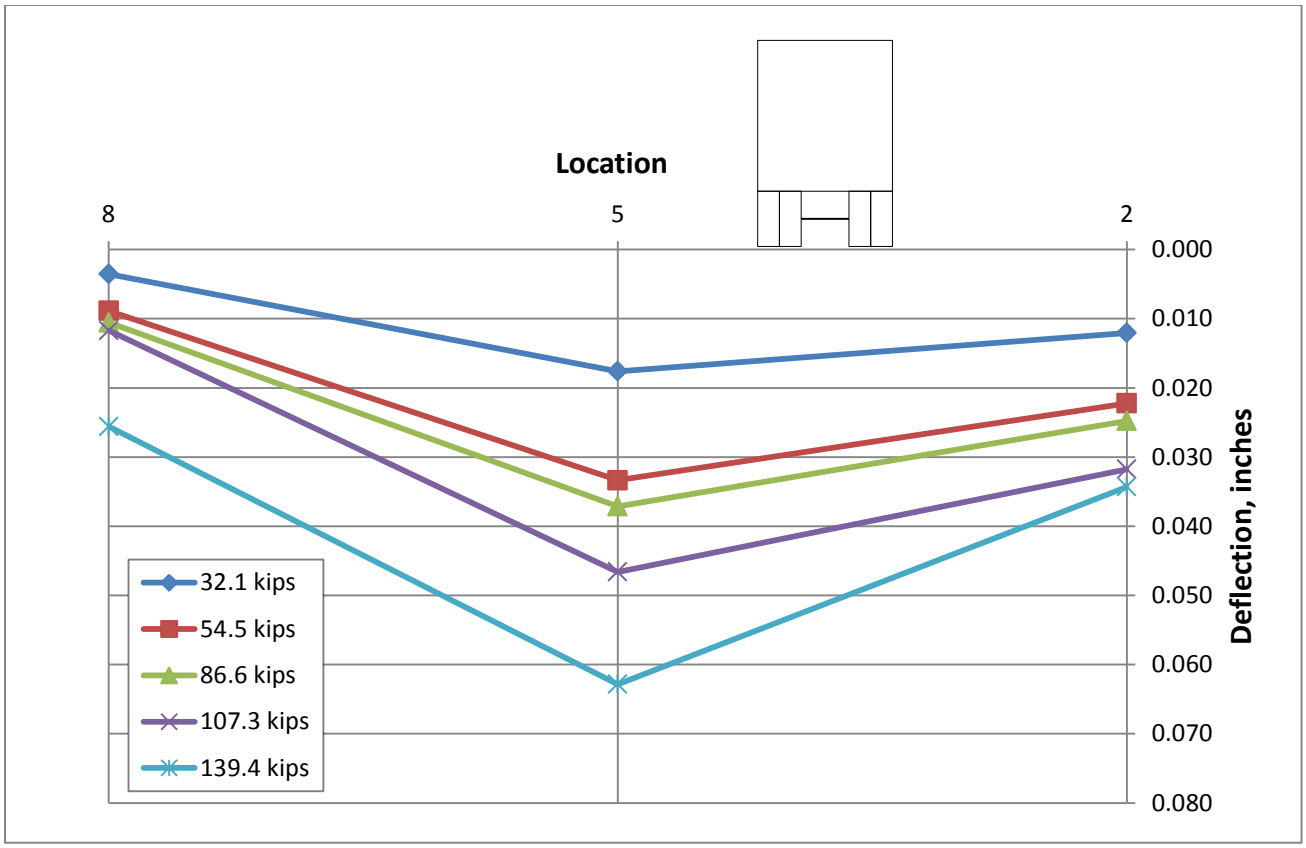

Figure 5-25. Depot St. Bridge Midspan Load Distribution (Load in U-S Lane)

Table 5-20. Depot St. Midspan Load Distribution (Load in U-S Lane)

Run	Load	2	5	8
2	**32.1**	36.3%	53.0%	10.7%
4	**54.5**	34.5%	51.7%	13.8%
6	**86.6**	34.2%	51.2%	14.6%
8	**107.3**	35.3%	51.8%	13.0%
10	**139.4**	28.0%	51.2%	20.8%

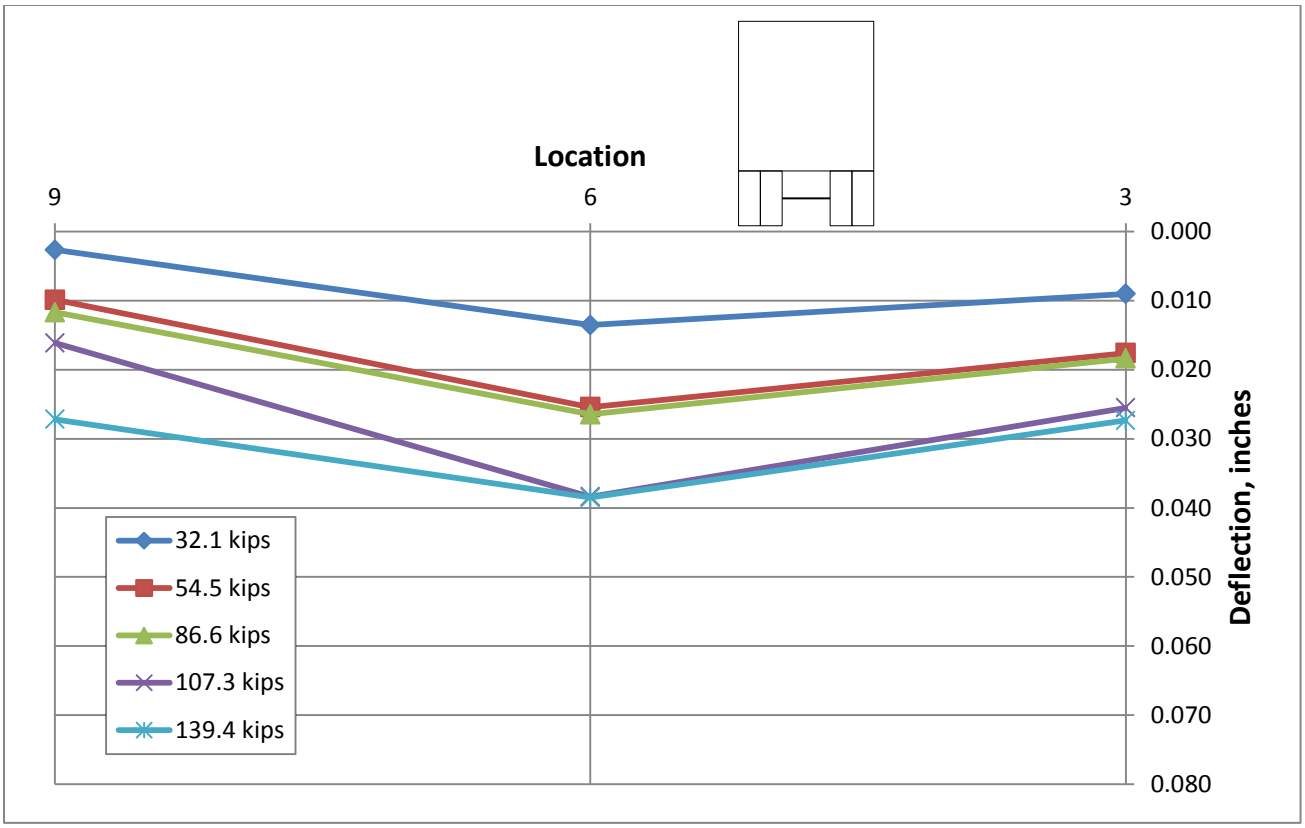

Figure 5-26. Depot St. Bridge North Quarter Point Load Distribution (Load in U-S Lane)

Table 5-21. Depot St. North Quarter Point Load Distribution (Load in U-S Lane)

Run	Load	3	6	9
2	**32.1**	35.8%	53.8%	10.4%
4	**54.5**	33.3%	48.1%	18.7%
6	**86.6**	32.5%	46.8%	20.7%
8	**107.3**	31.9%	48.0%	20.2%
10	**139.4**	29.4%	41.4%	29.2%

The maximum downward deflections for each quarter point are 0.039 in. for the north, 0.063 in. for midspan, and 0.039 in. for the south. The arches displayed consistent distribution behavior throughout the span of the bridge. Generally, the downstream arch had between ten and thirty percent of the total deflection, the center arch contained between forty and fifty percent,

while the upstream arch held between thirty and forty percent. For the deflections at the south quarter point, the percentages show that the center arch had more deflection than the downstream arch at all loading increments.

5.4 Finite Element Model Results

After developing the finite element models for each bridge, they were analyzed using the triple truck configuration from the live load test and the 72 kip rear tri-axle of a 150 kip coal truck. The coal truck rear tri-axle was analyzed by applying six, 12 kip tire point loads in the exact location at each quarter point utilized during live load testing. The rear tri-axle was oriented such that the middle axle of the three was directly over the quarter point. The layout of the tri-axle point loads for a typical quarter point is shown in Figure 5-27.

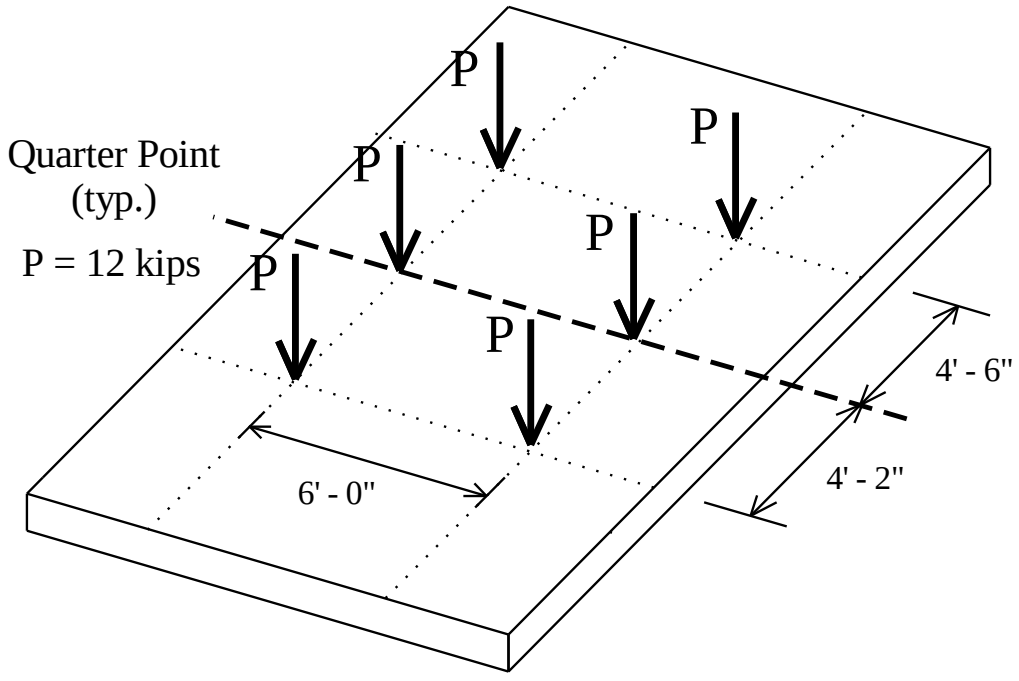

Figure 5-27. Coal Truck Rear Tri-Axle Model Loading Layout

The tri-axle loading was applied at locations halfway between the midpsan and each quarter point to validate that the instrument positions represented the critical locations along the bridge span. By using these load cases and comparing the results, a conclusion could be drawn as to what size coal trucks were simulated with the triple truck configuration. This helped in determining the kind of real coal traffic loads the bridge experienced during testing and how the measured response could be used in the future to provide a load rating recommendation if needed. However, load rating the bridges was not in the scope of this study.

5.4.1 Validating Critical Loading Locations

Before comparing results between the model and tests, the coal truck rear tri-axle load will be considered as it is applied at five locations along the span. Figures 5-28, 5-29, and 5-30 represent the Depot Street upstream arch deflections while the rear tri-axle load is placed in the upstream lane at the north quarter point, north three-eighths point, and midpsan, respectively. In each plot, the deformed arch shape is superimposed over the undeformed shape. In addition, measured vertical deflections from the three-vehicle load tests are included as discrete points. The deflections from the models and the tests were magnified by a thousand times to present a visual plot that could be read more easily.

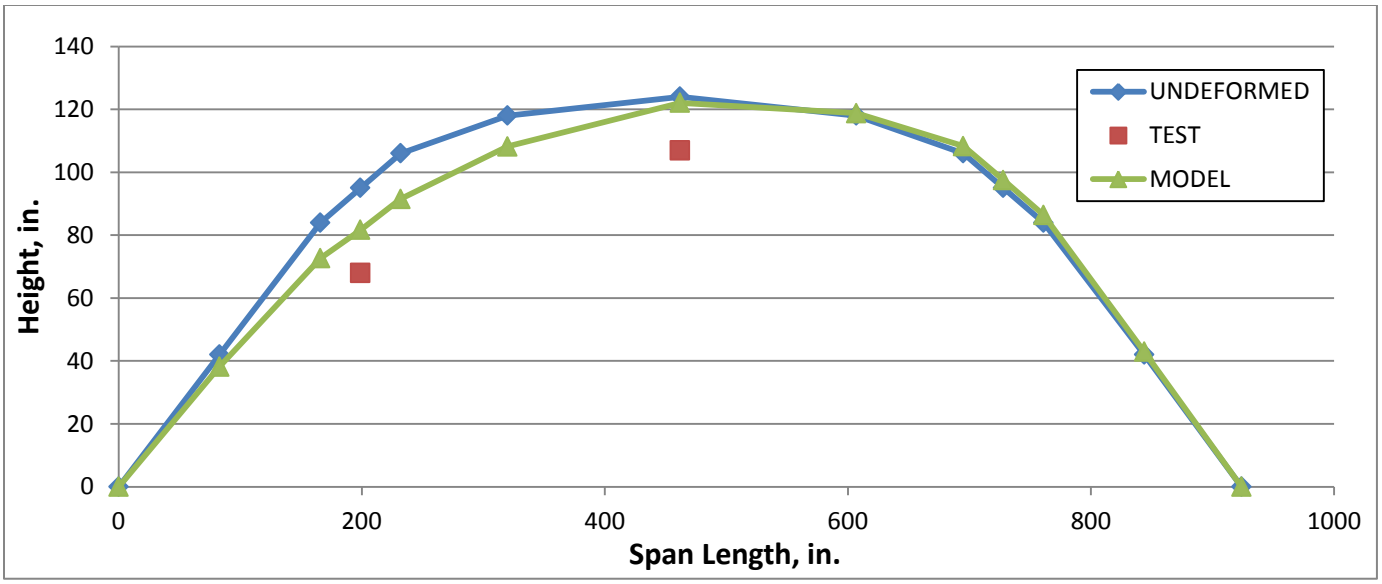

Figure 5-28. Depot St. U-S Arch Deflection (Load over North Quarter Pt.)

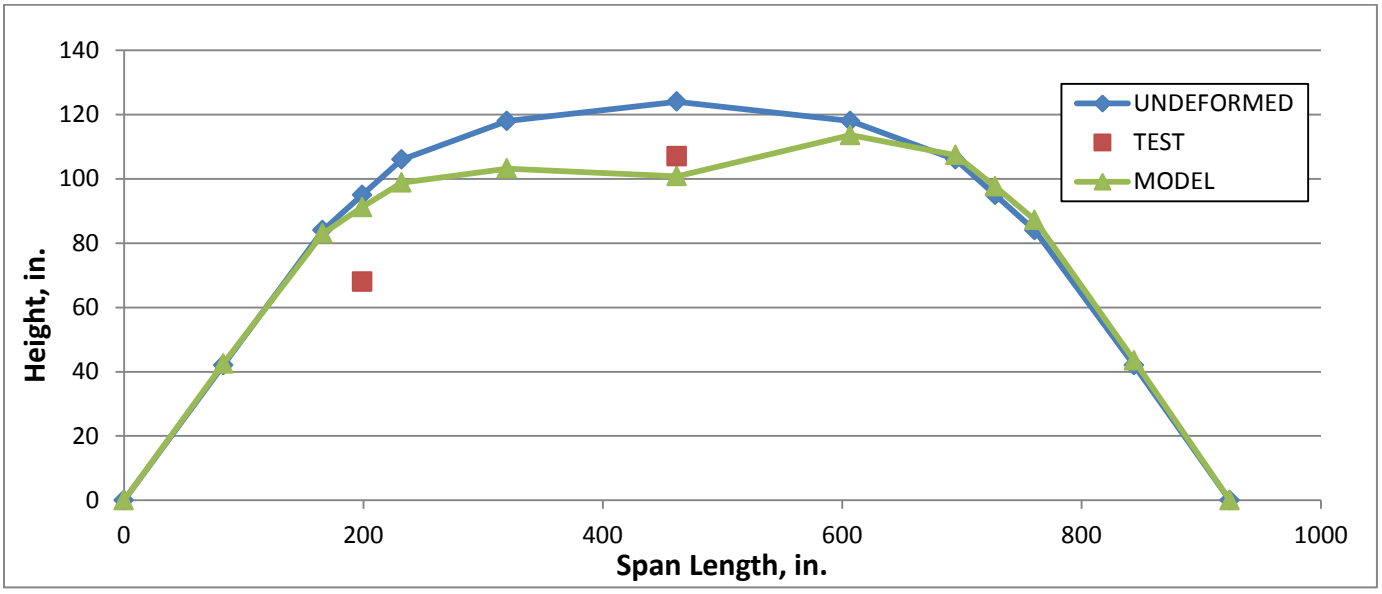

Figure 5-29. Depot St. U-S Arch Deflection (Load between North Quarter Pt. and Midspan)

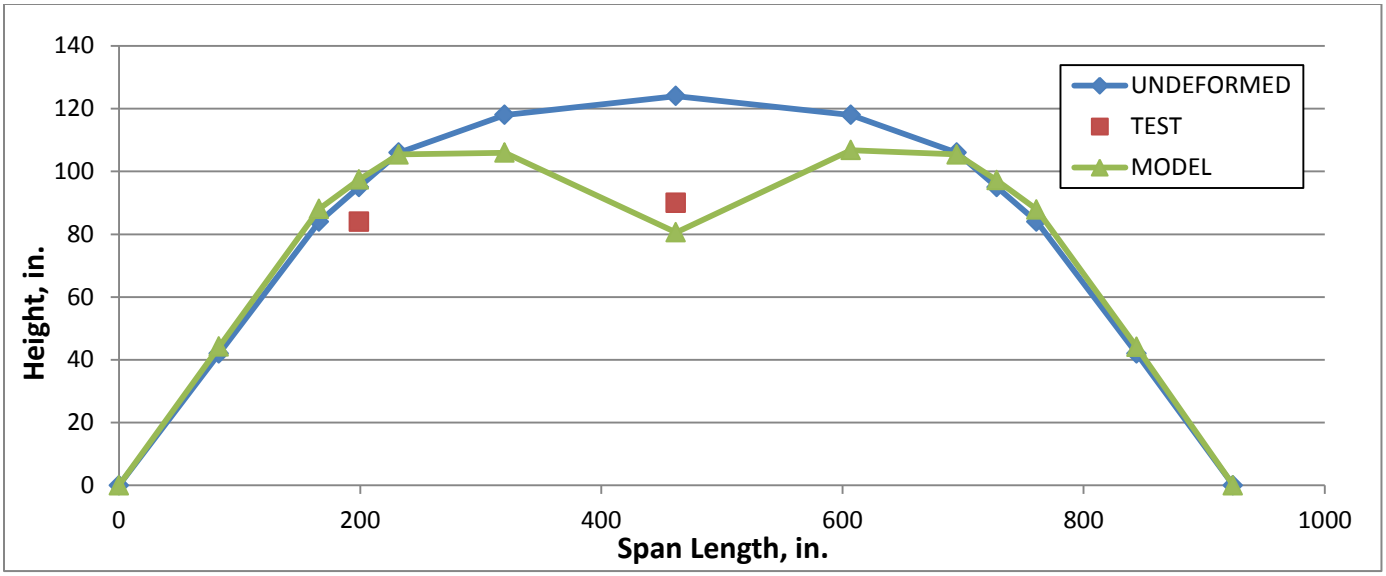

Figure 5-30. Depot St. U-S Arch Deflection (Load over Midspan)

From the plots of the arch deflection shape it is shown that placing the load halfway between the quarter point and the midspan does not create a critical deflection. The deflections experienced when the load was placed at the north three-eighths point were 0.004 at the north quarter point and 0.023 in. at midspan as shown in Figure 5-29. These values do not exceed the 0.013 in. deflection seen at the quarter point in Figure 5-28 or the 0.043 in. deflection at midspan as shown in Figure 5-30. This trend was repeated for other loadings at points between midspan and quarter points in both bridges. Because of this it is reasonable to conclude that the quarter point loading locations used during the test were sufficient in capturing the critical data desired.

5.4.2 Depot St. Bridge Model Test Load Deflections

After analyzing the model with the triple truck configuration, it was important to compare the results to those from the live load tests. By doing this the accuracy of the model could be determined, affecting the validity of conclusions drawn from the model. The following plots show the comparison between the model and the live load test results for the Main Street and

Depot Street Bridges. The following Depot Street plots in Figures 5-31, 5-32, and 5-33 reflect the arch behavior when the loads are located directly over the south quarter point in the downstream lane.

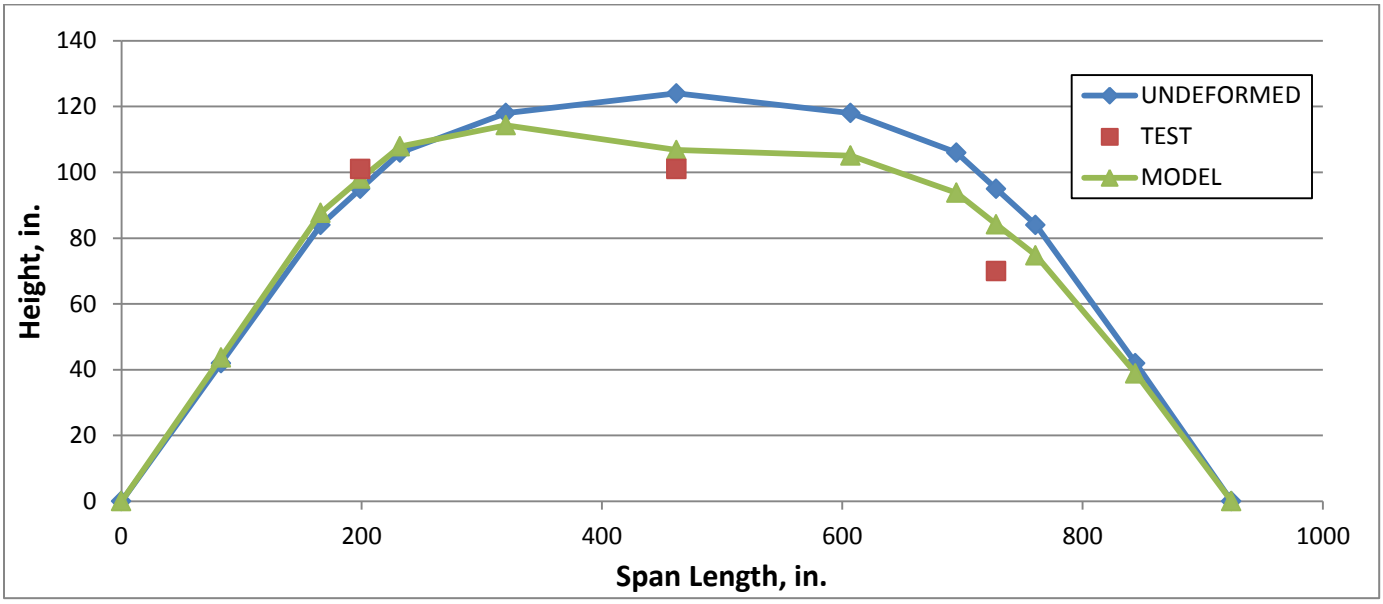

Figure 5-31. Depot St. Bridge Downstream Arch Deflection (Triple Truck Loading)

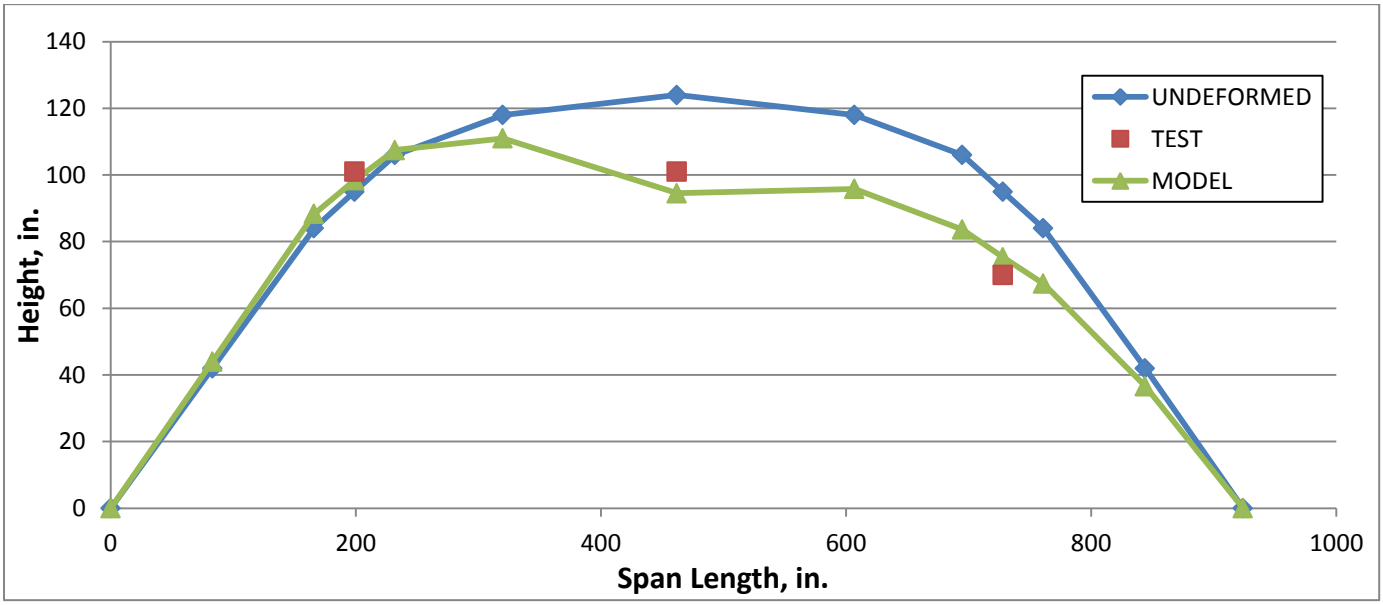

Figure 5-32. Depot St. Bridge Center Arch Deflection (Triple Truck Loading)

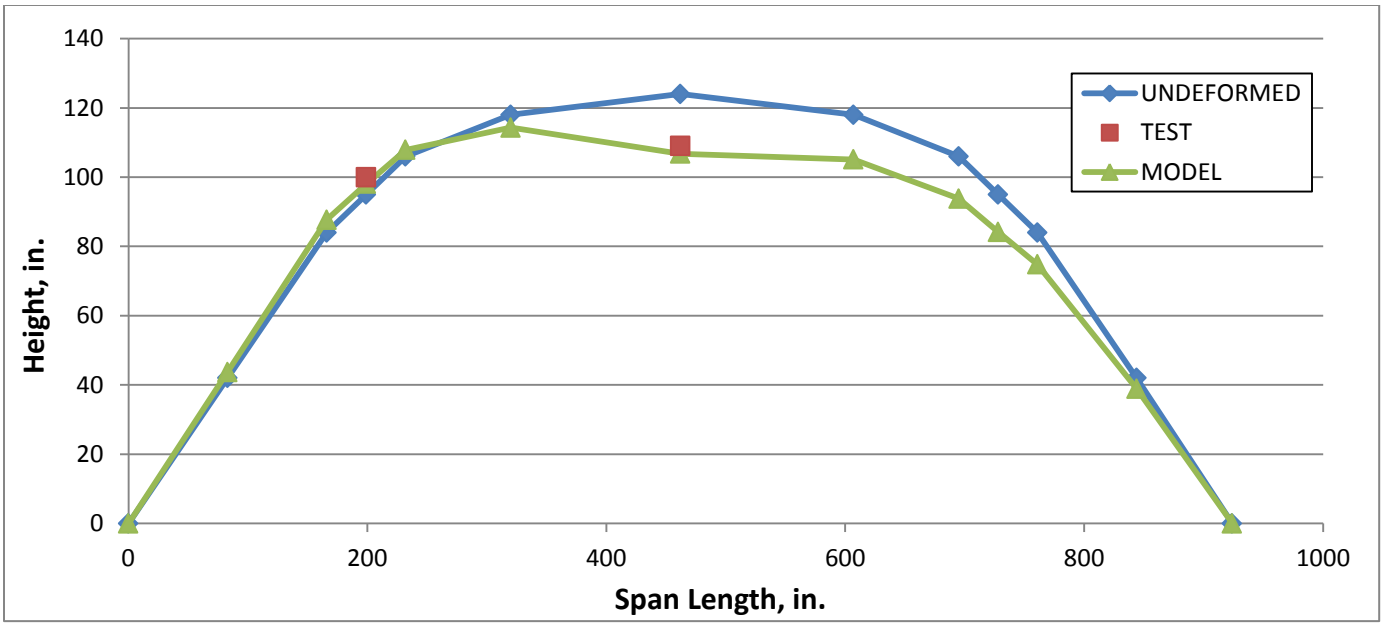

Figure 5-33. Depot St. Bridge Upstream Arch Deflection (Triple Truck Loading)

As shown in Figures 5-31, 5-32, and 5-33, the results obtained from the model match the arch shape from the live load tests. With the loading over the south quarter point, the deflections reflect expected arch behavior with downward deflection at the point of loading and midspan and slight uplift at the opposite quarter point. The deflection values as reported in Table 5-22 show that the results are within a reasonable range of each other, given the assumptions used in the model. This provides credibility to the model as an accurate representation of the actual arch behavior in the bridges. The maximum deflections recorded in these plots were found at midspan of the center arch with 0.040 in. from the live load test and 0.030 in. from the model. Given the small magnitude of the deflections seen in the live load test and the model, general accuracy of the global arch behavior is of more concern than individual deflection values matching precisely. It is interesting to note that the upstream and downstream arch deflections from the model closely match each other.

Table 5-22. Depot Street Model Arch Deflections (Triple Truck Loading)

Arch	Run	Quarter Point		
		North	Midspan	South
Upstream	Test	-0.005	0.015	N/A
	Model	-0.003	0.017	0.011
Center	Test	-0.011	0.040	0.038
	Model	-0.003	0.030	0.020
Downstream	Test	-0.006	0.023	0.025
	Model	-0.003	0.017	0.011

5.4.3 Main Street Model Test Load Deflections

For comparison of the Main Street Bridge deflections, the results from the triple truck loading at midspan in the downstream lane were used. Due to the traffic lane setup on the Main Street Bridge the loading in the downstream lane is located directly over the downstream arch rather than between arches. The deflected arch shapes for this loading are shown in Figures 5-34, 5-35, and 5-36.

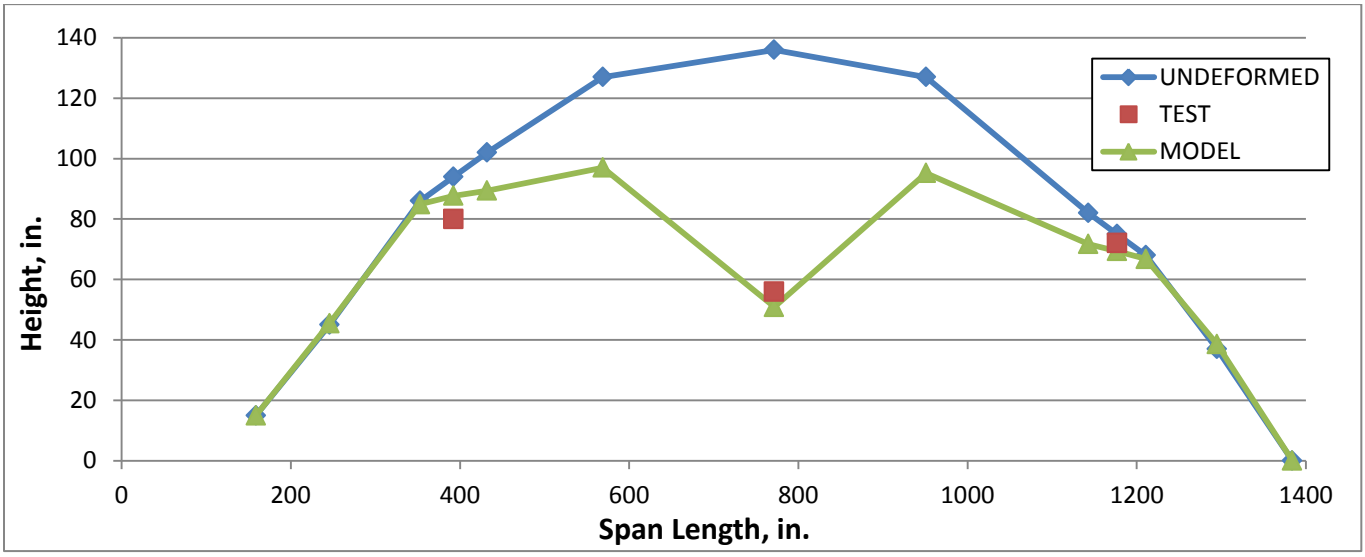

Figure 5-34. Main St. Bridge Downstream Arch Deflection (Triple Truck Loading)

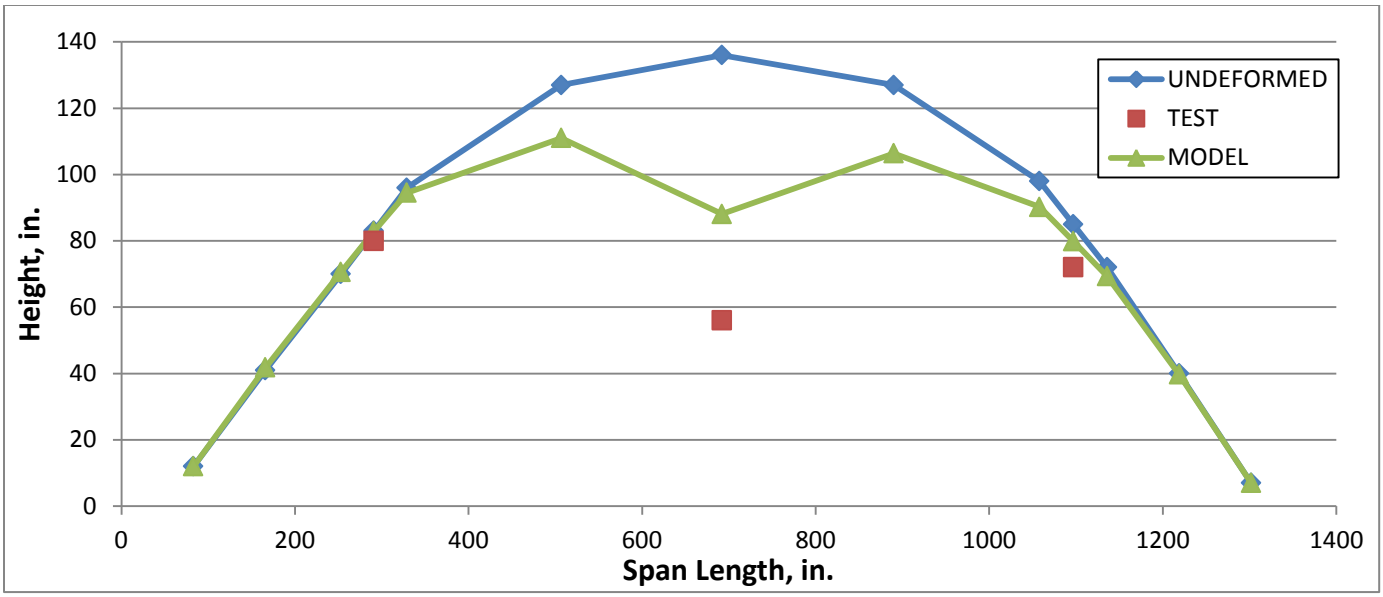

Figure 5-35. Main St. Bridge Center Arch Deflection (Triple Truck Loading)

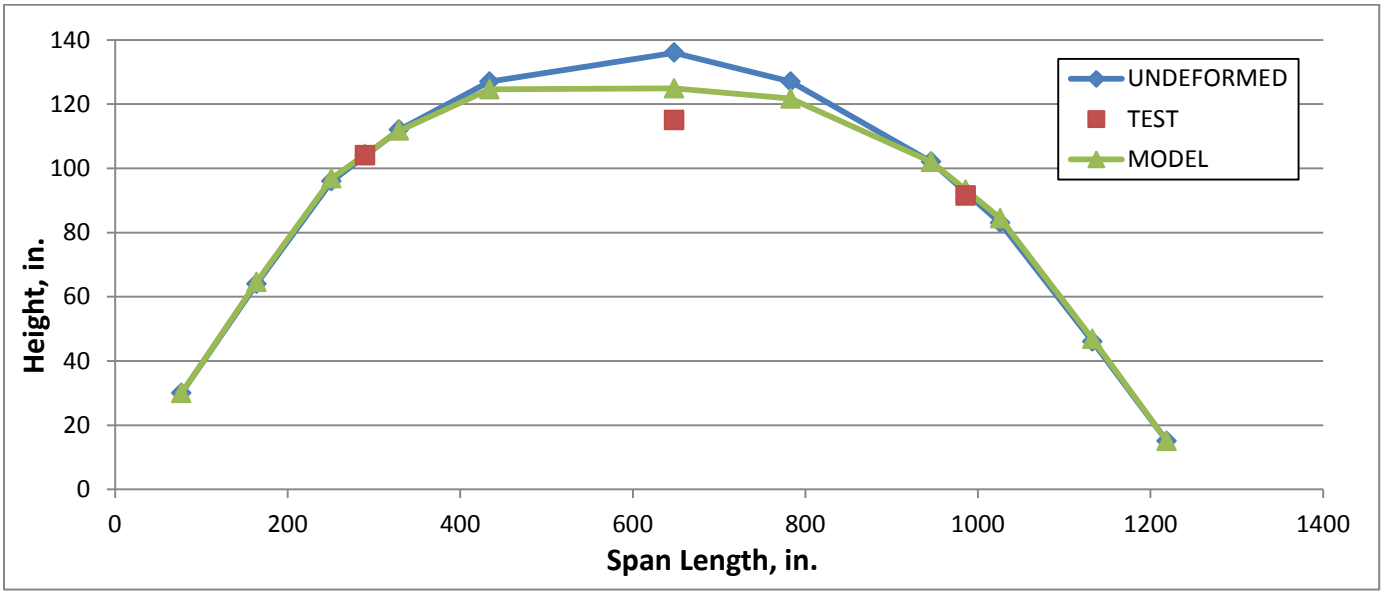

Figure 5-36. Main St. Bridge Upstream Arch Deflection (Triple Truck Loading)

From the plots it is shown that the downstream arch shows the most deflection with the center showing less and the upstream the least. The arch shapes follow the expected arch behavior from the loading at midspan with midspan experiencing the greatest downward

deflection and the other quarter points showing little downward deflection or uplift. Seeing the expected arch behavior helps demonstrate the bridge is still operating within a safe and serviceable condition. The results from the model follow the general deflected arch shapes seen in the tests and the arch deflection values are reported in Table 5-23. The maximum downward deflections were recorded at the loading location at midspan of the downstream arch. They were 0.080 in. for the live load test and 0.085 in. for the model simulation. The precision of these critical values provides further evidence that the model simulates the behavior of the real arches.

Table 5-23. Main Street Model Arch Deflections (Triple Truck Loading)

Arch		Quarter Point		
		North	Midspan	South
Upstream	Test	0.000	0.021	0.001
	Model	0.000	0.011	-0.001
Center	Test	0.002	0.056	0.006
	Model	0.000	0.048	0.005
Downstream	Test	0.014	0.080	0.003
	Model	0.006	0.085	0.006

5.4.4 Main Street Model Coal Truck Deflections

With the triple truck load from the tests meant to simulate the rear tri-axle of a coal truck, the models were analyzed with the actual tri-axle load recorded on weighed coal trucks. Six point loads of 12 kips each were placed in such a way that the middle axle was directly over the quarter point. The bridge model analysis was conducted for the tri-axle load at each quarter point and the deflection values recorded. The Main Street Bridge plots in Figures 5-37, 5-38, and 5-39 represent the deflected shapes when the tri-axle load was placed over the midspan of the upstream lane.

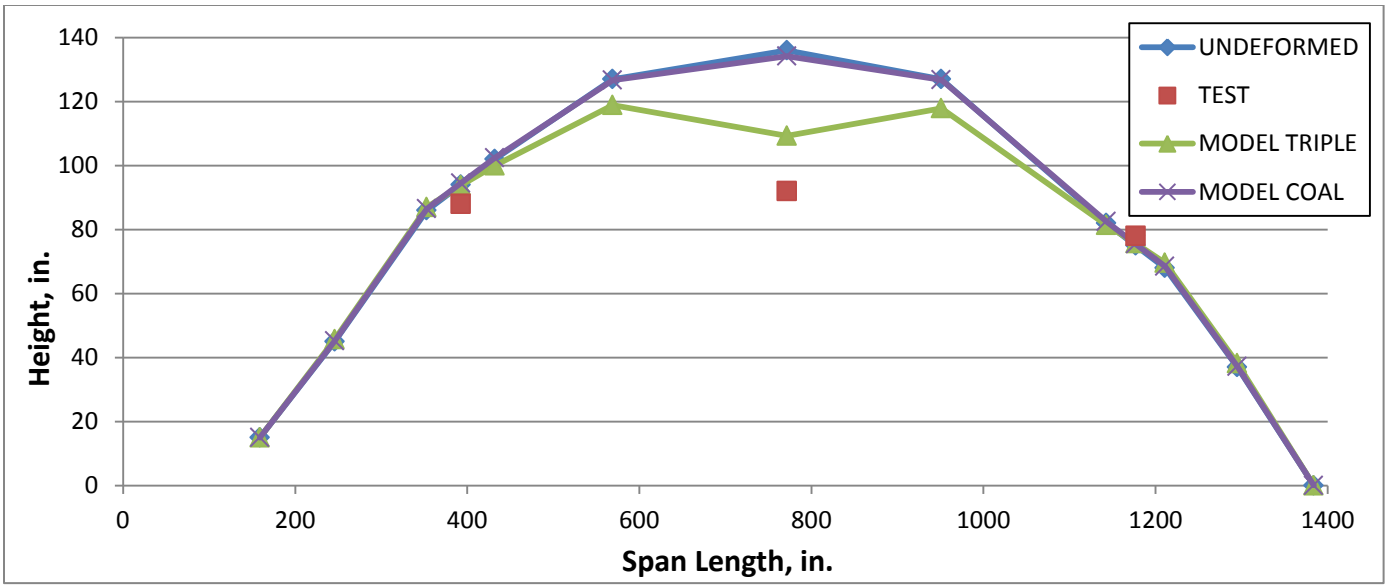

Figure 5-37. Main St. Bridge Downstream Arch Deflection (Triple Truck vs. Coal Tri-Axle)

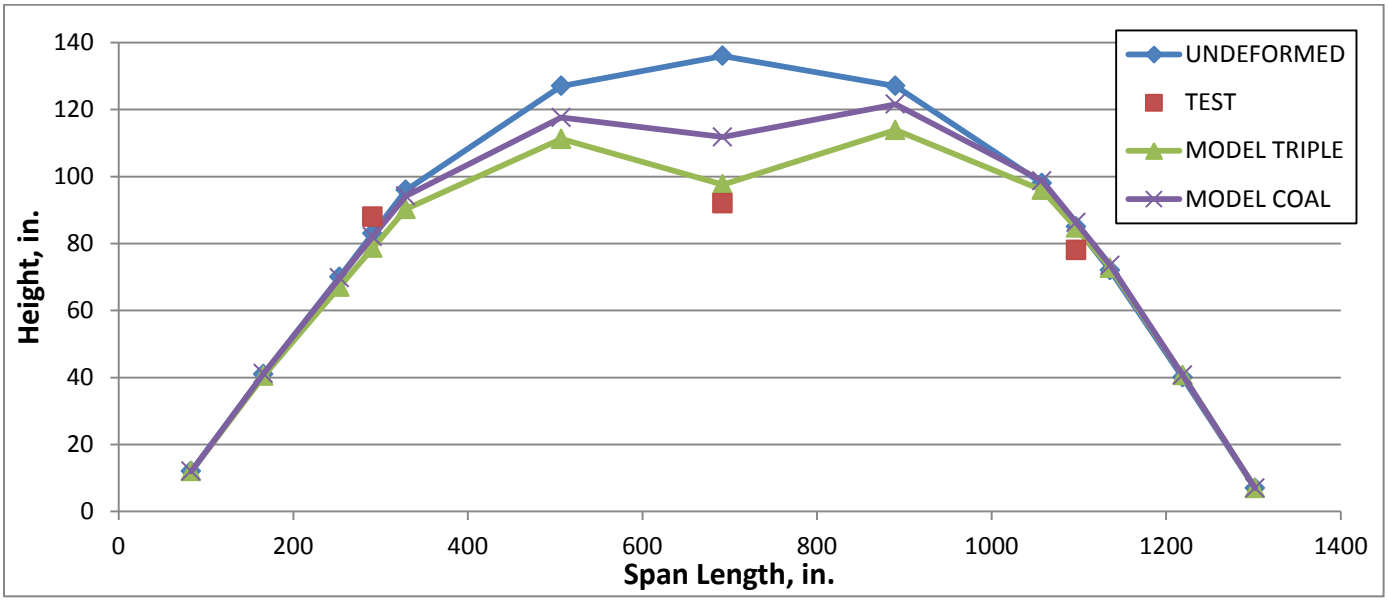

Figure 5-38. Main St. Bridge Center Arch Deflection (Triple Truck vs. Coal Tri-Axle)

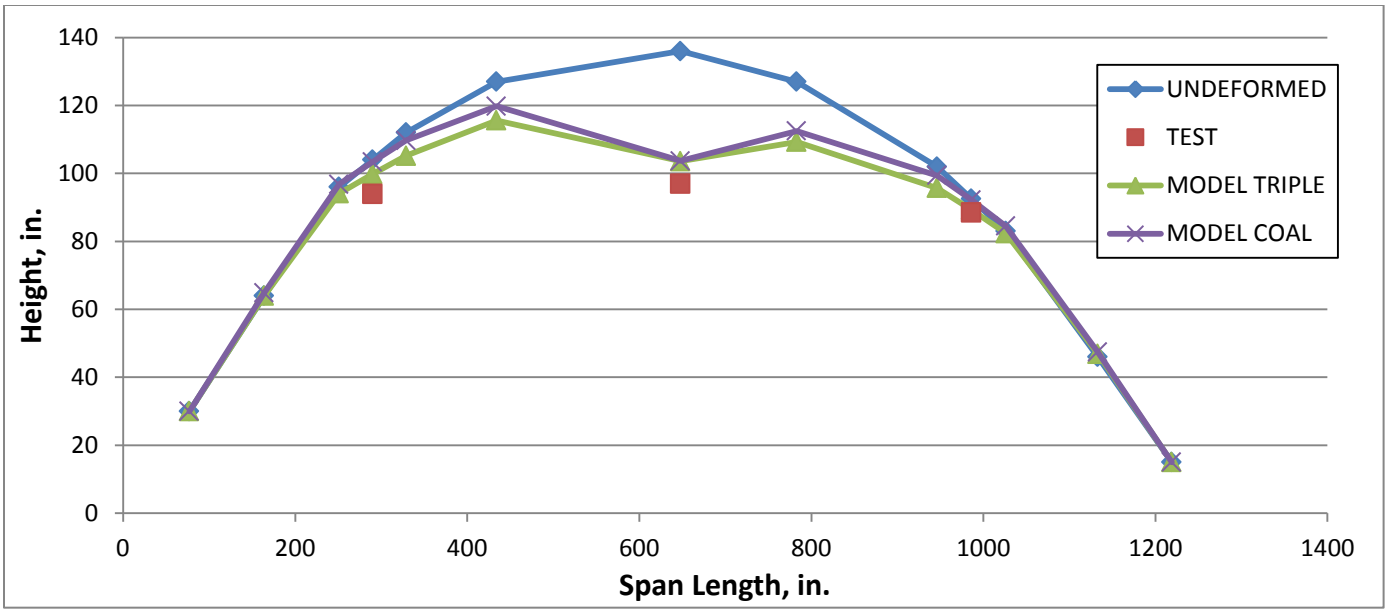

Figure 5-39. Main St. Bridge Upstream Arch Deflection (Triple Truck vs. Coal Tri-Axle)

As opposed to the triple truck configuration, the tri-axle load is not spread out over two lanes. Because of this localized placement there is less deflection in the arches not located directly below the load. This is shown in Figure 5-37 for the downstream arch where the tri-axle load causes a negligible amount of deflection when it is placed in the upstream lane. The center arch shows a reasonable amount of deflection and the upstream arch experiences the most deflection from the tri-axle load. This behavior follows what is expected from the placement of the tri-axle load in the model. The maximum downward deflection of 0.032 in. occurs at the location of the load at midspan in the upstream arch. The deflection results from the triple truck and tri-axle model analyses are compared in Table 5-24.

Table 5-24. Main Street Model Arch Deflections (Triple Truck vs. Coal Rear Tri-Axle)

Arch		Quarter Point		
		North	Midspan	South
Upstream	Triple	0.004	0.032	0.003
	Coal	0.001	0.032	0.000
Center	Triple	0.004	0.038	0.000
	Coal	0.001	0.024	-0.001
Downstream	Triple	0.000	0.027	-0.001
	Coal	-0.001	0.002	-0.001

Table 5-24 indicates that the coal rear tri-axle produces results that mimic the triple truck loading at midpsan of the upstream arch. The precision in the bridge response helps verify that the triple truck loading scenario used in the live load tests was a good representation for the rear tri-axle of a 150 kip coal truck.

5.4.5 Depot Street Model Coal Truck Deflections

The Depot Street Bridge was analyzed with the coal truck tri-axle load using the same method as the Main Street Bridge. The results of the tri-axle load at midspan in the upstream lane are shown in the plots in Figures 5-40, 5-41, and 5-42.

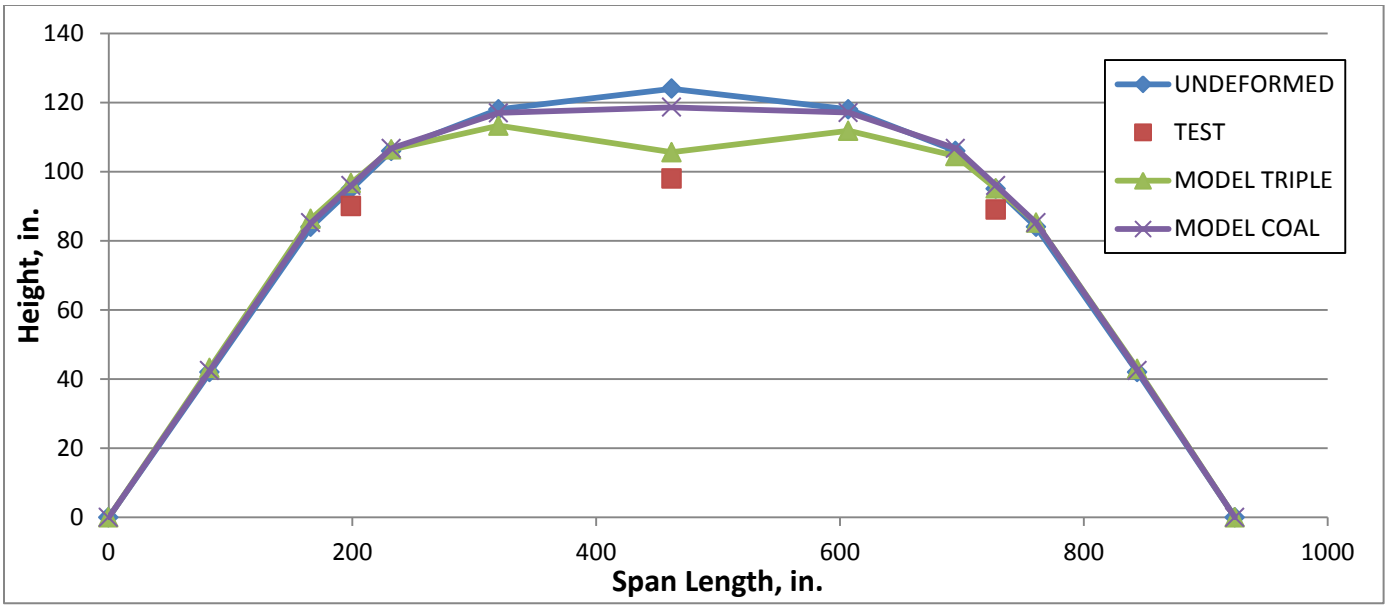

Figure 5-40. Depot St. Bridge Downstream Arch Deflection (Triple Truck vs. Coal Tri-Axle)

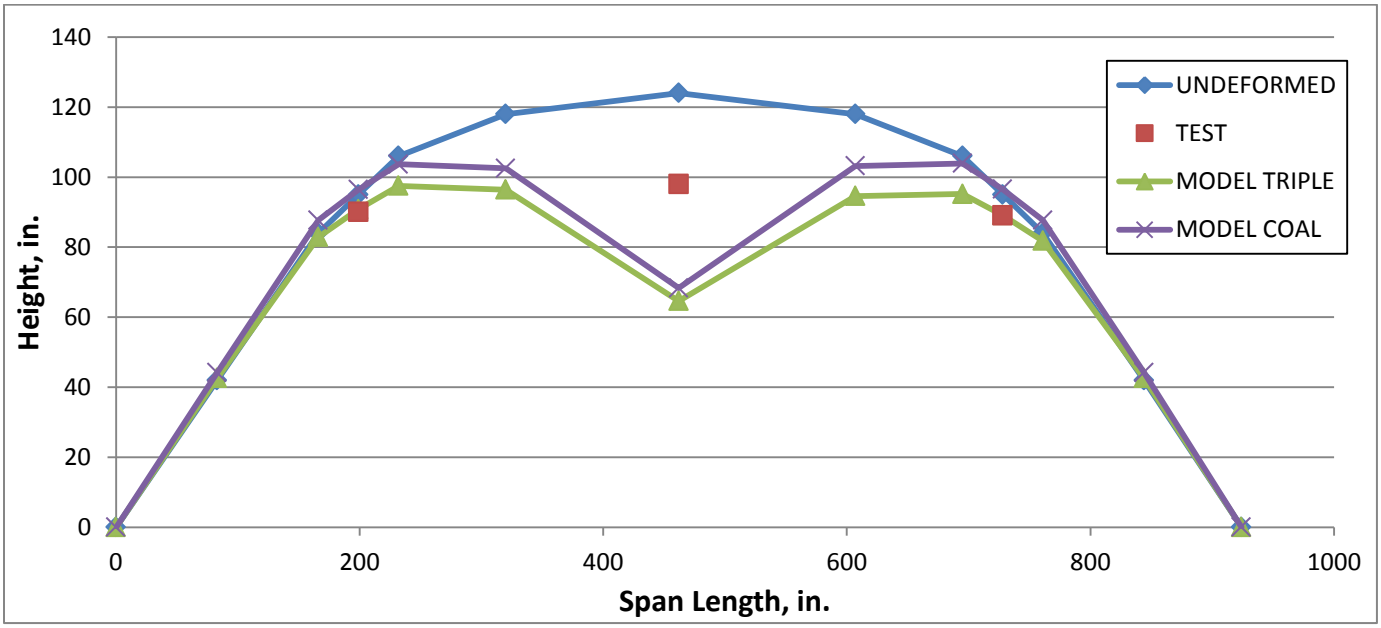

Figure 5-41. Depot St. Bridge Center Arch Deflection (Triple Truck vs. Coal Tri-Axle)

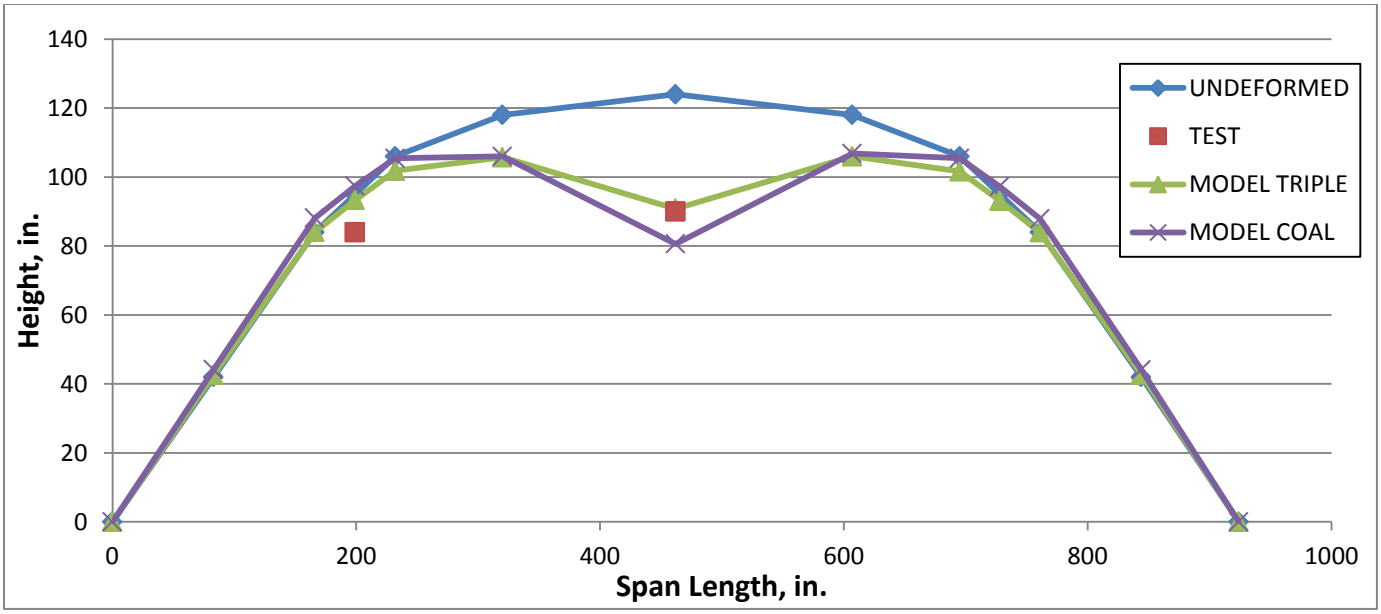

Figure 5-42. Depot St. Bridge Upstream Arch Deflection (Triple Truck vs. Coal Tri-Axle)

Due to the layout of traffic lanes on the Depot Street Bridge the loading is closer to the center arch than the outside arches. As expected, the plots show that the center arch experienced the most deflection with the arch opposite the loading showing a negligible amount. This was the case with the Main Street Bridge and shows that the model components located in close proximity to the load are affected greater than the components further away. The deflection values for comparison of the model loading scenarios are summarized in Table 5-25.

Table 5-25. Depot Street Model Arch Deflections (Triple Truck vs. Coal Rear Tri-Axle)

Arch		Quarter Point		
		North	Midspan	South
Upstream	Triple	0.002	0.033	0.002
	Coal	-0.002	0.043	-0.002
Center	Triple	0.004	0.059	0.006
	Coal	-0.001	0.056	-0.002
Downstream	Triple	-0.002	0.018	0.000
	Coal	-0.001	0.005	-0.001

Similar to the results seen in the Main Street Bridge model the tri-axle load is accurately represented by the triple truck configuration, especially at the critical location of maximum deflection at midspan of the center arch. The maximum deflection for the tri-axle load was 0.056 in. as compared to 0.059 in. for the triple truck configuration.

Overall when looking at the deflections from the models and live load tests, certain trends emerge. The midspan deflections, especially at critical locations came within a reasonable accuracy to conclude that the model acts similarly at midspan to the actual bridges. However the models consistently displayed less deflection than the live load tests at the north and south quarter points. This does not follow the usual trend with models as they are typically more flexible than the actual structure due to their idealization and difficulty in modeling small details that increase the stiffness of real structures. One such reason for these models being stiffer at their quarter points could be due to the complexity of the load path from the deck to the arch. A more detailed and refined model could eliminate these differences and produce more accurate results. However, since the deflections are small in magnitude and are the outer quarter points do not represent the majority of maximum deflections the model is an overall accurate representation of the global behavior of the arch bridges.

5.4.6 Main Street Model Strains

After analyzing the global behavior of the bridge through the deflection data, it is also important to look at how the model simulates local behavior by examining the strain in the arches. As discussed in Chapter 4, the model stresses were calculated using both internal axial forces and moments with the equation: $\sigma = P/A \pm M/Z$. The strains at the bottom, middle, and top of the arch were calculated and plotted alongside the strains from the live load tests for

comparison. The strain distribution for Location 1 (north quarter point of downstream arch) with the load directly overhead is shown below in Figure 5-43.

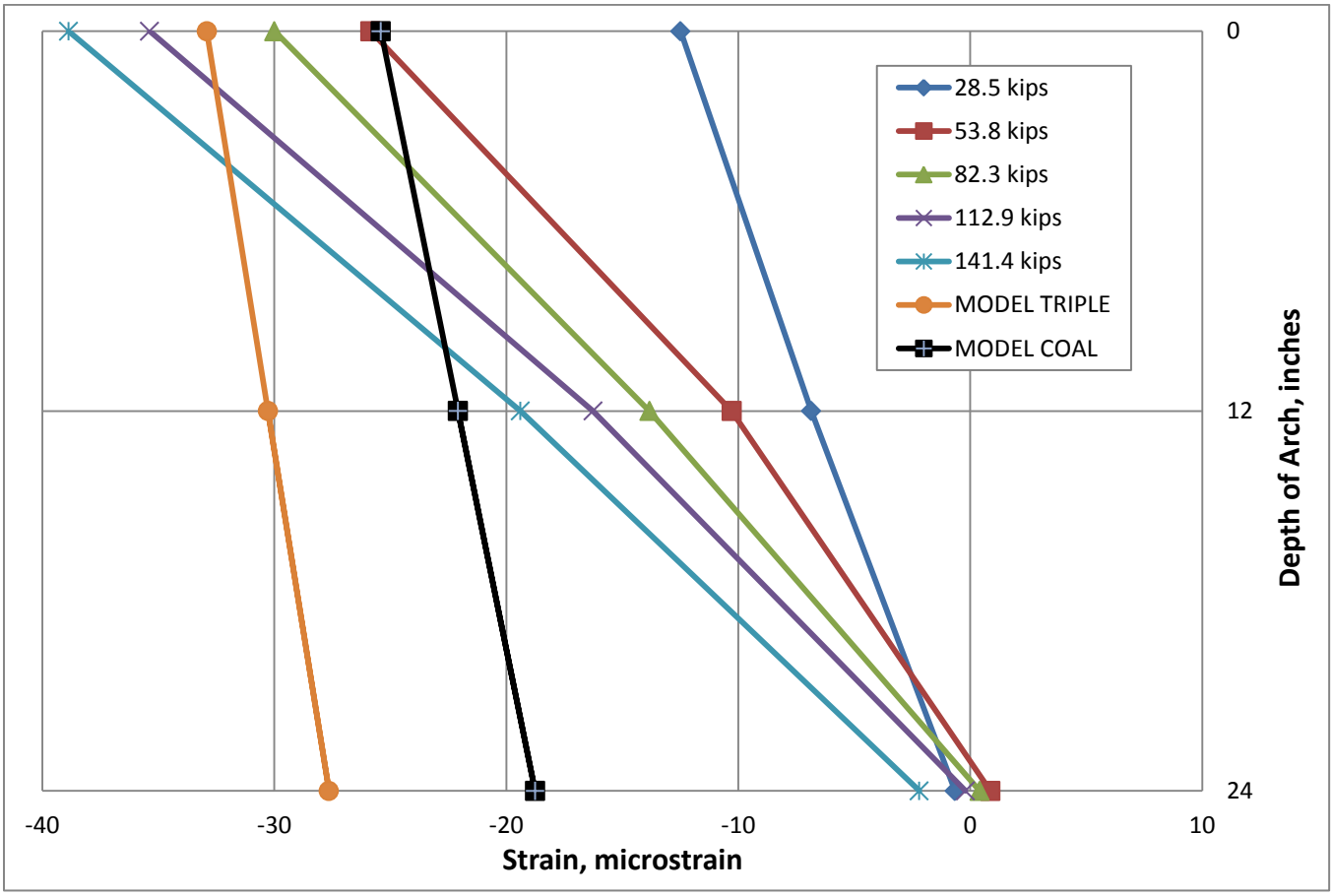

Figure 5-43. Main St. Model Location 1 Strain Distribution (Load over Location 1)

In Figure 5-43 model strains from the triple truck loading are shown with an orange trendline and model strains from the coal truck rear tri-axle are represented by a black trendline. The strains show maximum compressive strains at the top of the arch that approach those seen during live load testing but have much more compression in the bottom of the arch than shown by the live load tests. With the load directly over this location, it would be expected that large positive moments in the arch would be causing the bottom of the arch to experience tensile

bending stresses. This causes the arch to show strain distributions with large compressive strains at the top and negligible strains at the bottom as shown by the live load test distributions. However as seen from Figure 5-43, the model seems to be experiencing smaller bending moments in the arch than the live load tests, accounting for the difference in the distributions. The strain distributions at the Location 1 are shown again in Figure 5-44 with the load over Location 7 (opposite end of the bridge).

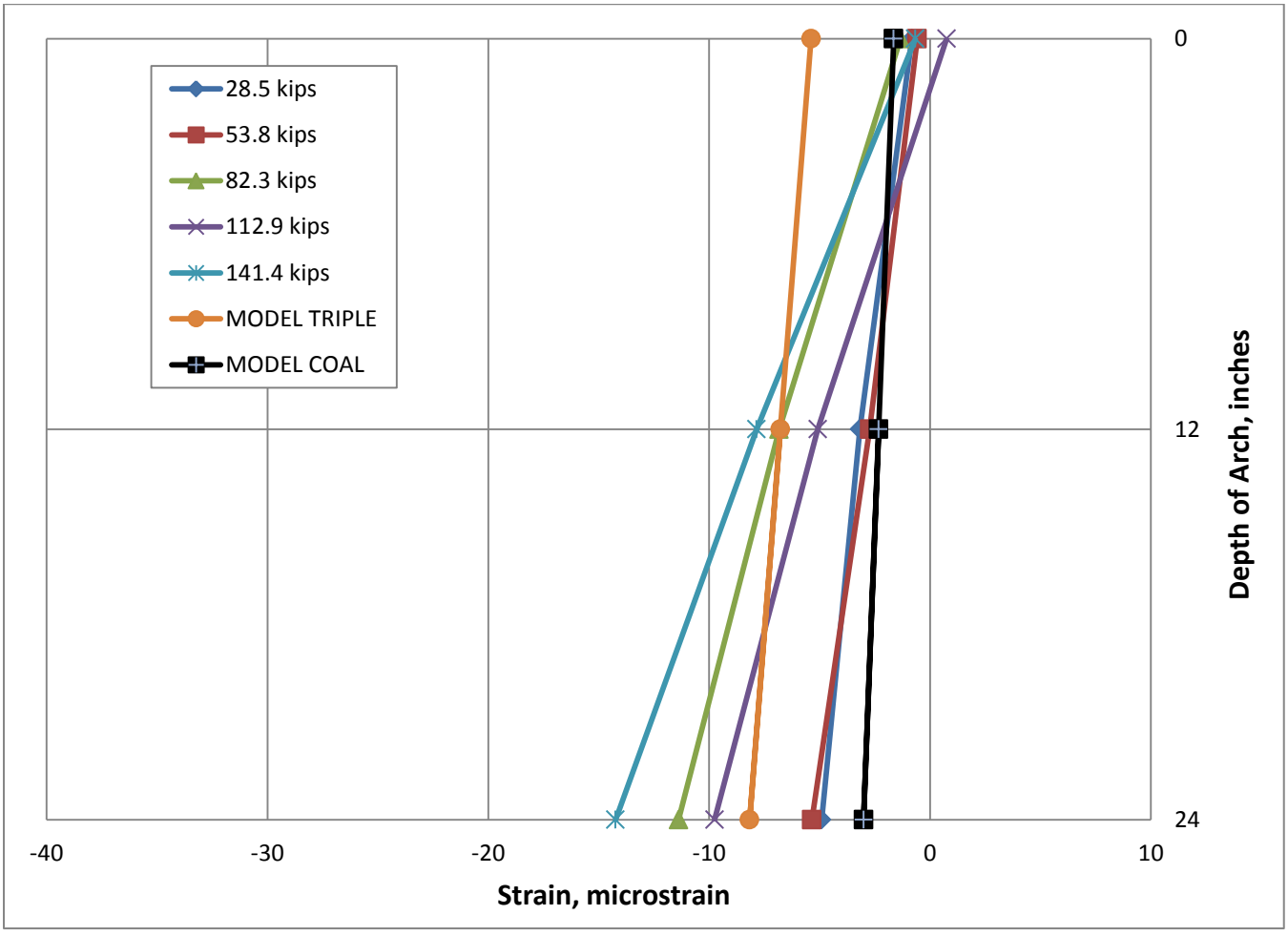

Figure 5-44. Main St. Model Location 1 Strain Distribution (Load over Location 7)

From Figure 5-44 the model strains follow the trend expected with the loading location. The model strain distributions show greater compression at the bottom than the top of the arch. This is the opposite of the behavior seen when the load was directly over Location 1. With such small strains shown in the distributions, the model provides a good representation of the local arch behavior in this scenario. The final strain distribution plot for Location 1 on the Main Street Bridge is shown in Figure 5-45 when the load is over Location 4 (midspan).

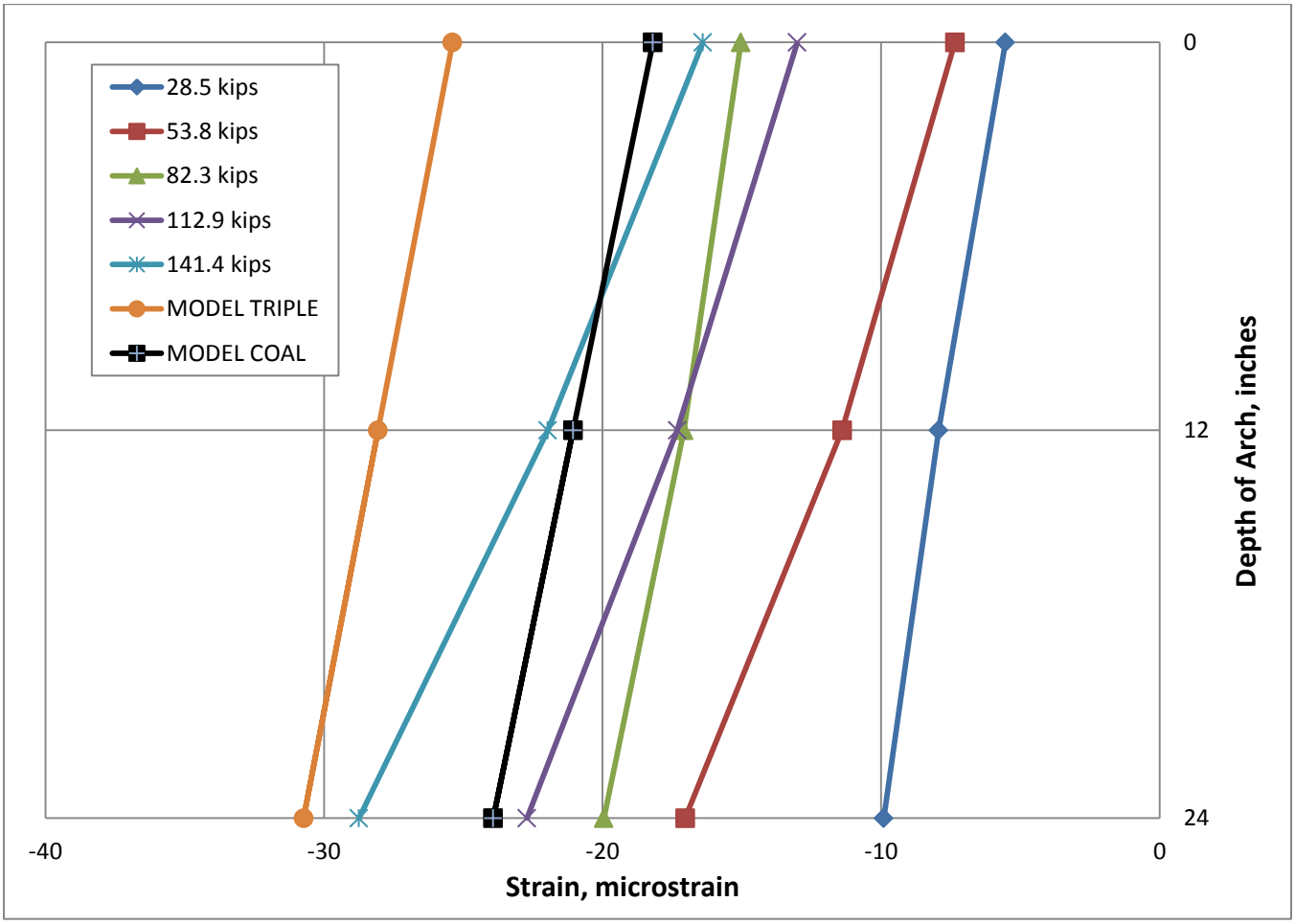

Figure 5-45. Main St. Model Location 1 Strain Distribution (Load over Location 4)

Figure 5-45 shows the strain distributions with compression throughout the depth of the arch. The model strains from the different loading scenarios both have maximum compressive

strains at the bottom of the arch which accurately portray the maximum strains seen with the heaviest loads from the live load tests. With the load at midspan, the gradient of the model strain distributions matches more closely with the live load test distributions, proving again that the model simulates local behavior of the arches well in certain situations.

After comparing model strains to live load strains for the three different loading locations, it can be seen that the maximum model strain values are within a reasonable range of those from the live load tests. The model strain distributions have less variance throughout the depth, leading to the conclusion that the bending stresses from the internal moments in the model are less than in the actual bridge with the live load tests. This is not of concern when assessing the validity of the model since the model is only a simple representation of the bridges. However, with a more refined model the local behavior may match more closely. It is worth noting that the model did produce linear strain distributions consistent with elastic behavior. This shows that, similar to the conclusions from the live load tests, the loads used on the models did not exceed the capacity of the bridge.

Further comparison between the live load arch strains and model arch strains for the Main Street Bridge are reported in Figures 5-46, 5-47, and 5-48. The positioning of the load in the downstream lane is showed in relation to the arches. Similar to the load distribution plots in Sections 5.2.3 and 5.3.3, each strain profile plot represents the strains recorded at each quarter point with the load directly over the respective location. Model and test strains in the plots represent strains from the bottom face of the arch.

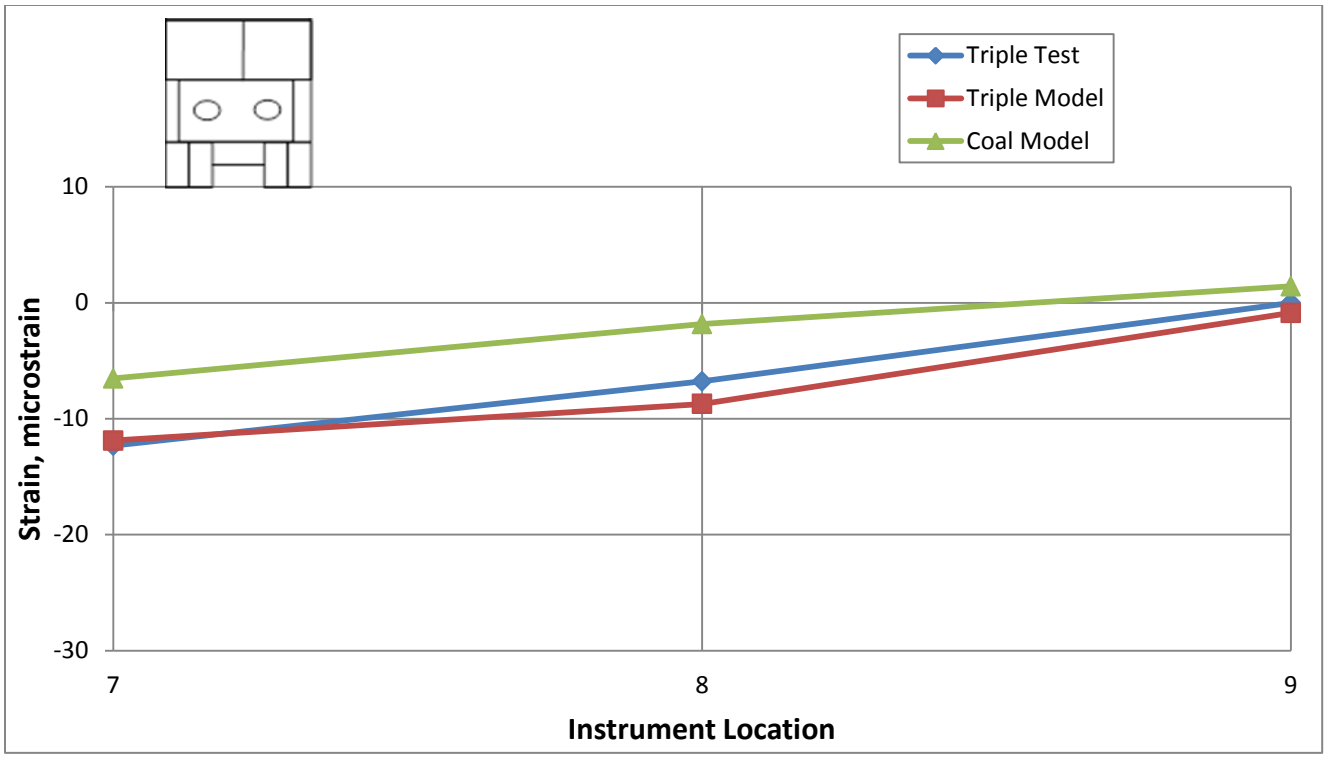

Figure 5-46. Main St. Bridge South Quarter Point Strain Profile (Load in D-S Lane)

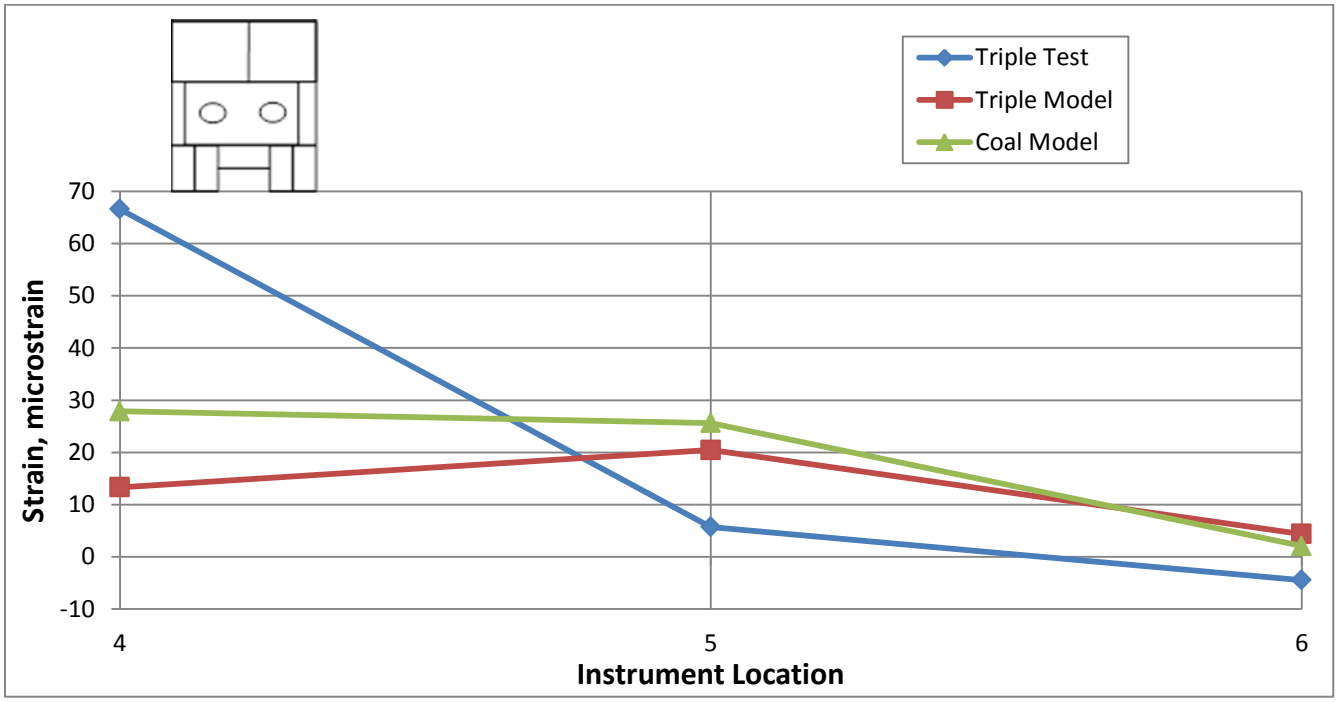

Figure 5-47. Main St. Bridge Midspan Strain Profile (Load in D-S Lane)

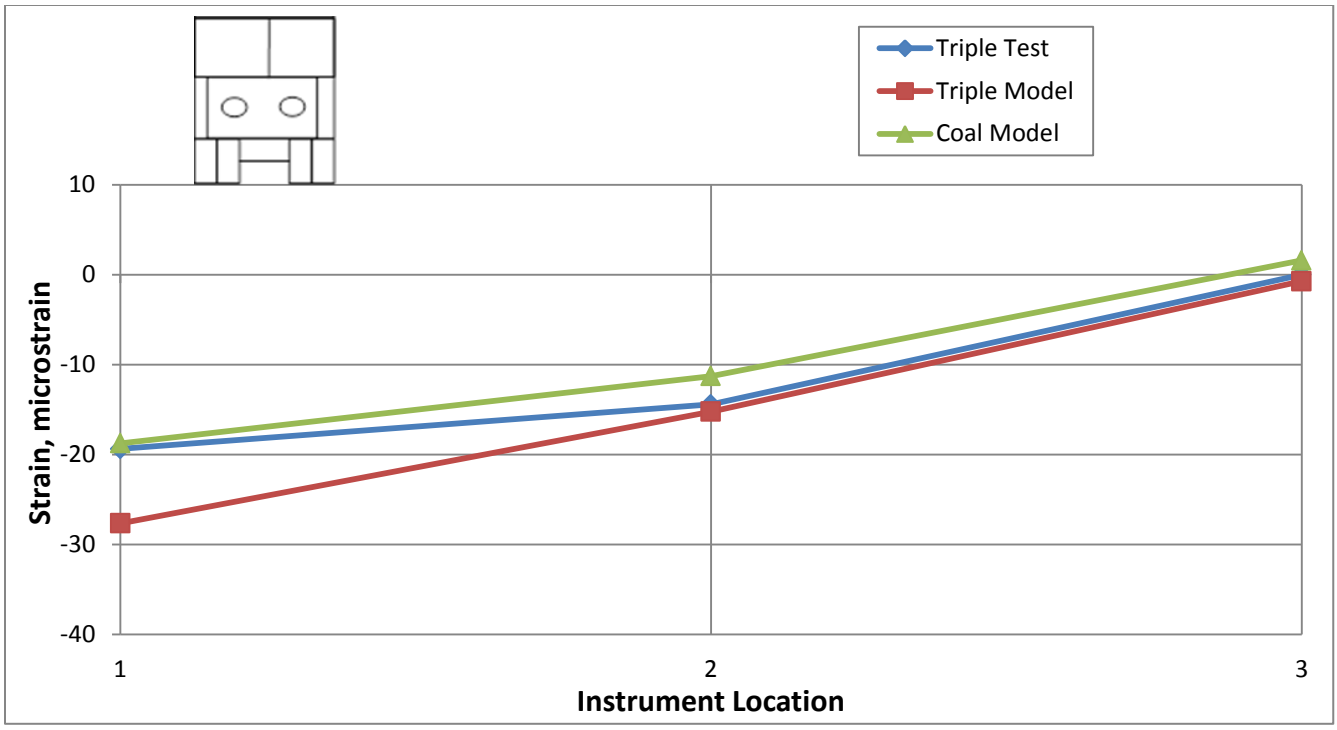

Figure 5-48. Main St. Bridge North Quarter Point Strain Profile (Load in D-S Lane)

The strains at the north and south quarter point locations in Figures 5-46 and 5-48 show expected arch behavior with the greatest compressive strain directly below the load and diminishing as the location becomes further from the load. The midspan strains show anomalous results with tensile arch strains ranging in magnitude across the arches. When comparing the results, the strains from the Main Street Bridge model are slightly larger than those from the live load tests. This trend indicates that the components of the bridge are more flexible than the actual bridge which conflicts with the trend shown in the deflection results. A possible explanation for this could be the setup of the model and how the load is transferred from the deck to the arch. Analyzing and refining the model further could produce more accurate model results.

5.4.7 Depot Street Model Strains

In the same manner as the Main Street Bridge, strains from the finite element model of the bridge were plotted next to the strains from the live load tests. Strain distribution plots through the arch depth and strain profiles at each quarter point were used for comparison. The strain distribution through the arch depth at Location 3 (north quarter point of upstream arch) with the load directly overhead is shown in Figure 5-49.

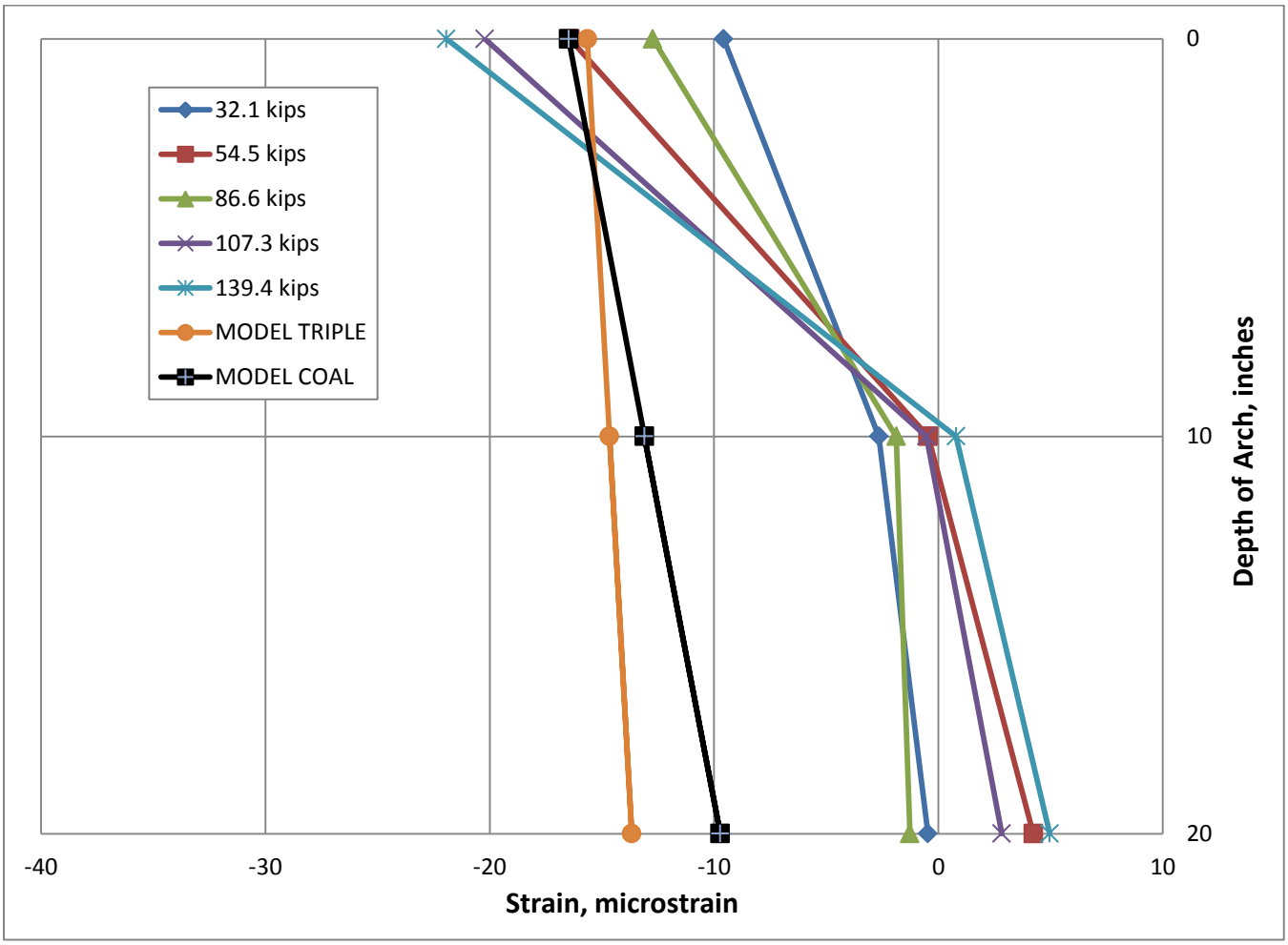

Figure 5-49. Depot St. Model Location 3 Strain Distribution (Load over Location 3)

Figure 5-49 shows the model strain distributions are very similar to those seen in Figure 5-43 for the Main Street Bridge. The maximum model compressive strains at the top of the arch are within a few microstrain of those from the live load tests. Again the model strain distributions have less variance throughout the depth, showing more compressive strain at the bottom than the live load tests. As stated earlier, this is most likely due to less bending stress being produced in the model arches. Figure 5-50 shows the strain distributions at Location 3 when the load is at Location 1 (opposite end of the bridge).

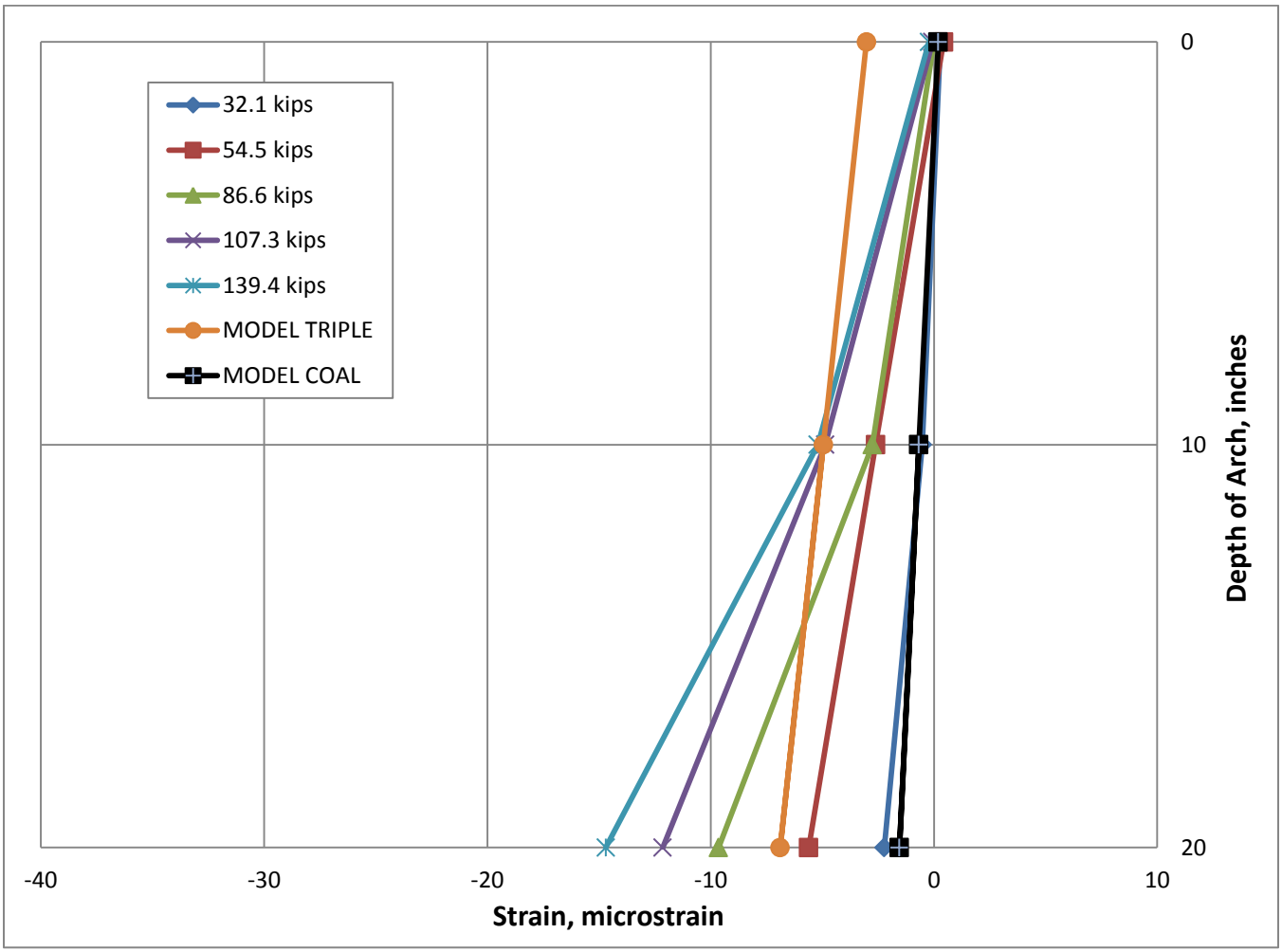

Figure 5-50. Depot St. Model Location 3 Strain Distribution (Load over Location 1)

Figure 5-50 is similar to the plot shown in Figure 5-44 for the Main Street Bridge. The model strain distributions show a better representation of the live load strain throughout the entire depth. The linear behavior with the compression at the bottom of the arch also matches expected behavior as uplift is expected at Location 3 with the load at the opposite end of the bridge. Even though the model strains are less than the live load strains for comparable loading, the strains are small enough that this is not of concern. The final strain distribution plot for Location 3 is shown in Figure 5-51 when the load is at Location 2 (midspan).

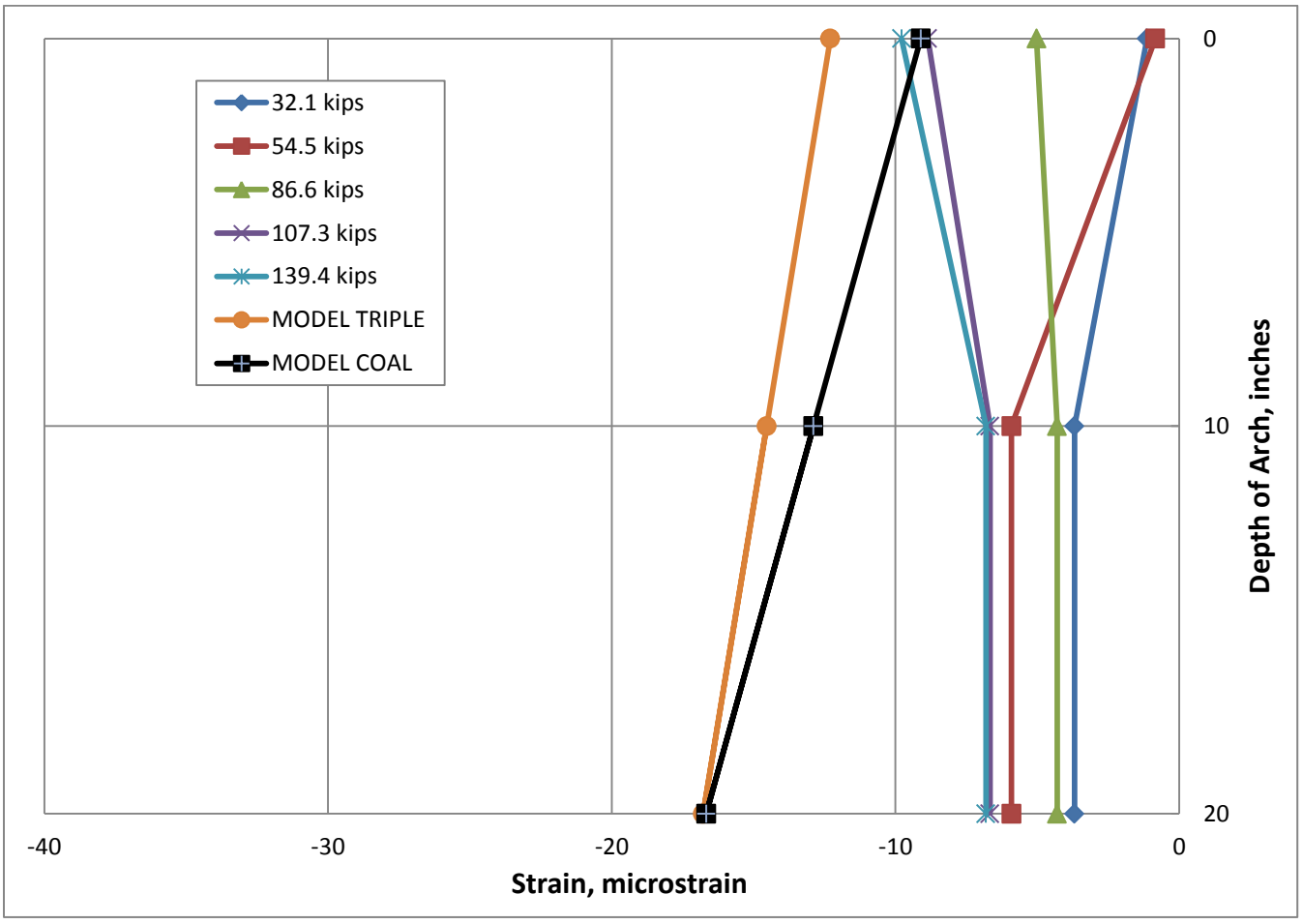

Figure 5-51. Depot St. Model Location 3 Strain Distribution (Load over Location 2)

In Figure 5-51, the model strain distributions match the same behavior as seen in Figure 5-45 for the Main Street Bridge. However in Figure 5-51 the live load strain distributions are not following the expected linear strain behavior. Instead of showing the expected compressive arch behavior as seen in the model strain distributions, the live load distributions are sporadic at the top with small amounts of compression throughout the depth.

After comparing model strains to live load strains for the three different loading locations, it can be seen that the maximum model strain values are within a reasonable range of those from the live load tests. The conclusion that the bending stresses from the internal moments in the model are less than in the actual bridge with the live load tests was drawn from the plots. This is not of concern when assessing the validity of the model since the model is only a simple representation of the bridges. However, with a more refined model the local behavior may match more closely. It is worth noting that the model did produce linear strain distributions consistent with elastic behavior. This shows that, similar to the conclusions from the live load tests, the loads used on the models did not exceed the capacity of the bridge. The strain distributions for the triple truck loading and the coal truck rear tri-axle matched more closely with the Depot Street Bridge model than the Main Street Bridge model. The reason for this is not certain but may have to do with the more symmetric profile of the Depot Street Bridge and the lack of skew across its span.

The following plots in Figures 5-52, 5-53, and 5-54 represent the strain comparisons between the live load tests and model for the Depot Street Bridge. Unlike the Main Street Bridge, these results are taken from the model with the loads located in the upstream lane of the bridge. Each quarter point is represented in the plots and the strains of each arch are compared for the triple truck loading and the coal truck rear tri-axle loading.

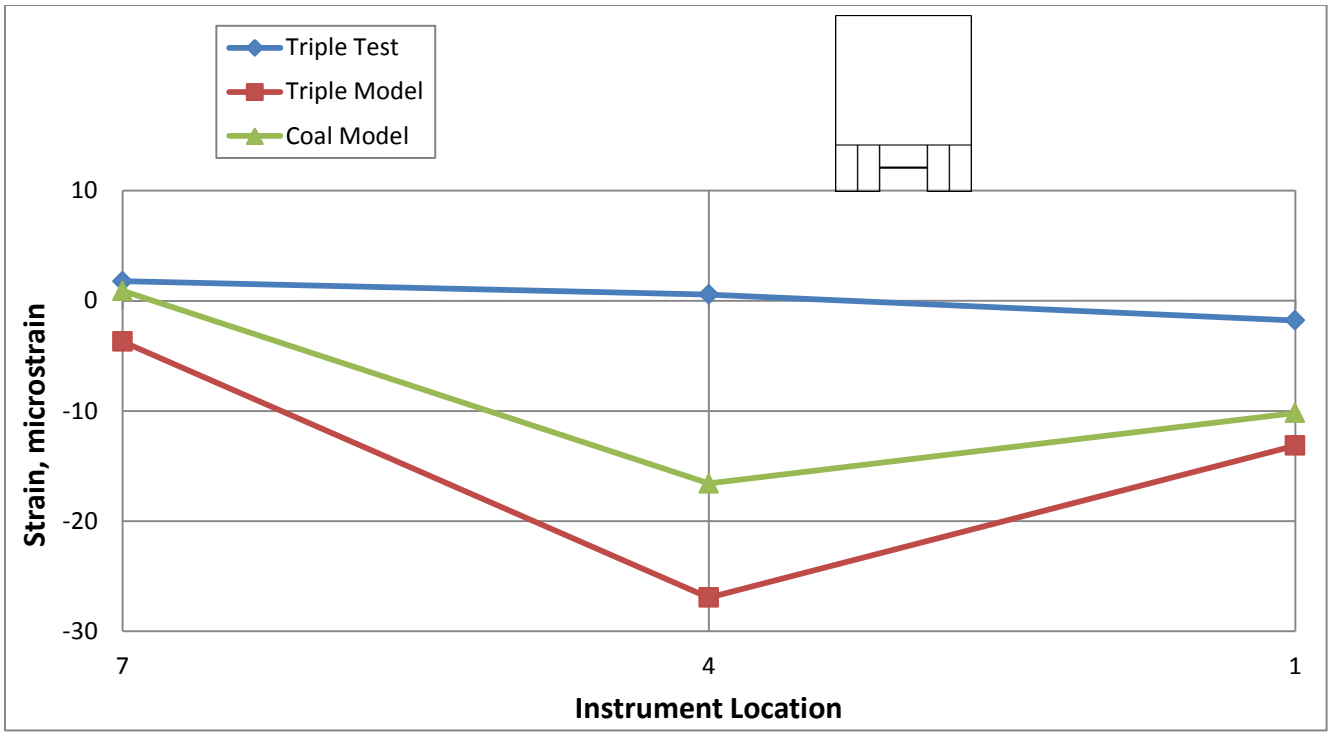

Figure 5-52. Depot St. Bridge South Quarter Point Strain Profile (Load in U-S Lane)

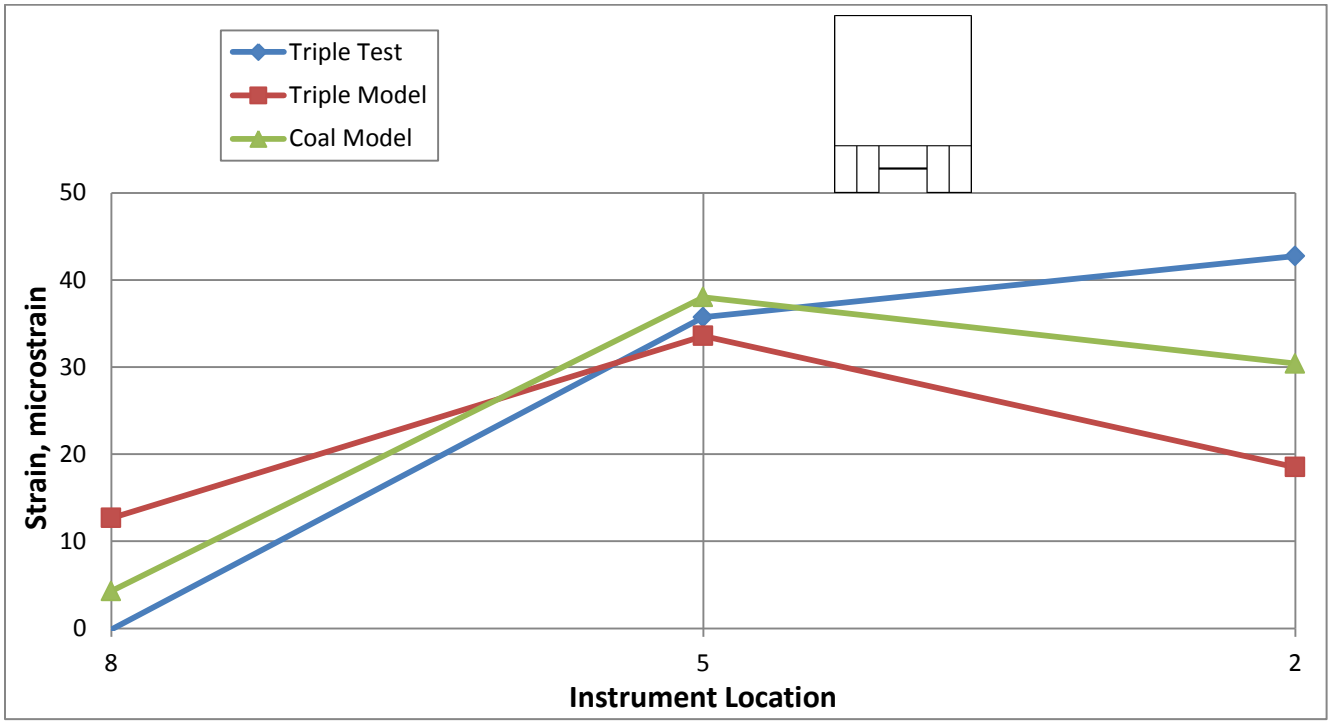

Figure 5-53. Depot St. Bridge Midspan Strain Profile (Load in U-S Lane)

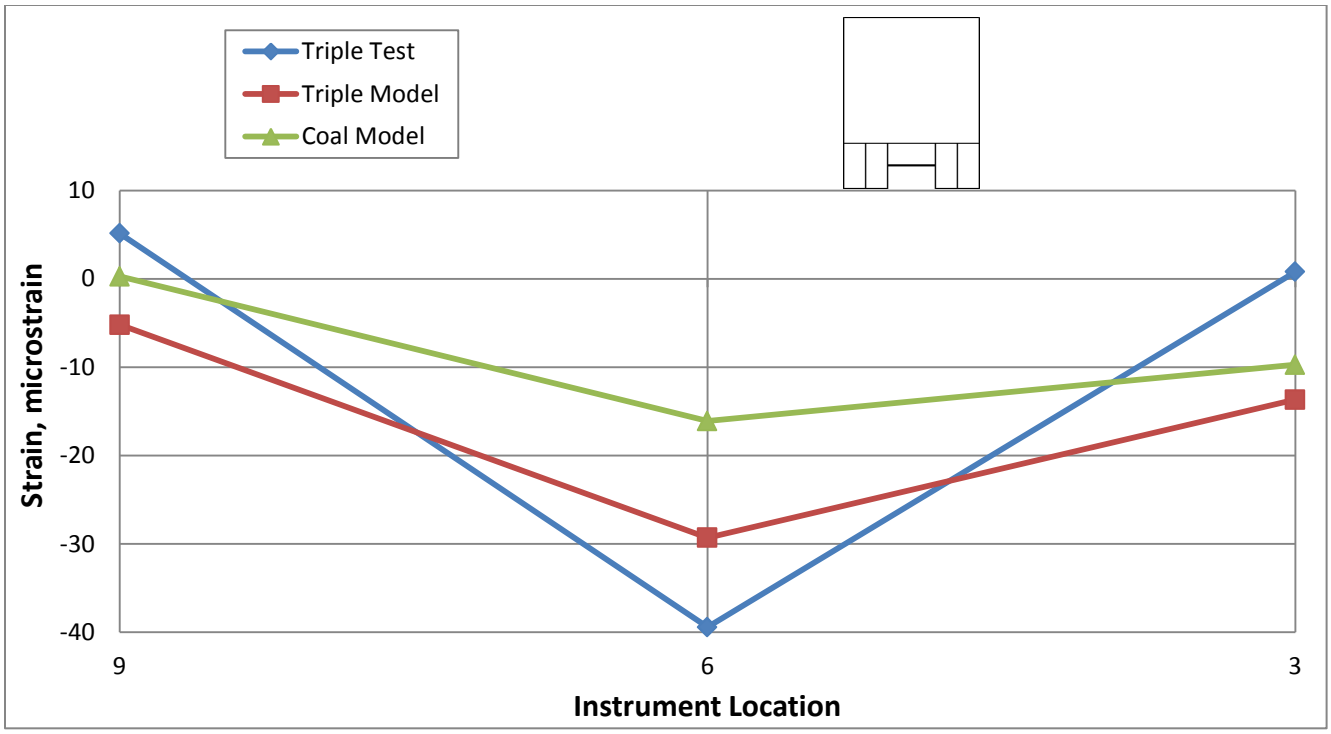

Figure 5-54. Depot St. Bridge North Quarter Point Strain Profile (Load in U-S Lane)

As with the Main Street Bridge results, the strain profiles show expected arch behavior at the south and north quarter points. At midspan the strains from the live load test show an unexpectedly large amount of tensile strain as compared to the small strains resulting from the model. These results are hard to explain and do not reflect the desired arch behavior. The strains from the coal tri-axle and triple truck loadings in the model have comparable magnitudes at every quarter point in the above plots. This reinforces the conclusion from the deflection comparison that the triple truck loading is a good representation for the rear tri-axle of a 150 kip coal truck. Also, when looking at the critical compressive strain value of 40 microstrain for the live load test the model results closely match. This shows that the model accurately captured the peak strain value and is a good representation of the actual bridge.

Overall when comparing the strains from the live load test to the model, accuracy is obtained in most situations with a few exceptions. This trend is consistent for both bridges and could be attributed to the need for refinement of the models. An example of unacceptable accuracy was the anomalous midspan strains from the Main Street Bridge model. From these comparisons it can be concluded that the local behavior trends of the arches was generally represented by the model but the level of refinement prevented the model from accurately matching exact strain values to those seen in the live load tests.

Chapter 6 - Conclusions and Recommendations

After comparing and analyzing the results obtained from the live load tests and finite element models, conclusions regarding the condition of the arch bridges were made. These conclusions helped shape the recommendations made to VDOT regarding the load rating of the bridges. These conclusions and recommendations are summarized in the following sections.

6.1 Summary of Results

6.1.1 Main Street Bridge

- During live load testing, loading the downstream lane produced the maximum bridge response in the downstream arch. The maximum downward deflection was 0.080 in. at midspan of the downstream arch with the triple truck loading of 141.9 kips at midspan in the downstream lane. The maximum uplift from the live load test was -0.009 in. at the opposite end of the arch over which the triple truck configuration was located.
- The maximum compressive strain was -38.9 με at the top of the downstream arch at the north quarter point. This relates to a compressive stress of 155 psi and resulted from the triple truck loading located over the south quarter point in the downstream lane.
- The maximum tensile strain was 66.6 με at the bottom of the downstream arch at midspan. This relates to a tensile stress of 266 psi and resulted from the load located directly over that location.
- When analyzing the bridge with the SAP2000 model, the maximum response followed the same trend as the live load test. The maximum downward deflection was 0.085 in. at midspan of the downstream arch with the triple truck load directly above in the downstream lane. The maximum downward deflection with the 72 kip rear coal truck tri-

axle was 0.084 in. at the same location. The maximum uplift from the model with the triple truck configuration was -0.006 in. at the south quarter point of the downstream arch when the load was over the north quarter point in the downstream lane. The maximum uplift from the tri-axle load was -0.004 in. at the same location.

- The maximum strains experienced by the model also followed the trends of the live load test. The maximum compressive strain from the model was -30.3 με (121 psi) at the north quarter point of the downstream arch with the triple truck load over the south quarter point in the downstream lane. For the tri-axle load the maximum compressive strain in the model was -22.1 με (88.4 psi) at the same arch location and loading location.
- The maximum tensile strain in the model from the triple truck load was 14.9 με (59.6 psi) at midspan of the downstream arch with the load directly overhead. From the tri-axle load the maximum tensile strain was 26.1 με (104.4 psi) at midspan of the center arch with the load at midspan in the downstream lane.

6.1.2 Depot Street Bridge

- During live load testing, the maximum bridge response was experienced by the center arch due to the traffic lane positioning. The maximum downward deflection was 0.064 in. and 0.063 in. with the triple truck loading at midspan in the downstream and upstream lane, respectively. The maximum uplift from the live load test was -0.011 in. at the north quarter point of the center arch with the triple truck configuration over the south quarter point in the downstream lane.
- The maximum compressive strain was -39.8 με at the middle of the center arch at the north quarter point. This relates to a compressive stress of 274 psi and resulted from the triple truck loading located at midspan in the upstream lane.

- The maximum tensile strain was 42.7 με at the bottom of the upstream arch at midspan. This relates to a tensile stress of 171 psi and resulted from the load located directly over that location.
- When analyzing the bridge with the SAP2000 model, the maximum response followed the same trend as the live load test. The maximum downward deflection was 0.058 in. and 0.059 in. with the triple truck loading at midspan in the downstream and upstream lane, respectively. Likewise, the maximum downward deflection was 0.053 in. and 0.056 in. with the rear coal truck tri-axle at midspan in the downstream and upstream lane, respectively. The maximum uplift from the model with the triple truck configuration was -0.004 in. at the north quarter point of the downstream arch when the load was over the south quarter point in the downstream lane. The maximum uplift from the tri-axle load was -0.004 in. at the same location.
- The maximum strains experienced by the model also followed the trends of the live load test. The maximum compressive strain from the model was -31.9 με (220 psi) at the north quarter point of the center arch with the triple truck load over the south quarter point in the downstream lane. For the tri-axle load the maximum compressive strain in the model was -20.8 με (143 psi) at the same arch location and loading location.
- The maximum tensile strain in the model from the triple truck load was 5.8 με (39.9 psi) at midspan of the center arch with the load directly overhead in the upstream lane. From the tri-axle load the maximum tensile strain was 8.2 με (56.4 psi) at the same arch location and loading location.

6.2 Conclusions

- Due to the behavior seen from the data collected during testing, it is believed that the bridges are still functioning well considering their age and history of extreme loadings.
- The magnitudes of the deflections and strains resulting from the range of loading scenarios were relatively small, providing evidence that the capacities of the bridges are still fully capable of safely supporting typical coal traffic loads.
- The purpose for using several load increments for testing the bridge was to determine if the global behavior of the bridge is linear elastic. As can be seen in the maximum deflection plots, generally, the load-versus-deflection plots are linear. This implies that there is excess capacity of the bridges beyond the largest test loads achieved with the three trucks. The three-truck loading concentrated 141.9 kips of load at each test location and was chosen to mimic the rear triple axles of the coal hauling tractor trailers that traverse this bridge. With linear load-versus-deflection response up to this loading, it is expected that the capacity of this bridge will be more than the triple truck combination used in the tests. This is due to the additional capacity of the reinforced concrete arch beyond the linear elastic range.
- From the quarter point load distribution plots, the deck shows proper distribution of load between the three arches through deflections which are proportional to the loading location. This allows for redundancy in the bridge, so if an arch were to begin to show distress under load (inelastic behavior), the other arches would be able to share the load and a failure of the bridge would be avoided.
- The linear strain distributions through the arch depth showed approximate linear elastic behavior in most cases for both bridges. In a few instances the strains did not show linear

elastic behavior most likely due to apparent surface distress at the instrument location. However, overall strain distribution results from the live load tests were favorable.

- The deflection results from the finite element models accurately represent those obtained from live load testing, especially at the critical locations. The maximum values and locations from the triple truck configuration in the live load tests were correctly simulated in the model, providing evidence that the models could capture the global behavior of the bridges accurately.
- The model strain results showed expected arch behavior and accurately represented the live load results in certain locations. However, the local behavior was not as accurately represented by the models as the global behavior from the deflection results was.
- The coal truck rear tri-axle produced strains and deflections very similar to those produced by the triple truck configuration in the models. This was important in showing that the triple truck scenario used in live load testing was a good representation of the rear tri-axle of a 150 kip coal truck that is typical in daily bridge traffic.

6.3 Recommendations

- As concluded from the test results, it will not be necessary to post the bridge to eliminate trucks similar to the test loads. In the short term, the bridge has shown that it is capable of handling such loadings.
- Due to the patching along the arches, there are concerns about the long term deterioration of the bridge combined with these loads. Because of this, it is recommended that the inspection of this bridge be moved to a shorter cycle. This will help to ensure the patching is not experiencing severe delamination from the mature concrete, which could affect the bridge's effective capacity.

References

AASHTO (2008). Bridging the Gap: Restoring and Rebuilding the Nation's Bridges. Washington, D.C.

ASCE (2009). Infrastructure Fact Sheet: Bridge Report Card. Washington, D.C.

Bakht, B., and L. G. Jaeger. "Bridge Testing: A Surprise Every Time. *Journal of Structural Engineering* 116.5 (1990): 1370-1383.

Baxter, D. J., and T. A. Balan. "Design of the Fulton Road Bridge Precast Segmental Concrete Arches." *Journal of Bridge Engineering* 13.5 (2008): 476-482.

Cai, C. S., M. Shahawy, and A. El-Saad. "Non-Destructive Testing of Field Bridges in Florida. *Proceedings of SPIE, The International Society for Optical Engineering* 3400 (1998): 19-30.

Cai, C.S., and M. Shahawy. "Understanding Capacity Rating of Bridges from Load Tests." *Practice Periodical on Structural Design and Construction* 8.4 (2003): 209-216.

Carrato, J. L., C. H. Hague, and H. R. Sandberg. "Load Rating Criteria for Existing Concrete Bridges." *Concrete International* 22.2 (2000): 45-51.

Chajes, M. J., H. W. Shenton III, and D. O'Shea. "Bridge-Condition Assessment and Load Rating Using Nondestructive Evaluation Methods." *Transportation Research Record* 2.1696 (2000): 83-91.

Chajes, M. J., and H. W. Shenton III. "Using Diagnostic Load Tests for Accurate Load Rating of Typical Bridges." *Proceedings of the Structures Congress and Exposition* (2005): 9-19.

Garrett, G. P. “Analytical Load Rating of an Open-Spandrel Arch Bridge: Case Study.” *Journal of Bridge Engineering* 12.1 (2007): 13-20.

Laffranchi, M., and P. Marti. “Robert Maillart's Curved Concrete Arch Bridges." *Journal of Structural Engineering* 123.10 (1997): 1280-1286.

Lok, M. S., and A. J. Lamanna. “Study of Turkish Bridge Standards Involving a Reinforced Concrete Arch Bridge.” *Journal of Performance of Constructed Facilities* 20.3 (2006): 274-280.

Marefat, M. S., E. Gargary, and S. Ataei. “Load Test of a Plain Concrete Arch Railway Bridge of 20-m Span.” *Construction & Building Materials* 18.9 (2004): 661-667.

McGrath, T. J., and E. P. Mastroianni. “Finite-Element Modeling of Reinforced Concrete Arch under Live Load.” *Transportation Research Record* .1814 (2002): 203-210.

Neely, W. D., T. E. Cousins, and J. J. Lesko. “ Evaluation of In-Service Performance of Tom’s Creek Bridge Fiber-Reinforced Polymer Superstructure.” *Journal of Performance of Constructed Facilities* 18.3 (2004): 147-158.

Nowak, A.S., S. Kim, and P. R. Stankiewicz. “Analysis and Diagnostic Testing of a Bridge.” *Computers & Structures* 77.1 (2000): 91-100.

Radic, J., Z. Savor, and A. Kindij. “Innovations in Concrete Arch Bridge Design.” *Proceedings of the Institution of Civil Engineers. Bridge Engineering* 159.3 (2006): 121-126.

Ranasinghe, A. P., and W. L. Gottshall. “Numerical Load Rating of Reinforced Concrete Compression Members: Demonstration with Connecticut Arch Bridges.” *Transportation Research Record* .1814 (2002): 145-153.

Saraf, V., A. F. Sokolik, and A. S. Nowak. “Proof Load Testing of Highway Bridges.” *Transportation Research Record* .1541 (1996): 51-57.

Sartor, R. R., M. P. Culmo, and J. T. DeWolf. “Short-Term Strain Monitoring of Bridge Structures.” *Journal of Bridge Engineering* 4.3 (1999): 157-164.

Viola, E., L. Panzacchi, and F. Tornabene. “General Analysis and Application to Redundant Arches under Static Loading.” *Construction & Building Materials* 21.5 (2007): 1129-1143.

Weidner, J., J. Prader, N. Dubbs, F. Moon, and A.E. Aktan. “Structural Identification of Bridges to Assess Safety and Performance.” *Proceedings of the 2009 Structures Congress*, April 30 - May 2, 2009, Austin, TX, 119-124.

Zhang, J., C. Li, F. Xu, and X. Yu. “Test and Analysis for Ultimate Load-Carrying Capacity of Existing Reinforced Concrete Arch Ribs.” *Journal of Bridge Engineering* 12.1 (2007): 4-12.

Zanardo, G., C. Pellegrino, C. Bobisut, C. Modena. “Performance Evaluation of Short Span Reinforced Concrete Arch Bridges.” *Journal of Bridge Engineering* 9.5 (2004): 424-434.

Appendix A - Live Load Test Data

Table A-1. Main Street Bridge Deflections (in)

TEST TRUCK INFORMATION				DEFLECTOMETER LOCATION								
Stop	Lane	Position on Bridge	Load (kips)	1	2	3	4	5	6	7	8	9
1.1	U-S	North Qtr. Pt.	28.5	0.003	0.011	0.008	0.001	0.007	0.006	-0.002	-0.004	-0.002
1.2	U-S	Midspan		-0.001	-0.001	-0.001	0.007	0.016	0.010	0.000	-0.002	0.003
1.3	U-S	South Qtr. Pt.		-0.003	-0.002	-0.003	0.003	0.003	0.001	0.003	0.008	0.009
2.1	D-S	South Qtr. Pt.	28.5	-0.001	-0.002	-0.002	0.010	0.003	0.000	0.008	0.007	0.003
2.2	D-S	Midspan		0.004	-0.001	0.000	0.021	0.012	0.002	0.000	0.000	0.000
2.3	D-S	North Qtr. Pt.		0.013	0.007	0.002	0.002	0.003	0.001	0.000	-0.001	-0.001
3.1	U-S	North Qtr. Pt.	53.8	0.008	0.028	0.020	0.000	0.008	0.008	-0.002	-0.005	-0.004
3.2	U-S	Midspan		0.002	0.002	0.003	0.013	0.035	0.024	-0.001	-0.004	0.002
3.3	U-S	South Qtr. Pt.		-0.004	-0.004	-0.004	0.005	0.007	0.002	0.005	0.014	0.016
4.1	D-S	South Qtr. Pt.	53.8	-0.003	-0.003	-0.002	0.015	0.003	0.000	0.019	0.011	0.004
4.2	D-S	Midspan		0.005	-0.002	-0.001	0.048	0.023	0.005	-0.002	-0.002	0.000
4.3	D-S	North Qtr. Pt.		0.026	0.012	0.004	0.009	0.009	0.003	-0.004	-0.005	-0.003
5.1	U-S	North Qtr. Pt.	82.3	0.009	0.028	0.023	0.005	0.020	0.017	-0.003	-0.004	-0.004
5.2	U-S	Midspan		0.003	0.006	0.006	0.018	0.041	0.025	-0.001	0.002	0.007
5.3	U-S	South Qtr. Pt.		-0.003	-0.004	-0.003	0.008	0.015	0.007	0.007	0.024	0.018
6.1	D-S	South Qtr. Pt.	82.3	-0.003	-0.004	-0.003	0.031	0.010	0.001	0.020	0.016	0.005
6.2	D-S	Midspan		0.013	0.001	0.000	0.051	0.030	0.006	0.002	0.003	0.000
6.3	D-S	North Qtr. Pt.		0.031	0.019	0.005	0.018	0.013	0.002	-0.003	-0.003	-0.003

TEST TRUCK INFORMATION				DEFLECTOMETER LOCATION								
Stop	Lane	Position on Bridge	Load (kips)	1	2	3	4	5	6	7	8	9
7.1	U-S	North Qtr. Pt.	112.9	0.013	0.044	0.034	0.003	0.020	0.017	-0.005	-0.005	-0.008
7.2	U-S	Midspan		0.006	0.014	0.012	0.021	0.055	0.036	-0.003	-0.001	0.003
7.3	U-S	South Qtr. Pt.		-0.005	-0.005	-0.005	0.014	0.027	0.013	0.007	0.027	0.022
8.1	D-S	South Qtr. Pt.	112.9	-0.005	-0.006	-0.006	0.031	0.008	-0.001	0.033	0.022	0.006
8.2	D-S	Midspan		0.012	-0.001	-0.003	0.075	0.039	0.007	0.004	0.006	0.001
8.3	D-S	North Qtr. Pt.		0.042	0.023	0.006	0.034	0.026	0.005	-0.006	-0.005	-0.007
9.1	U-S	North Qtr. Pt.	141.4	0.025	0.049	0.035	0.013	0.028	0.020	-0.007	-0.008	-0.009
9.2	U-S	Midspan		0.006	0.011	0.010	0.044	0.066	0.039	-0.003	-0.001	0.004
9.3	U-S	South Qtr. Pt.		-0.007	-0.008	-0.008	0.020	0.028	0.013	0.019	0.034	0.026
10.1	D-S	South Qtr. Pt.	141.4	-0.007	-0.009	-0.008	0.037	0.017	0.005	0.036	0.030	0.015
10.2	D-S	Midspan		0.014	0.002	0.000	0.080	0.056	0.021	0.003	0.006	0.001
10.3	D-S	North Qtr. Pt.		0.043	0.035	0.014	0.034	0.028	0.009	-0.008	-0.006	-0.006

Table A-2. Main Street Bridge Strains (με)

TEST TRUCK INFORMATION				STRAIN TRANSDUCER LOCATION										
Stop	Lane	Position on Bridge	Load (kips)	1-bot	1-mid	1-top	2-bot	2-mid	2-top	4	5	6	7	8
1.1	U-S	North Qtr. Pt.	28.5	-0.1	-2.2	-2.7	-1.1	-4.5	-0.5	-2.4	-0.7	0.3	-0.9	-2.0
1.2	U-S	Midspan		-3.7	-2.9	-0.6	-7.8	-4.2	-0.1	7.8	3.1	-2.2	-2.6	-7.6
1.3	U-S	South Qtr. Pt.		-1.6	-0.4	0.6	-2.8	-1.1	-0.1	2.8	0.1	0.2	-0.3	-1.4
2.1	D-S	South Qtr. Pt.	28.5	-4.9	-3.2	-0.8	-2.8	-1.6	0.3	-0.4	-0.5	-0.4	-6.3	-2.8
2.2	D-S	Midspan		-9.9	-7.9	-5.5	-6.5	-4.1	0.3	25.3	1.5	-1.1	-7.9	-8.3
2.3	D-S	North Qtr. Pt.		-0.7	-6.9	-12.5	-2.6	-5.4	0.0	-7.2	-1.2	-0.7	-2.4	-5.4

TEST TRUCK INFORMATION				STRAIN TRANSDUCER LOCATION											
Stop	**Lane**	**Position on Bridge**	**Load (kips)**	**1-bot**	**1-mid**	**1-top**	**2-bot**	**2-mid**	**2-top**	**4**	**5**	**6**	**7**	**8**
3.1	U-S	North Qtr. Pt.	53.8	2.7	-3.6	-4.7	4.1	-6.8	-1.0	-6.1	-2.2	1.4	-0.7	-2.3
3.2	U-S	Midspan		-5.2	-5.8	-1.9	-13.1	-7.5	0.1	11.2	5.4	-5.7	-3.4	-11.5
3.3	U-S	South Qtr. Pt.		-3.1	-2.2	0.3	-3.6	-1.8	0.1	5.1	-0.7	0.3	-0.9	-6.9
4.1	D-S	South Qtr. Pt.	53.8	-5.3	-2.7	-0.6	-2.0	-1.0	0.0	-5.7	-1.2	-0.3	-8.6	1.3
4.2	D-S	Midspan		-17.0	-11.4	-7.3	-7.9	-4.3	0.1	74.2	3.0	-1.7	-16.1	-11.8
4.3	D-S	North Qtr. Pt.		0.9	-10.3	-25.8	-2.6	-7.5	-0.4	-10.1	-0.5	-0.6	-3.8	-3.9
5.1	U-S	North Qtr. Pt.	82.3	0.9	-5.8	-5.2	-2.7	-10.4	-0.8	-3.9	-0.5	-1.1	-3.7	-6.4
5.2	U-S	Midspan		-6.0	-7.2	-2.9	-14.0	-10.0	0.0	18.4	5.8	-4.8	-6.2	-17.4
5.3	U-S	South Qtr. Pt.		-3.7	-2.6	-0.3	-6.3	-3.4	0.1	6.7	2.5	-1.8	-2.6	-3.2
6.1	D-S	South Qtr. Pt.	82.3	-11.4	-6.8	-1.3	-4.7	-2.0	0.3	13.7	0.1	-0.4	-13.8	-4.3
6.2	D-S	Midspan		-20.0	-17.1	-15.0	-11.1	-7.0	0.2	42.1	6.5	-1.1	-19.0	-13.2
6.3	D-S	North Qtr. Pt.		0.4	-13.8	-30.0	-1.5	-10.0	-0.4	10.5	2.3	0.4	-7.2	-5.2
7.1	U-S	North Qtr. Pt.	112.9	3.9	-5.3	-5.7	7.1	-10.0	-1.5	-7.2	-0.6	1.9	-0.8	-4.8
7.2	U-S	Midspan		-6.4	-9.6	-3.3	-19.2	-14.0	-0.4	18.0	6.9	-4.2	-4.0	-21.1
7.3	U-S	South Qtr. Pt.		-6.8	-5.5	1.8	-11.5	-4.9	0.0	16.6	5.2	-0.3	-0.1	-13.7
8.1	D-S	South Qtr. Pt.	112.9	-9.7	-5.1	0.8	-3.2	-0.8	-0.2	7.7	0.2	0.3	-11.8	1.5
8.2	D-S	Midspan		-22.7	-17.3	-13.0	-10.1	-5.4	-0.6	63.8	7.1	-0.4	-27.1	-15.8
8.3	D-S	North Qtr. Pt.		-0.2	-16.3	-35.4	-1.3	-10.0	-1.6	26.4	5.0	1.5	-8.7	-7.1
9.1	U-S	North Qtr. Pt.	141.4	0.5	-12.0	-19.9	3.2	-14.9	-1.4	-8.0	-0.7	-0.1	-6.0	-10.2
9.2	U-S	Midspan		-16.7	-15.5	-7.4	-24.7	-17.3	-0.1	45.7	4.4	-8.0	-16.9	-31.0
9.3	U-S	South Qtr. Pt.		-10.2	-6.1	0.5	-13.0	-6.3	0.2	10.2	2.3	-3.4	-4.4	-14.1
10.1	D-S	South Qtr. Pt.	141.4	-14.2	-7.8	-0.7	-8.9	-3.9	0.1	9.9	0.3	-0.3	-12.3	-6.8
10.2	D-S	Midspan		-28.7	-22.0	-16.4	-20.9	-12.9	-0.3	66.6	5.7	-4.5	-30.3	-25.8
10.3	D-S	North Qtr. Pt.		-2.2	-19.4	-38.9	0.6	-14.4	-1.6	21.4	2.8	0.9	-11.4	-11.3

Table A-3. Depot Street Bridge Deflections (in)

TEST TRUCK INFORMATION				DEFLECTOMETER LOCATION							
Stop	Lane	Position on Bridge	Load (kips)	2	3	4	5	6	7	8	9
1.1	D-S	South Qtr. Pt.	32.1	0.003	-0.002	0.011	0.011	-0.002	0.008	0.006	-0.003
1.2	D-S	Midspan		0.005	0.000	0.005	0.019	0.003	0.002	0.012	0.002
1.3	D-S	North Qtr. Pt.		0.000	0.004	0.000	0.003	0.016	-0.002	0.000	0.012
2.1	U-S	North Qtr. Pt.	32.1	0.006	0.009	0.000	0.008	0.014	-0.003	0.000	0.003
2.2	U-S	Midspan		0.012	0.000	0.006	0.018	0.002	0.000	0.004	-0.002
2.3	U-S	South Qtr. Pt.		0.002	-0.003	0.011	0.005	-0.001	0.002	0.000	-0.005
3.1	D-S	South Qtr. Pt.	54.5	0.005	-0.003	0.021	0.017	-0.004	0.017	0.011	-0.005
3.2	D-S	Midspan		0.010	0.001	0.004	0.035	0.007	0.002	0.022	0.006
3.3	D-S	North Qtr. Pt.		0.002	0.008	-0.002	0.006	0.027	-0.003	0.002	0.024
4.1	U-S	North Qtr. Pt.	54.5	0.007	0.018	-0.003	0.010	0.025	-0.003	0.002	0.010
4.2	U-S	Midspan		0.022	0.001	0.007	0.033	0.001	0.001	0.009	-0.001
4.3	U-S	South Qtr. Pt.		0.005	-0.003	0.020	0.009	-0.005	0.007	0.003	-0.004
5.1	D-S	South Qtr. Pt.	86.6	0.007	-0.002	0.020	0.028	-0.001	0.015	0.019	-0.002
5.2	D-S	Midspan		0.008	0.005	0.008	0.033	0.017	0.003	0.022	0.017
5.3	D-S	North Qtr. Pt.		0.003	0.008	-0.001	0.016	0.027	-0.004	0.010	0.025
6.1	U-S	North Qtr. Pt.	86.6	0.017	0.018	-0.001	0.025	0.026	-0.003	0.007	0.012
6.2	U-S	Midspan		0.025	0.007	0.013	0.037	0.009	0.003	0.011	0.004
6.3	U-S	South Qtr. Pt.		0.013	0.000	0.022	0.019	-0.001	0.008	0.007	0.000

TEST TRUCK INFORMATION				DEFLECTOMETERS							
Stop	Lane	Position on Bridge	Load (kips)	2	3	4	5	6	7	8	9
7.1	D-S	South Qtr. Pt.	107.3	0.007	-0.003	0.027	0.026	-0.003	0.021	0.019	-0.002
7.2	D-S	Midspan		0.012	0.003	0.013	0.044	0.013	0.008	0.030	0.013
7.3	D-S	North Qtr. Pt.		0.006	0.010	-0.001	0.025	0.032	-0.005	0.015	0.031
8.1	U-S	North Qtr. Pt.	107.3	0.015	0.026	-0.002	0.025	0.038	-0.004	0.006	0.016
8.2	U-S	Midspan		0.032	0.011	0.012	0.047	0.017	0.001	0.012	0.004
8.3	U-S	South Qtr. Pt.		0.019	-0.001	0.025	0.027	-0.001	0.009	0.008	-0.004
9.1	D-S	South Qtr. Pt.	139.4	0.015	-0.005	0.038	0.040	-0.011	0.025	0.023	-0.006
9.2	D-S	Midspan		0.025	0.008	0.016	0.064	0.016	0.008	0.034	0.014
9.3	D-S	North Qtr. Pt.		0.008	0.021	-0.002	0.028	0.043	-0.006	0.014	0.036
10.1	U-S	North Qtr. Pt.	139.4	0.017	0.027	-0.003	0.031	0.039	-0.007	0.010	0.027
10.2	U-S	Midspan		0.034	0.011	0.018	0.063	0.028	0.006	0.026	0.005
10.3	U-S	South Qtr. Pt.		0.019	-0.004	0.039	0.032	0.002	0.020	0.012	-0.008

Table A-4. Depot Street Bridge Strains (με)

TEST TRUCK INFORMATION				STRAIN TRANSDUCER LOCATION												
Stop	Lane	Position on Bridge	Load (kips)	1	2	3-bot	3-mid	3-top	4	5	6-bot	6-mid	6-top	7	8	9
1.1	D-S	South Qtr. Pt.	32.1	-0.2	4.3	-2.5	-1.3	0.2	0.4	0.0	-2.1	-3.5	-0.1	0.4	0.0	-4.5
1.2	D-S	Midspan		-1.3	9.2	-2.4	-0.7	-0.5	-6.0	6.8	-4.2	-8.9	-2.2	-6.5	-0.3	-7.2
1.3	D-S	North Qtr. Pt.		-0.5	-3.0	1.5	1.6	-2.7	-2.1	-3.2	0.0	-7.2	-6.6	-1.8	-0.6	3.9
2.1	U-S	North Qtr. Pt.	32.1	-1.6	2.6	0.5	-1.9	-9.6	-3.3	3.8	-0.2	-11.1	-5.9	-2.1	0.0	2.0
2.2	U-S	Midspan		-2.9	25.5	-7.2	-3.7	-1.1	-5.3	18.8	-3.2	-9.2	-1.1	-2.2	0.5	-1.1
2.3	U-S	South Qtr. Pt.		-0.2	-4.5	-2.2	-0.5	0.3	1.0	-1.4	0.2	-2.6	-0.1	1.3	1.1	1.0

TEST TRUCK INFORMATION				STRAIN TRANSDUCER LOCATION												
Stop	**Lane**	**Position on Bridge**	**Load (kips)**	**1**	**2**	**3-bot**	**3-mid**	**3-top**	**4**	**5**	**6-bot**	**6-mid**	**6-top**	**7**	**8**	**9**
3.1	D-S	South Qtr. Pt.	54.5	0.0	5.6	-3.8	-1.1	1.3	2.8	0.6	-3.1	-4.4	0.2	0.9	-0.2	-8.2
3.2	D-S	Midspan		-2.3	19.5	-3.6	-0.2	0.2	-10.3	35.2	-7.0	-15.0	-3.5	-12.5	-0.1	-12.6
3.3	D-S	North Qtr. Pt.		-0.9	-3.7	3.8	3.4	-3.7	-3.1	-4.4	0.1	-12.1	-10.6	-3.7	-1.0	5.4
4.1	U-S	North Qtr. Pt.	54.5	-2.3	-0.5	4.2	-0.5	-16.4	-4.6	2.7	-0.6	-18.6	-10.5	-3.8	-0.4	3.4
4.2	U-S	Midspan		-5.0	46.1	-12.9	-5.9	-0.8	-9.8	42.1	-7.5	-17.1	-1.7	-4.7	-0.5	-5.6
4.3	U-S	South Qtr. Pt.		-0.4	-10.8	-5.6	-2.6	0.4	1.3	-4.8	-2.1	-3.8	-0.1	1.6	-1.0	-4.7
5.1	D-S	South Qtr. Pt.	86.6	-1.2	12.4	-4.6	-0.8	1.3	-3.4	7.7	-5.1	-10.3	-0.4	-5.1	0.0	-11.4
5.2	D-S	Midspan		-2.4	14.3	-0.4	2.0	-0.8	-7.4	17.4	-5.4	-19.9	-7.0	-11.1	0.1	-9.2
5.3	D-S	North Qtr. Pt.		-1.6	3.1	5.5	4.6	-2.9	-5.8	2.3	2.1	-13.1	-10.5	-8.1	-0.4	4.2
6.1	U-S	North Qtr. Pt.	86.6	-4.3	10.6	-1.3	-1.9	-12.7	-8.7	6.6	-3.6	-26.7	-10.9	-5.7	-0.2	1.2
6.2	U-S	Midspan		-5.1	24.2	-10.0	-4.3	-5.0	-9.7	13.3	-7.1	-20.8	-4.8	-4.3	-0.5	-5.8
6.3	U-S	South Qtr. Pt.		-0.3	4.4	-9.6	-2.8	0.0	2.8	3.4	-6.2	-9.0	-0.8	1.5	-1.5	-7.6
7.1	D-S	South Qtr. Pt.	107.3	-0.4	9.6	-5.3	-1.9	1.2	1.8	5.6	-5.5	-10.2	-0.4	-0.9	-0.4	-12.6
7.2	D-S	Midspan		-2.9	20.7	-3.5	-0.1	-0.7	-9.9	20.1	-7.5	-22.7	-7.0	-14.5	0.1	-14.6
7.3	D-S	North Qtr. Pt.		-2.7	6.7	3.2	3.1	-4.5	-8.8	6.4	-1.7	-22.2	-14.1	-11.6	-0.3	2.0
8.1	U-S	North Qtr. Pt.	107.3	-4.8	4.7	2.8	-0.5	-20.2	-9.9	3.0	-2.4	-32.0	-17.1	-7.2	-1.1	3.1
8.2	U-S	Midspan		-7.4	41.3	-13.4	-6.7	-8.9	-14.1	22.0	-10.2	-30.8	-8.0	-7.4	-1.2	-6.2
8.3	U-S	South Qtr. Pt.		-2.3	12.0	-12.1	-4.9	-0.1	-1.5	5.4	-7.4	-14.2	-1.7	-0.3	-1.5	-8.2
9.1	D-S	South Qtr. Pt.	139.4	-2.5	14.4	-16.9	-4.9	-0.6	-2.7	4.5	-13.8	-16.6	-3.0	-4.1	-3.1	-19.1
9.2	D-S	Midspan		-8.1	43.1	-18.3	-4.5	-7.4	-21.0	34.0	-19.3	-38.7	-13.3	-20.6	-3.9	-20.5
9.3	D-S	North Qtr. Pt.		-5.5	-6.8	-2.8	2.2	-18.8	-16.1	-2.9	-9.0	-34.9	-25.7	-16.6	-5.5	0.5
10.1	U-S	North Qtr. Pt.	139.4	-5.9	5.5	5.0	0.8	-21.9	-12.3	9.1	-1.6	-39.4	-22.0	-10.8	0.1	5.1
10.2	U-S	Midspan		-8.5	42.7	-15.6	-6.8	-9.8	-18.5	35.7	-13.6	-39.8	-9.2	-13.8	-0.1	-14.2
10.3	U-S	South Qtr. Pt.		-1.8	10.3	-14.7	-5.2	-0.2	0.6	2.8	-8.1	-16.8	-1.7	1.8	-0.8	-10.1

Appendix B - Live Load Test Strain Plots

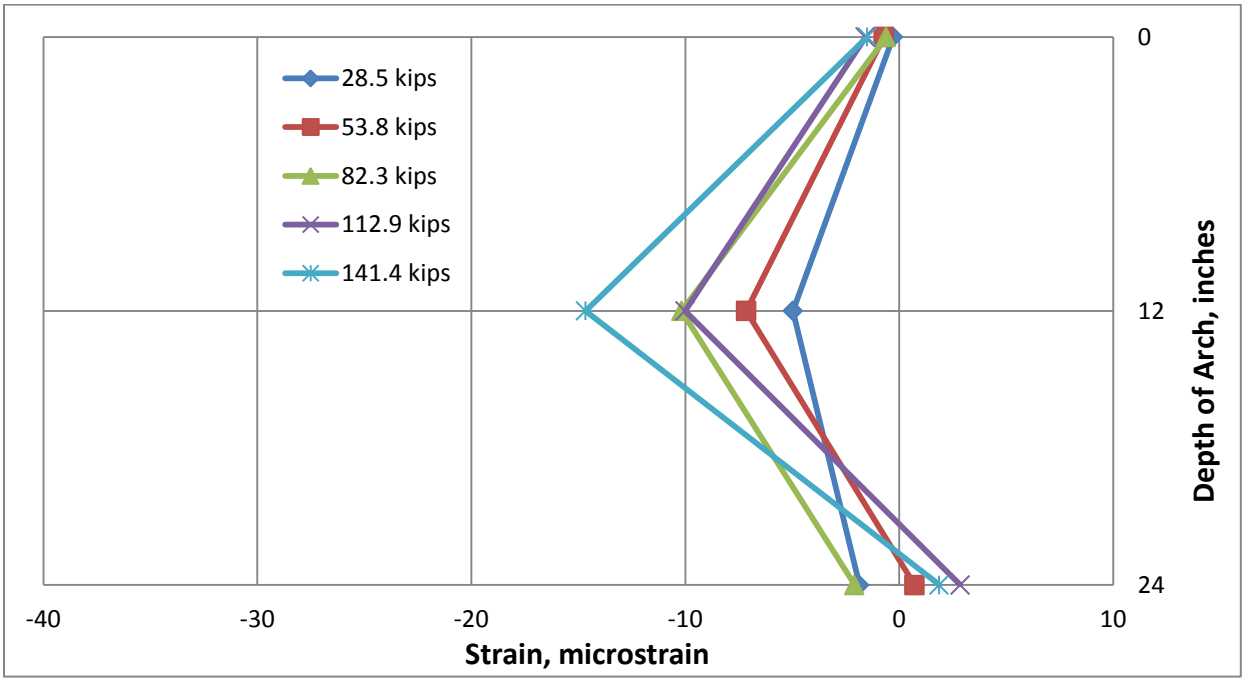

Figure B-1. Main St. Bridge Location 2 Strain Distribution (Load over Location 2)

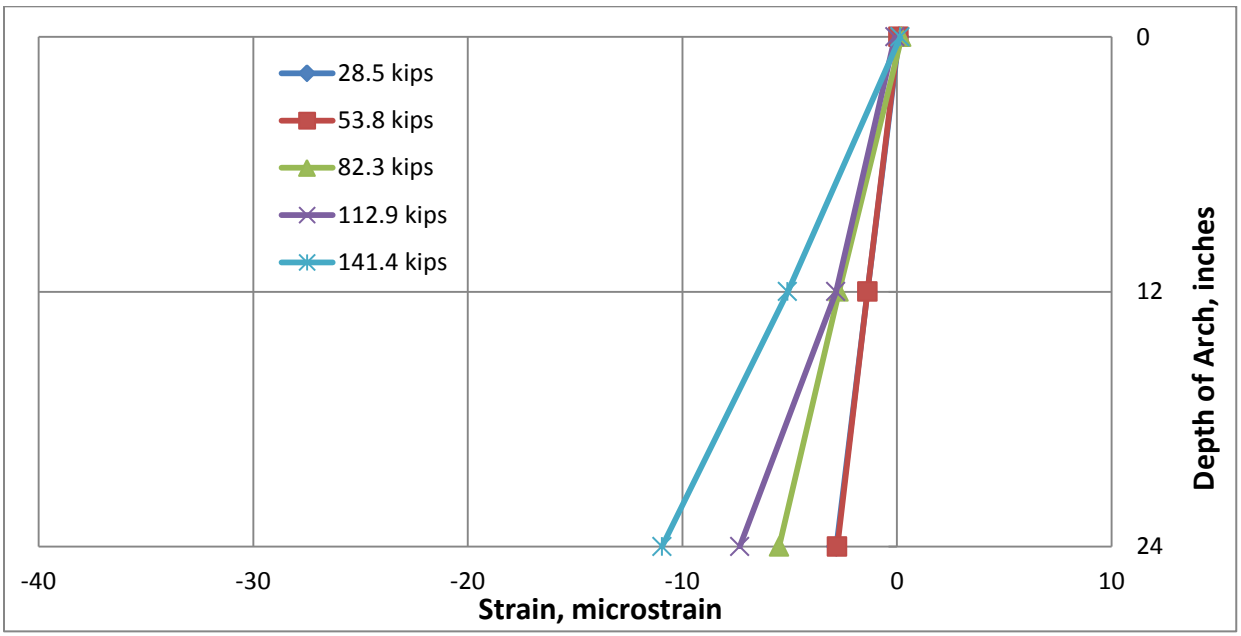

Figure B-2. Main St. Bridge Location 2 Strain Distribution (Load over Location 8)

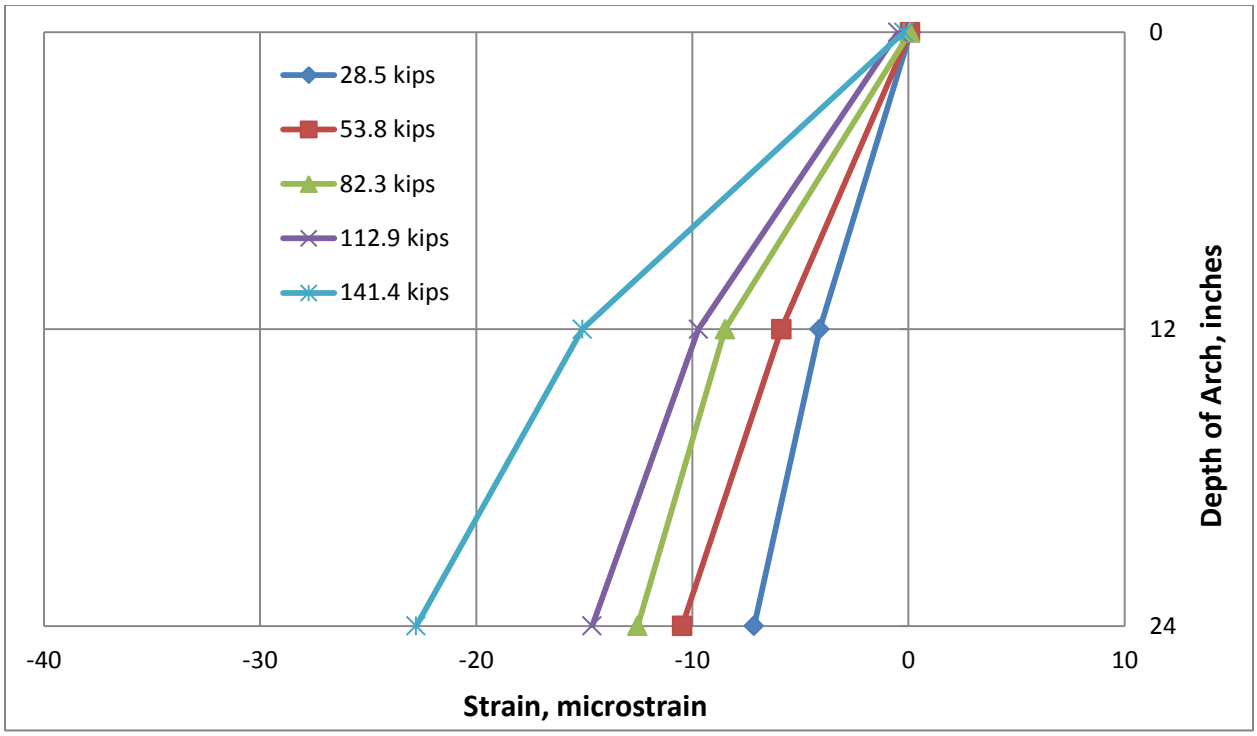

Figure B-3. Main St. Bridge Location 2 Strain Distribution (Load over Location 5)

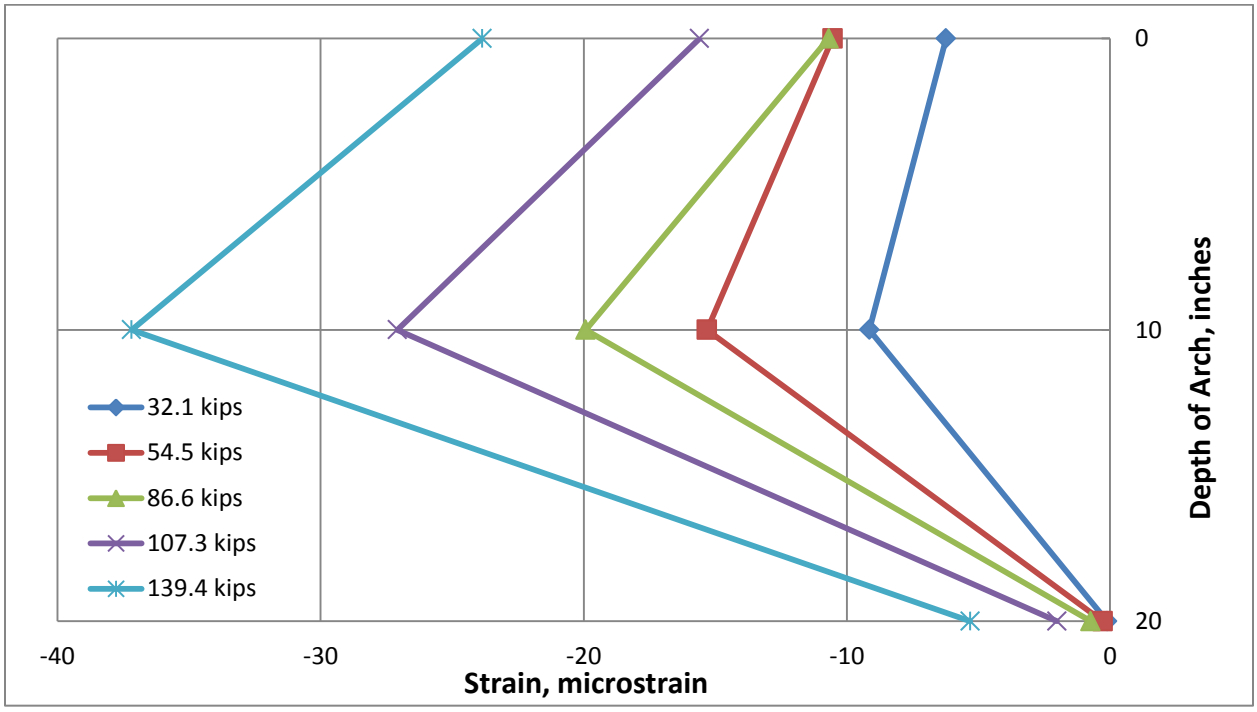

Figure B-4. Depot St. Bridge Location 6 Strain Distribution (Load over Location 6)

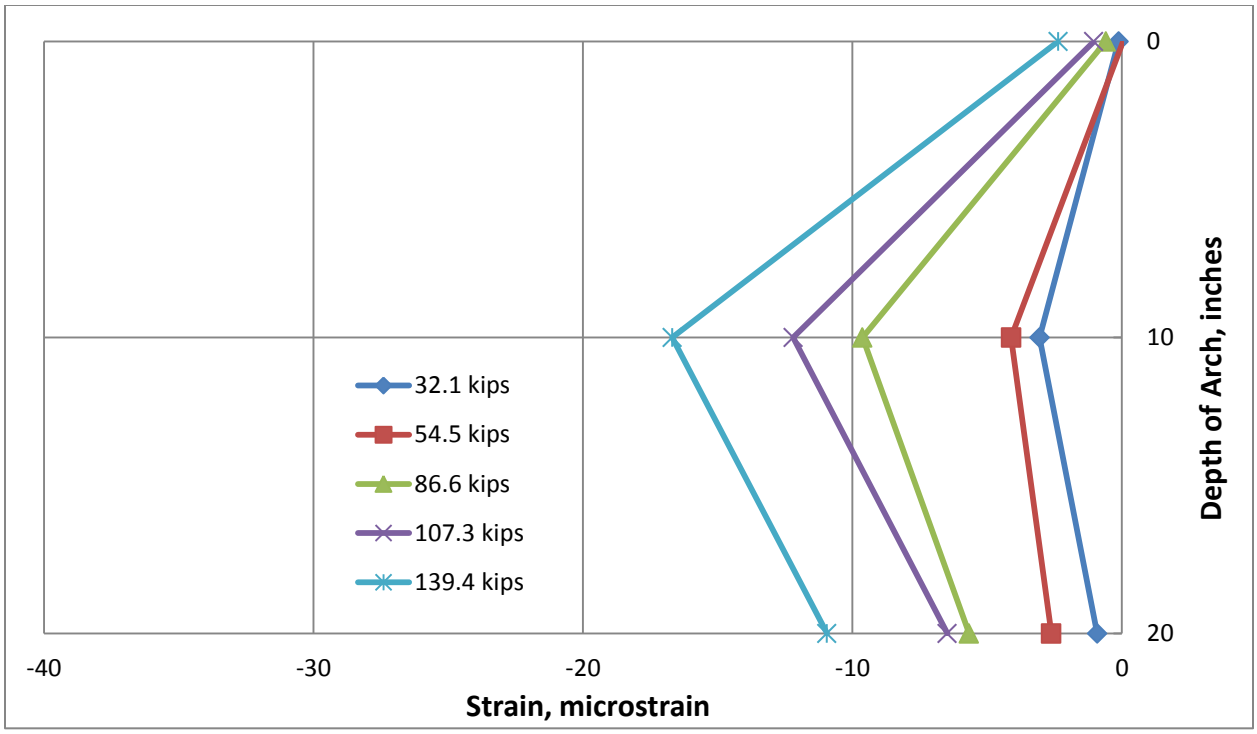

Figure B-5. Depot St. Bridge Location 6 Strain Distribution (Load over Location 4)

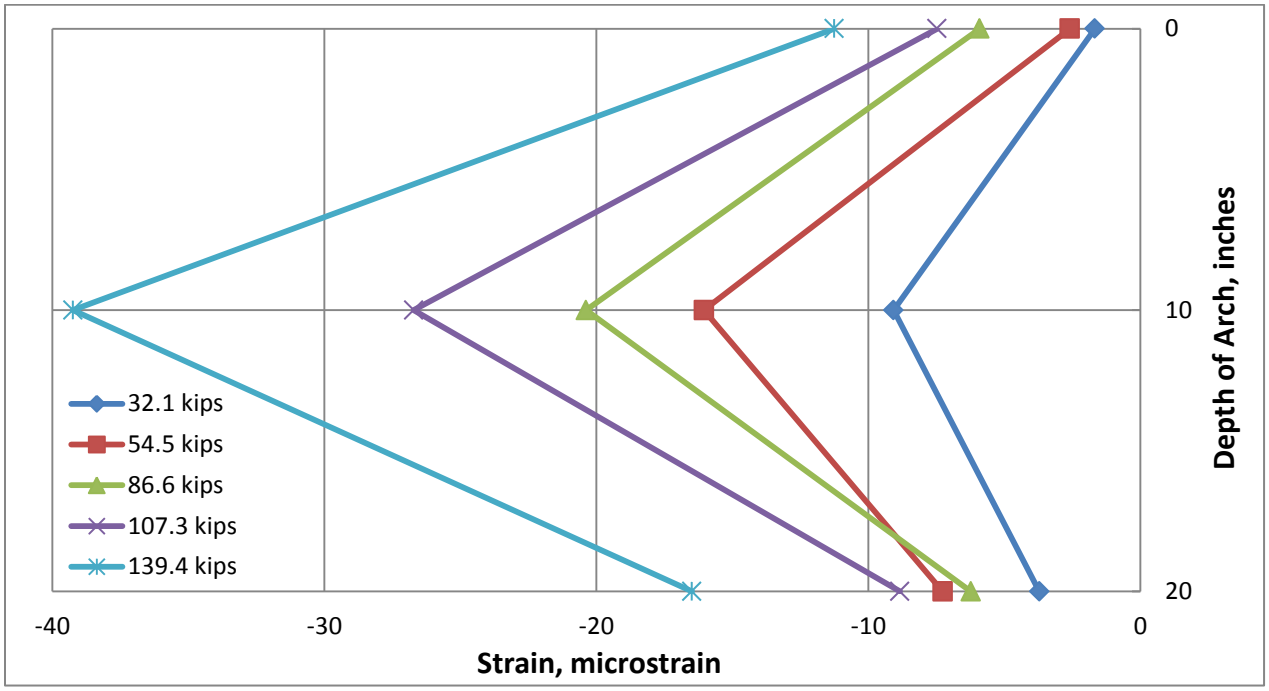

Figure B-6. Depot St. Bridge Location 6 Strain Distribution (Load over Location 5)

Appendix C - Live Load Test Load Distribution Tables

Table C-1. Main Street Bridge Load Distribution Deflections

Test Truck Info			North Deflectometers				Midspan Deflectometers				South Deflectometers			
LANE	Run	Loads	1	2	3	Total	4	5	6	Total	7	8	9	Total
U-S	1	28.5	0.003	0.011	0.008	0.022	0.007	0.016	0.010	0.034	0.003	0.008	0.009	0.019
D-S	2		0.013	0.007	0.002	0.022	0.021	0.012	0.002	0.035	0.008	0.007	0.003	0.017
U-S	3	53.8	0.008	0.028	0.020	0.056	0.013	0.035	0.024	0.072	0.005	0.014	0.016	0.034
D-S	4		0.026	0.012	0.004	0.042	0.048	0.023	0.005	0.076	0.019	0.011	0.004	0.034
U-S	5	82.3	0.009	0.028	0.023	0.059	0.018	0.041	0.025	0.083	0.007	0.024	0.018	0.049
D-S	6		0.031	0.019	0.005	0.054	0.051	0.030	0.006	0.088	0.020	0.016	0.005	0.040
U-S	7	112.9	0.013	0.044	0.034	0.091	0.021	0.055	0.036	0.112	0.007	0.027	0.022	0.056
D-S	8		0.042	0.023	0.006	0.070	0.075	0.039	0.007	0.121	0.033	0.022	0.006	0.062
U-S	9	141.4	0.025	0.049	0.035	0.109	0.044	0.066	0.039	0.149	0.019	0.034	0.026	0.078
D-S	10		0.043	0.035	0.014	0.093	0.080	0.056	0.021	0.157	0.036	0.030	0.015	0.081

Table C-2. Main Street Bridge Load Distribution Percentages

Test Truck Info		North Deflectometers			Midspan Deflectometers			South Deflectometers		
Run	Loads	1	2	3	4	5	6	7	8	9
1	28.5	12.9%	51.3%	35.8%	21.0%	48.3%	30.8%	16.8%	39.5%	43.7%
2		57.2%	33.3%	9.5%	59.5%	33.3%	7.1%	46.6%	38.3%	15.1%
3	53.8	14.3%	49.3%	36.3%	18.0%	48.5%	33.6%	13.1%	41.1%	45.8%
4		62.3%	29.4%	8.3%	63.2%	30.6%	6.2%	56.1%	32.8%	11.1%
5	82.3	15.4%	46.6%	37.9%	21.1%	48.9%	30.0%	14.4%	49.0%	36.6%
6		56.8%	34.3%	8.9%	58.1%	34.6%	7.3%	49.1%	38.9%	12.0%
7	112.9	14.4%	48.4%	37.2%	18.4%	49.0%	32.6%	11.7%	48.4%	39.9%
8		59.4%	32.4%	8.2%	61.9%	32.4%	5.7%	53.9%	36.4%	9.7%
9	141.4	23.2%	44.9%	31.9%	29.3%	44.4%	26.3%	23.8%	43.4%	32.8%
10		46.8%	37.7%	15.5%	51.1%	35.5%	13.4%	44.7%	36.8%	18.5%

Table C-3. Depot Street Bridge Load Distribution Deflections

Test Truck Info			South Deflectometers			Midspan Deflectometers				North Deflectometers			
Lane	Run	Loads	4	7	Total	2	5	8	Total	3	6	9	Total
D-S	1	32.1	0.011	0.008	0.019	0.005	0.019	0.012	0.035	0.004	0.016	0.012	0.032
U-S	2		0.011	0.002	0.013	0.012	0.018	0.004	0.033	0.009	0.014	0.003	0.025
D-S	3	54.5	0.021	0.017	0.037	0.010	0.035	0.022	0.067	0.008	0.027	0.024	0.058
U-S	4		0.020	0.007	0.027	0.022	0.033	0.009	0.064	0.018	0.025	0.010	0.053
D-S	5	86.6	0.020	0.015	0.035	0.008	0.033	0.022	0.063	0.008	0.027	0.025	0.061
U-S	6		0.022	0.008	0.030	0.025	0.037	0.011	0.072	0.018	0.026	0.012	0.056
D-S	7	107.3	0.027	0.021	0.048	0.012	0.044	0.030	0.086	0.010	0.032	0.031	0.073
U-S	8		0.025	0.009	0.034	0.032	0.047	0.012	0.090	0.026	0.038	0.016	0.080
D-S	9	139.4	0.038	0.025	0.063	0.025	0.064	0.034	0.123	0.021	0.043	0.036	0.100
U-S	10		0.039	0.020	0.059	0.034	0.063	0.026	0.123	0.027	0.039	0.027	0.093

Table C-4. Depot Street Bridge Load Distribution Percentages

Test Truck Info		South Deflectometers		Midspan Deflectometers			North Deflectometers		
Run	Loads	4	7	2	5	8	3	6	9
1	32.1	58.5%	41.5%	13.4%	53.6%	33.0%	12.3%	49.7%	38.0%
2		83.3%	16.7%	36.3%	53.0%	10.7%	35.8%	53.8%	10.4%
3	54.5	55.6%	44.4%	14.5%	52.9%	32.6%	13.1%	46.3%	40.7%
4		73.6%	26.4%	34.5%	51.7%	13.8%	33.3%	48.1%	18.7%
5	86.6	58.2%	41.8%	13.4%	52.2%	34.4%	13.3%	44.8%	41.9%
6		72.2%	27.8%	34.2%	51.2%	14.6%	32.5%	46.8%	20.7%
7	107.3	56.1%	43.9%	13.7%	51.3%	35.0%	13.9%	44.0%	42.1%
8		74.8%	25.2%	35.3%	51.8%	13.0%	31.9%	48.0%	20.2%
9	139.4	60.7%	39.3%	20.2%	51.9%	27.9%	21.0%	42.9%	36.1%
10		65.4%	34.6%	28.0%	51.2%	20.8%	29.4%	41.4%	29.2%

Appendix D - Main Street Bridge Model Arch Deflection Plots

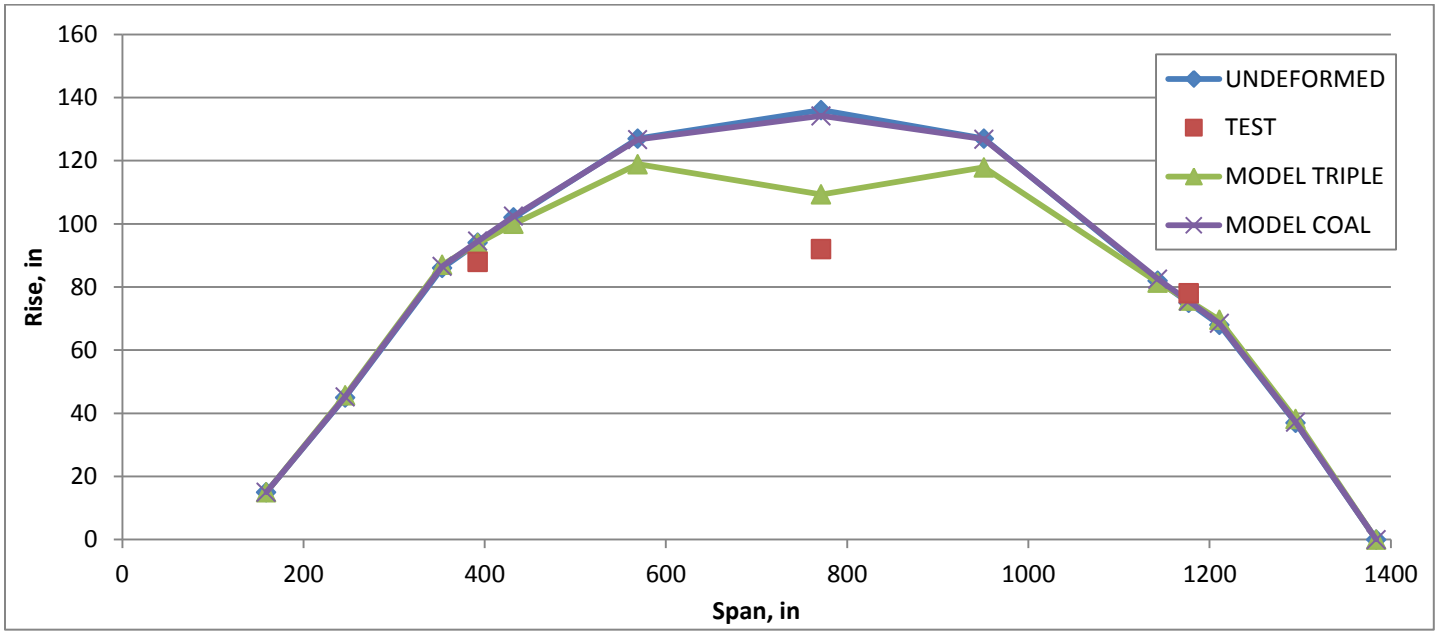

Figure D-1. Main St. Downstream Arch (Load at North Quarter Pt. in U-S Lane)

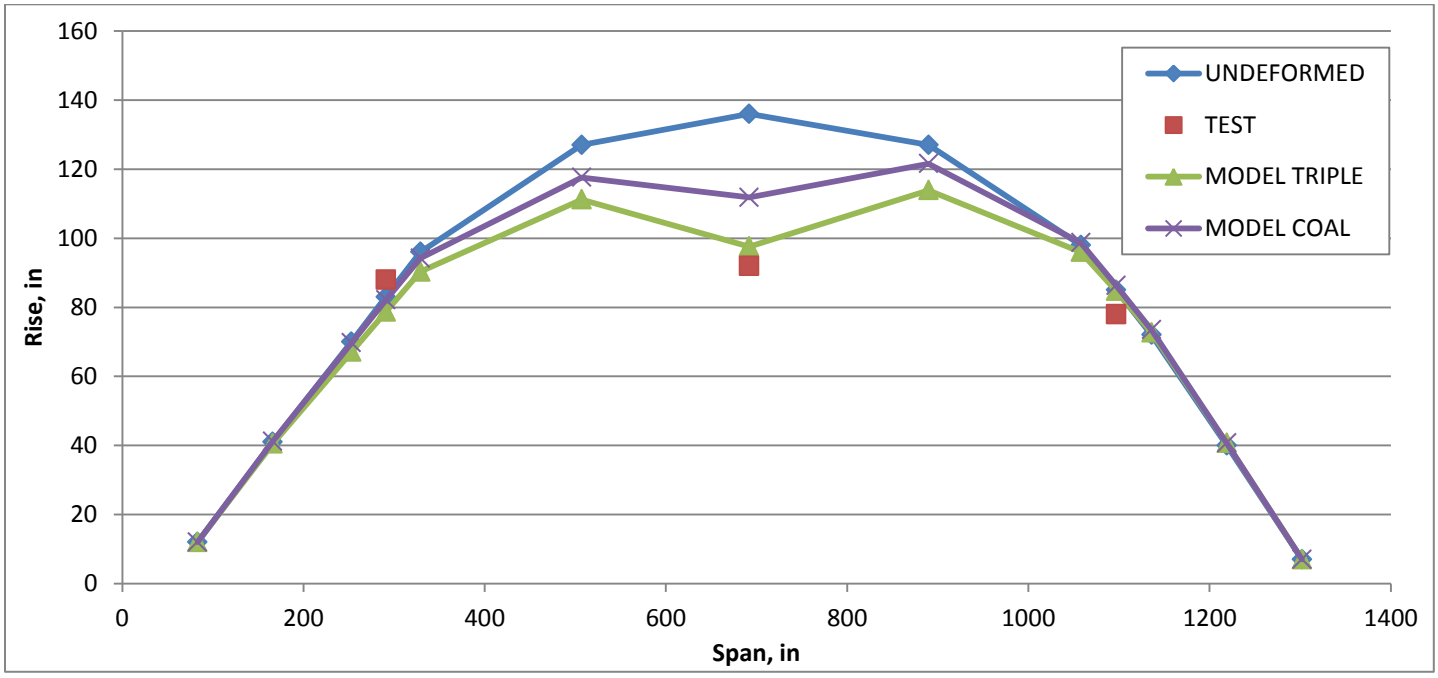

Figure D-2. Main St. Center Arch (Load at North Quarter Pt. in U-S Lane)

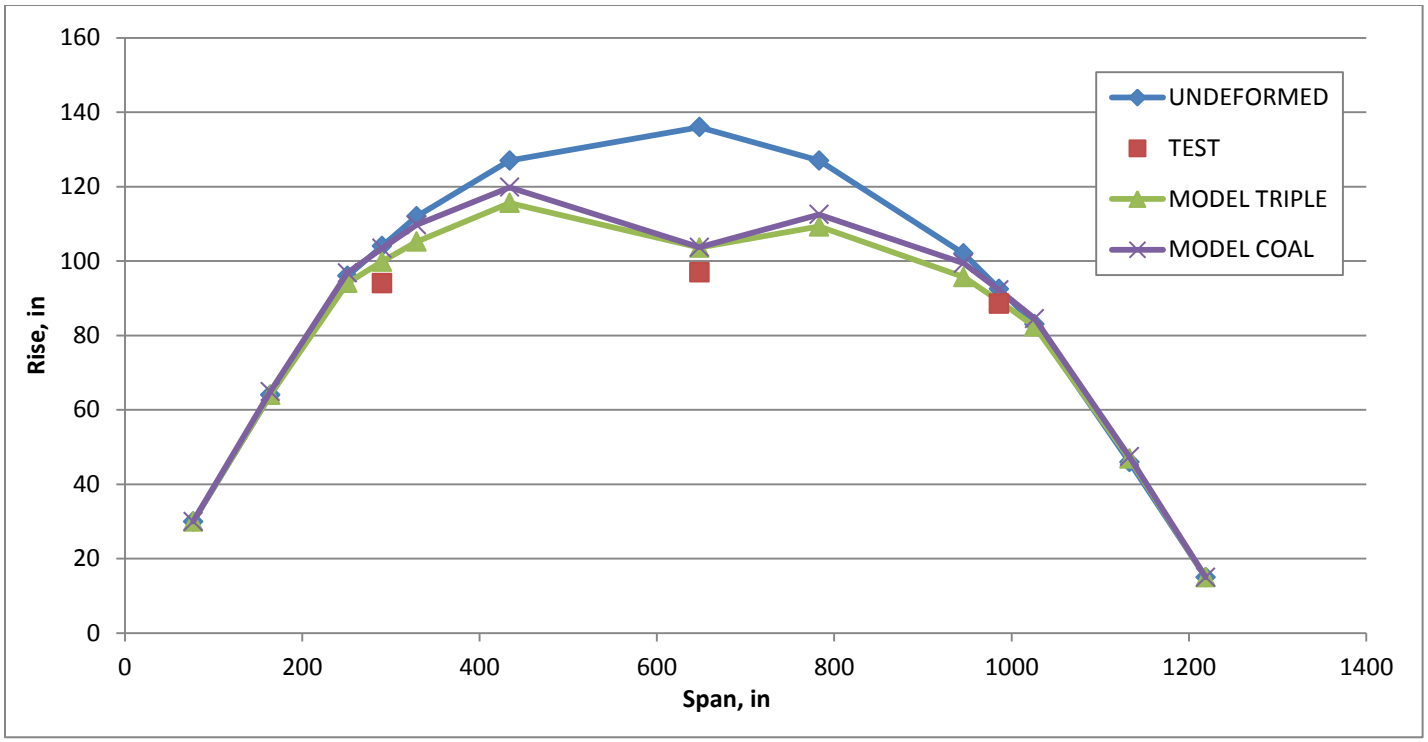

Figure D-3. Main St. Upstream Arch (Load at North Quarter Pt. in U-S Lane)

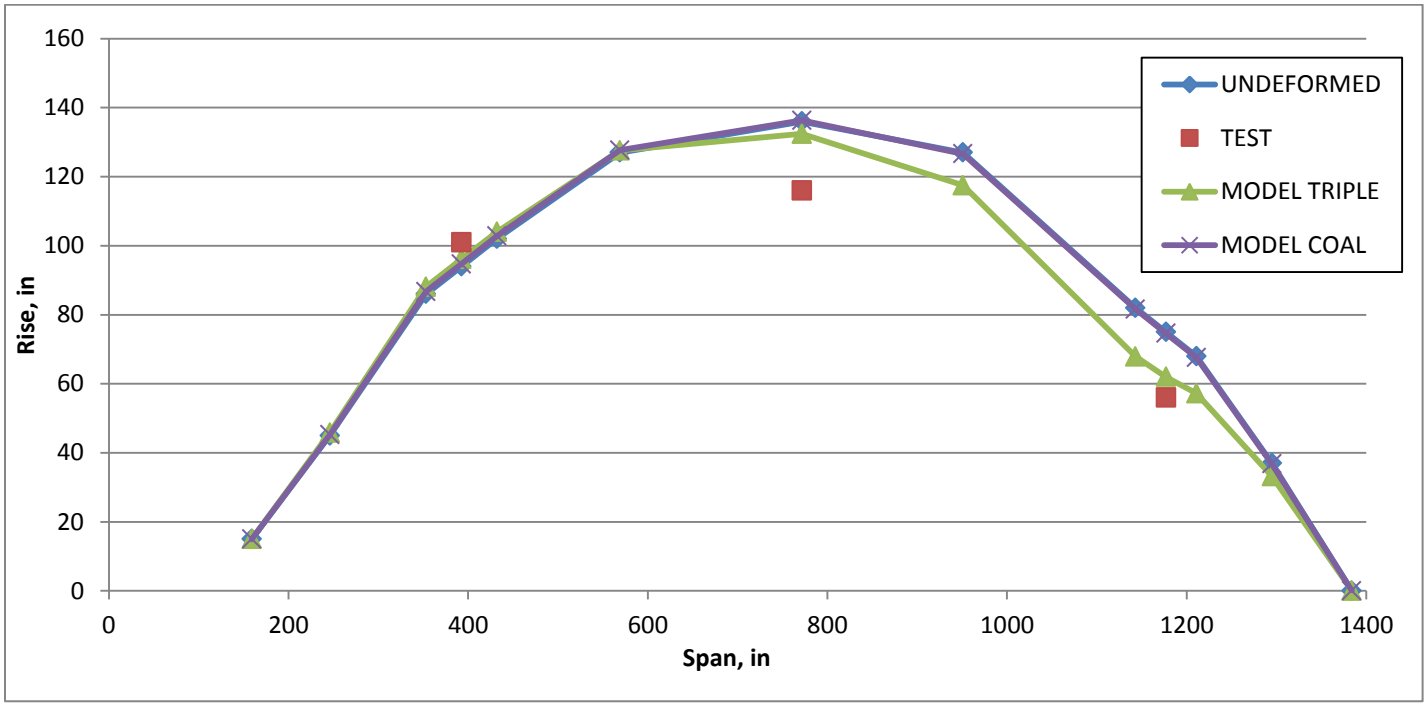

Figure D-4. Main St. Downstream Arch (Load at South Quarter Pt. in U-S Lane)

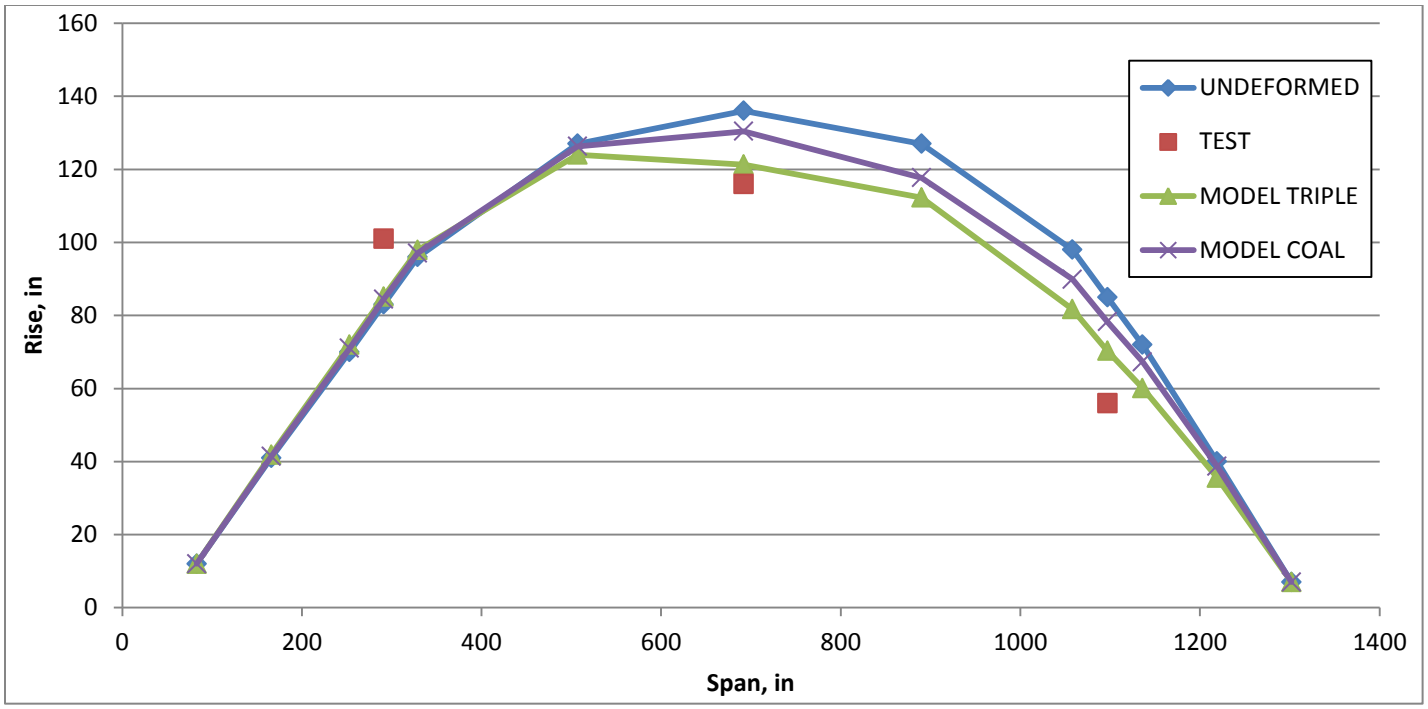

Figure D-5. Main St. Center Arch (Load at South Quarter Pt. in U-S Lane)

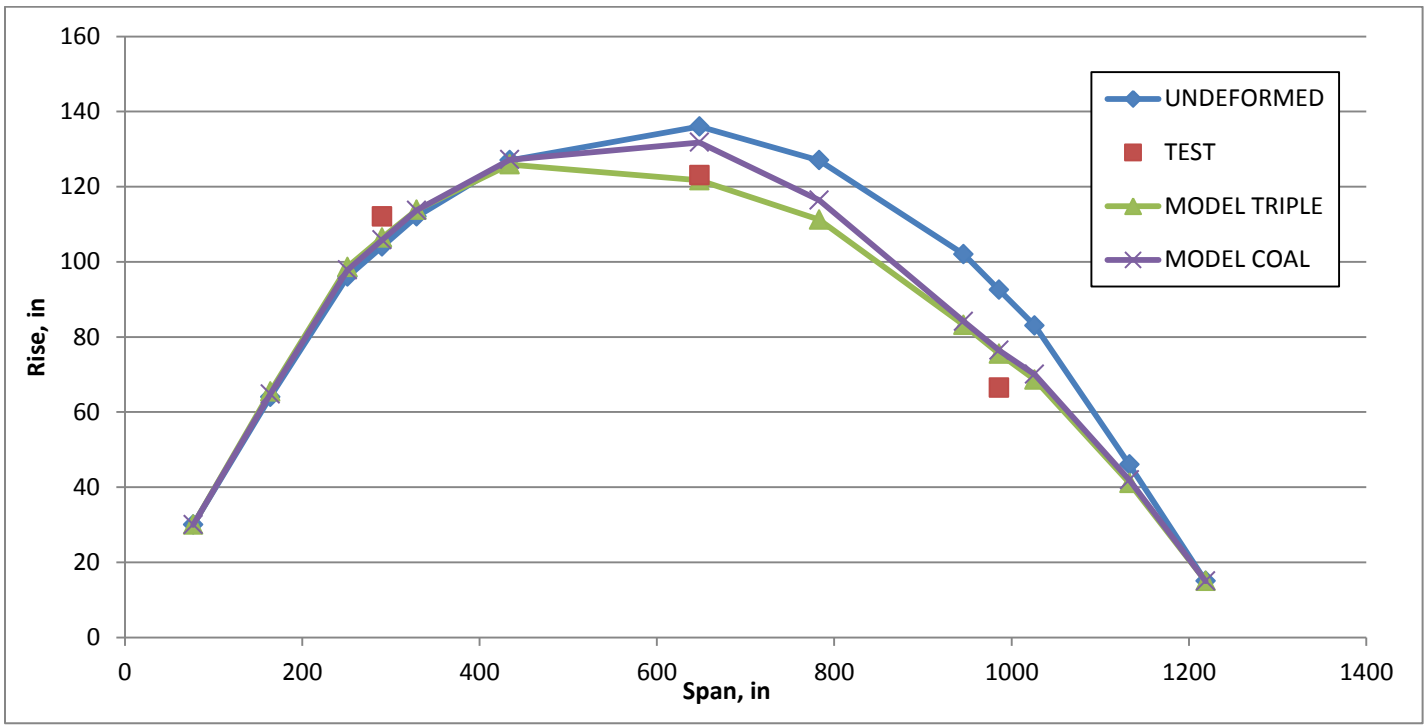

Figure D-6. Main St. Upstream Arch (Load at South Quarter Pt. in U-S Lane)

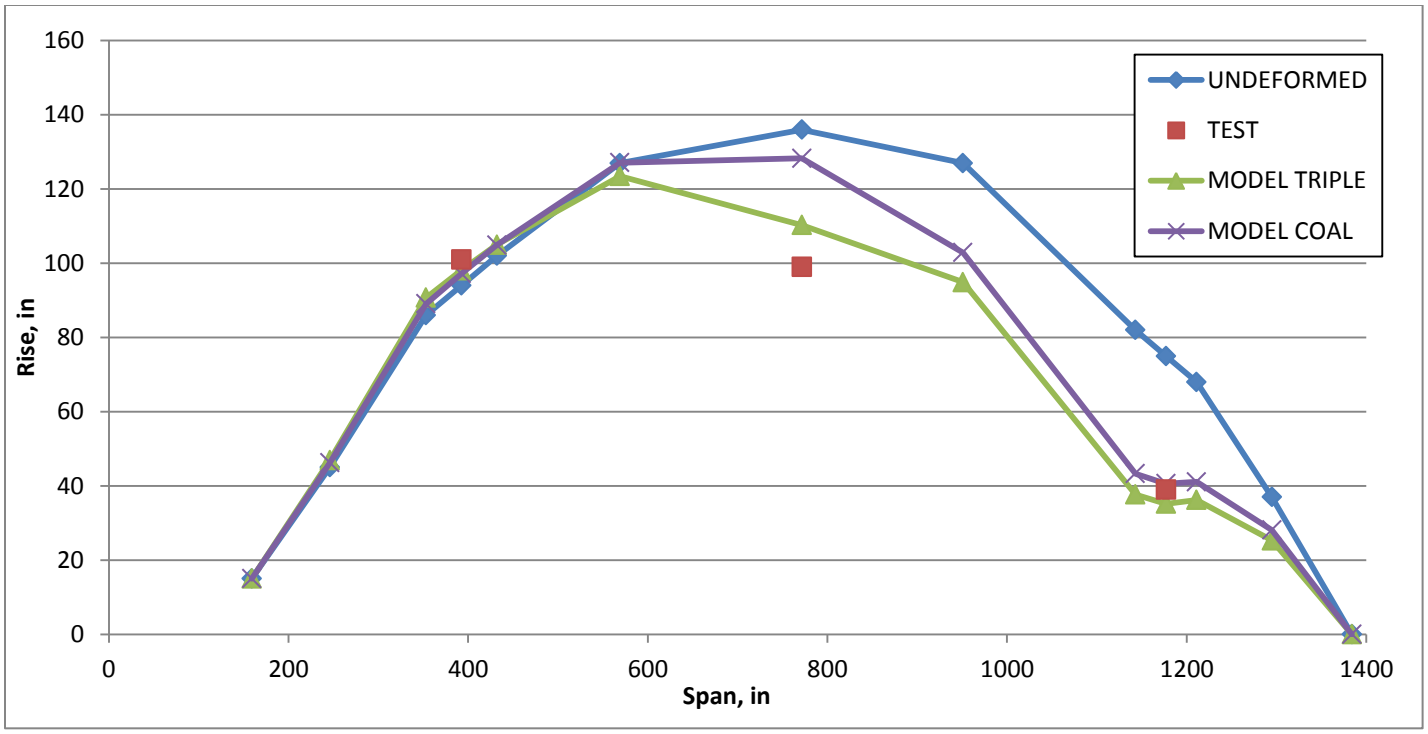

Figure D-7. Main St. Downstream Arch (Load at South Quarter Pt. in D-S Lane)

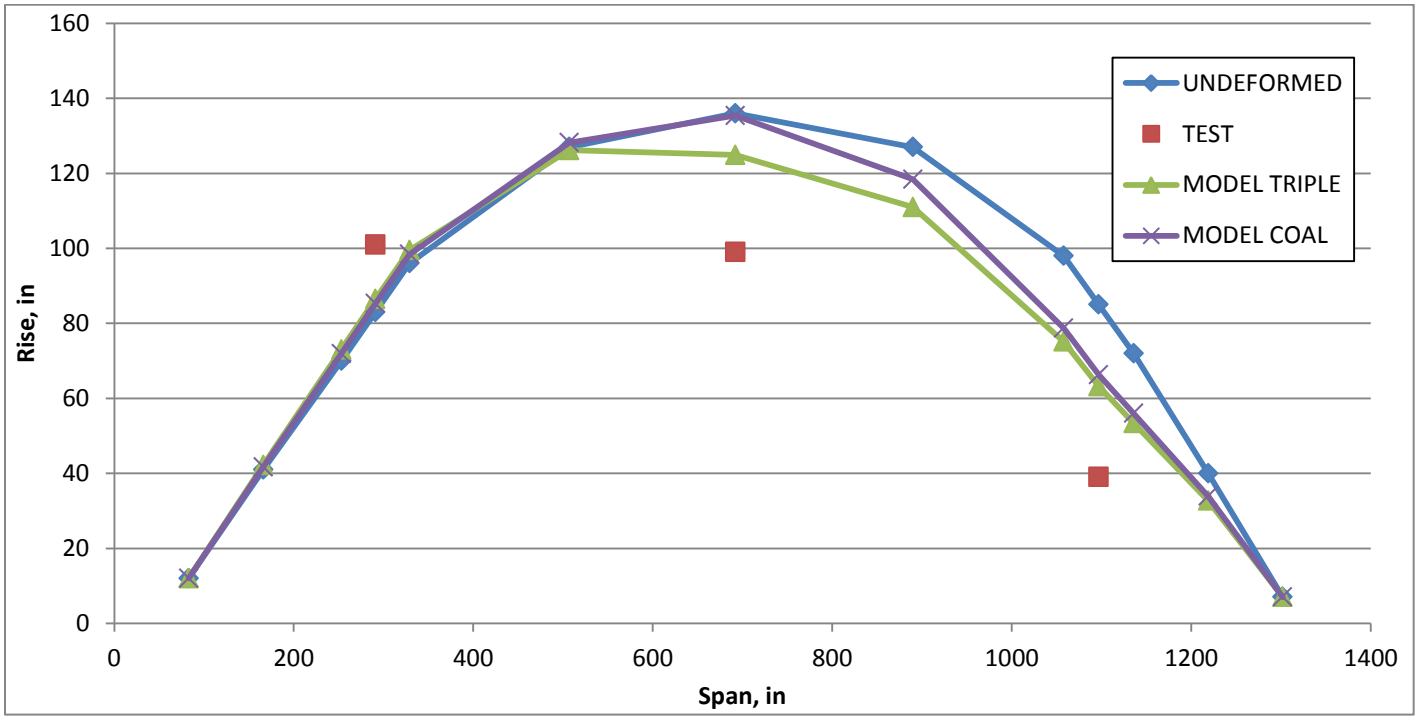

Figure D-8. Main St. Center Arch (Load at South Quarter Pt. in D-S Lane)

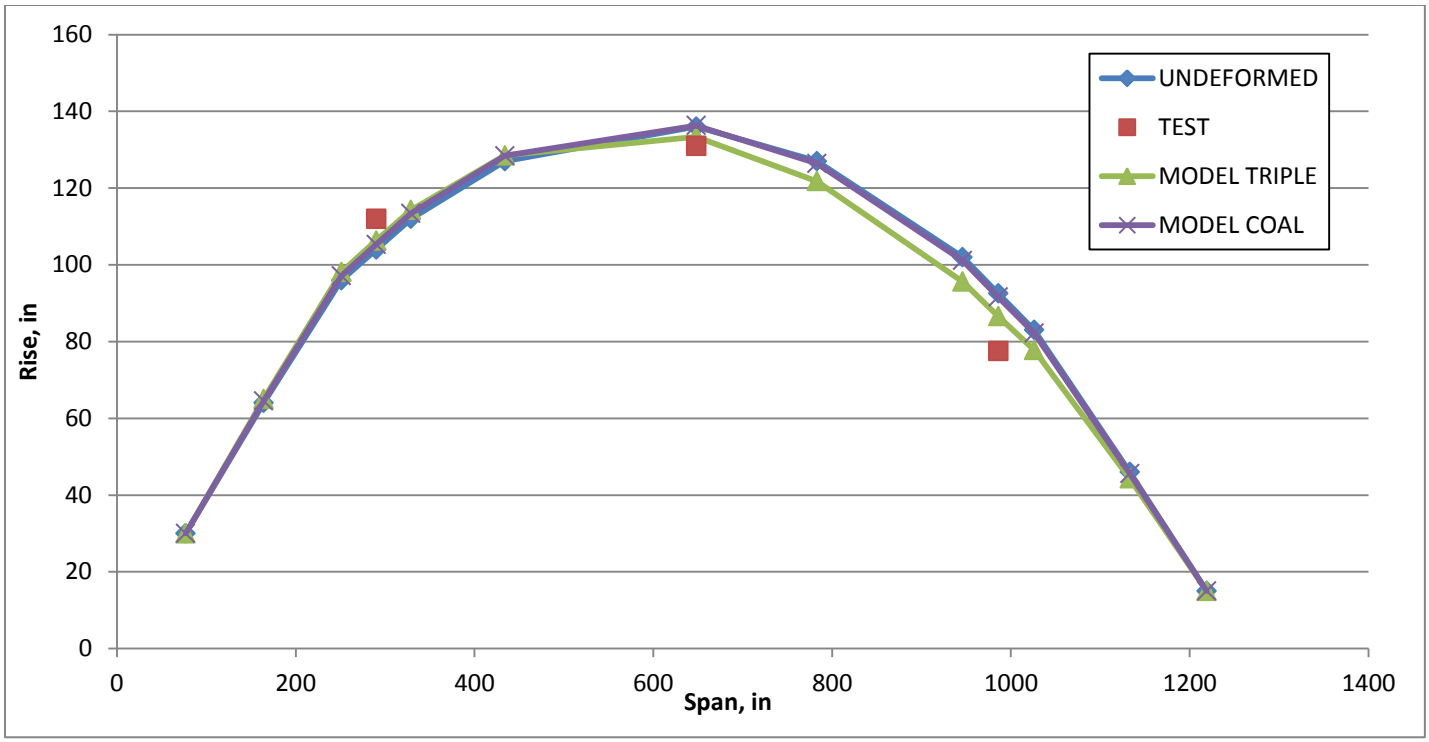

Figure D-9. Main St. Upstream Arch (Load at South Quarter Pt. in D-S Lane)

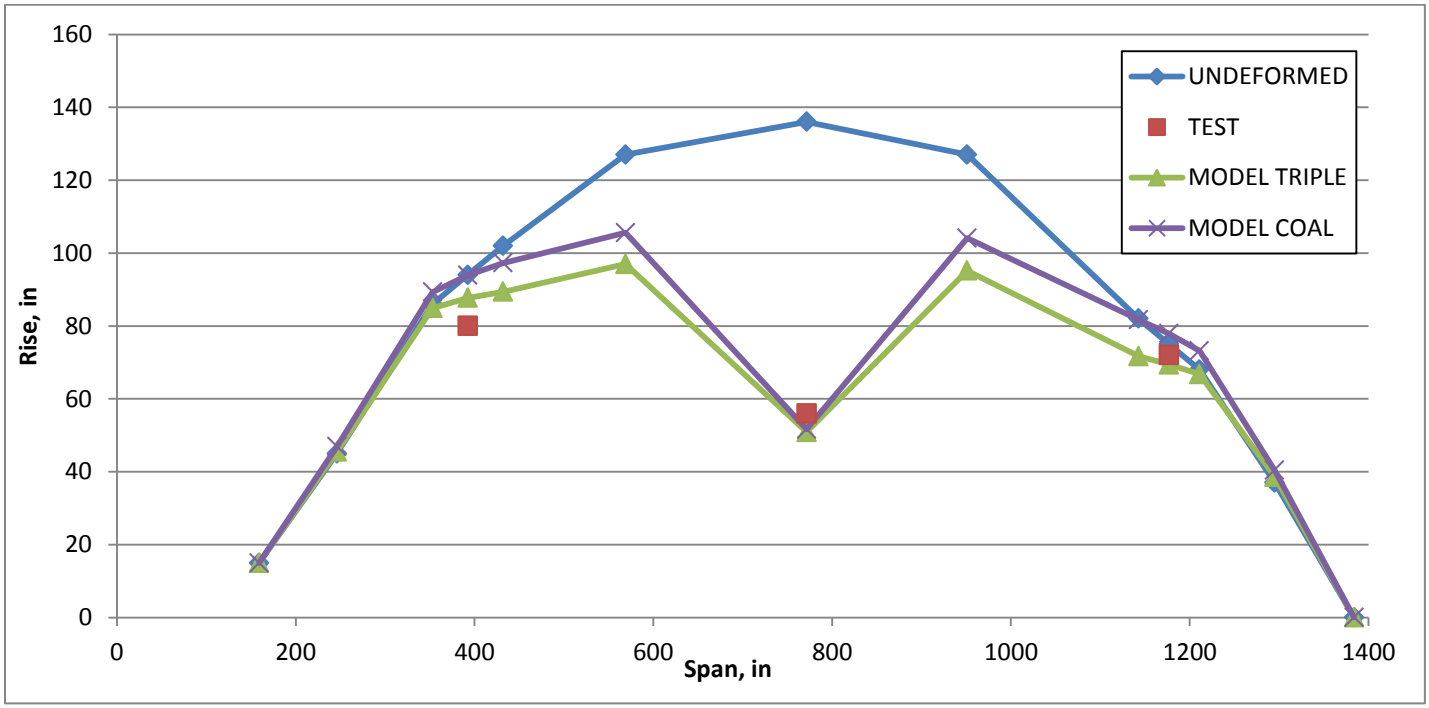

Figure D-10. Main St. Downstream Arch (Load at Midspan in D-S Lane)

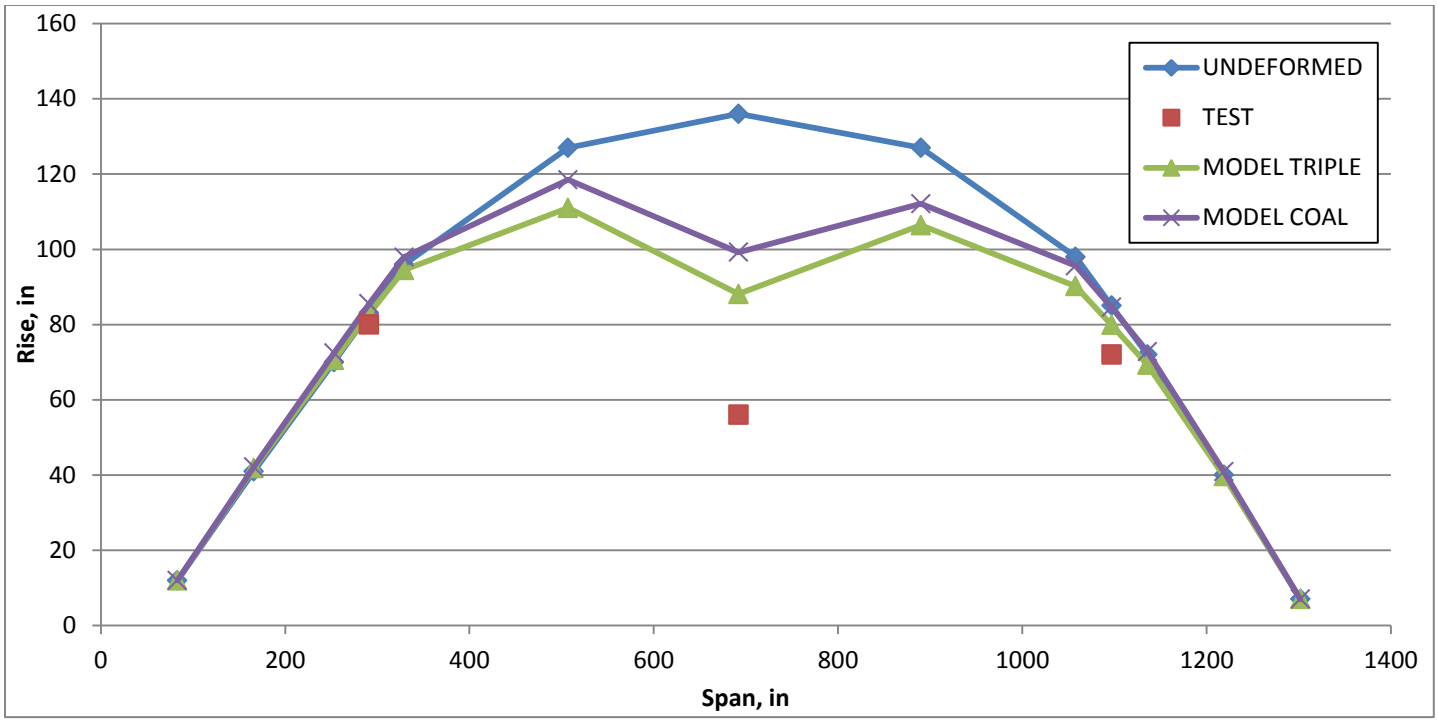

Figure D-11. Main St. Center Arch (Load at Midspan in D-S Lane)

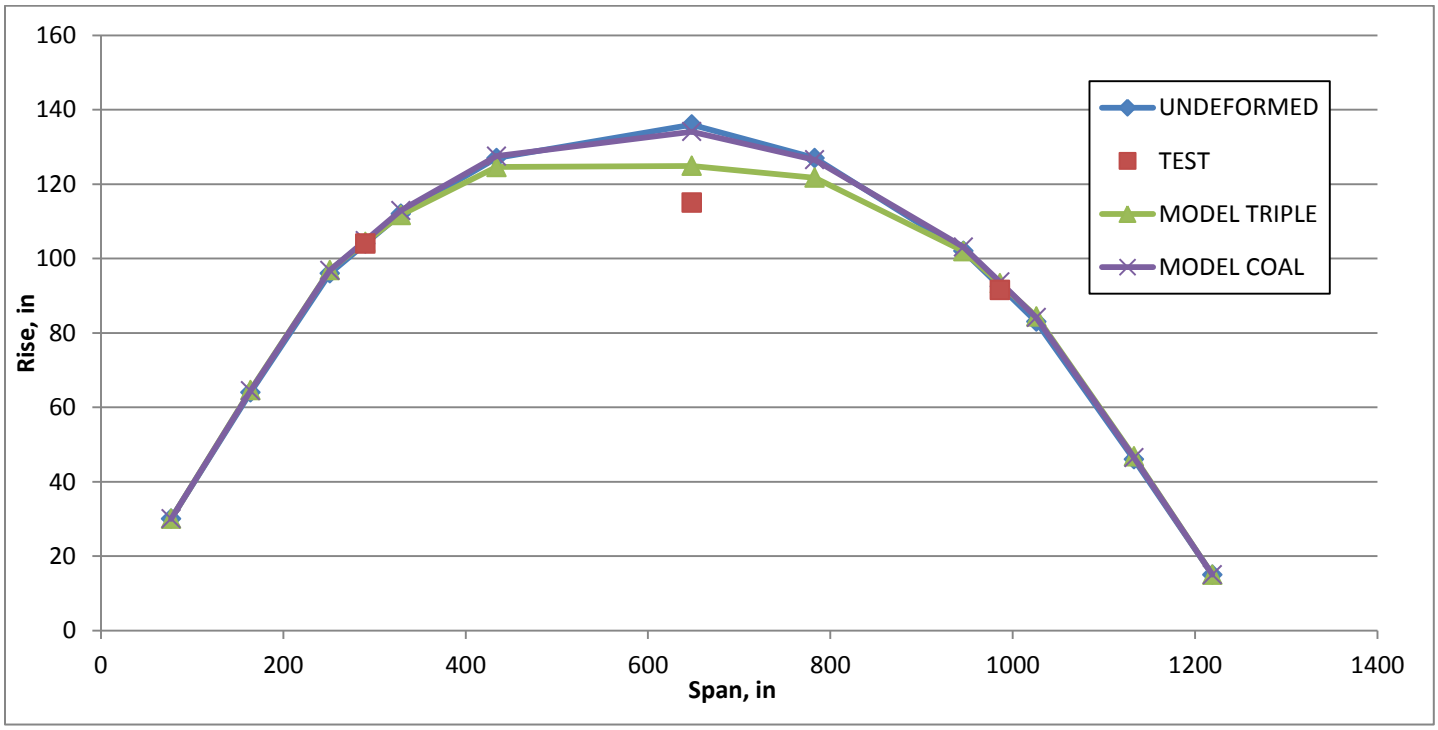

Figure D-12. Main St. Upstream Arch (Load at Midspan in D-S Lane)

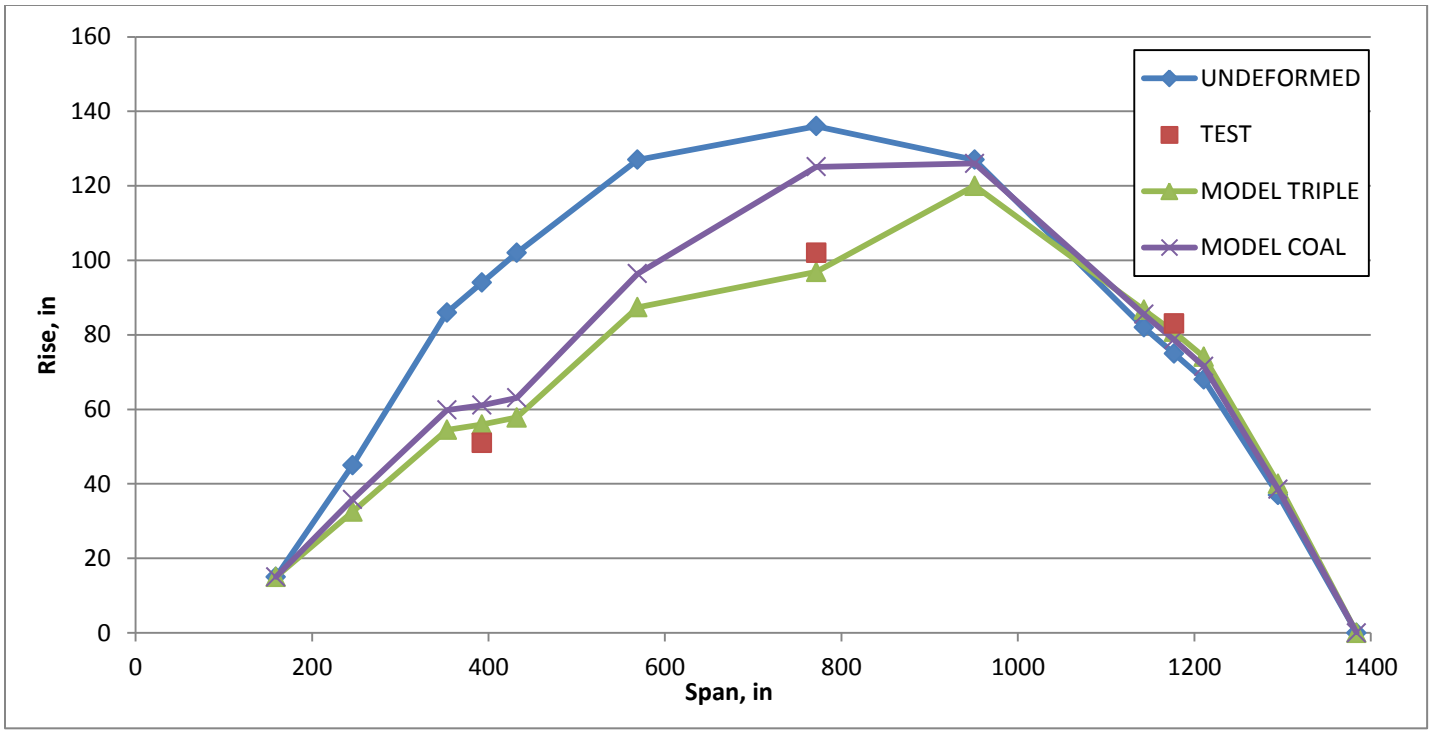

Figure D-13. Main St. Downstream Arch (Load at North Quarter Pt. in D-S Lane)

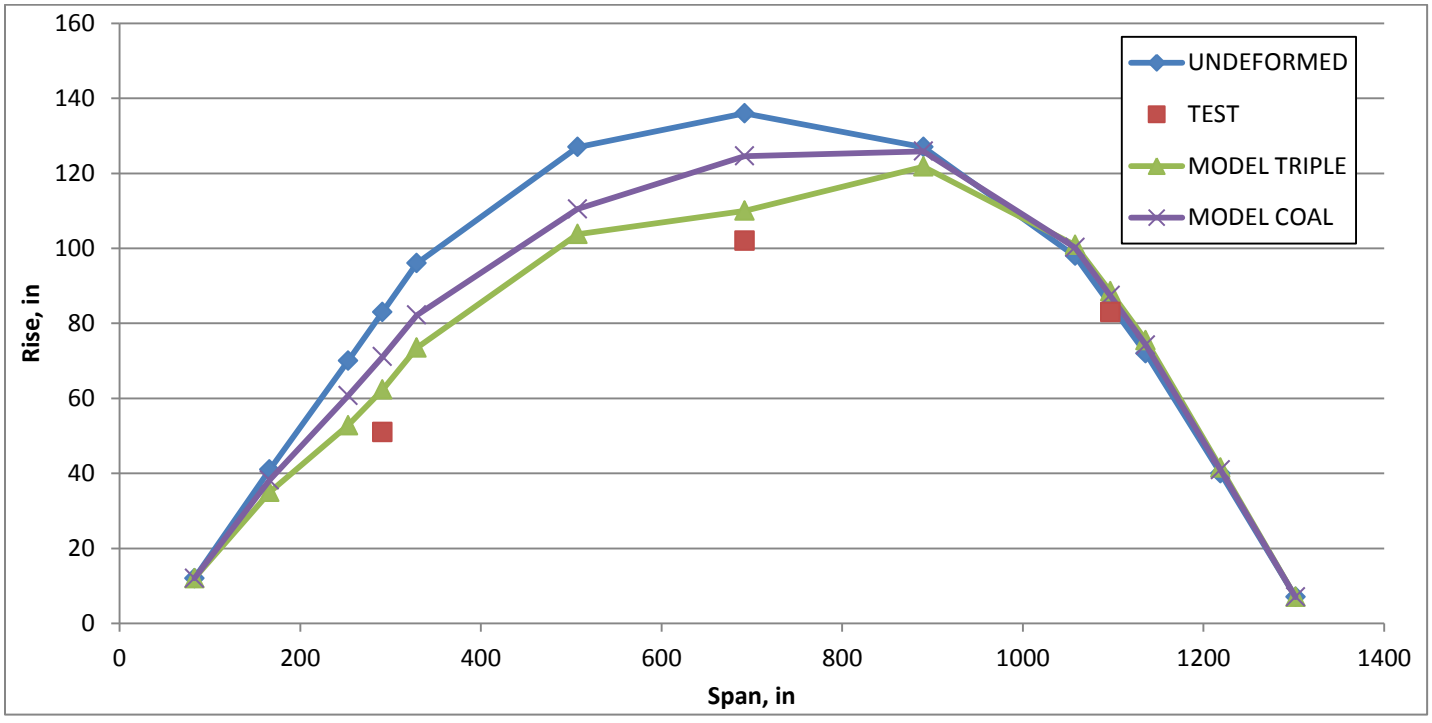

Figure D-14. Main St. Center Arch (Load at North Quarter Pt. in D-S Lane)

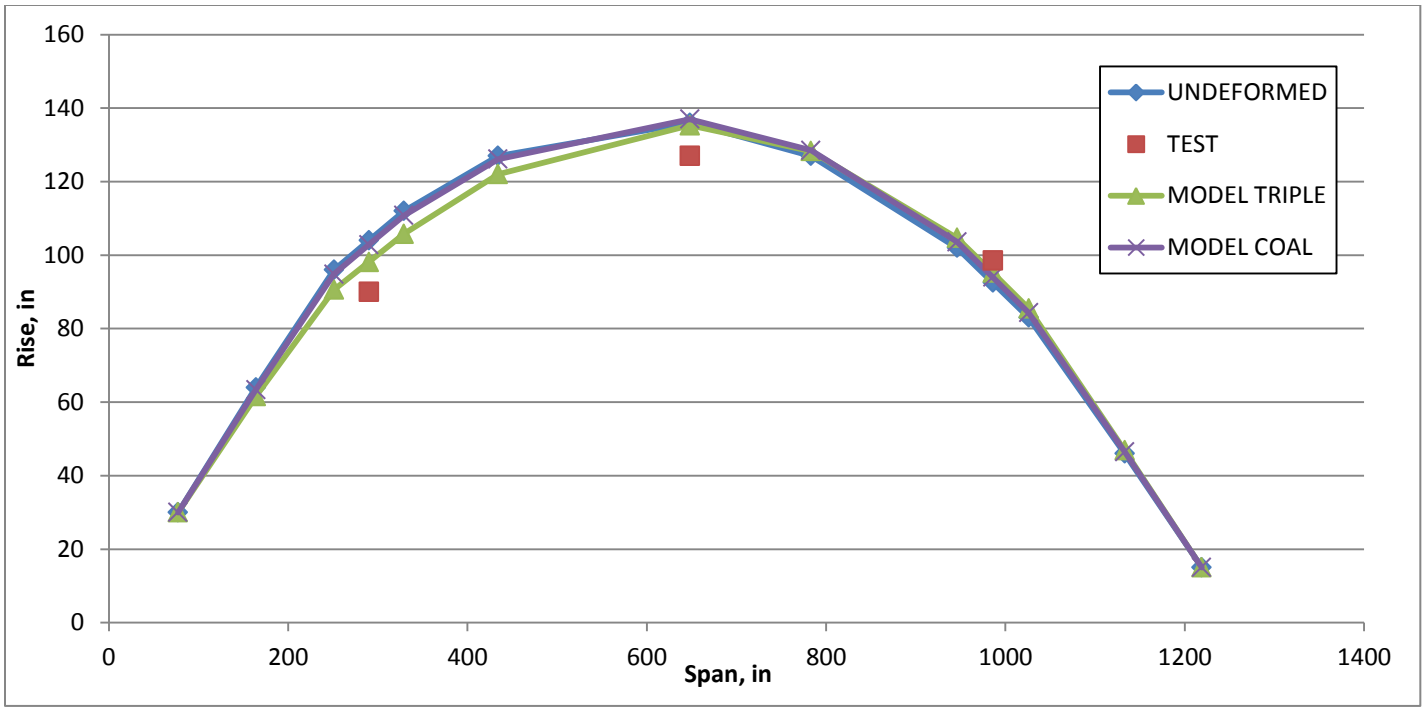

Figure D-15. Main St. Upstream Arch (Load at North Quarter Pt. in D-S Lane)

Appendix E - Depot Street Bridge Model Arch Deflection Plots

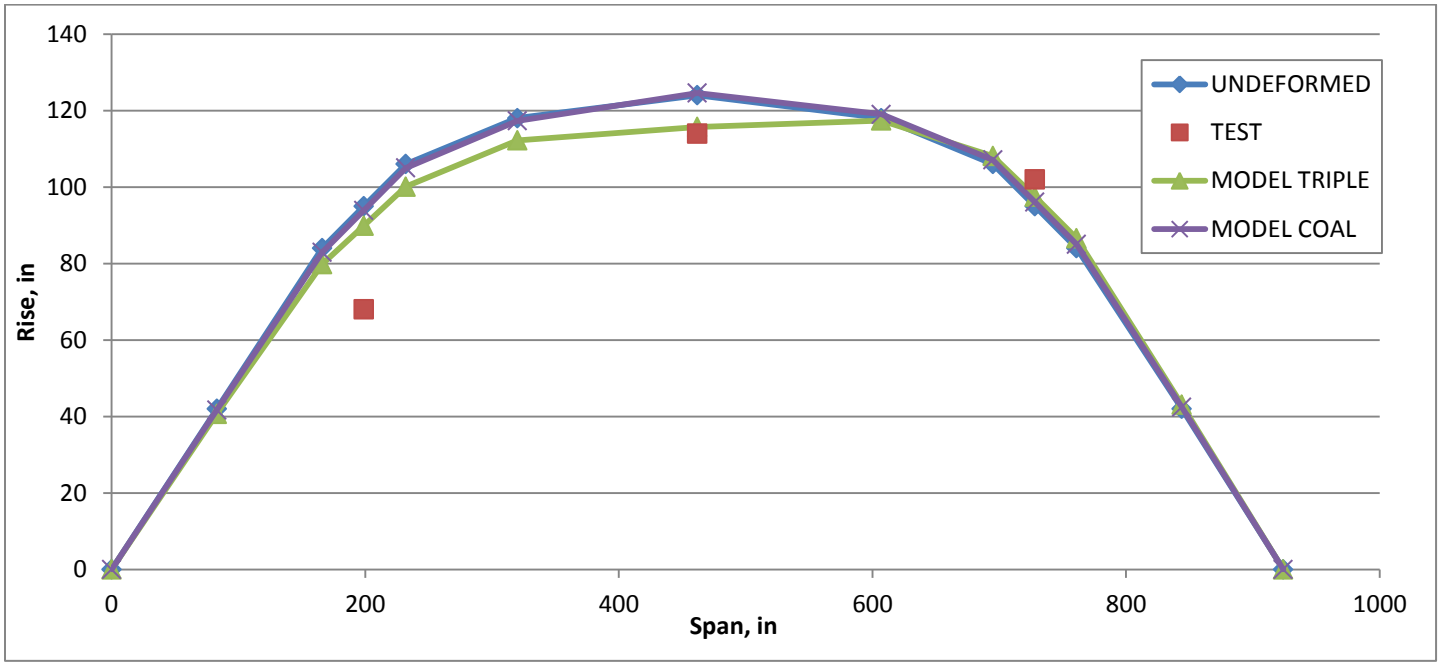

Figure E-1. Depot St. Downstream Arch (Load at North Quarter Pt. in U-S Lane)

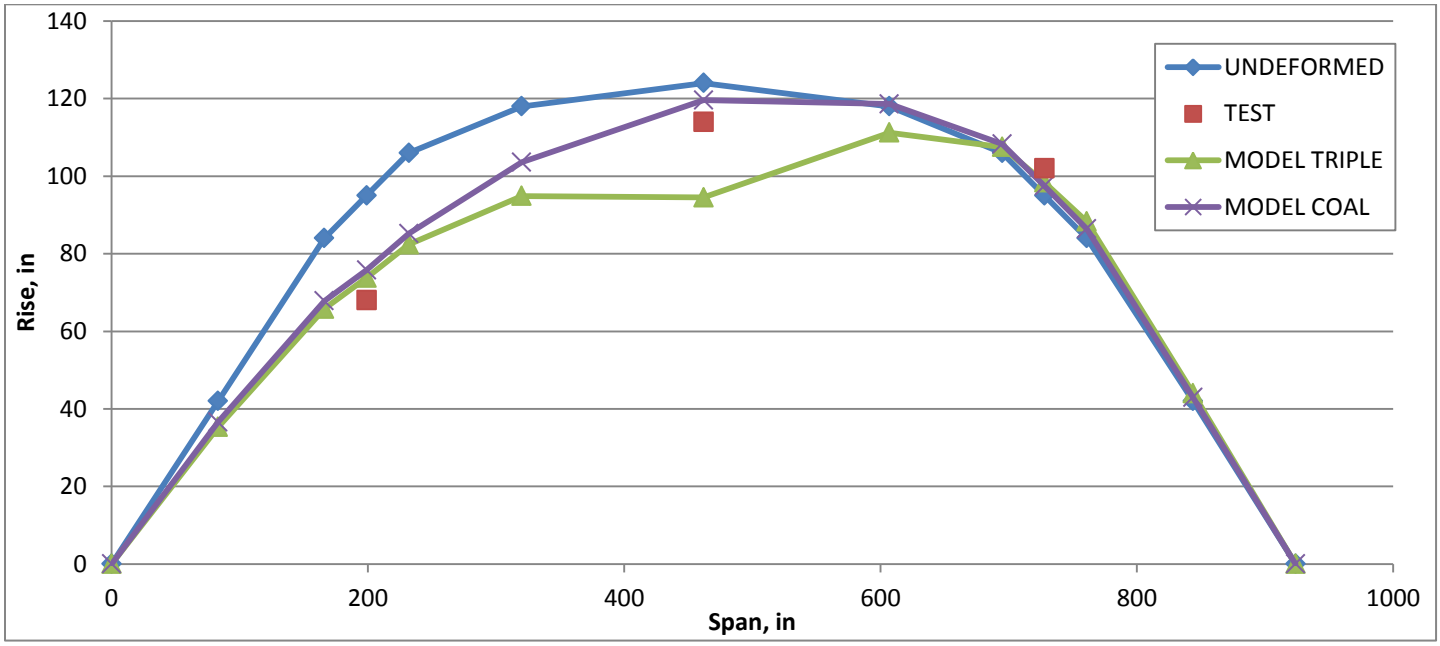

Figure E-2. Depot St. Center Arch (Load at North Quarter Pt. in U-S Lane)

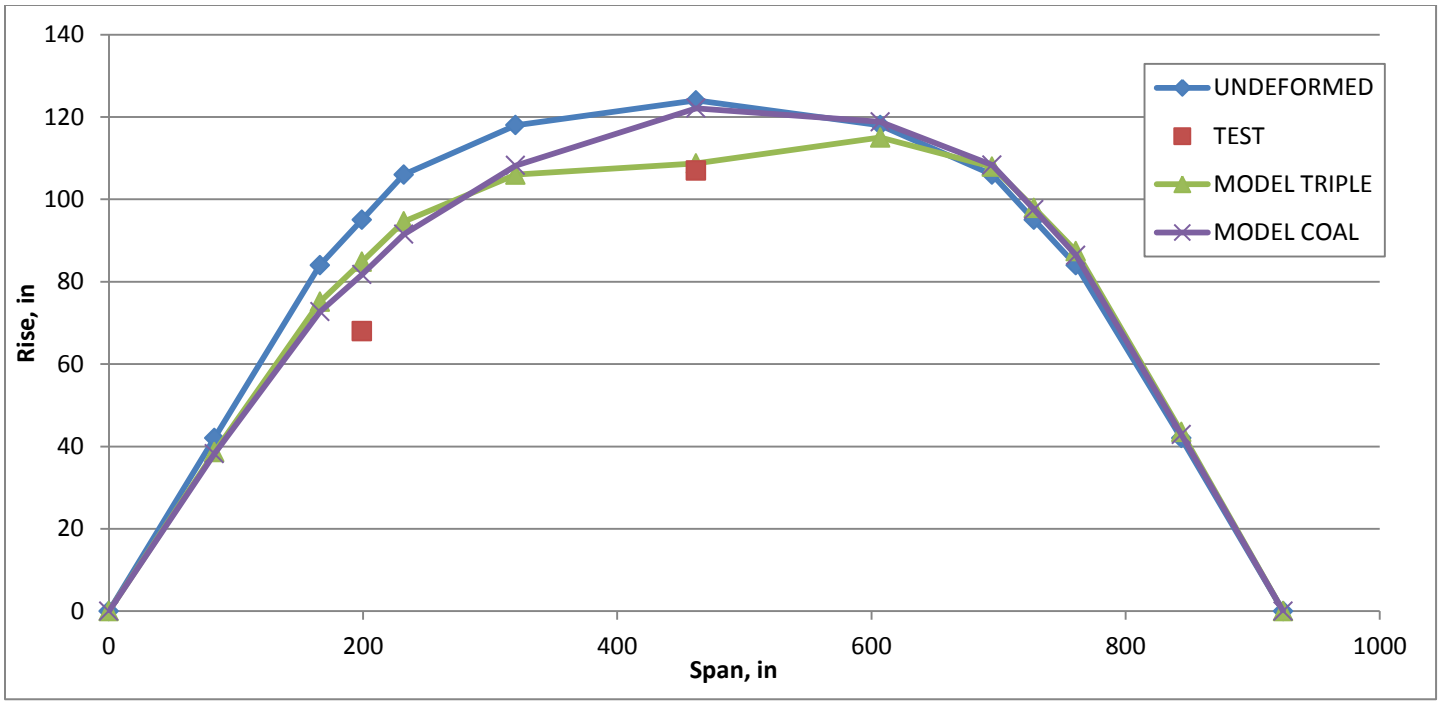

Figure E-3. Depot St. Upstream Arch (Load at North Quarter Pt. in U-S Lane)

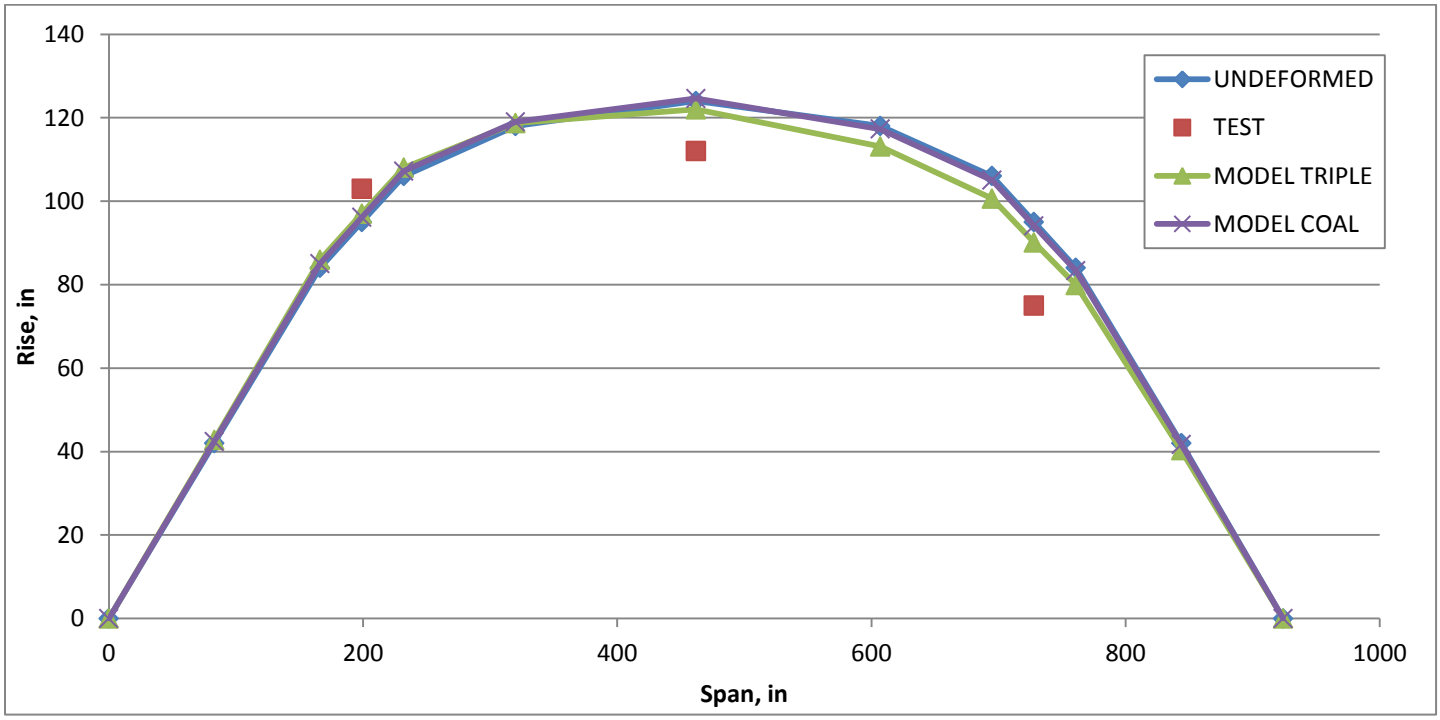

Figure E-4. Depot St. Downstream Arch (Load at South Quarter Pt. in U-S Lane)

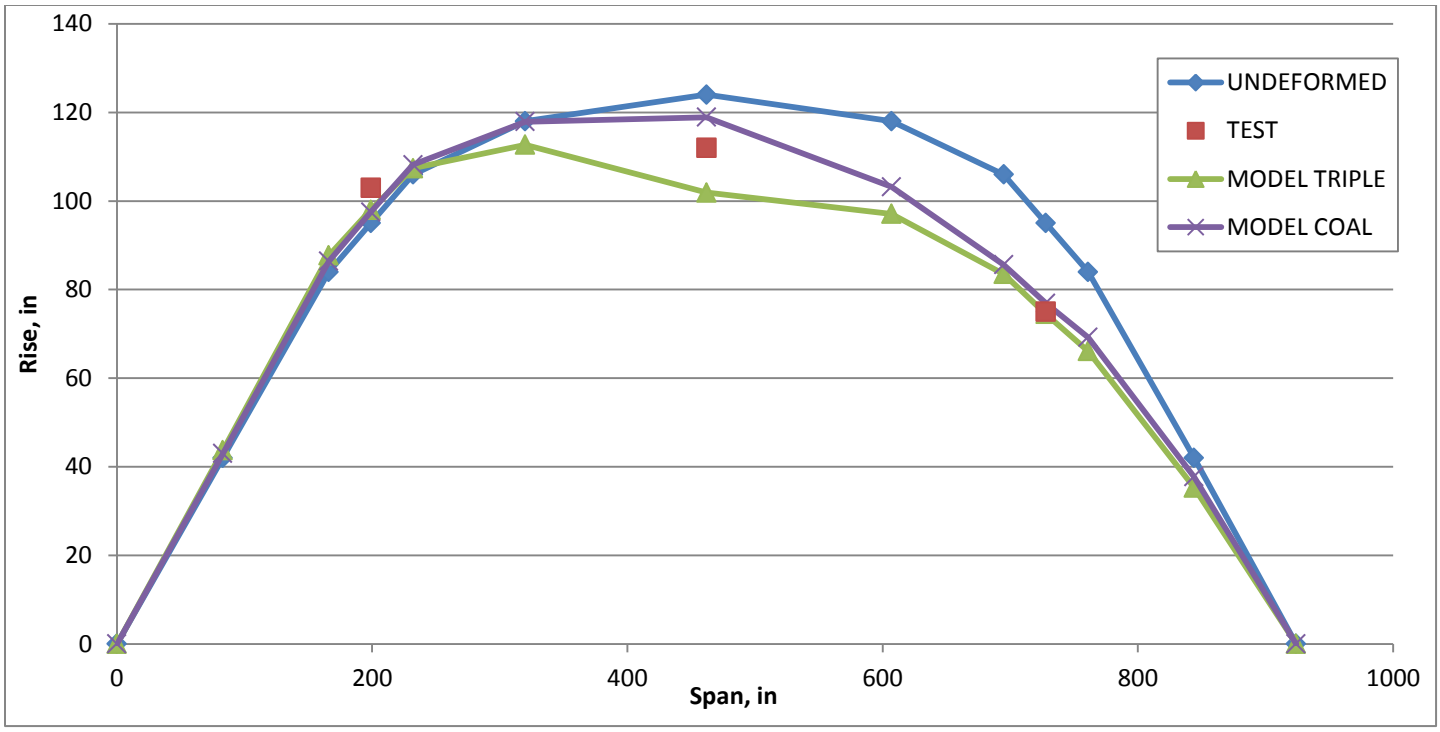

Figure E-5. Depot St. Center Arch (Load at South Quarter Pt. in U-S Lane)

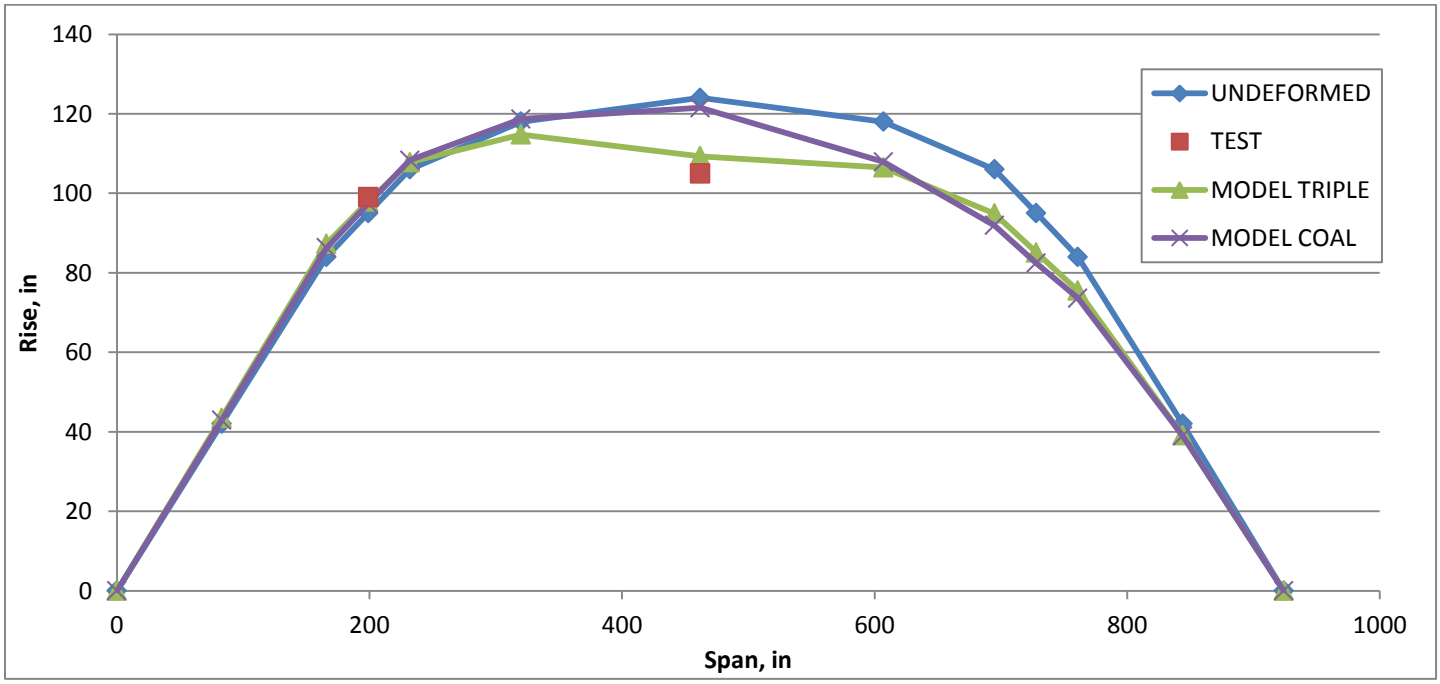

Figure E-6. Depot St. Upstream Arch (Load at South Quarter Pt. in U-S Lane)

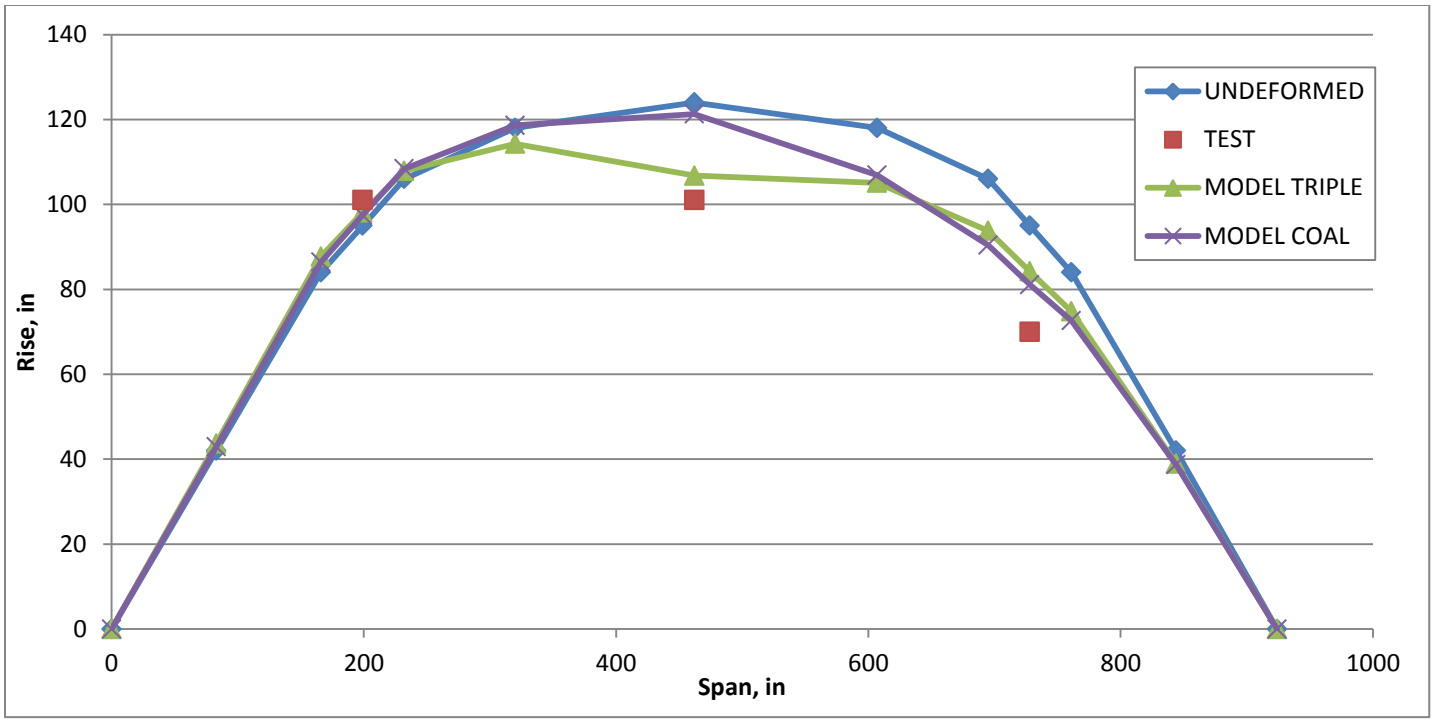

Figure E-7. Depot St. Downstream Arch (Load at South Quarter Pt. in D-S Lane)

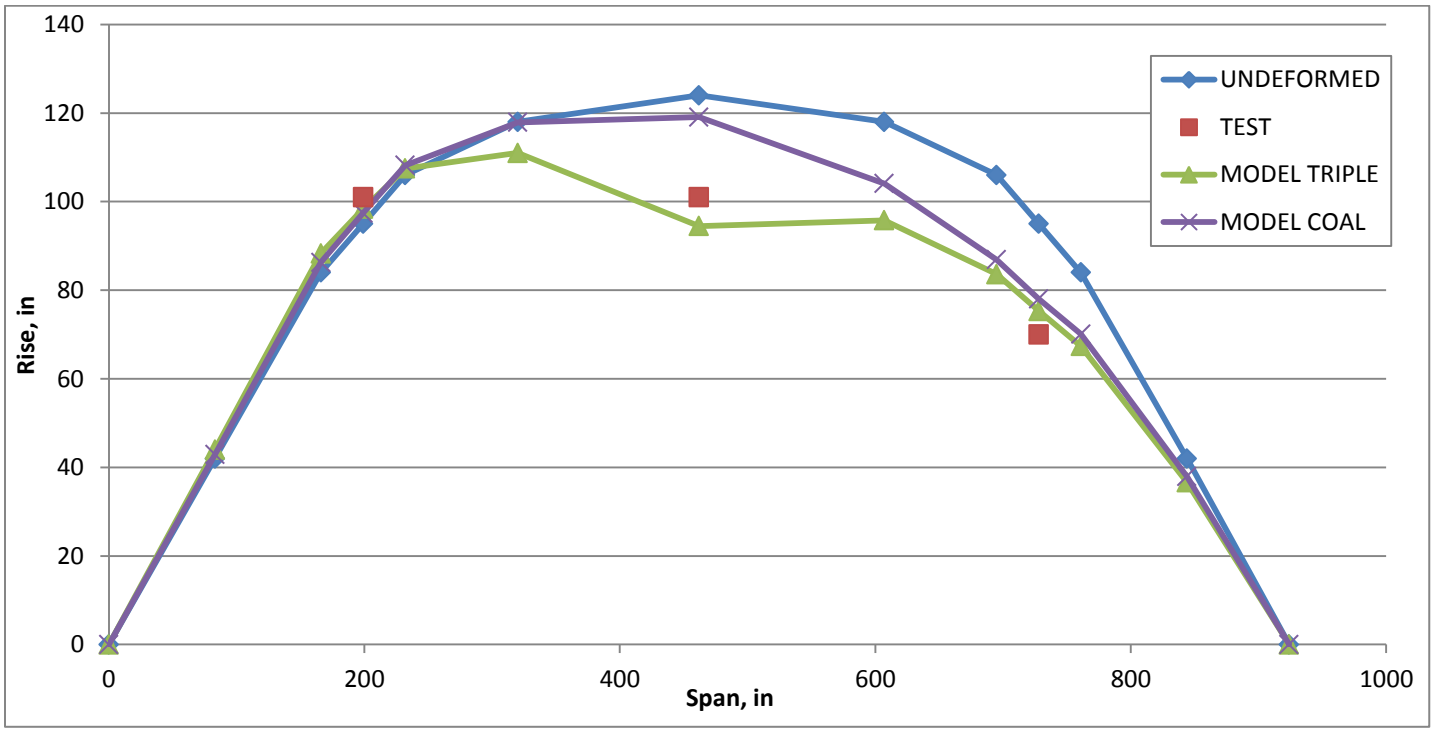

Figure E-8. Depot St. Center Arch (Load at South Quarter Pt. in D-S Lane)

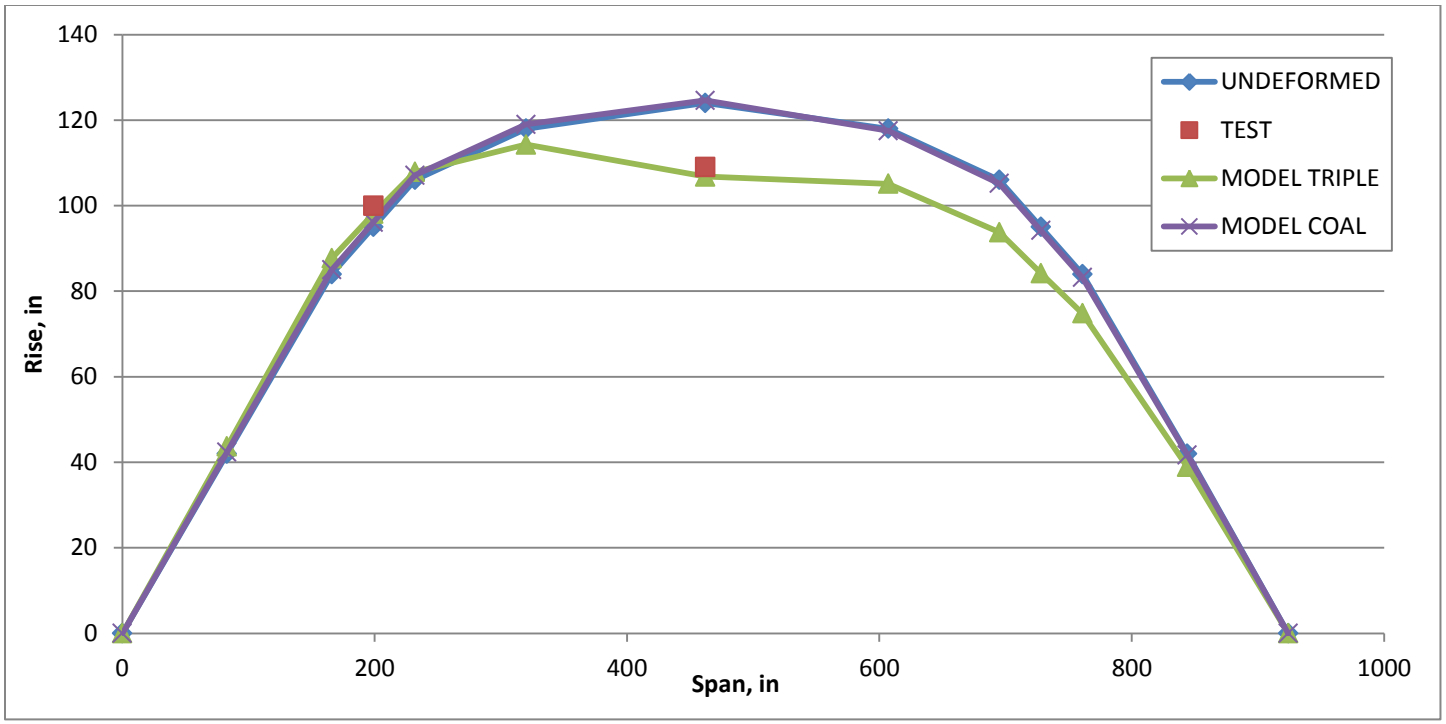

Figure E-9. Depot St. Upstream Arch (Load at South Quarter Pt. in D-S Lane)

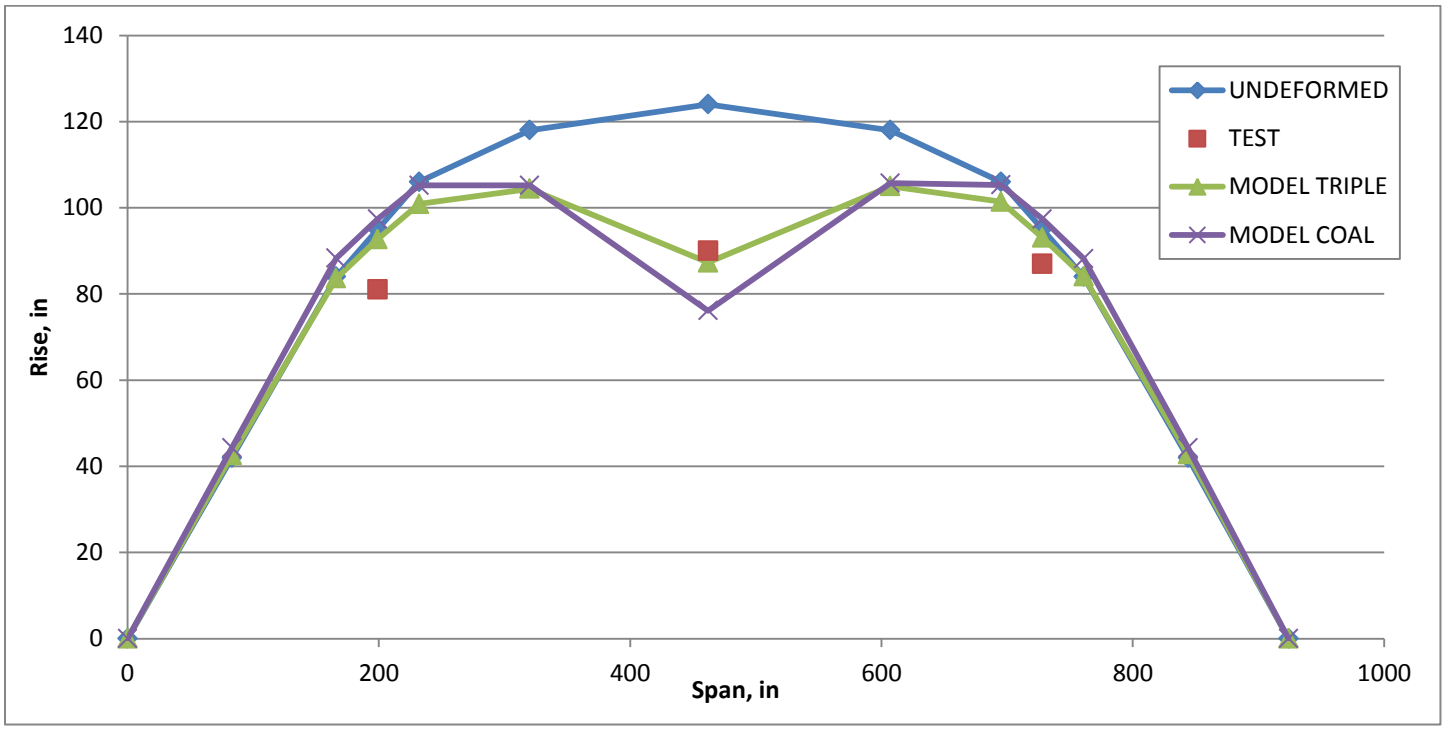

Figure E-10. Depot St. Downstream Arch (Load at Midspan in D-S Lane)

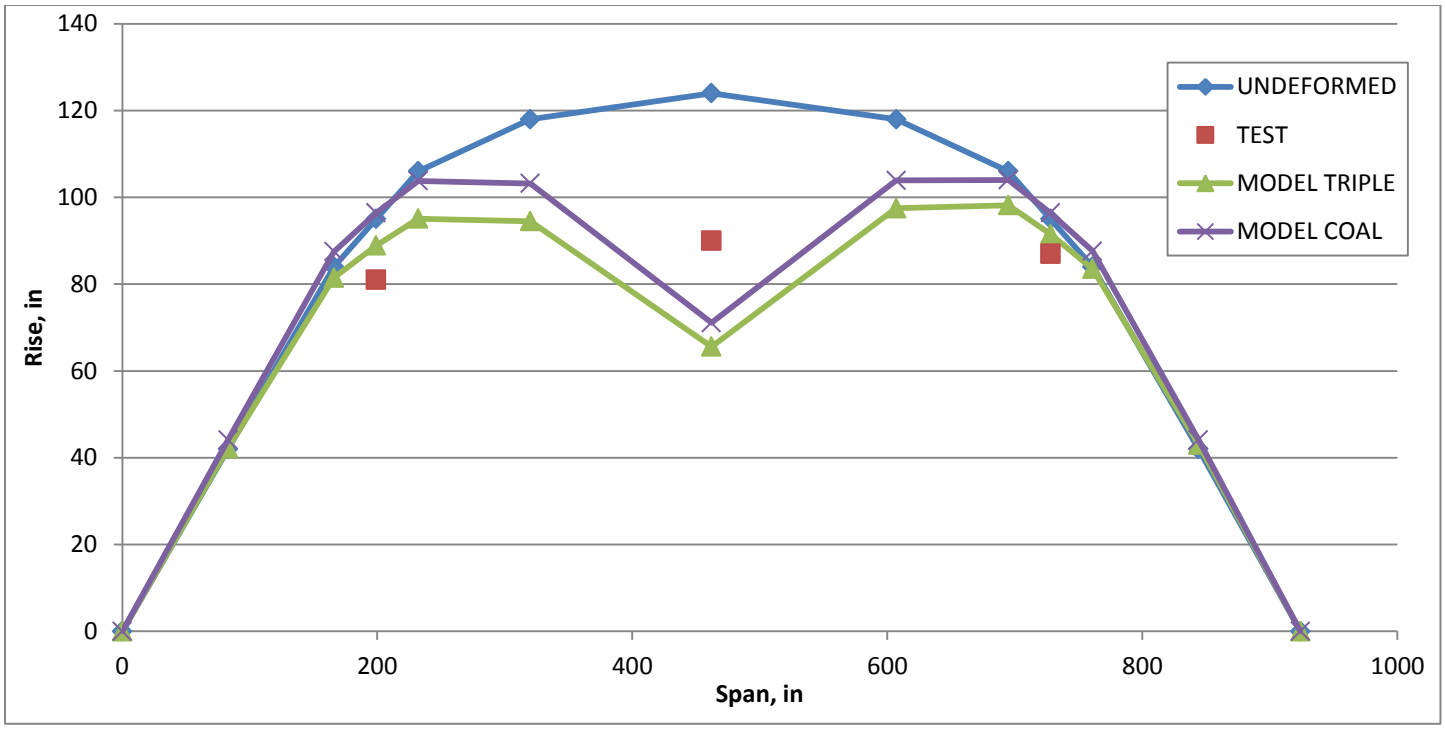

Figure E-11. Depot St. Center Arch (Load at Midspan in D-S Lane)

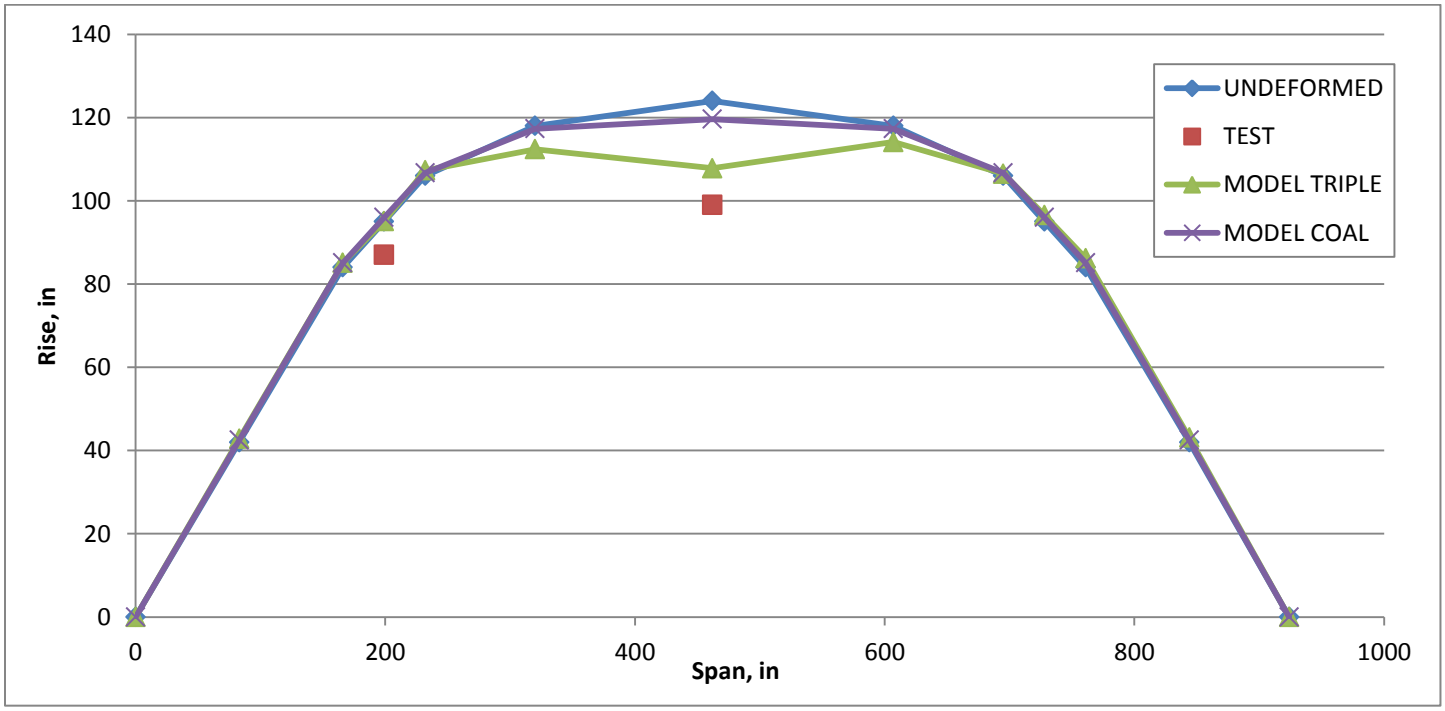

Figure E-12. Depot St. Upstream Arch (Load at Midspan in D-S Lane)

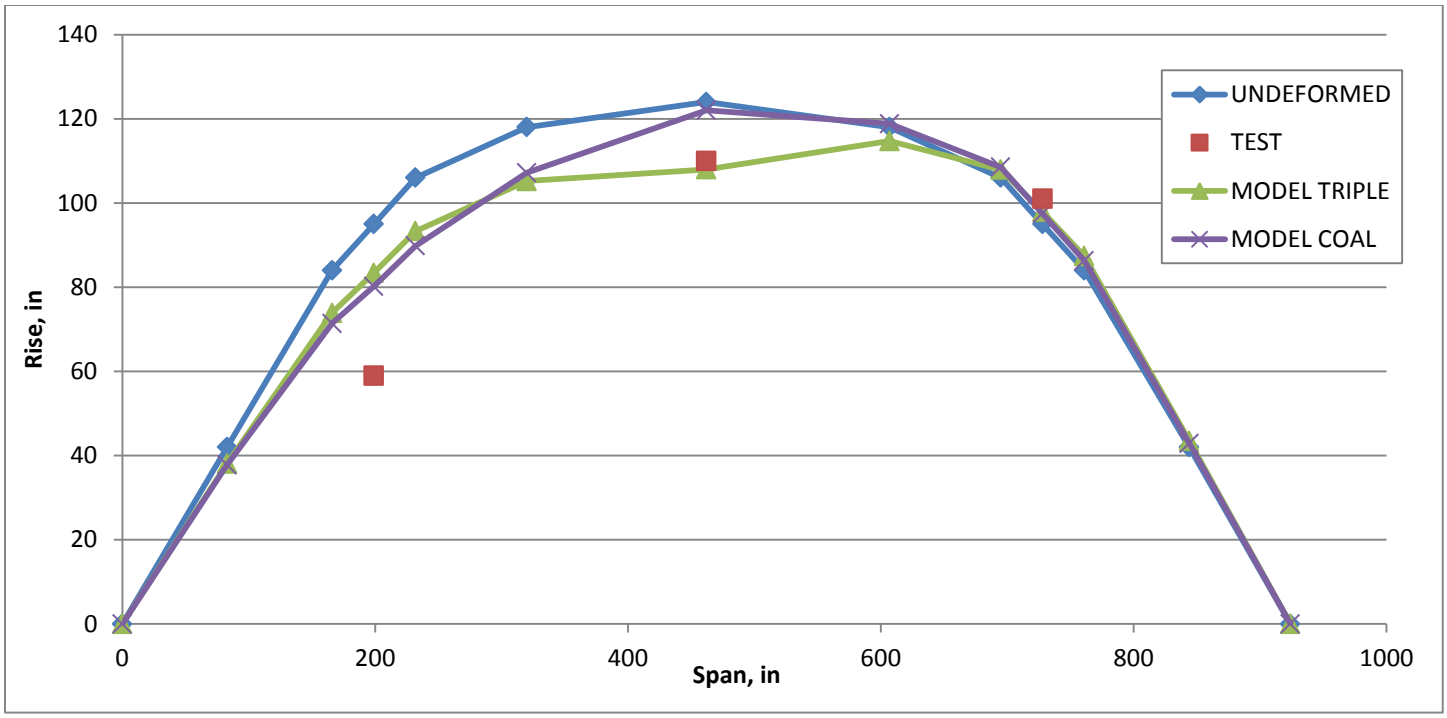

Figure E-13. Depot St. Downstream Arch (Load at North Quarter Pt. in D-S Lane)

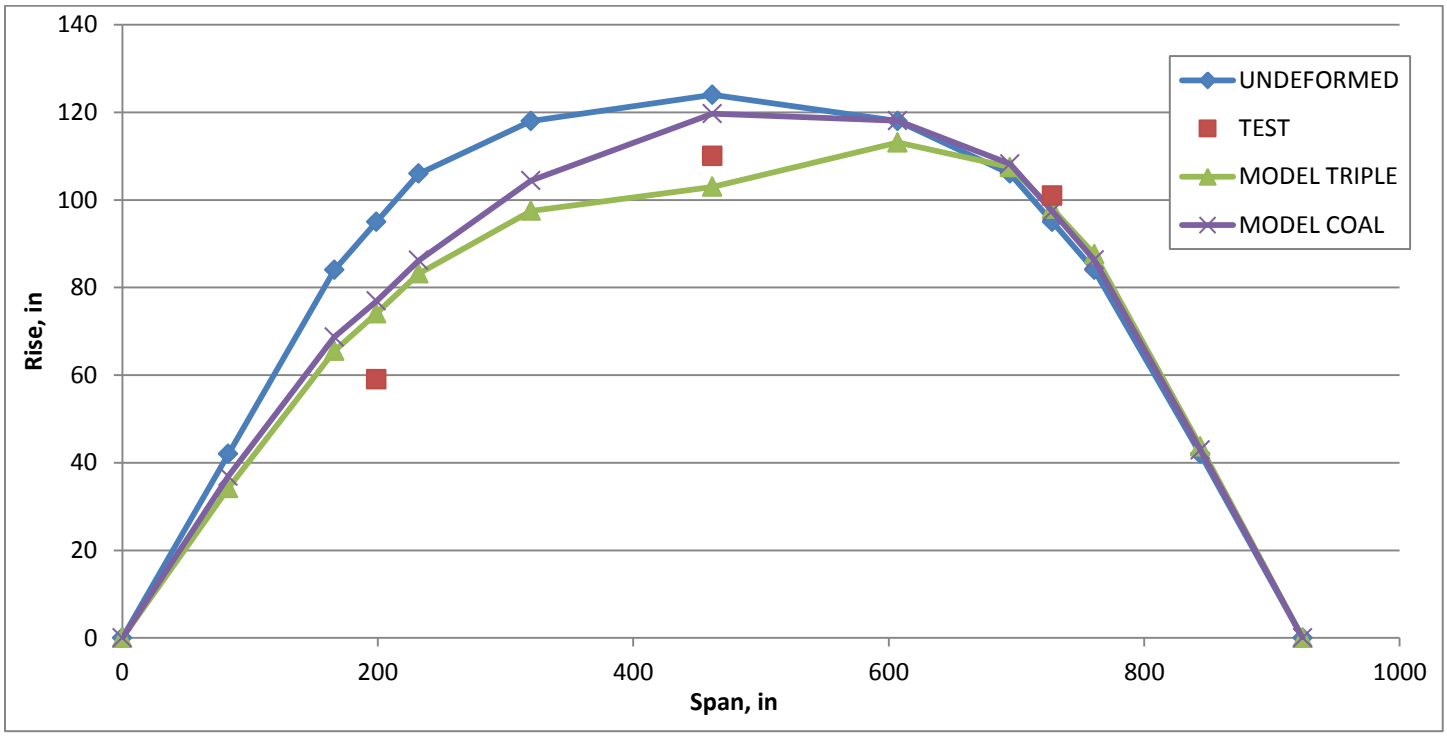

Figure E-14. Depot St. Center Arch (Load at North Quarter Pt. in D-S Lane)

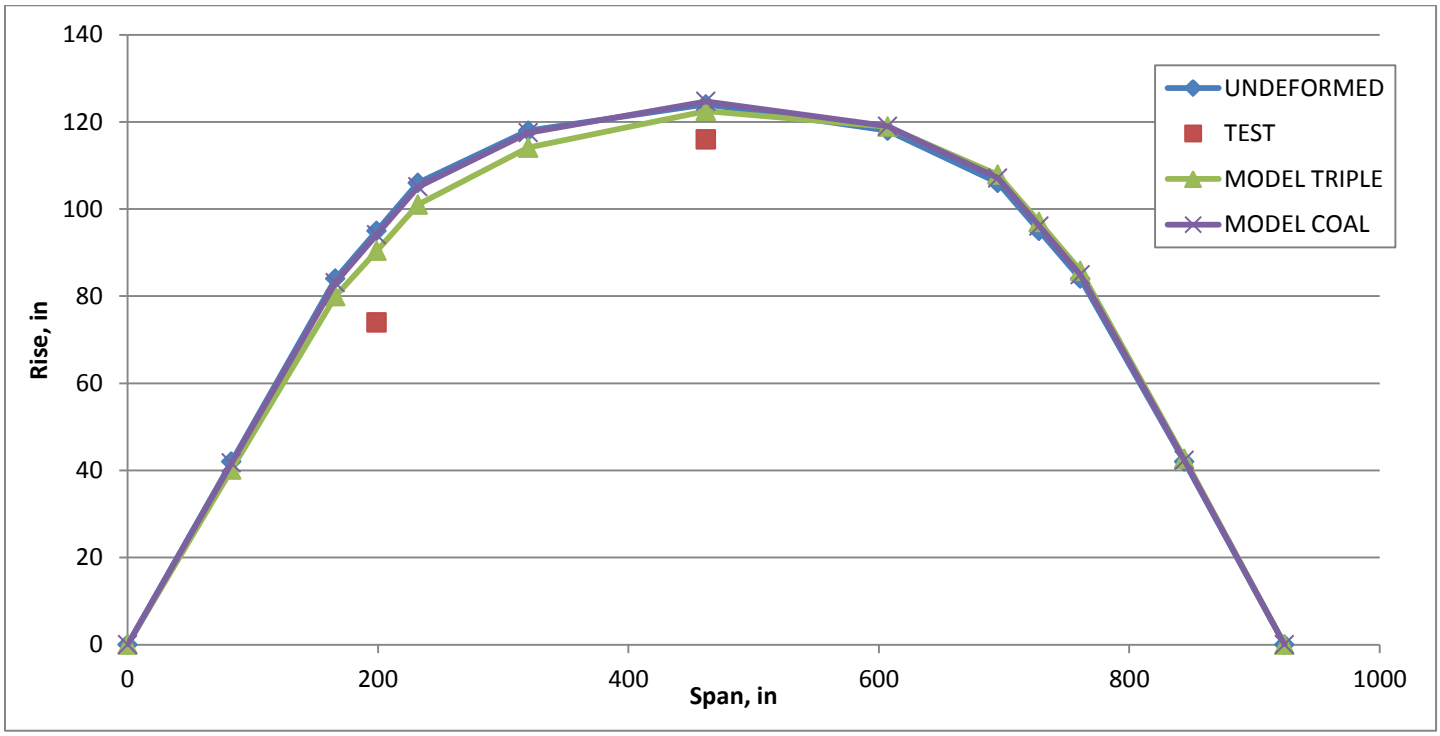

Figure E-15. Depot St. Upstream Arch (Load at North Quarter Pt. in D-S Lane)

Appendix F - Model Arch Strain Profiles

Table F-1. Main Street Bridge Strains (Load in U-S Lane)

LOADING INFORMATION		STRAIN TRANSDUCER LOCATION								
Position on Bridge	Scenario	1	2	3	4	5	6	7	8	9
North Quarter Pt.	Triple Test	-12.0	-14.9	N/A	-8.0	-0.7	-0.1	-6.0	-10.2	N/A
	Triple Model	-6.8	-9.1	-8.1	-5.4	-4.0	-1.2	-2.7	-4.4	-4.9
	Coal Model	0.5	-2.2	-5.8	-0.9	-0.8	-2.5	-0.3	-1.1	-1.6
Midspan	Triple Test	-15.5	-17.3	N/A	45.7	4.4	-8.0	-16.9	-31.0	N/A
	Triple Model	-8.6	-15.5	-11.2	3.1	11.9	8.0	-9.0	-13.9	-15.2
	Coal Model	-0.3	-9.9	-8.3	0.1	2.1	14.1	-0.3	-6.2	-13.4
South Quarter Pt.	Triple Test	-6.1	-6.3	N/A	10.2	2.3	-3.4	-4.4	-14.1	N/A
	Triple Model	-1.8	-5.9	-4.4	-0.2	4.4	3.9	-1.7	-10.0	-9.4
	Coal Model	-0.3	-2.2	-1.7	-0.1	1.1	-1.8	0.8	-7.1	-4.5

Table F-2. Main Street Bridge Strains (Load in D-S Lane)

LOADING INFORMATION		STRAIN TRANSDUCER LOCATION								
Position on Bridge	Scenario	1	2	3	4	5	6	7	8	9
South Quarter Pt.	Triple Test	-7.8	-3.9	N/A	9.9	0.3	-0.3	-12.3	-6.8	N/A
	Triple Model	-8.2	-4.5	-1.7	6.2	-1.2	1.3	-11.9	-8.7	-0.9
	Coal Model	-3.0	-1.2	-0.7	-2.6	-4.6	-0.5	-6.5	-1.8	1.4
Midspan	Triple Test	-22.0	-12.9	N/A	66.6	5.7	-4.5	-30.3	-25.8	N/A
	Triple Model	-30.7	-17.0	-3.3	13.3	20.4	4.4	-28.7	-20.2	-4.2
	Coal Model	-23.9	-10.1	-0.2	27.9	25.6	2.1	-24.1	-15.4	-0.1
North Quarter Pt.	Triple Test	-19.4	-14.4	N/A	21.4	2.8	0.9	-11.4	-11.3	N/A
	Triple Model	-27.6	-15.2	-0.7	-4.6	-1.3	-1.3	-11.9	-9.5	-1.7
	Coal Model	-18.8	-11.3	1.6	-8.4	-8.2	-0.8	-4.4	-4.0	-0.8

Table F-3. Depot Street Bridge Strains (Load in U-S Lane)

LOADING INFORMATION		STRAIN TRANSDUCER LOCATION								
Position on Bridge	Scenario	1	2	3	4	5	6	7	8	9
North Quarter Pt.	Triple Test	-5.9	5.5	0.8	-12.3	9.1	-39.4	-10.8	0.1	5.1
	Triple Model	-6.7	4.7	-13.7	-12.9	9.8	-29.3	-3.1	3.1	-5.2
	Coal Model	-1.4	-5.8	-9.7	-2.6	-7.1	-16.1	0.5	-0.7	0.3
Midspan	Triple Test	-8.5	42.7	-6.8	-18.5	35.7	-39.8	-13.8	-0.1	-14.2
	Triple Model	-16.0	18.5	-16.8	-32.5	33.6	-30.9	-6.2	12.7	-8.2
	Coal Model	-15.6	30.4	-16.7	-21.4	38.0	-13.8	-1.2	4.3	-1.2
South Quarter Pt.	Triple Test	-1.8	10.3	-5.2	0.6	2.8	-16.8	1.8	-0.8	-10.1
	Triple Model	-13.1	5.2	-6.9	-26.9	4.8	-10.7	-3.7	-0.7	-1.1
	Coal Model	-10.2	-5.1	-1.5	-16.6	-6.4	-2.8	0.9	-0.3	-0.3

Table F-4. Depot Street Bridge Strains (Load in D-S Lane)

LOADING INFORMATION		STRAIN TRANSDUCER LOCATION								
Position on Bridge	Load Scenario	1	2	3	4	5	6	7	8	9
South Quarter Pt.	Triple Test	-2.5	14.4	-4.9	-2.7	4.5	-16.6	-4.1	-3.1	-19.1
	Triple Model	-4.4	2.7	-2.9	-28.2	8.9	-13.1	-15.1	6.4	-7.7
	Coal Model	1.0	-0.3	-0.2	-15.5	-5.9	-2.8	-11.3	-5.7	-1.7
Midspan	Triple Test	-8.1	43.1	-4.5	-21.0	34.0	-38.7	-20.6	-3.9	-20.5
	Triple Model	-5.5	10.1	-7.0	-29.2	31.3	-32.5	-17.9	20.2	-13.6
	Coal Model	-0.8	3.7	-0.9	-20.4	36.1	-21.3	-17.2	33.0	-18.0
North Quarter Pt.	Triple Test	-5.5	-6.8	2.2	-16.1	-2.9	-34.9	-16.6	-5.5	0.5
	Triple Model	-0.9	-1.2	-3.0	-9.9	2.9	-26.2	-7.2	4.3	-14.8
	Coal Model	-0.2	-0.7	1.1	-2.5	-6.5	-15.1	-1.5	-6.5	-11.0

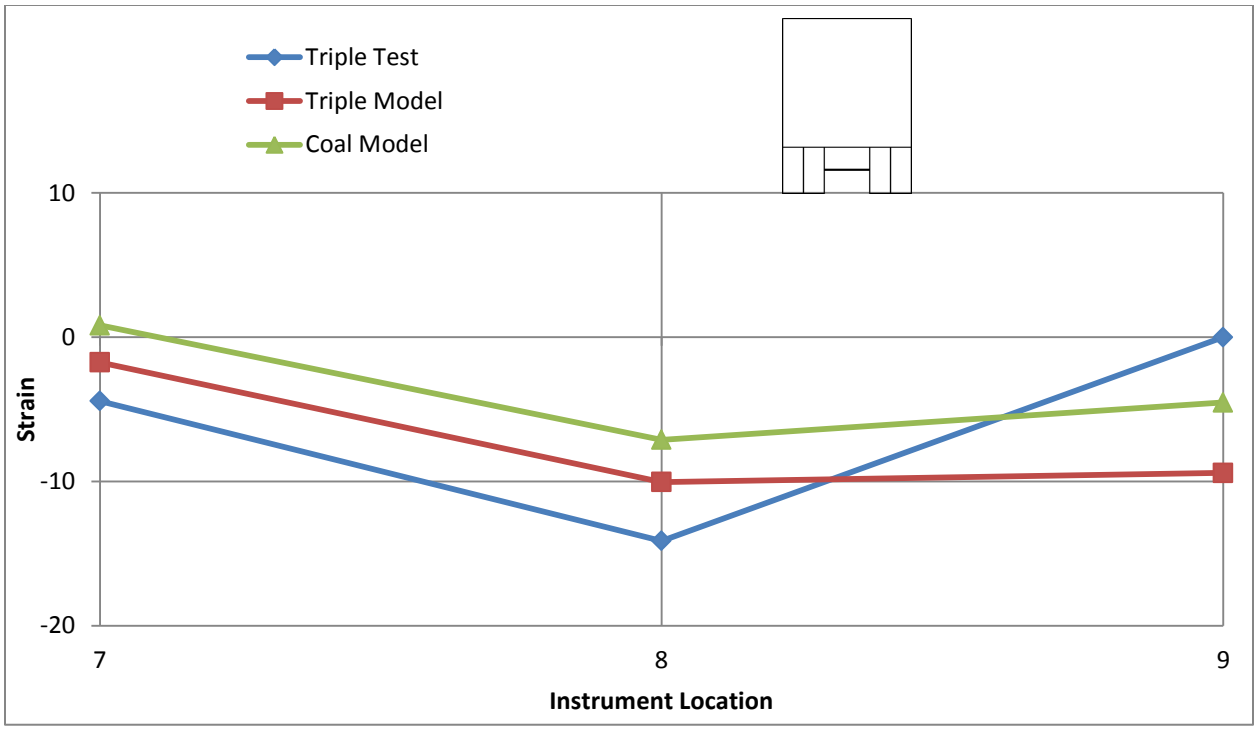

Figure F-1. Main St. Bridge South Quarter Point Strain Profile (Load in U-S Lane)

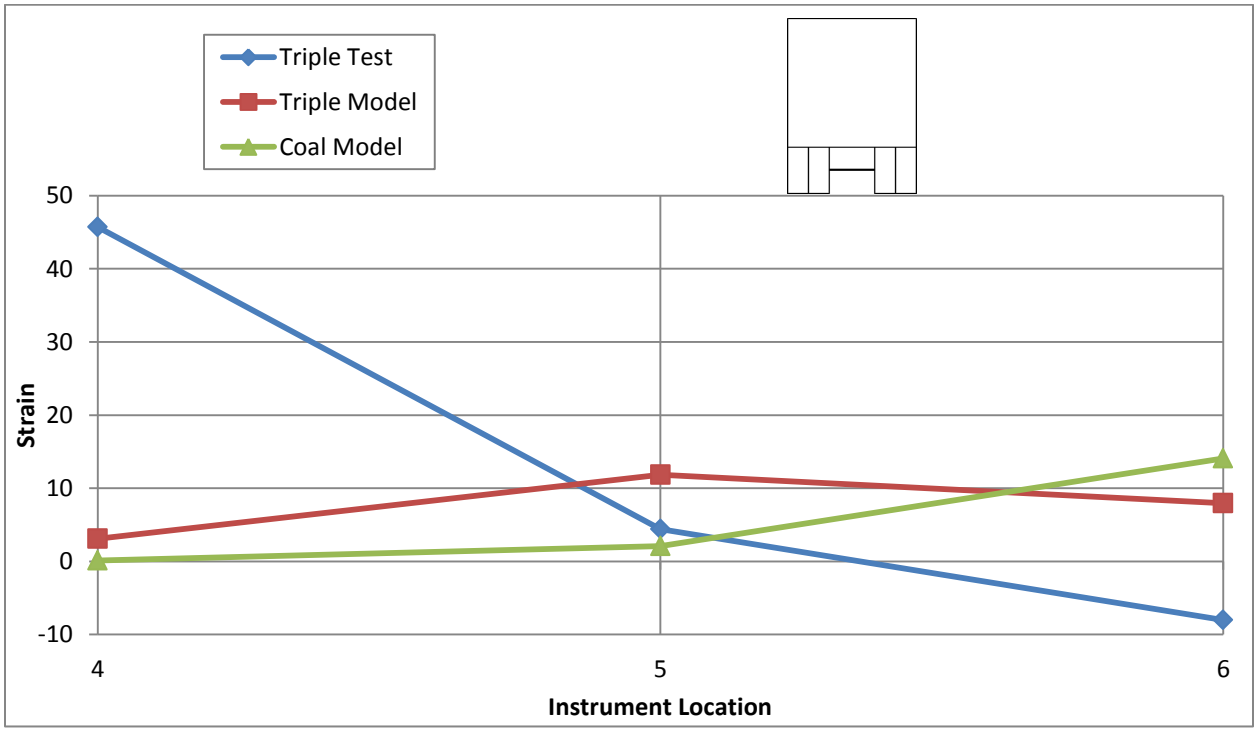

Figure F-2. Main St. Bridge Midspan Strain Profile (Load in U-S Lane)

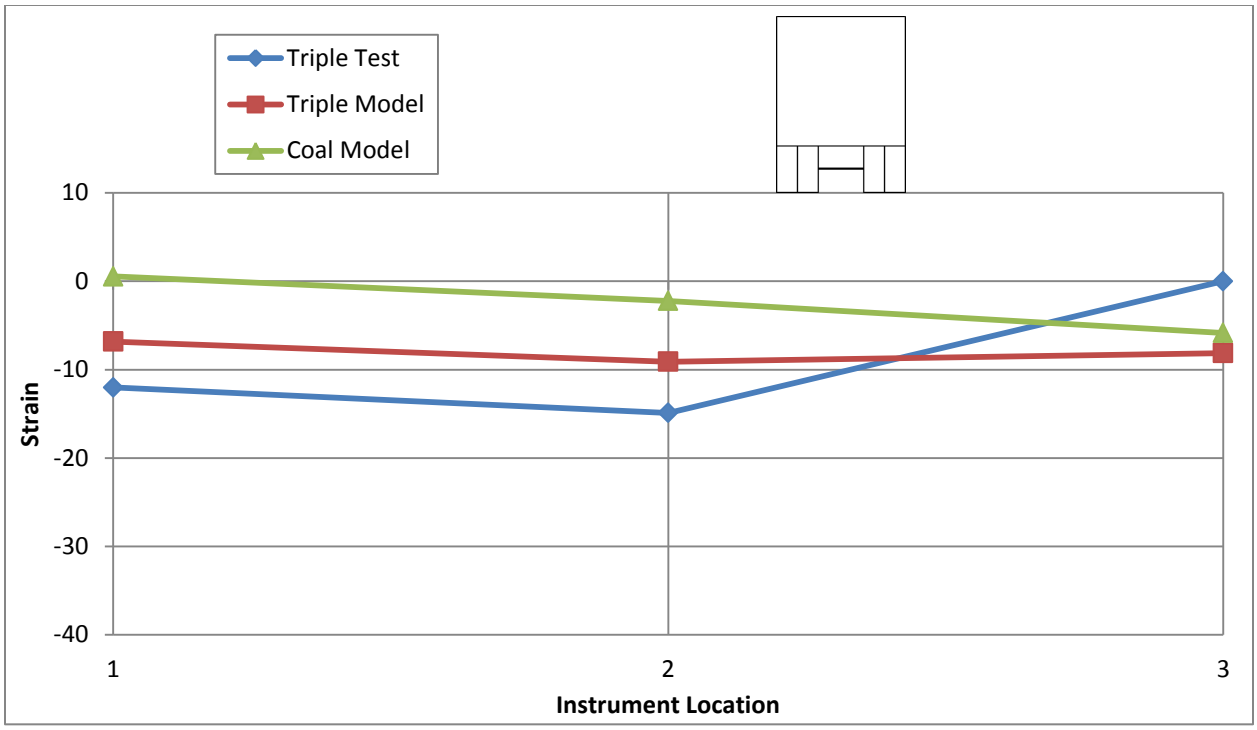

Figure F-3. Main St. Bridge North Quarter Point Strain Profile (Load in U-S Lane)

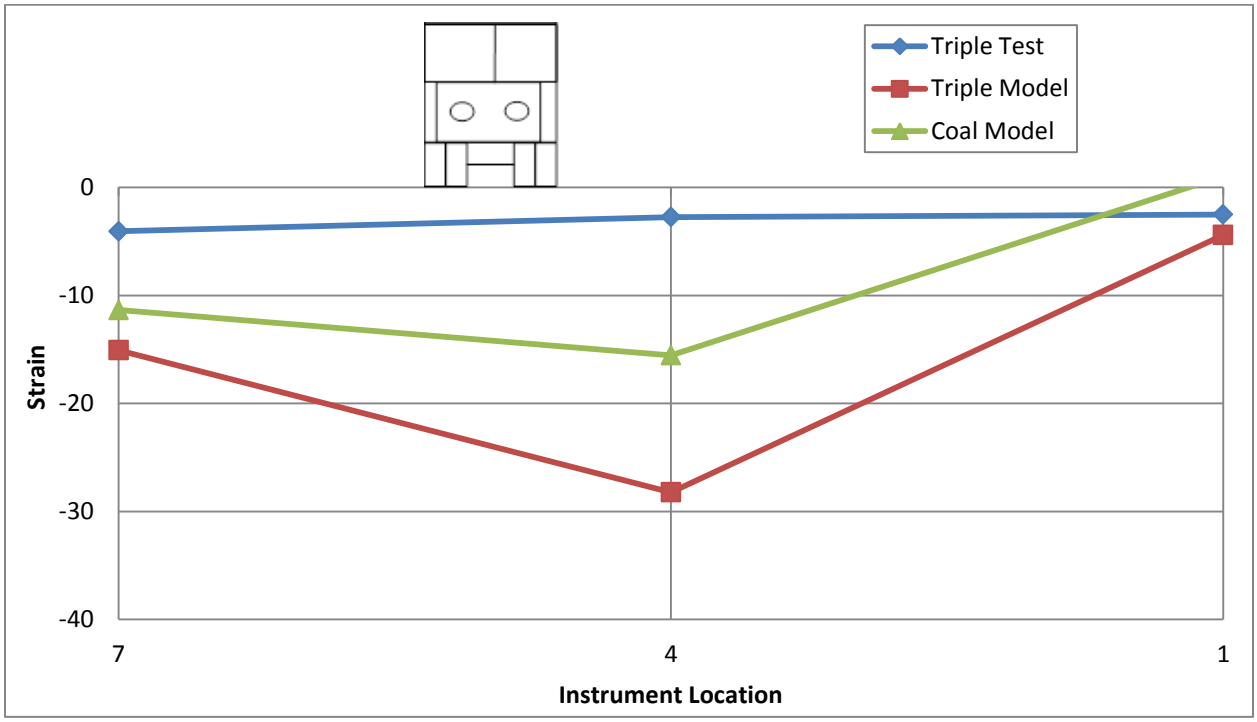

Figure F-4. Depot St. Bridge South Quarter Point Strain Profile (Load in D-S Lane)

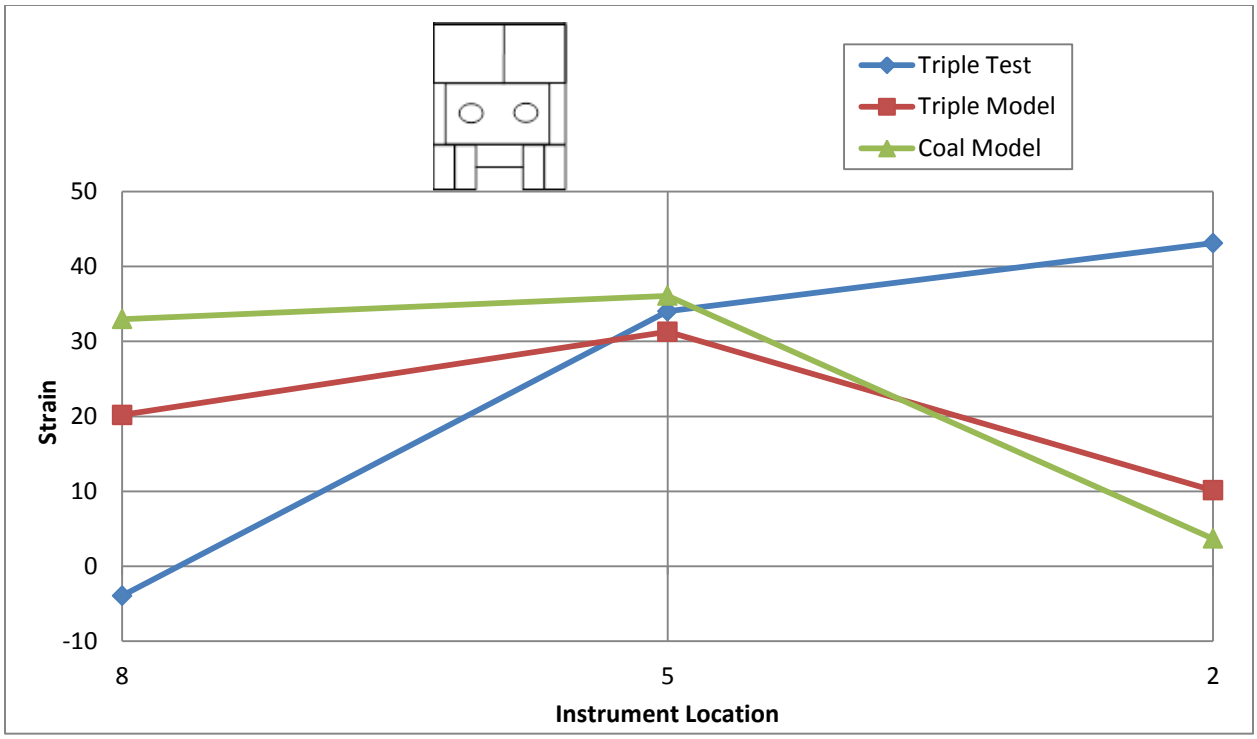

Figure F-5. Depot St. Bridge Midspan Strain Profile (Load in D-S Lane)

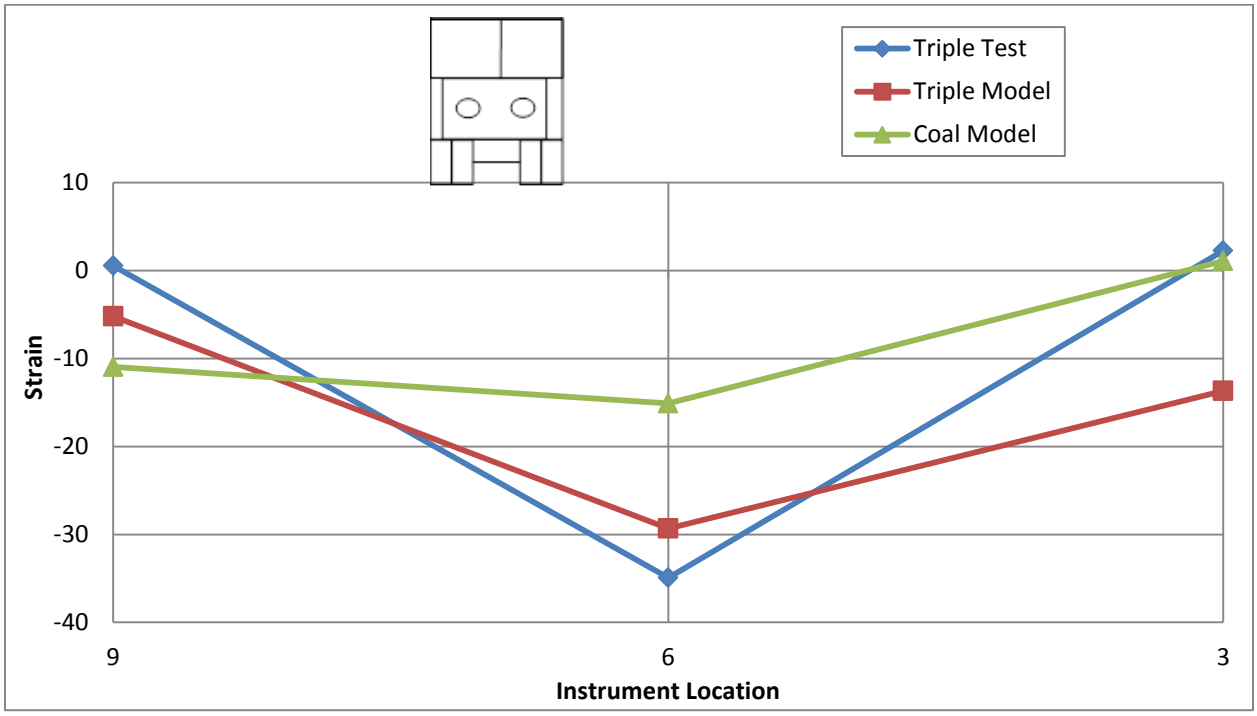

Figure F-6. Depot St. Bridge North Quarter Point Strain Profile (Load in D-S Lane)